# Origin and characteristics of plant signals in surface and subrecent sediments of the southwest African continental slope

Ursprung und Charakteristika von Pflanzensignalen in Oberflächen- und subrezenten Sedimenten des südwestafrikanischen Kontinentalhanges

Dissertation
zur Erlangung des Grades und Titels
einer Doktorin der Naturwissenschaften
- Dr. rer. nat. -

angenommen
bei der Fakultät für Mathematik und Naturwissenschaften
der Carl von Ossietzky Universität Oldenburg

von

Tanja Badewien
geboren am 01.12.1983 in Leer

Erstgutachter: Prof. Dr. Jürgen Rullkötter
Zweitgutachter: Prof. Dr. Hans-Jürgen Brumsack

Eingereicht am: 27.02.2015
Disputation am: 22.04.2015

The following parts of this thesis have been published,
are submitted to or in preparation for publication:

Chapter 2: Badewien, T., Vogts, A., Rullkötter, J. *n*-Alkane distribution and stable carbon isotope composition in leaf waxes of $C_3$ and $C_4$ plants Angola. Submitted to Organic Geochemistry.

Chapter 3: Vogts, A., Schefuß, E., Badewien, T., Rullkötter, J., 2012. *n*-Alkane parameters from a deep sea sediment transect off southwest Africa reflect continental vegetation and climate conditions. Organic Geochemistry 47, 109-119.

Chapter 4: Vogts, A., Badewien, T., Rullkötter, J., Schefuß, E. Stable hydrogen isotopic composition of continental precipitation is reflected by δD ratios of land plant-derived *n*-alkanes in marine sediments off southwest Africa. In preparation for submission to Organic Geochemistry.

Chapter 5: Badewien, T., Vogts, A., Rullkötter, J. Influence of Late Pleistocene and Holocene climate on vegetation distribution in southwest Africa elucidated from sedimentary *n*-alkanes - differences between 12°S and 20°S. In revision after review by Quaternary Science Reviews.

Parts of this thesis were presented by the author
at the following meetings and conferences:

Badewien, T., Schefuß, E., Vogts, A., Rullkötter, J., 2010. Rain forest and savanna: What marine sediments tell about African vegetation. Jahrestagung der Afrikagruppe deutscher Geowissenschaftler (AdG), Frankfurt, Germany (25th to 26th June), oral presentation.

Badewien, T., Schefuß, E., Vogts, A., Rullkötter, J., 2010. Leaf wax components in recent sediments from the SW-African continental slope: Conclusions about terrestrial vegetation. 6th North German Organic Geochemistry Meeting, Hamburg, Germany (2nd September), oral presentation.

Badewien, T., Rullkötter, J., 2011. Terrestrial *n*-alkanes in ocean margin sediments regarding distance to the continent. 25th International Meeting on Organic Geochemistry (IMOG), Interlaken, Switzerland (18th to 23th September), poster presentation.

## Abstract

Information on continental vegetation zones and climatic parameters can be derived from long chain *n*-alkanes in marine geological archives. This thesis extends the potentially available informations by reporting the *n*-alkane parameters (chain length distribution, stable carbon and/or hydrogen isotopic compositions) of plant species from southwest Africa and in sediments off southwest Africa in different approaches.

For the first part of the thesis, 41 $C_3$ and 11 $C_4$ plant species from the wood- and shrubland of Angola were analysed. Their *n*-alkane data were combined with literature data available for $C_3$ plants of the rain forest (north of Angola) and for $C_3$ and $C_4$ plants of the savannah (south of Angola). The combined database constitutes a continental transect and reveals an increase in the $\delta^{13}C$ ratio of $C_3$ plants towards the south. This increase is probably due to latitudinal changes of environmental conditions like water stress, light intensity and incorporation of recycled $CO_2$. In addition, the distribution patterns of the *n*-alkanes reveal an increase in the chain length towards the south for $C_3$ and $C_4$ plants. Climatic and environmental factors (mean annual temperature, aridity indices and a vertical temperature gradient) possibly controlling the carbon number distribution were correlated to the chain length. The results of the correlations are discussed.

The two subsequent studies investigate an isobathic transect of surface sediment samples from the southeast Atlantic (1°N to 28°S). One study evaluates how the *n*-alkane chain length distribution and stable carbon isotopic composition reflect the adjacent continental vegetation. To estimate the $C_4$ contribution to the sediments, a binary mixing equation was employed using different *n*-alkane parameters as end member values for $C_3$ and $C_4$ plants. In southwest Africa, the vegetation changes from $C_3$ dominated in the equatorial rain forest to $C_4$ dominated towards the south. The calculated $C_4$ abundance reflects the continental vegetation if long-range transport by winds and rivers is taken into account. The four northern samples of the transect probably receive large amounts of aeolian material from distant locations and were excluded for further climatic deductions. The $C_4$ abundances of the other samples correlate significantly with the mean annual precipitation and the aridity indices in the catchment areas. The subsequent study also deals with the isobathic transect and evaluates how the hydrogen isotopic composition of *n*-alkanes reflects the δD composition of the continental precipitation. The δD ratios of the $C_{29}$, $C_{31}$ and $C_{33}$ *n*-alkanes vary only slightly among each other and along the transect. The total

δD variation of the precipitation is higher than the total δD variation of the *n*-alkanes. The best correlations of the *n*-alkane δD values with continental precipitation δD values at different distances to the coast were found for locations at 350 km inland. The correlations are similar if seasonal precipitation is taken into account. Despite the huge differences in environmental conditions and vegetation composition throughout the transect, the apparent fractionation is largely constant. The evaluation of other *n*-alkane parameters leads to the conclusion that the change of the δD composition due to the change of aridity is compensated by the concurrent δD variation due to the change of plant groups.

The last study of this thesis draws conclusions on the past vegetation changes in southwest Africa and contains implications on the influence of different climatic parameters on the past vegetation. Two sediment cores from the southeast Atlantic (12°S and 20°S) covering the current interglacial and parts of the last glacial were analysed for their *n*-alkane parameters. The sampling location of the southern core is adjacent to a $C_4$ dominated region and reveals a fairly uniform contribution of $C_4$ material to the sediments during the last 23 ka. In contrast, the core at 12°S covering the last 73 ka indicates a $C_4$ domination during the Last Pleistocene, a $C_3$ domination during the Holocene and a gradual change of the vegetation during deglaciation. During deglaciation, the increasing atmospheric $CO_2$ content correlates well with the $\%C_4$ values. Compared to the Holocene, the last glacial is characterised by lower $pCO_2$ values, whereby $C_4$ plants have an advantage over $C_3$ plants. During the Late Pleistocene, smaller $\%C_4$ fluctuations were detected which do not occur simultaneously with Heinrich Stadials or Antarctic warming periods. Instead, the local insolation at the end of the growing season shows great similarities with the $\%C_4$ fluctuations.

## Zusammenfassung

Informationen über die kontinentalen Vegetationszonen und das Klima können aus langkettigen *n*-Alkanen in marinen geologischen Archiven abgeleitet werden. Diese Dissertation erweitert diese potentiell verfügbaren Informationen, indem die *n*-Alkanparameter (Kettenlängenverteilung, stabile Kohlenstoff- und Wasserstoffisotopenverhältnisse) von verschiedenen Pflanzenarten aus Südwestafrika und in Sedimenten des Südostatlantiks im Rahmen verschiedener Projekte analysiert wurden.

Der erste Teil dieser Dissertation befasst sich mit der Analyse von 41 $C_3$- und 11 $C_4$-Pflanzen aus Baum- und Buschlandschaften von Angola. Die Ergebnisse wurden in eine Datenbank integriert, die bereits Daten von $C_3$-Pflanzen des Regenwaldes (nördlich von Angola) und von $C_3$- und $C_4$-Pflanzen aus der Savanne (südlich von Angola) enthielt. Die erweiterte Datenbank stellt damit einen südwestafrikanischen Transekt dar und zeigt einen breitengradabhängigen Anstieg der stabilen Kohlenstoffisotopenverhältnisse der $C_3$-Pflanzen an. Dieser Anstieg wird vermutlich durch verschiedene Umweltbedingungen wie Wasserstress, Lichtintensität und Aufnahme von $CO_2$ aus mineralisierter Biomasse verursacht. Darüber hinaus steigt die Kettenlänge der *n*-Alkane in Richtung Süden für die $C_3$- und $C_4$-Pflanzen an. Klimatische und umweltbedingte Faktoren (Jahresmitteltemperaturen, Ariditätsindizes und vertikaler Temperaturgradient) beeinflussen möglicherweise die Kohlenstoffzahlverteilung und werden mit den Kettenlängen korreliert. Die Ergebnisse der Korrelationen werden diskutiert.

Die zwei darauf folgenden Studien untersuchen einen isobathischen Transekt von Oberflächensedimenten des Südostatlantiks (1°N bis 28°S). Eine der Studien legt dar, inwiefern die Kettenlängenverteilung und die stabilen Kohlenstoffisotopenverhältnisse der *n*-Alkane die aktuellen Vegetationszusammensetzungen der benachbarten Gebiete auf dem Kontinent widerspiegeln. Der $C_4$-Anteil in den Sedimenten wurde mit Hilfe der Endgliederwerte verschiedener *n*-Alkanparameter für die $C_3$- und $C_4$-Pflanzen berechnet. Auf dem südwestafrikanischen Kontinent wechselt die Vegetation vom $C_3$-dominierten Regenwald in der Region des Äquators zu $C_4$-dominierten Gebieten in Richtung Süden. Der berechnete $C_4$-Anteil in den Sedimenten spiegelt die kontinentale Vegetation wider, wenn der Ferntransport von Pflanzenteilen mittels Winden und Flüssen berücksichtigt wird. Die vier nördlichsten Sedimentproben enthalten vermutlich einen signifikanten Anteil an Pflanzenmaterial, welches von weiter entfernten Regionen stammt, und

wurden für klimatische Rekonstruktionen nicht berücksichtigt. Die $C_4$-Anteile in den südlicheren Proben korrelieren signifikant mit dem mittleren Jahresniederschlag und den Ariditätsindizes der Ursprungsgebiete. Die weitere Studie zu dem isobathischen Transekt bewertet, inwiefern die Wasserstoffisotopenzusammensetzung der *n*-Alkane den Deuteriumanteil des kontinentalen Niederschlags widerspiegelt. Die δD-Werte der $C_{29}$-, $C_{31}$- und $C_{33}$-*n*-Alkane variieren nur leicht untereinander und im Verlauf des Transekts. Die Schwankung der δD-Werte des kontinentalen Niederschlags ist höher als die der *n*-Alkane. Die δD-Werte der *n*-Alkane werden mit den δD-Werten des kontinentalen Niederschlags in Gebieten mit verschiedenen Entfernungen zur Küste korreliert und zeigen die besten Korrelationen für Gebiete mit 350 km Abstand zur Küste. Wenn saisonaler Niederschlag mit einbezogen wird, sind die Korrelationen ähnlich. Trotz der großen Unterschiede der Umweltbedingungen und der Vegetationszusammensetzung im Verlauf des Transekts ist die isotopische Fraktionierung nahezu konstant. Unter Einbeziehung anderer *n*-Alkanparameter wird darauf geschlossen, dass die Veränderung der δD-Werte, bedingt durch die wechselnde Aridität, durch die Veränderung der δD-Werte kompensiert wird, die durch den Wechsel der Pflanzengruppen verursacht wird.

In der letzten Studie dieser Dissertation werden Rückschlüsse auf vergangene Vegetationsveränderungen in Südwestafrika gezogen sowie der Einfluss verschiedener klimatischer Faktoren auf die Vegetation untersucht. Dazu wurden zwei Sedimentkerne aus dem Südostatlantik (12°S und 20°S), die das aktuelle Interglazial und das letzte Glazial abdecken, auf *n*-Alkanparameter untersucht. Der südliche Kern erhält Pflanzenmaterial von den benachbarten, $C_4$-dominierten Gebieten und zeigt einen recht einheitlichen Beitrag von $C_4$-Material zu den Sedimenten während der letzten 23 ka. Im Gegensatz dazu gibt der Kern von 12°S, der die letzten 73 ka umfasst, Hinweise auf eine $C_4$-dominierte Vegetation während des Jungpleistozäns, auf $C_3$-dominierte Vegetation während des Holozäns und auf einen graduellen Wechsel der Vegetation während der Deglaziation. Während der Deglaziation korreliert der zunehmende atmosphärische $CO_2$-Gehalt gut mit den $\%C_4$-Werten. Im Vergleich zum Holozän zeichnet sich das letzte Glazial durch niedrigere $pCO_2$-Werte aus, die $C_4$-Pflanzen einen Vorteil gegenüber $C_3$-Pflanzen verschaffen. Für das Jungpleistozän werden kleinere $\%C_4$-Schwankungen gefunden, welche nicht zeitgleich mit Heinrich Stadialen oder zu Zeiten Antarktischer Erwärmung stattfanden. Die $\%C_4$-Schwankungen zeigen dafür große Ähnlichkeit mit der lokalen Sonneneinstrahlung am Ende der Vegetationsperiode.

## Table of content

## Figure captions

(Abbreviated)

## Table captions

(Abbreviated)

# Abbreviations

## Latin characters

| | |
|---|---|
| $\%C_3$ | Calculated $C_3$ abundance |
| $\%C_4$ | Calculated $C_4$ abundance |
| °C | Degree Celsius |
| °E | Degree East (longitude) |
| °N | Degree North (latitude) |
| °S | Degree South (latitude) |
| a | Year |
| AA | Arabian Anticyclone |
| ABF | Angola-Benguela-Front |
| AC | Angola Current |
| ACL | Average chain length |
| $ACL_{X-Y}$ | Average chain length of the *n*-alkanes with X to Y carbon atoms |
| AdG | “Afrikagruppe deutscher Geowissenschaftler” |
| arithm. average | Arithmetic average |
| ASE | Accelerated Solvent Extractor |
| AW | Antarctic warming periods |
| BC | Benguela Current |
| BCC | Benson-Calvin cycle |
| BP | Before present |
| bsf | Below sea floor |
| ca. | Circa |
| CAB | Congo Air Boundary |
| CAM | Crassulacean Acid Metabolism |
| cf. | compare |
| cm | Centimeter |
| CPI | Carbon preference index |
| $CPI_{X-Y}$ | Carbon preference index for *n*-alkanes in the chain length interval X to Y |
| DB-5ht | Non polar capillary column for high temperature gas chromatography |
| DFG | “Deutsche Forschungsgemeinschaft” |
| DM | Dry matter |
| e.g. | For example, abbreviaton of “exemplii gratia” (Latin) |

| | |
|---|---|
| FID | Flame ionisation detector |
| Fig. | Figure |
| g | Gram |
| GC | Gas chromatograph, abbreviation is used for gas chromatography in Chapters 3 and 4 |
| GC-FID | Gas chromatography with a flame ionisation detector |
| GeoB | Geosciences of the University of Bremen |
| HS | Heinrich Stadial |
| i.d. | Inner diameter |
| i.e. | That is, abbreviation of “id est” (Latin) |
| ICBM | Institute for Chemistry and Biology of the Marine Environment |
| IMOG | International Meeting on Organic Geochemistry |
| IOW | Leibniz Institute for Baltic Sea Research |
| irm-MS | Isotope ratio monitoring mass spectrometer |
| ITCZ | Intertropical Convergence Zone |
| ka | 1000 years, abbreviation of “kiloannus” (Latin) |
| kg | Kilogram |
| km | Kilometre |
| L | Major low pressure cell |
| l | Litre |
| LGM | Last Glacial Maximum |
| m | Metre |
| MAD | Median absolute deviation |
| MARUM | Center for Marine Environmental Sciences |
| mg | Milligram |
| min | Minute |
| mm | Millimetre |
| MSTFA | N-methyl-N-(trimethylsilyl)-trifluoroacetamide |
| n | Number of samples |
| n.d. | Not determined |
| NAA | North Atlantic Antizyclone |
| NE | Northeasterly |
| NEM | North East African monsoon |
| NHC | Northern Hadley Cell |
| no., nos. | Number, numbers, abbreviaton of “numero” (Latin) |
| $n_X$ | Number of samples used for parameter X |
| ODP | Ocean Drilling Project |

| | |
|---|---|
| OIPC | Online isotopes in precipitation calculator |
| OM | Organic mateer |
| p | Probability |
| $pCO_2$ | Partial pressure of carbon dioxide |
| PEP | Phosphoenolpyruvate |
| PEP-C | Phosphoenolpyruvate carboxylase |
| PM | Plant material |
| PP | Photosynthetic pathway |
| ppmV | Parts per million by volume |
| $P_{WMA}$ | Weighted mean average of precipitation |
| r | Pearson correlation coefficient |
| $r^2$ | Coefficient of determination |
| RSD | Relative standard deviation |
| $R_{St}$ | Isotope ratio of a standard sample |
| Rubisco | Ribulose-1,5-bisphosphate carboxylase oxygenase |
| RuBP | Ribulose-1,5-bisphosphate |
| RV | Research vessel |
| $R_X$ | Isotope ratio of a sample |
| s | Second |
| SAA | South Atlantic Anticyclone |
| SD | Standard deviation |
| SE | Southeasterly |
| SEM | South East African monsoon |
| SHC | Southern Hadley Cell |
| SIA | South Indian Anticyclone |
| SLAP | Standard light Antarctic precipitation, standard substance |
| SST | Sea surface temperature |
| SW | Southwest |
| TIC | Total inorganic carbon |
| TOC | Total organic carbon |
| $U_{37}^{K'}$ | Ketone unsaturation index |
| v/v | Volumetric content |
| V-SMOW | Vienna-Standard Mean Ocean Water, standard substance |
| V-PDB | Vienna-Pee Dee Belemnite, standard substance |
| vs. | Versus |
| WAM | West African Monsoon |
| WMA | Weighted mean average |

| | |
|---|---|
| WR | Walvis Ridge |
| wt | Weight |
| XRF | X-ray fluorescence |

**Greek characters**

| | |
|---|---|
| $\delta D_L$ | Stable hydrogen isotope composition of lipids |
| $\delta^{13}C$ | Stable carbon isotope composition ($^{13}C/^{12}C$) relative to the V-PDB standard in per mil (‰) |
| $\delta^{13}C_{OM}$ | Stable carbon isotope composition of the organic material |
| $\delta^{13}C_P$ | Carbon isotopic composition of $C_3$ plants |
| $\delta^{13}C_{WMA}$ | Weighted mean averaged molecular stable carbon isotope composition |
| $\delta^{13}C_{WMAX-Y}$ | Weighted mean average of the stable carbon isotope composition of *n*-alkanes with X to Y carbon atoms |
| $\delta^{13}C_X$ | Stable carbon isotope composition of the *n*-alkane with X carbon atoms |
| $\delta^{18}O$ | Stable oxygen isotope composition ($^{16}O/^{18}O$) relative to the V-PDB standard |
| $\delta D$ | Stable hydrogen isotope composition ($^{2}H/^{1}H$) relative to the V-SMOW standard in per mil (‰) |
| $\delta D_P$ | Hydrogen isotope composition of precipitation |
| $\delta D_{WMA}$ | Weighted mean averaged molecular stable hydrogen isotope composition |
| $\delta D_X$ | Stable hydrogen isotope composition of the *n*-alkane with X carbon atoms |
| $\delta_X$ | Delta value of a substance X |
| $\varepsilon_a$ | Apparent stable hydrogen isotope fractionation |
| $\varepsilon_{aCX}$ | Apparent hydrogen isotopic fractionation between continental precipitation and the *n*-alkane with X carbon atoms |
| $\varepsilon_{aWMA29-33}$ | Apparent hydrogen isotopic fractionation between the continental precipitation and the weighted mean average of odd carbon numbered *n*-alkanes with 29 to 33 carbon atoms |
| µm | Micrometre |
| σ | Standard deviation |

# 1. Introduction

The deposition of organic matter in lacustrine or marine sediments provides a valuable archive of environmental conditions in their catchment areas. Insights into past and current climatic conditions are necessary to understand the factors influencing climate and their consequences. This knowledge is needed to assess how the environment will react to climatic changes in the future. Today, studies on sedimentary archives gain more importance with regard to the antropogenically induced changes in the climatic system and their effects (IPCC, 2013).

Valuable tools employed in palaeoclimatic studies are biomarkers. Biomarkers are compounds, e.g. in sediments, which are unambiguously linked to the organisms they originate from (Rullkötter, 2003). To analyse past vegetation zones, long chain *n*-alkanes have proven to be valuable biomarkers. *n*-Alkanes are constituents of the outer wax layer of terrestrial plants. When entering the geological realm, they remain unaltered over long time scales. Sedimentary *n*-alkanes can be linked to their terrestrial plant origin and, thus, serve as (bio-)markers for this specific life form. In order to derive pertinent information on past conditions from geological archives, the current vegetation and the relationship between present-day vegetation and sedimentary archives need to be studied. With this background knowledge, past climatic conditions can be reconstructed. For instance, the differences in the sedimentary isotopic compositions of *n*-alkanes can be used to draw conclusions on the hydrologic conditions in the continental source areas of the *n*-alkanes (e.g., Eglinton and Hamilton, 1967; Schefuß et al., 2005; Castañeda et al., 2009; Collins et al., 2011).

The African continent, especially its southwestern section, is an ideal investigation area for terrestrial *n*-alkanes. There, the vegetation zones are arranged broadly parallel to the latitudes, and transport of terrestrial *n*-alkanes to the sediments occurs mainly along zonal patterns (Dupont and Wyputta, 2003; Mayaux et al., 2004).

## 1.1. The photosynthetic pathways

Terrestrial plants are divided into three groups according to their photosynthetic pathways. All terrestrial plants fix $CO_2$ through their opened stomata (Fig. 1.1). Inside the mesophyll cell, the $CO_2$ is in chemical equilibrium with aqueous bicarbonate and is incorporated into the Benson-Calvin cycle (Fig. 1.1a). This cycle comprises three steps. At first, the $CO_2$ is used to carboxylate ribulose-1,5-bisphosphate (RuBP) producing two $C_3$ molecules (glycerate-3-phosphate). This reaction is catalysed by

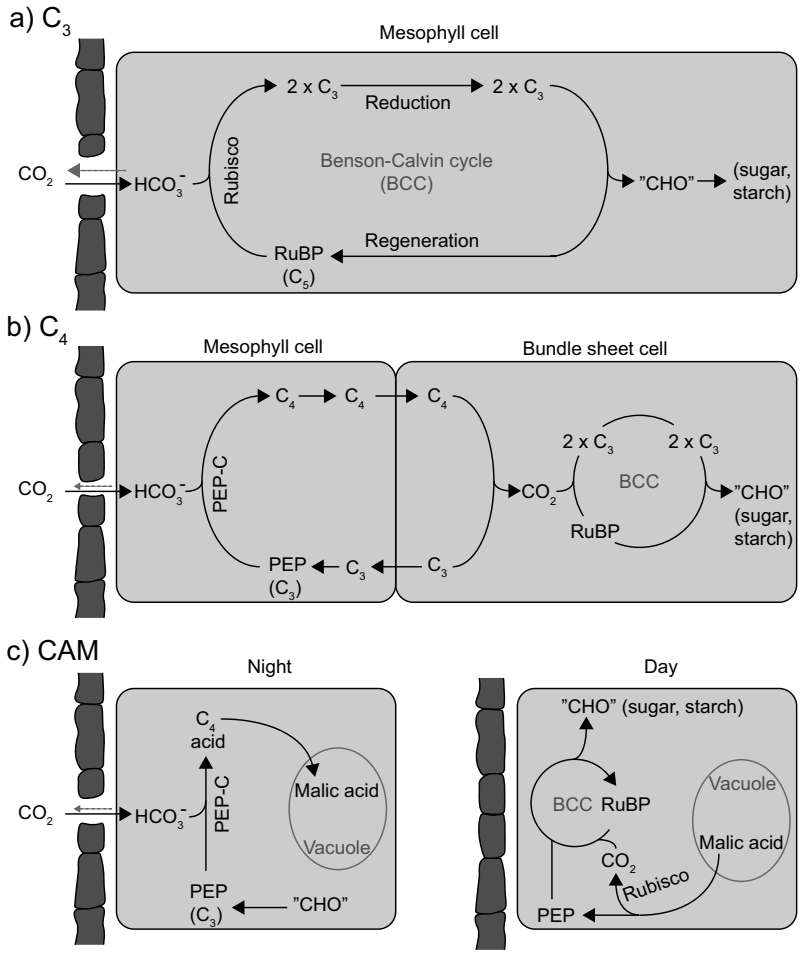


**Fig 1.1:** The photosynthetic pathways of terrestrial plants a) for $C_3$ species, b) for $C_4$ species and c) for CAM species; BCC - Benson-Calvin cycle; Rubisco - ribulose-1,5-bisphoshate carboxylase oxygenase; RuBP- ribulose-1,5-bisphosphate; PEP - phosphoenolpyruvate; PEP-C - phosphoenolpyruvate carboxylase; “CHO” - starch and other carbohydrates (after Leegood, 1999a,b).

the enzyme ribulose-1,5-bisphosphate carboxylase/oxygenase (Rubisco). Glycerate-3-phosphate is further reduced to triose-phosphate (also a $C_3$ molecule). In the third step, fructose-6-phosphate is formed and used to regenerate RuBP or to synthesise starch and other carbohydrates. The so-called $C_3$ plants use this way of $CO_2$ assimilation. As Rubisco is bifunctional, it also catalyses the oxygenation of RuBP. This process called photorespiration inhibits the carboxylase reaction. Thereby, the carbon assimilation can be depressed by up to 40% although losses vary highly with changing environmental conditions (Leegood, 1999b).

The $C_4$ plants developed biochemical variations of the process used by the $C_3$ plants to prevent photorespiration by concentrating $CO_2$ around Rubisco (Fig. 1.1b). $C_4$ plants also use the Benson-Calvin cycle but preconcentrate $CO_2$ before it enters the cycle. Therefore, $C_4$ plants have two specialised cell types (mesophyll and

bundle-sheath cells) which together are known as Kranz anatomy. The mesophyll cells are reduced in size compared to $C_3$ plants but the reactions occurring in the $C_4$ mesophyll cells are viewed as a $CO_2$ pump concentrating $CO_2$ at the site of carbon fixation. In the mesophyll cells, $CO_2$ is fixed by phosphoenolpyruvate carboxylase (PEP-C) to yield a four-carbon acid. The acid is further reduced to aspartate or malate which are then exported to the bundle-sheath cells. A decarboxylation reaction releases $CO_2$ which then enters the Benson-Calvin cycle. PEP-C is not an oxygenase and has a higher affinity for $HCO_3^-$ than Rubisco for $CO_2$. Furthermore, the concentration of $CO_2$ is kept up to 10- to 20-fold higher around Rubisco than in the mesophyll cells, and Rubisco is saturated with $CO_2$. These adaptations not only lead to the prevention of photorespiration but also to higher rates of carbon assimilation (Ehleringer et al., 1997; Leegood, 1999a; Keeley and Rundel, 2003; Tipple and Pagani, 2007).

Another variation of the $C_3$ pathway also reduces photorespiration by concentrating $CO_2$ around Rubisco (Fig. 1.1c). In the Crassulacean Acid Metabolism (CAM), the initial fixation of $CO_2$ by PEP-C and the subsequent fixation by Rubisco in the Benson-Calvin cycle in the same tissue are temporally separated. The stomata are open at night when the temperatures and, therefore, water loss are reduced. $CO_2$ is converted to malic acid and stored in vacuoles. During the day, malic acid is decarboxylated to provide $CO_2$ for the Benson-Calvin cycle. This process concentrates $CO_2$ around Rubisco leading to up to 60 times higher daytime $CO_2$ levels compared to ambient levels. However, CAM plants may also open stomata at daytime and incorporate $CO_2$ directly into the Benson-Calvin cycle ($C_3$ photosynthesis). CAM plants are $C_3$ plants as seedlings and the CAM pathway is first induced at the beginning of the dry season. Subsequently, many plants stay facultative CAM plants (Leegood, 1999a; Lüttge, 2002, 2004).

## 1.2. The wax layer and its biosynthesis

The precursor compound class of the wax layer substances are fatty acids which are also part of the wax layer. The biosynthesis of fatty acids is a complex, repetitive cycle in which an initial acetyl group is elongated by a $C_2$ unit and by further $C_2$ units per subsequent cycle. When the acyl chain has a length of $C_{16}$ or $C_{18}$, it is released from the cycle as a fatty acid. At this length, the fatty acids are spatially separated depending on their need for membrane or wax synthesis. For wax synthesis, further elongation of the fatty acids is similar to the initial cycle. After elongation, the fatty acids follow the reductive pathway to yield, e.g., aldehydes or the decarbonylation pathway which leads to the formation of ketones or *n*-alkanes (Kunst and Samuels,

2003; Shepherd and Wynne Griffiths, 2006). Due to decarbonylation, odd-numbered *n*-alkanes are typical for land plants (Eglinton and Eglinton, 2008).

Long chain saturated hydrocarbons synthesised in this way are transported to the plant surface where they form a wax layer. The wax layer protects the plant against ultraviolet radiation, bacterial and fungal pathogens and reduces non-stomatal water loss (Kolattukudy, 1976; Kunst and Samuels, 2003; Shepherd and Wynne Griffiths, 2006). The thickness of the wax layer is variable. Many plants react to higher irradiation, lower temperatures or water stress with an increase in the wax layer thickness (Shepherd and Wynne Griffiths, 2006). In addition, the distribution pattern of the different compound classes and the carbon number distribution of substances within a compound class change due to the influence of environmental factors.

### 1.3. Transport of waxes from the plant into the sediment

Waxes are removed from the plant surface by winds (e.g., during dust storms), leaf-to-leaf contact or the impact of rain drops. The plant waxes and their components form aerosols by this abrasion or by biomass burning (Simoneit et al., 1988; Swap et al., 1996; Shepherd and Wynne Griffiths, 2006; Simoneit, 2006). In dry areas with loose soil cover, dust is easily eroded and transported by wind, but dust erosion is less important in forests (Chester, 2003). By wind abrasion, the plant waxes are transferred intact to the atmosphere whereas they may be altered during biomass burning (Simoneit, 2002; Schefuß et al., 2003a). During biomass burning, temperature, aeration and burn duration determine the molecular changes and the transformation of the organic material. Moist wood burns more slowly than dry wood because additional energy is needed to vaporise the moisture. Dry wood burning may cause oxygen-limited conditions. Thus, moist and dry wood burning may result in incomplete combustion and increased production of smoke (Simoneit, 2002). Smouldering conditions (<300°C) prevail in the rain forest while the vegetation in the savannah mainly burns under flaming conditions (>300°C; Simoneit, 2002). In general, the dryer the vegetation, the easier it starts to burn (Barbosa et al., 1999).

In the atmosphere, particles of different origin and size become interspersed. Wind-blown dust and plant particles are coarser than particles from combustion processes (ca. 10 µm and up to 2 µm in diameter, respectively; Chester, 2003). The difference in size leads to different residence times in the atmosphere. Particles with a diameter of >100 µm remain in the atmosphere for several minutes to several hours, small particles (<1 µm in diameter) up to several weeks. Thereby, small particles are commonly transported several thousands of kilometres. In general, the smaller the particles, the further they are transported (Morales, 1986).

Aerosols travel with the prevailing winds and are removed from the atmosphere by gravitation or precipitation (Prospero et al., 1983; Simoneit, 2006). If the particles are transported towards the ocean and they reach the water surface, they coagulate, which enhances their sinking velocity. Marine organisms may ingest these flocs and aggregate them into faecal pellets leading to even higher sinking velocities (Simoneit, 2006). Due to the high sinking rates of the flocs and the faecal pellets, ocean currents play a minor role in the dispersal of terrestrial material (Fischer and Wefer, 1996; Dupont and Wyputta, 2003).

In addition to aeolian transport, plant lipids may be transported by river water and deposited near the river mouth (Burdige, 2005). In southwest Africa, four large rivers, the Ogooué, the Congo, the Kunene and the Orange, discharge into the Atlantic Ocean (Bremner and Willis, 1993; Gingele, 1996; Dai and Trenberth, 2002). In the sediments, long chain *n*-alkyl compounds are relatively resistant against degradation and, over time, form an archive containing information on the adjacent continental vegetation (Cranwell, 1981).

### 1.4. *n*-Alkane isotope composition

The carbon and hydrogen isotopic compositions of *n*-alkanes are preserved during transport and in the sediments (Schidlowski, 1987; Schefuß et al., 2004; Sachse et al., 2012). Chemically, isotopes are indistinguishable, but the physical difference in atomic radii causes reactions or other processes to require slightly more energy if a heavier isotope is involved. Bonds between lighter isotopes are weaker than bonds between heavier isotopes causing light isotopes to react slightly more readily. The partitioning of isotopes between two substances or two phases of a substance with different isotopes is called isotope fractionation. Isotope fractionation occurs by isotope exchange reaction and/or kinetic processes. Isotope exchange reactions (thermodynamic or equilibrium fractionation) are involved in reactions which are in equilibrium. These fractionations are temperature dependent leading to no isotope fractionation at very high temperatures and increasing fractionation at lower temperatures. Thermodynamic fractionation leads to differences in the distribution of isotopes between reactant and product. Reactant and product are the same substances, but have final masses differing from their initial masses. Kinetic fractionation depends on the different reaction rates of isotopes and leads to differences between the heavy and the light isotope in reaction or transport rates. The kinetic effect results in an accumulation of the light isotope in the product and is normally associated with evaporation, diffusion or enzymatic reactions. In contrast

to thermodynamic fractionation, kinetic fractionation is irreversible or unidirectional and usually much larger than thermodynamic fractionation. The isotopic composition of a compound is expressed as delta (δ) value according to the following equation

$$\delta_X = \left( \frac{R_X}{R_{St}} - 1 \right) \times 1000\ (‰) \qquad \textbf{Equation 1.1}$$

where $R_X$ is the isotope ratio of a sample and $R_{St}$ the defined isotope ratio of a standard (Schidlowski, 1987; Hoefs, 2004; Sulzman, 2007).

### 1.4.1. Stable carbon isotopic composition

Natural carbon-containing materials comprise about 98.9% of the lighter carbon, $^{12}C$, and 1.1% of the heavier carbon, $^{13}C$. The relative amount of $^{13}C$ to $^{12}C$ is called the stable carbon isotopic composition and is expressed as the $\delta^{13}C$ value relative to the Vienna-Pee Dee Belemnite standard. $C_3$ and $C_4$ plants discriminate to a different degree against $^{13}C$ allowing conclusions about the relative abundances of these plant types in past vegetation as derived from sedimentary biomarkers (Pancost and Boot, 2004).

The $\delta^{13}C$ value of plant material depends on the $^{13}C$ content of the carbon source, i.e., $CO_2$, as well as the isotope effects during assimilation of $CO_2$ and biosynthesis (Hayes, 1993). The $^{13}C$ content of $CO_2$ varied over time but during the Pleistocene the variation was minimal (Pancost and Boot, 2004). Different effects cause fractionation of $^{12}C$ and $^{13}C$ in terrestrial plants. At first, $CO_2$ enters the plant cell via diffusion, dissolves and is converted into $HCO_3^-$ (Fig. 1.1). For $C_3$ plants, this causes a fractionation of about 4.4‰. The fractionation in the following enzymatic fixation of $CO_2$ by RuBP is larger and leads to a fractionation of about -20 to -40‰ (Fig. 1.1a). This fractionation is mainly responsible for the $\delta^{13}C$ value of $C_3$ plants (Schidlowski, 1987; Hayes, 1993). Additionally, local, environmental and plant specific factors may alter the $\delta^{13}C$ values of $C_3$ plants (Arens et al., 2000). These factors and the effects on the carbon isotopic composition are summarised in Table 1.1.

For $C_4$ plants, the dominant effect of fractionation is the diffusion of $CO_2$ into the cell. The enzymatic fixation by PEP-C only leads to a small fractionation (-2 to -3‰, Fig. 1.1b; Schidlowski, 1987; Hayes, 1993). No further fractionation would occur if the bundle sheath cells were gas tight but some $CO_2$ and $HCO_3^-$ likely leaks into the mesophyll cells. The extent of leakiness determines to which extend fractionation occurs by Rubisco (Farquhar, 1983; Farquhar et al., 1989).

The different isotopic discrimination leads to $\delta^{13}C$ values for the entire plant material in the range of -23 to -34‰ and -6 to -23‰ for $C_3$ and $C_4$ plants, respectively.

**Table 1.1:** The influence of ecological conditions on the carbon isotopic composition of $C_3$ plants ($\delta^{13}C_P$, adopted from Arens et al., 2000).

| Factor | Effect on $\delta^{13}C_P$ | Ecological conditions |
|---|---|---|
| Osmotic stress | +3 to +10‰ | High-salinity soils, extreme at high $pCO_2$ |
| Reduced $pCO_2$ with altitude | +3 to +7‰ | High mountains |
| Water stress, low relative humidity | +3 to +6‰ | Arid and semiarid climate |
| Growth form and deciduousness | -3 to +3‰ | Variation between trees, forbs and grasses and between evergreen and deciduous species |
| Seasonal variation | -2 to +2‰ | Strongest effect in semiarid and arid climate |
| Age of the plant (juvenile vs. adult) | -2‰ in juvenile plants | Seedling or sapling vs. reproductive individual |
| Sun vs. shade leaves | -1 to -3‰ in the sun | Variation due to position in the canopy relative to direction of sun |
| Low temperature | -3‰ | Polar regions during ice house times, high altitude |
| Low nutrients | -4‰ | Nutrient-poor soils |
| Recycled $CO_2$ | -1 to -5‰ | Within closed canopies or where soil outgassing is high (boreal forest) |
| Low light | -5 to -6‰ | Forest understory |

CAM plants use both, PEP-C and Rubisco, to fix carbon (Fig. 1.1c) and, thus, their carbon isotopic composition spans the ranges of $C_3$ and $C_4$ plants (-10 to -33‰; Schidlowski, 1987). During biosynthesis, the synthesised lipids become more depleted in $^{13}C$. This leads to more negative $\delta^{13}C$ values for the *n*-alkanes by 3.6‰ on average compared to the total leaf surface lipid extract (Monson and Hayes, 1980; Collister et al., 1994). The $\delta^{13}C$ ranges of $C_3$ and $C_4$ plants do not overlap, which renders the stable carbon isotope ratio the most widely accepted tool to determine if organic material in sediments originates from either $C_3$ or $C_4$ plants. However, CAM plants may disturb the reliability of these assessments. But the distribution of CAM plants today is sparse and usually limited to ecological niches. For most investigation areas, it is unlikely that CAM plants bias these assessments. In geological archives, leaves and their features (such as Kranz anatomy) are seldom preserved but morphologically degraded material is omnipresent. Marine and lacustrine sediments contain a mixture of marine and terrestrial organic material. Therefore, bulk parameters are not used to distinguish between $C_3$ and $C_4$ plants. Instead, specific biomarkers, like long chain *n*-alkanes, which are derived mainly from land

plants, are used for such investigations (Pancost and Boot, 2004).

### 1.4.2. Stable hydrogen isotopic composition

Hydrogen has two stable isotopes. The abundance of protium ($^1$H) is 99.98% while that of deuterium (D) is 0.02%. δD ratios are expressed relative to Vienna-Standard Mean Ocean Water (V-SMOW; Hoefs, 2004). The different factors influencing the δD composition of plants are summarised in Fig. 1.2. The main hydrogen source for plants is soil water which in turn is derived from precipitation. The hydrogen isotopic composition of precipitation is highly variable but mainly depends on isotope fractionation during evaporation and condensation. Three effects mainly alter the δD content of the precipitation. If water evaporates the vapour is depleted in D. But if the vapour condenses and precipitates the precipitation is isotopically heavier than the vapour. In a series of precipitation cycles precipitation becomes progressively lighter. Air masses lose moisture over the continents leading to lighter precipitation further inland (continental effect). The temperature effect is relevant in regions outside the tropics where the temperatures are highly variable. At cooler temperatures, the isotopic fractionation between vapour and water is higher. In tropical regions with a high seasonality of precipitation, the amount effect leads to isotopically lighter precipitation at higher precipitation rates (Sachse et al., 2012). This effect is associated with several processes. As air rises and cools to saturation, condensate falls through other droplets that formed below and exchanges with them. The droplets can grow larger by taking on more vapour as they fall. When the droplets exit the cloud they can evaporate into dry air. Thereby, isotopically light isotopes vaporise preferentially and the remaining liquid is heavier. In addition, the droplets exchange with vapour in unsaturated air below the cloud. The liquid becomes more enriched in the heavy isotope. The probability of encounters between falling droplets and

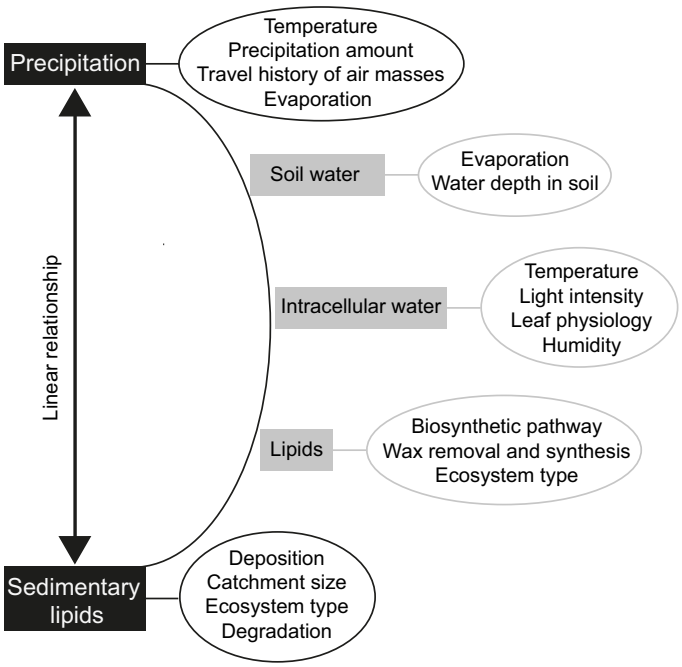


**Fig. 1.2:** Factors influencing the δD composition of sedimentary lipids (after Sachse et al., 2012).

vapour is higher in humid air. Thus, evaporation and exchange lead to heavier gentle tropical rain. Although the amount effect is considered a tropical effect it occurs to a lesser extent also at mid-latitudes in summer (Sharp, 2007).

The isotopic composition of soil water and groundwater largely reflect the isotopic composition of the precipitation. Due to surface soil evaporation, the composition in the upper part of the soil may be altered especially in arid climates. However, plants in these regions often have deep roots and take up water from deeper parts of the soil water or groundwater which are isotopically unaltered by evaporation (Sachse et al., 2012).

The isotopic composition of the source water remains unaltered during uptake of water by the root. The δD values of root water can be different from the leaf water due to transpiration or water loss from the leaves. During biosynthesis, the synthesised components become further depleted in D compared to leaf water. Biosynthesis involves enzymatic reactions where hydrogen is added, removed or exchanged and derived from different precursors with varying δD values. Therefore, each pathway of lipid synthesis leads to different δD compositions in the product. The lipids with the smallest δD variations compared to the source water are *n*-alkyl compounds. Decarbonylation of *n*-alkanoic acids leads to *n*-alkanes which are more depleted in D (ca. 25‰) than their precursor molecules. The mechanisms leading to isotope fractionation are currently unknown. In addition, the influence of environmental factors like salinity, growth rate or light intensity altering the hydrogen isotopic composition of lipids are currently poorly understood (Chikaraishi and Naraoka, 2007; Sachse et al., 2012).

Despite the several alterations of the hydrogen isotopic composition of precipitation, δD values of lipids from terrestrial plants primarily depend on the mean precipitation δD values. In sedimentary records, the hydrogen isotopic composition remains unaltered compared to the plant material at lower temperatures. The *n*-alkane δD values span ranges between -100 and -300‰ (Sachse et al., 2012). The δD values of *n*-alkanes are used to deduce past hydrological variations. In sediment samples from the Congo Fan spanning the last 20 ka, δD values of *n*-alkanes were interpreted to indicate wetter or drier continental contitions (more negative and more positive δD values, respectively) which in turn gives insight into the changes of past atmospheric circulation (Schefuß et al., 2005). Furthermore, *n*-alkane δD values are used to record changes in mountain range uplift (Polissar et al., 2009). Mountain range uplift occurs over multimillion-year timescales, which makes it difficult to separate effects of changing climate and atmospheric circulation from changes in δD precipitation due to uplift. To account for this effect, coeval records from the foreland

to the mountain range are compared (Hren et al., 2010). However, due to the incomplete understanding of the relative importance of plant physiological versus climatic parameters in determing leaf-wax *n*-alkane δD values, these studies are limited to qualitative interpretations (Sachse et al., 2012).

## 1.5. General distribution of $C_3$ and $C_4$ plants

Today, the majority of terrestrial plant species use the $C_3$ pathway. The CAM pathway is used by ca. 6% of the plant species and the $C_4$ pathway by approximately 3%. Despite their low percentage among the plant species, $C_4$ plants cover more than 35% of the Earth´s land surface. More than 50% of the $C_4$ species belong to the grass family (Sage et al., 1999a,b). The $C_4$ pathway occurs especially in tropical and warm temperate grasses and sedges wheras most temperate grasses, trees and shrubs are $C_3$ plants (Sage, 2001; Eglinton and Eglinton, 2008). Due to their high water use efficiency, CAM plants thrive where water supply is limited. CAM is found in virtually all terrestrial plant growth forms and is common in desert succulents and tropical epiphytes (Keeley and Rundel, 2003). Approximately 60% of all epiphytes are CAM plants, and CAM species inhabiting tropical rainforest outnumber typical desert species (Lüttge, 2004).

The $C_3$ pathway evolved 450 million years ago (Sage, 1999). At that time, the atmosphere contained very high $CO_2$ and very low $O_2$ concentrations (high $CO_2/O_2$ ratio) compared to today. The efficiency of Rubisco was enhanced and photorespiration was minimal. About 24 million years ago, the $CO_2/O_2$ ratio decreased to near-modern levels and the photosynthetic rate of $C_3$ plants was reduced by photorespiration. It is assumed that the $C_4$ mechanism evolved during that time in order to enhance photosynthetic efficacy. As the $C_4$ plant photosynthesis rate is not influenced by photorespiration, $C_4$ plants have an advantage over $C_3$ plants under these conditions (Tipple and Pagani, 2007).

The main factors controlling the abundance of $C_3$ and $C_4$ plants are temperature and light (Sage, 2001). The rate of photorespiration in $C_3$ plants is higher at high temperatures, aridity and high light intensities. To minimise water loss under these condition, $C_3$ plants reduce stomatal width, which reduces the internal $CO_2$ concentration. In contrast, $C_4$ plants are better adapted to these conditions. $C_4$ plants have less open stomata but the same photosynthetic rate because of the high concentration of $CO_2$ around Rubisco. However, the $C_4$ pathway consumes more energy than the $C_3$ pathway. But when the rate of photorespiration in $C_3$ plants rises, the energy cost of photosynthesis increases and may rise above that of $C_4$ plants. Photosynthetic energy cost is equal for $C_3$ and $C_4$ plants at 25 to 30°C and lower for

$C_4$ plants at >30°C. Thus, $C_3$ plants have an optimal $CO_2$ assimilation at lower temperatures than $C_4$ plants (Leegood, 1999a; Sage, 2001; Tipple and Pagani, 2007). Furthermore, $C_4$ plants have a better water use efficiency because they preconcentrate $CO_2$ and reduce stomata width, which leads to a minimised water loss without a drop in photosynthesis rate (Leegood, 1999a; Sage, 2001; Tipple and Pagani, 2007).

$C_4$ plants outcompete $C_3$ plants if they have access to moderate to high light intensities (Sage, 2001). $C_3$ and $C_4$ plants have nearly the same rates of photosynthesis at low light intensities. If the light intensity increases, photosynthesis rates of both, $C_3$ and $C_4$ plants, increase, but rates for $C_4$ plants increase more steeply than for $C_3$ plants (Björkman and Berry, 1973; Björkman, 1976). $C_4$ plants dominate where they receive at least 30 to 50% of full sunlight intensities but rarely occur in forest canopies where light intensities are <20% of full sunlight. Shaded environments are cooler and more humid so that $C_3$ plants open their stomata more widely than they otherwise would allowing for higher $CO_2$ levels inside shaded plants. Therefore, $C_3$ plants outcompete $C_4$ plants at low light intensities (Sage, 2001).

On geological timescales, the atmospheric $CO_2$ level is another controlling factor for the abundance of $C_3$ and $C_4$ plants. At lower atmospheric $CO_2$ levels, the photosynthetic rate is reduced in $C_3$ plants. In contrast, the photosynthetic rate of $C_4$ plants is unaffected by $pCO_2$. Lower $pCO_2$ decreases the cross-over temperature above which $C_4$ plants have an advantage compared to $C_3$ plants (Ehleringer et al., 1997; Collatz et al., 1998). That means, at a constant temperature of, e.g., 20°C $C_4$ plants are favoured by a $pCO_2$ of 200 ppmV and $C_3$ plants by a $pCO_2$ of 400 ppmV. But at 400 ppmV $pCO_2$ and 35°C, $C_4$ plants have an advantage compared to $C_3$ plants (Ehleringer et al., 1997).

A secondary factor which controls the occurrence of $C_3$ and $C_4$ plants is aridity. $C_4$ plants have a higher water use efficiency than $C_3$ plants and, therefore, thrive in arid regions. In addition, fire is more common in arid regions. In contrast to $C_3$ species, $C_4$ grasses have tissues which protect them partly underground against fire. Fire kills or inhibits the growth of $C_3$ plants which further promotes the dominance of $C_4$ plants in arid regions (Sage, 2001).

The seasonality of precipitation is a factor influencing the $C_3$ and $C_4$ abundance in grasslands. Grasslands with cool-season precipitation are $C_3$ dominated while $C_4$ grasses are abundant in monsoon grasslands with summer precipitation. Other secondary factors favouring $C_4$ plant abundance are low soil nitrogen or nutrient supply, moderate salinity or herbivory (Leegood, 1999a; Sage, 2001; Tipple and Pagani, 2007).

In contrast to $C_3$ and $C_4$ plants, CAM plants tolerate drought on a daily or seasonal basis and grow slowly. CAM is rather a strategy for stress survival but not for high productivity and dominance. Therefore, CAM plants do not compete with $C_3$ or $C_4$ plants for the same area but occupy ecological niches (Leegood, 1999a; Keeley and Rundel, 2003; Lüttge, 2004). Today, the competitive factors between $C_3$ and $C_4$ plants lead to a higher abundance of $C_4$ plants in hot, high light and dry environments, like tropical and subtropical regions.

## 1.6. Current climate and the distribution of $C_3$ and $C_4$ plants in Africa

The distribution of $C_3$ and $C_4$ plants on the southwestern African continent is related to temperature and atmospheric circulation because these factors determine the occurrence and length of the wet seasons (Fig. 1.3a,b). The Intertropical Convergence Zone (ITCZ) follows the maximum of solar heating. The ITCZ passes over large parts of Africa because Africa is located north and south of the equator. In northwestern Africa, the ITCZ remains north of the equator all year long due to the asymmetry of the West African continent. Above the Atlantic Ocean, a high-pressure area prevails throughout the year north and south of 20°N and 20°S, respectively (the North Atlantic Anticyclone, NAA, and the South Atlantic Anticyclone, SAA). Due to the pressure difference, the winds are roughly directed from the Atlantic anticyclones towards the ITCZ. The ITCZ separates the northern and southern wind systems, the North-East trades or Harmattan and the South-Western trades, respectively. Another convergence zone, the Congo Air Boundary, separates the winds from the Atlantic and the Indian Ocean. Where the Congo Air Boundary and the ITCZ meet, a low pressure area prevails (e.g., the Angolan Low in the Southern Hemisphere; Philander et al., 1996; Gasse, 2000; Nicholson, 2000).

The ITCZ is followed by the so-called tropical rainbelt, a region associated with abundant rainfall. In the equatorial region, the ITCZ and the rainbelt pass twice a year leading to a humid zone with two seasonal rainfall maxima (Fig. 1.3c). The seasonality of the precipitation increases towards the South with summer rains and winter droughts. The precipitation of central and southwestern Africa originates from the SAA (Fig. 1.3a,b). During austral summer, the trade winds from the SAA and the West African monsoon system are directed towards the Angolan Low causing the summer rain. During winter, however, the SE trades are directed towards the ITCZ in the Northern Hemisphere causing winter drought in southwestern Africa. The precipitation over southern Africa is influenced by the warm Agulhas current. During austral summer, the moisture converges and causes precipitation (“winter rain”; Nicholson, 2000; Gasse et al., 2008). However, this view on the connection

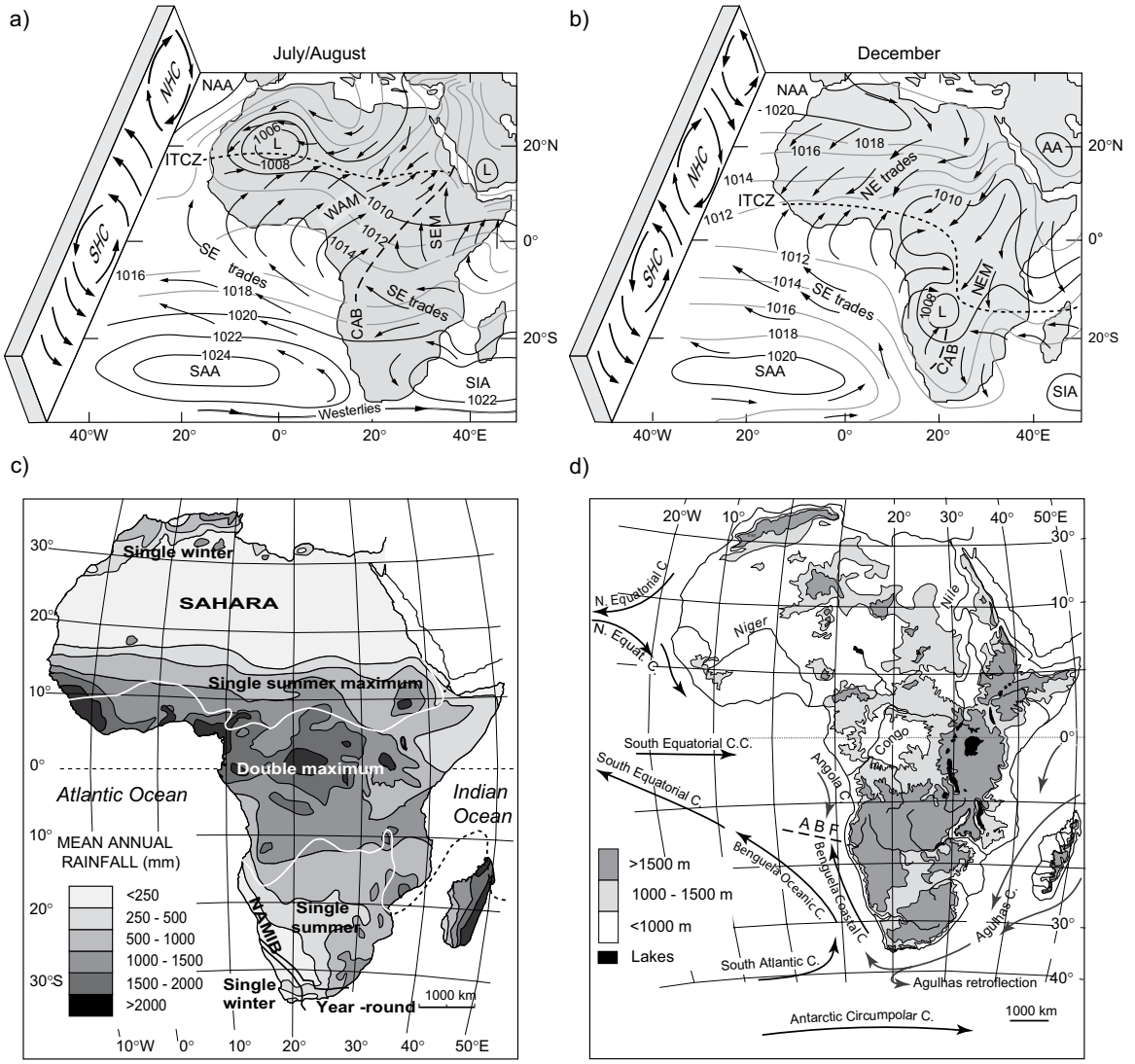


**Fig. 1.3:** Some aspects of the present-day African climate (from Gasse et al., 2008): Low-level wind and pressure patterns during a) austral winter and b) austral summer, c) mean annual rainfall and rainfall regimes and d) major African surface features and oceanic surface currents. NAA - North Atlantic Anticyclone; SAA - South Atlantic Anticyclone; AA - Arabian Anticyclone; SIA - South Indian Anticyclone; L - major low pressure cells; WAM - West African Monsoon; NEM - North East African monsoon; SEM - South East African monsoon; ITCZ - Intertropical Convergence Zone (dotted line); CAB - Congo Air Boundary (dashed line); SHC - southern Hadley Cell; NHC - northern Hadley Cell; ABF - Angola-Benguela- Front.

of the West African monsoon system and the ITCZ is currently being re-evaluated (Nicholson, 2009, 2013). One important aspect is the possible dissociation of the ITCZ from the main region of precipitation. It is further suggested that local evaporation rather than moisture from the Atlantic is the main moisture source for the monsoon (Nicholson, 2009).

South of the tropics, the zonal patterns are altered by topographic and oceanic

influences which lead to an East-West asymmetry (Fig. 1.3d). The flat topography in the tropics enables moist air masses from the Atlantic to reach far into the East. But the highlands in East Africa and the Great Escarpment, a high altitude area in southern Africa, further south limit the flow of these air masses to extend further east contributing to the aridity in the hinterland. The Great Escarpment limits the inland penetration of “winter rain”. In the east, it intercepts moisture brought by the SE trade winds from the Indian Ocean (Gasse et al., 2008; Nicholson, 2000). The arid Namib Desert is located adjacent to a cold near-coastal ocean current (Fig. 1.3d). There, the cold water reduces the flux of vapour inland. The cold temperatures are due to several upwelling cells. The cells are located between 34°S to 15°S along the Benguela Coastal Current which flows from the southern part of the African continent towards the equator (Nicholson, 2000; Gasse et al., 2008).

The decreasing precipitation from the tropics towards the south is accompanied by a decrease in mean annual temperature. The changes in temperature and precipitation are reflected in the zonation of the vegetation. Near the equator, where temperature and precipitation are high, tropical rain forest prevail. Further north and south, the vegetation composition is altered from woodlands via shrublands to grasslands. This means, the vegetation gradually changes from a continuous stand of trees with interlocking canopies via an open stand of trees or bushes to a land cover mainly consisting of grasses. These changes are characterised by a decreasing woodiness ($C_3$ plants) and increasing $C_4$ plant abundance. However, in the winter rain area of the southern part of Africa, $C_3$ plants dominate again (Whittaker, 1975; White, 1983).

## 1.7. Past conditions - globally and specifically in Africa

The current patterns of atmospheric circulation and vegetation cover differ from past conditions. During the last glacial and the Last Glacial Maximum (LGM, the period of maximum global ice volume, ca. 21 ka), the climate in most parts of Africa was cooler and dryer than today. During the LGM the mean annual temperature was ca. 3°C lower than today. Due to the lower temperatures, the NE and SE trade wind were stronger. Therefore, the movement of the ITCZ was probably contracted resulting in a position further south and further north during austral winter and summer, respectively (Frierson et al., 2007; Gasse et al., 2008; Collins et al., 2011). Along the western coast of southern Africa, the climate was wetter than today which was caused by a northward movement of the “winter rain” area (Chase and Meadows, 2007).

The temperature changes during different glaciation stages of the Quaternary are

due to glacial-interglacial fluctuations which are in turn caused by changes in the Earth´s orbital parameters. These orbital parameters are mainly obliquity (the angle of the Earth´s axial tilt), precession (rotation of the Earth´s axis) and eccentricity (the amount by which the Earth´s orbit deviates from a circle). These periodic parameters mainly determine the amount of insolation reaching the Earth. During glacials, decreased insolation leads to a decrease in global temperatures and, thus, to a decrease in the atmospheric $CO_2$ concentration and the build up of large ice sheets (Hays et al., 1976; Pierrehumbert, 2010). Due to their linear correlation, the concentration of $pCO_2$ in air bubbles of ice cores gives insight into past temperatures (Barnola et al., 1987). In addition, the global ice volume is recorded in the oxygen isotopic composition of foraminifera found in sedimentary archives. The more $H_2O$ is stored in ice sheets, the heavier is the isotopic composition of the remaining water in the oceans. The foraminifera incorporate the $\delta^{18}O$ of the water in which they live into their shells. However, water temperature and salinity also have an effect on the $\delta^{18}O$ composition. These variances are globally more uniform in the deep ocean. To minimise effects of temperature and salinity on the foraminiferal $\delta^{18}O$ value, benthic foraminifera are used for $\delta^{18}O$ stacks. Stacks are averaged $\delta^{18}O$ records from multiple sites and provide a global climate signal (Lisiecki and Raymo, 2005).

During the last glacial (ca. 74 ka to 15 ka; Sanchez Goñi and Harrison, 2010) several climatic oscillations occurred. An example for a rapid climate change are Dansgaard-Oeschger cycles, which are characterised by warming followed by cooling in Greenland. Some of the cold intervals are associated with Heinrich Events (Alley, 1998; Sanchez Goñi and Harrison, 2010). In the North Atlantic, debris of ice rafting in sediments (Heinrich layers) were found and associated with intervals of cooler temperatures (Heinrich Stadials; Heinrich, 1988; Broecker et al., 1992; Sanchez Goñi and Harrison, 2010). The cooler temperatures are a result of iceberg discharges in the North Atlantic. In the North Atlantic, cold and salty water sinks into the deep ocean (North Atlantic deep water formation). To substitute this water, surface waters from the tropics are drawn towards the North Atlantic. If the supply of fresh water, e.g., delivered by ice melt, is increased, surface waters are diluted and weaken the North Atlantic deep water formation (Alley, 1998). In this case, the drawing of tropical, warm waters from the Southern Hemisphere towards the North Atlantic is also weaker, leading to a cooling in the Northern Hemisphere. In contrast, the Southern Hemisphere is heated (Broecker, 1998; EPICA, 2006).

## 1.8. Motivation and outline of this thesis

Although research in the development of *n*-alkanes as biomarkers and their use as indicator of vegetation distribution is widely validated, there are still several knowledge gaps. The *n*-alkane parameter, especially their $\delta^{13}C$ values for $C_3$ and $C_4$ plants, respectively, are used to deduce past vegetation distribution. For this purpose, the molecular $\delta^{13}C$ values of *n*-alkanes in waxes from $C_3$ and $C_4$ plants (end member values) are required. Rommerskirchen et al. (2006b) and Vogts et al. (2009) analysed plant species from southern and equatorial Africa. They compiled available literature data on the *n*-alkane parameters to provide end member values for palaeoenvironmental studies. Here, plant species from Angola, situated between equatorial and southern Africa, were analysed to fill the geographical gap in south-western Africa and to expand the database.

Sedimentary studies revealed inconsistencies which were related to the sediment material retrieved from different water depths. Here, surface sediments of an isobathic transect recovered off southwest Africa were analysed for their *n*-alkane chain length distribution and stable carbon isotope composition. It was evaluated if the *n*-alkane parameter reflect the current vegetation on the adjacent continent.

For the same isobathic transect, the hydrogen isotopic composition of the *n*-alkanes and its connections to the δD composition of the continental precipitation were analysed.

In palaeovegetation studies, significant differences between the Late Pleistocene and the Holocene in terms of $C_3$ and $C_4$ distribution in Africa were found (e.g., Rommerskirchen et al., 2003, 2006a; Collins et al., 2011). To gain insight into the mechanisms responsible for the local distribution of $C_3$ and $C_4$ plants during these time frames, two sediment cores from the southeast Atlantic covering the Holocene and parts of the Late Pleistocene were investigated.

This thesis aims to answer these outstanding questions:

- Is there a continuous trend of *n*-alkane parameters for $C_3$ and $C_4$ plants from the rain forest via the wood- and shrubland towards the savannah?
- Which deductions are possible from the average chain length of the long chain *n*-alkanes on climatic conditions?
- Do the *n*-alkane parameters of surface sediments reflect the recent vegetation composition on the African continent?
- Can sediment-derived *n*-alkane parameters and end member values from plant material be used to deduce vegetation composition in the catchment area?
- Which current environmental conditions (precipitation, aridity) control the vegetation composition?

- Does the sedimentary *n*-alkane stable hydrogen isotope composition mirror the hydrogen isotope composition of the continental precipitation?
- Does the apparent fractionation between the stable hydrogen isotope compositions of lipids and precipitation depend on climatic conditions or on vegetation composition?
- Which climatic parameters are reflected by vegetation changes?
- Are single sample approaches (i.e., one sample per glaciation stage) representative?

## 1.9. Outline of the author´s contribution

The objectives of this thesis follow up on results and open questions in the theses by Florian Rommerskirchen (2006) and Angela Vogts (2011). This thesis contains four manuscripts which are published in, in revision after review, submitted to and in preparation for international peer-reviewed journals. This includes two first and two co-author manuscripts of the author of this thesis. In the following, the contribution of the author herself to each project is outlined, and a short summary of each manuscript is given.

### 1.9.1. Chapter 2: *n*-Alkane distribution and stable carbon isotope composition in leaf waxes of $C_3$ and $C_4$ plants from Angola

This chapter deals with the analysis of the distribution of *n*-alkanes and their carbon isotopic composition in plant samples from Angola. The author herself selected the samples, organised the cooperation and retrieved the plant leaf samples from the herbarium in Bonn (Germany). The samples were worked up by the author herself and scientific assistants as well as laboratory assistants were supervised by the author. The author interpreted the results, developed the manuscript concept and wrote the manuscript. The author was supported by Angela Vogts (IOW, Warnemünde, Germany) and Jürgen Rullkötter (ICBM, University of Oldenburg, Germany).

In this project, 41 $C_3$ plants and 11 $C_4$ plants were analysed for their *n*-alkane distribution and molecular carbon isotope composition. The samples originate from the wood- and shrubland located between the rain forest and the savannah. The *n*-alkane end member database, a literature survey of *n*-alkane data for vegetation reconstruction, was updated and the updated *n*-alkane parameters are provided. The end member data do not change significantly when calculated with either the arithmetic average or the median. From the rain forest via the wood- and shrubland towards the savannah, the molecular isotopic composition of the $C_3$ plants

becomes heavier, which is probably due to changing environmental conditions like water stress, light intensity and incorporation of recycled $CO_2$. The *n*-alkane chain length increases towards the south for the $C_3$ and the $C_4$ plants. For palaeoenvironmental studies, the chain length may not be a direct indicator for the vegetation distribution in contrast to the carbon isotopic composition. Instead, the chain length may be a parameter for the plant growth height or the tree abundance.

### 1.9.2. Chapter 3: *n*-Alkane parameters from a deep sea sediment transect off southwest Africa reflect continental vegetation and climate conditions

This manuscript contains the analysis of the carbon isotopic composition of land plant-derived *n*-alkanes and their distribution in an isobathic transect off southwest Africa. This project is a joint project of the theses by Angela Vogts (2011) and the author as well as the author´s diploma thesis. The samples were analysed by the author herself as part of her diploma thesis. Additional analyses (bulk parameters) were performed by technical assistants supervised by Angela Vogts. The initial interpretation of the results was part of the author´s diploma thesis. However, after her diploma thesis, the interpretation of the results was significantly expanded. The advanced interpretation of the results, the concept of the manuscript and the writing of the manuscript was conducted by Angela Vogts. However, the author was involved in all parts after her diploma thesis and took part in the further handling of the manuscript. In addition, Enno Schefuß (MARUM, University of Bremen, Germany) and Jürgen Rullkötter (ICBM, University of Oldenburg, Germany) supported the development of the manuscript by discussion of the results.

Sediment samples from an isobathic transect off southwest Africa between 2°N and 28°S were analysed. The vegetation on the continent changes from $C_3$ to $C_4$ dominated towards the south. This change is reflected by the sedimentary *n*-alkane parameters. The chain lengths and the molecular stable isotope composition both increase towards the south and were found to be suitable parameters to estimate the $C_4$ plant contribution to the sediments. The calculated $C_4$ proportion in the sediments strongly correlates (i) with the $C_4$ abundance in continental catchment areas postulated by wind trajectories and river systems and (ii) with the mean annual precipitation and aridity indices in selected catchment areas.

### 1.9.3. Chapter 4: Stable hydrogen isotopic composition of continental precipitation is reflected by δD ratios of land plant-derived *n*-alkanes in marine sediments off southwest Africa

This chapter contains the interpretation of the hydrogen isotopic composition of the *n*-alkanes of the isobathic transect off southwest Africa analysed in Chapter 3. This project is also a joint project of the theses by Angela Vogts (2011) and the author. The samples were worked up by the author herself as part of her diploma thesis. Angela Vogts analysed the hydrogen isotopic composition and wrote the manuscript. The author was involved in all aspects regarding the development of the manuscript including the interpretation of the results. Further suggestions were made by Enno Schefuß (MARUM, University of Bremen, Germany) and Jürgen Rullkötter (ICBM, University of Oldenburg, Germany).

The long chain *n*-alkanes in sediment samples from an isobathic transect off southwest Africa between 2°N and 28°S (the same samples as in Chapter 3) were analysed for their δD composition. The δD values of the *n*-$C_{29}$, *n*-$C_{31}$ and *n*-$C_{33}$ alkanes were compared to the modelled hydrogen composition of the precipitation. The δD composition of the precipitation was modelled for continental locations along the postulated transport pathway of the plant material from the catchment area towards the ocean. For the δD values and the mean annual precipitation, the correlation coefficients are highest for locations with 350 km distance to the coast. Throughout the transect, the apparent fractionation between the *n*-alkanes and the precipitation is fairly constant although continental aridity and plant life form change. Sedimentary *n*-alkane hydrogen composition may be directly converted to the δD ratio of the continental precipitation but the vegetation composition should be evaluated concurrently.

### 1.9.4. Chapter 5: Influence of Late Pleistocene and Holocene climate on vegetation distribution in southwest Africa elucidated from sedimentary *n*-alkanes - differences between 12°S and 20°S

The final manuscript of this thesis draws conclusions on the vegetation distribution and the climate in southwest Africa during the Holocene and the last glacial. For this, two sediment cores (12°S and 20°S) were investigated for long chain *n*-alkane distribution and their carbon isotopic composition. The author herself selected the samples for the southern core, organised the cooperation and retrieved the sediment samples from the core repository in Bremen (Germany). For the core at 12°S, these tasks were performed by Angela Vogts. Samples of both cores were worked up by Angela Vogts and the author as well as several scientific assistants

and laboratory assistants were supervised by Angela Vogts or the author. Analyses of the bulk parameters were performed by technical assistants supervised by Angela Vogts or the author. The radiocarbon dating of selected samples was done by the Poznań Radiocarbon Laboratory (Poland). The evaluation of the results of the core at 12°S and 20°S was done by Angela Vogts and the author, respectively. The author interpreted the results of both cores, developed the manuscript concept and wrote the manuscript. The author was supported by Angela Vogts (IOW, Warnemünde, Germany) and Jürgen Rullkötter (ICBM, University of Oldenburg, Germany). In this thesis, the submitted version of the manuscript is included. However, the reviewer suggested further validation of the age models. Therefore, the revised version of the manuscript will contain additional radiocarbon ages of the southern core (analyses in progress), which may lead to a different age approximation.

The vegetation composition in southwest Africa archived in sediment cores from 12°S and 20°S during the last 73 and 23 ka, respectively, was investigated. All *n*-alkane parameters remain fairly uniform for the southern core indicating a constant $C_4$ domination. For this location, values from single samples overlap from the Last Glacial Maximum and the Holocene and are, therefore, not significantly representative for the stadial they derive from. In contrast, zthe vegetation changed from $C_4$ dominated during the Late Pleistocene to $C_3$ dominated during the Holocene for the northern core. During the deglaciation, the vegetation change occurs in accordance with the $pCO_2$ increase. Smaller vegetation fluctuations during the Late Pleistocene coincide with changes in the local insolation.

# 2. *n*-Alkane distribution and stable carbon isotope composition in leaf waxes of $C_3$ and $C_4$ plants from Angola

Tanja Badewien[a,*], Angela Vogts[b], Jürgen Rullkötter[a]

[a] Institute for Chemistry and Biology of the Marine Environment (ICBM), Carl von Ossietzky University of Oldenburg, Germany
[b] Leibniz Institute for Baltic Sea Research, Warnemünde (IOW), Germany

* Corresponding author. Tel.: +49 441 798 3627; fax: +49-441-798 3404.
E-mail address: t.badewien@icbm.de (Tanja Badewien).

This chapter has been submitted to Organic Geochemistry.

## 2.1. Abstract

Palaeoenvironmental assessment of past $C_3$ and $C_4$ vegetation distributions relies on end member data from plant analyses. In southwestern Africa, end member data of the carbon number distribution of *n*-alkanes from leaf waxes and their carbon isotopic composition were available for the rain forest and the savannah but not for the transition region, i.e. the wood- and shrubland. In this study, we analysed the *n*-alkane parameters of 41 $C_3$ plants and 11 $C_4$ plants from the wood- and shrubland of Angola. Our results revealed highly variable *n*-alkane parameters for individual plants. The combined results for the rain forest, the wood- and shrubland and the savannah show an increase in the average chain length (ACL) of $C_3$ and $C_4$ plants from the equator towards South Africa. The stable carbon isotopes of the *n*-alkanes become heavier towards the south for the $C_3$ plants. The mean values of the *n*-alkane parameters were calculated from the arithmetic average as well as the median, applying both averaging methods to *n*-alkane data from a sedimentary study led to similar vegetation reconstructions. In addition, correlation between ACL and growth height of the plants is discussed indicating that the ACL may be useful as a tree abundance parameter. Thus, the enlarged end member database strengthens the *n*-alkane parameters as tools for palaeoenvironmental studies.

## 2.2. Introduction

Palaeoenvironmental studies reconstruct past ecosystems and climate by employing, e.g., sedimentary plant remains such as leaf wax constituents. Leaf waxes cover all aerially exposed organs of higher land plants and form a protective layer (Eglinton and Hamilton, 1967; Shepherd and Wynne Griffiths, 2006). The wax layer contains a diverse mixture of different compound classes, e.g., fatty acids and long chain *n*-alkanes. The *n*-alkanes are largely resistant against degradation and, therefore, valuable biomarkers (Eglinton and Eglinton, 2008).

The analysis of sedimentary long chain *n*-alkanes reveals, e.g., the past continental vegetation in terms of $C_3$ and $C_4$ plant distribution (e.g., Feakins et al., 2005; Rommerskirchen et al., 2006a; Collins et al., 2011; Schefuß et al., 2011). Such studies are based on the different carbon fixation pathways of $C_3$ and $C_4$ plants, which lead to the production of *n*-alkanes with different carbon isotopic compositions. The differences in carbon uptake lead to a more negative carbon isotopic composition of the $C_3$ plants compared to the $C_4$ plants. Atmospheric $CO_2$ enters the plant cell through the stomata, is enzymatically fixed and directly incorporated into the Calvin-Benson-Bassham Cycle in the case of $C_3$ plants. $C_4$ plants preconcentrate the $CO_2$ before it enters the Calvin-Benson-Bassham Cycle because their stomata are smaller in order to minimise water loss. This leads to an advantage of $C_4$ plants (mainly grasses) compared to $C_3$ plants in hot, arid regions like savannahs. $C_3$ plants (nearly all trees and shrubs) dominate in wetter regions like wooded areas (for an overview see, e.g., Tipple and Pagani, 2007; Eglinton and Eglinton, 2008).

In addition to the isotopic differences, plant studies from Africa show differences in the *n*-alkane chain length distribution of $C_3$ and $C_4$ plants (Rommerskirchen et al., 2006b; Vogts et al., 2009). $C_3$ savannah plants produce longer chain *n*-alkanes than the $C_3$ rain forest plants, and the average chain length (ACL) of the *n*-alkanes is even higher for $C_4$ grasses from the savannah. In these studies, plants mainly from the equatorial region and from Namibia and South Africa were analysed. For the transition zone, no plant data were available to verify the trends in chain length.

In this study, we have reduced the geographical gap between equatorial and southern Africa by analysing $C_3$ and $C_4$ plant species from Angola. We further evaluate changes in the distribution pattern of the *n*-alkanes and their carbon isotopic composition in southwest Africa by combining the data of Rommerskirchen et al. (2006b), Vogts et al. (2009) and from this study. The combined dataset constitutes improved end member background information for palaeoenvironmental studies.

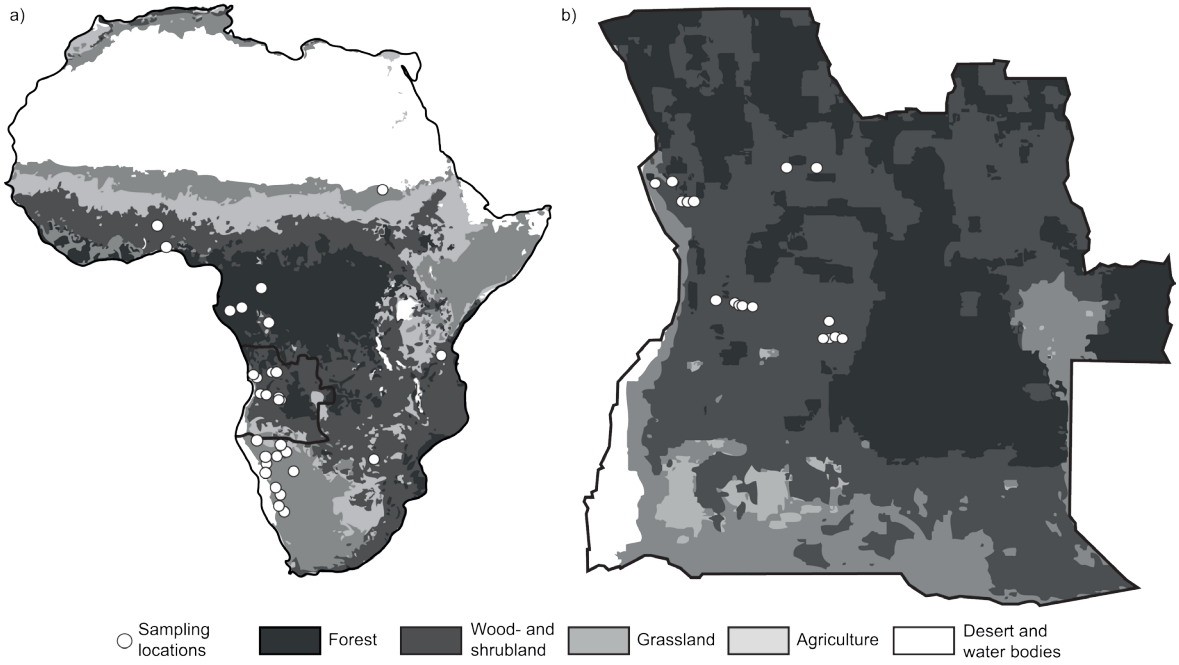


**Fig. 2.1:** Vegetation of a) Africa and b) Angola (after Mayaux et al., 2004) including the sampling locations of the plant material analysed by a) Vogts et al. (2009), Rommerskirchen et al. (2006b) and this study and b) this study.

## 2.3. Material and methods

### 2.3.1. Sample material and study area

The plant material was collected from the deciduous wood- and shrubland in northern and central Angola (Fig. 2.1; White, 1983; Mayaux et al., 2004). The wood- and shrubland is defined as a transition zone between forest and grassland. In the forest, trees using the $C_3$ pathway dominate and in the grasslands $C_4$ grasses are abundant. In the wood- and shrubland, trees cover up to 40% of the area, shrubs more than 15% and grasses between 15 and <40% (Mayaux et al., 2004).

The plants were sampled in August and September 2006 and in June 2007 by W. Lobin and T. Leyens (University of Bonn, Germany) who assigned the family and species identities (Supplementary Table 2.S1). The plants were kept between newspaper sheets or fixed on sheets of paper with paper adhesive. The plants were stored at room temperature at the herbarium in Bonn (Germany).

## 2.3.2. Analytical methods

### *2.3.2.1. Extraction and sample preparation*

The organic compounds were extracted from 5 to 380 mg dry and ground plant material by using an Accelerated Solvent Extractor (ASE 200, Dionex) with $CH_2Cl_2$ and MeOH (9/1, v/v, 3 x 5 min, 70 bar, 100°C) as solvents. Squalane was added as an internal standard. The extract was dissolved in *n*-hexane and insoluble components were removed by filtration over dry $NaSO_4$. In the *n*-hexane-soluble fraction, the aliphatic/alicyclic hydrocarbons were separated from the aromatic and polar heterocomponent fractions by medium pressure liquid chromatography (Radke et al., 1980).

In the aliphatic fraction, the *n*-alkanes were analysed by gas chromatography (Agilent 6890) with flame ionisation detector, helium as carrier gas and a high-temperature column (J&W, DB-5ht, 30 m length, 0.25 mm i.d., 0.1 µm film thickness). The injector temperature was raised from 60°C to 350°C (held for 2 min) at a rate of 480°C $min^{-1}$.The temperature of the gas chromatograph (GC) oven was raised from 60°C (3°C $min^{-1}$) to 350°C and then held for 5 min. *n*-Docosanoic acid methyl ester was added as the injection standard. The individual *n*-alkanes were identified by comparison of the retention times with those of a standard mixture. Based on signal intensity and the internal standard, the *n*-alkane abundances were calculated and reported as µg $g^{-1}$ plant material dry wt. The recovery of the internal standard was better than 80% except for Rubiaceae I and Cyperaceae I (recovery >40%; for the consecutive numeration of the plant species see Supplementary Table 2.S1). Blank samples of purified sand and storage material (newspaper sheets, paper adhesive) went through the same procedure and showed no significant contamination interfering with the long chain *n*-alkanes.

### *2.3.2.2. Molecular carbon isotope analysis*

Some samples contained substances (partly) coeluting with *n*-alkanes. To avoid possible interference during isotope analysis, the *n*-alkanes of these samples were separated from the branched and cyclic saturated hydrocarbons by urea adduction (Rommerskirchen et al., 2006b). The stable carbon isotopic composition was determined by an Agilent 6890N GC coupled to a Thermo Finnigan MAT 253 isotope ratio mass spectrometer (irm-MS) via a combustion interface (GC-III). The gas chromatography conditions were identical to those used for the *n*-alkane quantification with the exception of the injector and oven temperatures. The injector temperature was programmed from 60°C (held 8 s) to 305°C (held 2 min) at a rate of 10°C $min^{-1}$.

The GC oven was programmed from 60°C (held 2 min) to 300°C (held 18 min) at a rate of 3°C $min^{-1}$. Where samples had been treated by urea adduction, the final oven temperature was held for 38 min due to the inclusion of an additional standard (*n*-$C_{42}$-alkane). The instrument was calibrated by injection of repeated pulses of $CO_2$ of known carbon isotopic composition at the beginning and the end of each run.

For quality control, certified and lab standards (*n*-alkanes and fatty acid methyl esters) were measured between the sample runs. Squalane with known isotopic composition was used as an internal standard. Where squalane had been removed during urea adduction, it was added to the samples prior to isotope analysis. The relative standard deviation of the internal standard was 2.3%. The analyses were run at least in duplicate and yielded values with a difference of less than 0.5‰.

#### *2.3.2.3. Isotopic composition of the plant material*

The bulk isotopic composition of the plant material was determined by a Carlo Erba Elemental Analyser 1108 coupled to a Thermo Finnigan MAT 252 irm-MS. The results were blank-corrected according to Werner et al. (1999). The relative standard deviation of a certified lab standard was 0.9%. The analyses were run at least in duplicate with a difference of values of 0.3‰ on average.

### 2.3.3. Classification of the photosynthetic pathway

The mean $\delta^{13}C$ values of the bulk plant material were between -31 and -11‰ (Supplementary Table 2.S2). The literature $\delta^{13}C$ values for $C_3$ plants are in the range of -34 to -23‰ whereas $C_4$ plants are isotopically heavier (-23 to -6‰; Schidlowski, 1987). Applying these values to our plant samples led to a total of 11 $C_4$ and 41 $C_3$ plants. For each of two Fabaceae (VIII and IX; Supplementary Table 2.S2), only single $\delta^{13}C$ value was available which points to the $C_3$ pathway. In the literature, these plants are also described as $C_3$ plants (Sage et al., 1999b). The $\delta^{13}C$ values of CAM (Crassulacean Acid Mechanism) plants overlap with those of $C_3$ and $C_4$ plants (Schidlowski, 1987). However, none of the plants analysed here was reported to use the CAM pathway (Sayed, 2001).

## 2.4. Results

### 2.4.1. *n*-Alkane distribution

All samples showed an odd-over-even *n*-alkane predominance which is also represented by the values of the carbon preference index (CPI) for the $C_{25}$ to $C_{35}$ *n*-alkanes (Supplementary Table 2.S3; Marzi et al., 1993). The $CPI_{25\text{-}35}$ values ranged

between 2 and 40 with an average of 8. For Apiaceae I no CPI was calculated because no even numbered *n*-alkanes in the range of $C_{25}$ to $C_{35}$ were detected.

In general, individual plants showed great differences in the *n*-alkane distribution patterns regardless of the photosynthetic pathway used. The distribution patterns were either dominated by one, two or three *n*-alkanes (Supplementary Table 2.S4). The $C_{31}$ *n*-alkane dominated in 41% and the $C_{29}$ *n*-alkane in 36% of the $C_3$ plants. For the $C_4$ plants, the $C_{31}$ homologue was dominant in 64% of the specimens. For the six families of which at least three species were analysed, the dominating *n*-alkane changed for four families within a family. For instance, either the $C_{29}$, the $C_{31}$ or the $C_{33}$ *n*-alkane was most abundant in the Asteraceae ($C_3$ plants). The average chain length (ACL; Poynter, 1989) for the odd-numbered $C_{25}$ to $C_{35}$ *n*-alkanes ranged from 27.4 to 32.5 and from 29.0 to 31.3 for the $C_3$ and the $C_4$ plants, respectively (Supplementary Table 2.S3).

### 2.4.2. Carbon isotope composition

The carbon isotope compositions of the *n*-alkanes were in the range reported before for land plants (e.g., Bi et al., 2005; Rommerskirchen et al., 2006b; Vogts et al., 2009). The $\delta^{13}C$ values showed high variabilities for plants of a given photosynthetic pathway. Those for the $C_3$ plants ranged from -44 to -29‰ (Supplementary Table 2.S2). For the $C_4$ plants, the range was smaller (from -27 to -19‰). In addition, the $\delta^{13}C$ values of compounds within one plant differed up to 3.2‰ (Fabaceae XI, *Brachystegia wangermeeana*, $C_3$ plant) and up to 4.6‰ (Poaceae VIII, $C_4$ plant), respectively. In contrast, the $\delta^{13}C$ values of the different *n*-alkanes of some of the plants were within the error margin of the measurements.

Two $C_3$ plants (Fabaceae VII and Crassulaceae I) showed $\delta^{13}C$ values for the different *n*-alkanes around -43‰, which is 3 to 4‰ lighter than in the other $C_3$ plants. Similarly light values for $C_3$ plants were also found by Vogts et al. (2009). The weighted mean average of the $\delta^{13}C$ values for the odd-numbered *n*-alkanes from $C_{27}$ to $C_{33}$ ($\delta^{13}C_{WMA27\text{-}33}$) strongly varied from -44.0 to -26.4‰ for $C_3$ plants and from -23.2 to -19.9‰ for $C_4$ plants (Supplementary Table 2.S2).

## 2.5. Discussion

### 2.5.1. The *n*-alkane parameters for the wood- and shrubland plants

All samples contain longer chain *n*-alkanes with an odd-over-even predominance typical for land plants (Supplementary Table 2.S4; Eglinton et al., 1962; Collister et al., 1994). All $CPI_{25\text{-}35}$ values are between 2 and 40 (Supplementary Table 2.S3).

CPI values of wax alkanes extending over such a large range were also found by Bush and McInerney (2013), Rommerskirchen et al. (2006b) and Vogts et al. (2009). Five plants show CPI values <3. Vogts et al. (2009) found lower CPI values for plants containing low concentrations of *n*-alkanes (<250 µg $g^{-1}$ dry wt.; Supplementary Table 2.S4). In this study, low and high CPI values occur in plants with both low and high concentrations of *n*-alkanes. This is in agreement with Hoffmann et al. (2013), who did not find a correlation between CPI values and *n*-alkane concentration.

A combination of the results for *n*-alkane distribution and carbon isotopic composition of individual plants is shown in Fig. 2.2 as averaged $C_3$ and $C_4$ plant data for wood- and shrubland. Because the analysed plants show considerable variability in the *n*-alkane parameters, we investigated the effect of applying different averaging methods, i.e. the arithmetic average and the median. The histograms calculated from the arithmetic average show the dominance of the $C_{29}$ and $C_{31}$ *n*-alkanes in

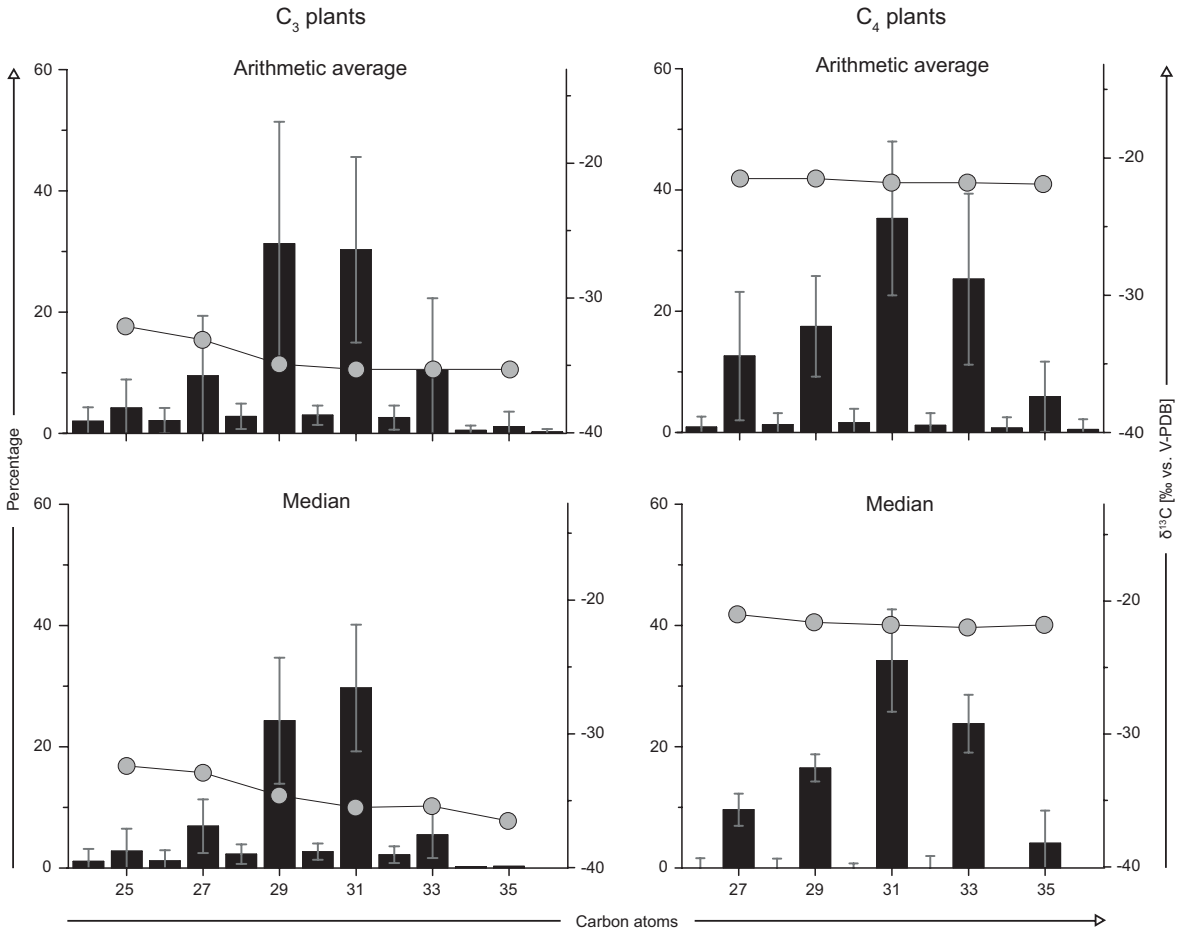


**Fig. 2.2:** Plants from Angola: Mean values of the distribution of *n*-alkanes (in % homologue of the displayed *n*-alkanes, histograms) and the $\delta^{13}C$ values of the odd-numbered *n*-alkanes (grey circles) calculated by the arithmetic average and the median for the $C_3$ and the $C_4$ plants (n= 41 and n= 11, respectively). Grey bars indicate the standard deviation (arithmetic average) and the median absolute deviation (median) of the individual *n*-alkanes.

the $C_3$ plants (both ca. 31%), followed by the $C_{27}$ and $C_{33}$ homologues, both with nearly equal percentages (ca. 10%). The $C_4$ plants are dominated by the $C_{31}$ alkane (35%), followed by the $C_{33}$ homologue. Both *n*-alkanes together account for more than 50% of the sum of all homologues. The $C_{27}$ and $C_{29}$ *n*-alkanes are of lower importance (ca. 15% each).

The *n*-alkane $\delta^{13}C$ values of the $C_3$ plants and the $C_4$ plants range between -37 and -32‰ and between -22 and -21‰, respectively. With increasing chain length, the $\delta^{13}C$ values tend to become more negative. This trend is more distinct for the $C_3$ (3‰) than the $C_4$ plants (1‰). The isotopic composition changes presumably because the different *n*-alkanes are produced at different times during the growth of the leave (Collister et al., 1994; Chikaraishi and Naraoka, 2007). This difference in the timing of the *n*-alkane biosynthesis may also explain the isotopic differences of the *n*-alkanes within individual plants (Supplementary Table 2.S2).

The distribution patterns for the $C_3$ and the $C_4$ plants were calculated by median to minimise effects of extreme values (Fig. 2.2). The median *n*-alkane parameters are similar to those based on the arithmetic average and the percentages and the $\delta^{13}C$ values differ only slightly. The percentages of the even numbered *n*-alkanes, however, are systematically - although only slightly - lower when the median is calculated (up to 2%).

### 2.5.2. Enhanced $C_3$ and $C_4$ plant end member database

#### *2.5.2.1. Different averaging methods*

Rommerskirchen et al. (2006b) and Vogts et al. (2009) compiled *n*-alkane data in averaged histograms for $C_3$ and $C_4$ plants, respectively, to be used as vegetation proxies in palaeoenvironmental studies. The *n*-alkane parameters for the wood- and shrubland are fairly similar if calculated either by the arithmetic average or the median. To identify possible discrepancies between both averaging methods in a larger $C_3$ and $C_4$ plant dataset, we combined our results with the end member database compiled by Vogts et al. (2009; Supplementary Tables 2.S2, 2.S3 and 2.S4). When looking at differences of averaged parameters, such as ACL or $\delta^{13}C_{WMA}$, it has to be considered that different carbon number ranges of both parameters are used in the literature. For instance, plant studies have used an ACL ranging from $C_{27}$ to $C_{35}$ (Rommerskirchen et al., 2006b), from $C_{25}$ to $C_{35}$ (Vogts et al., 2009) or from $C_{21}$ to $C_{35}$ (Carr et al., 2014). In addition, sedimentary studies have used the ranges of $C_{29}$ to $C_{33}$ (Vogts et al., 2012) or $C_{27}$ to $C_{33}$ (Rommerskirchen et al., 2006a) to determine the past vegetation composition. The range variations for the $\delta^{13}C_{WMA}$

**Table 2.1:** Different end member values of higher plant wax *n*-alkane parameters: Mean values for average chain length (ACL) and weighted mean average (WMA) of $\delta^{13}C$ values as well as standard deviation (SD) and median absolute deviation (MAD) for the different *n*-alkane ranges combining data for $C_3$ and $C_4$ plants compiled by Vogts et al. (2009), Rommerskirchen et al. (2006b) and in this study; number of analysed species (n): $n_{ACL,C3}$= 110, $n_{ACL,C4}$= 189, $n_{\delta13CWMA,C3}$= 103, $n_{\delta13CWMA,C4}$= 41; ACL after Poynter (1989).

| Parameter | Range | Arithmetic average | | Median | | SD | | MAD | |
|---|---|---|---|---|---|---|---|---|---|
| | | $C_3$ | $C_4$ | $C_3$ | $C_4$ | $C_3$ | $C_4$ | $C_3$ | $C_4$ |
| ACL | 25-35 | 29.81 | 30.69 | 29.85 | 30.83 | 1.1 | 0.9 | 0.7 | 0.5 |
| | 27-33 | 30.00 | 30.62 | 29.97 | 30.76 | 0.9 | 0.8 | 0.6 | 0.5 |
| | 27-35 | 30.06 | 30.75 | 30.04 | 30.85 | 0.9 | 0.9 | 0.7 | 0.5 |
| | 29-33 | 30.39 | 31.16 | 30.36 | 31.16 | 0.8 | 0.5 | 0.5 | 0.3 |
| $\delta^{13}C_{WMA}$ [‰] | 25-35 | -35.1 | -21.9 | -34.9 | -21.7 | 3.0 | 1.9 | 1.9 | 1.3 |
| | 27-35 | -35.1 | -22.0 | -34.9 | -21.8 | 3.0 | 1.9 | 1.9 | 1.3 |
| | 29-33 | -35.3 | -22.0 | -35.3 | -22.1 | 2.9 | 1.9 | 1.9 | 1.6 |

values in these studies are akin to those of the ACL. Therefore, we list several ranges of ACL and $\delta^{13}C_{WMA}$ for the $C_3$ and the $C_4$ plants in Table 2.1. For the calculation of the mean values, all $C_3$ and $C_4$ plant data obtained by Rommerskirchen et al. (2006b), Vogts et al. (2009) and in this study are used regardless of the growth form or the photosynthetic subtype.

The arithmetic averages for the different ranges of ACL are around 30.0 for the $C_3$ plants (Table 2.1) and higher for the $C_4$ plants (ca. 30.8). These distribution patterns are similar to those for $C_3$ plants reported by Vogts et al. (2009) and for $C_4$ plants analysed by Rommerskirchen et al. (2006b). The $\delta^{13}C_{WMA}$ values for the $C_3$ plants are ca. -35.2‰, the $C_4$ plants are heavier at ca. -22.9‰ (Table 2.1). Both averaging methods for the different ACL ranges yield nearly equal results for the $C_3$ plants. The median values for the $C_4$ plants are slightly higher than the values for the arithmetic average (max. 0.14). The $\delta^{13}C_{WMA}$ values for $C_3$ and $C_4$ plants are nearly equal with a maximum in differences of 0.2‰. However, the values for the arithmetic average and the median are most consistent if they are calculated using the most abundant *n*-alkanes ($C_{29}$ to $C_{33}$). Therefore, it is recommended that an ACL including the main *n*-alkanes should be applied in (palaeo)vegetation assessment. Overall, even though individual plants differ among each other in the distribution patterns and the isotopic composition, the mean values remain stable, even if calculated by different methods.

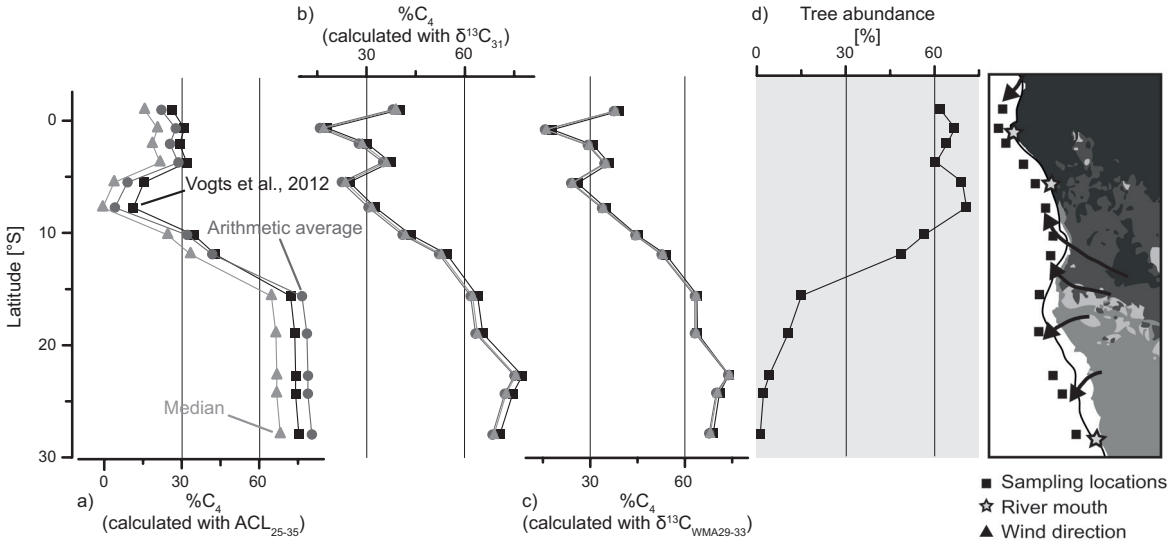


**Fig. 2.3:** Comparison of the calculation of $\%C_4$ by the different end member values (a, b, c) and the tree abundance calculated with $ACL_{27\text{-}33}$ end member values for trees and grasses (d; ACL after Poynter, 1989). Calculations with the end member data used by Vogts et al. (2012; black rectangle) and the enlarged end member dataset of this study averaged by the arithmetic average (dark grey circles) and the median (light grey triangles); sedimentary *n*-alkane data from Vogts et al. (2012); the map depicts the sampling locations, the adjacent continental vegetation (for the colour code see Fig. 2.1) and transport pathways of the plant material (wind, rivers; wind direction after Dupont and Wyputta, 2003).

### *2.5.2.2. Vegetation distribution estimated using different end member values*

We used the enlarged end member dataset to evaluate possible effects on the conclusions of palaeoenvironmental studies by applying the end member values of Vogts et al. (2009) and those of this study (both arithmetic average and median) to a transect of surface sediments off southwest Africa (Vogts et al., 2012). The vegetation on the adjacent continent covers $C_3$ (rain forest) as well as $C_4$ plant dominated regions (grassland) and the transition zone (Fig. 2.3). The contribution of CAM plants to the sediments was assumed to be negligible. We employed the binary mixing equation used by Vogts et al. (2012) to calculate the $C_4$ plant abundance. For estimating $\%C_4$ by $\delta^{13}C$ values, only the results for $\delta^{13}C_{31}$ are shown; the results for $\delta^{13}C_{29}$ and $\delta^{13}C_{33}$ were similar, and the results for the three end member values are in good accordance.

When comparing three different *n*-alkane parameters ($ACL_{25\text{-}35}$, $\delta^{13}C_{31}$ and $\delta^{13}C_{WMA29\text{-}33}$; Fig. 2.3a-c), the highest accordance was obtained for the calculations using $\delta^{13}C_{31}$ and $\delta^{13}C_{WMA29\text{-}33}$ with differences of 1% $C_4$ on average. The good accordance for the calculation of $\%C_4$ by isotopic compositions may be due to the relation between isotopic composition and photosynthetic pathway (O'Leary,

1981; Schidlowski, 1987). The $C_3$ and $C_4$ end member values differ by ca. 13‰ for both averaging methods, and values for $C_3$ and $C_4$ plants do not overlap (Table 2.1).

The differences between the arithmetic average and the median are higher for the $ACL_{25-35}$ than for the isotope data (Fig. 2.3a). Compared to Vogts et al. (2012), the discrepancies extend up to 7 and 12% $C_4$ for the arithmetic average and the median, respectively. These discrepancies are caused by the end member value difference between the two averaging methods. The end member values for the $C_3$ plants are similar for the arithmetic average and the median. But for the $C_4$ plants, the end member values differ by 0.14 (Table 2.1). Furthermore, the differences between the $C_3$ and $C_4$ end member values are small (0.9 and 1.0, respectively) while the relative standard deviations and the relative median absolute deviations are high. This leads to the relatively high variations in the calculated $C_4$ plant abundance.

Although the comparison of the different calculation methods for $ACL_{25-35}$ showed some differences, the general dominance of either $C_3$ or $C_4$ plants is apparent even though the studies on end member plant data are limited surveys. Altogether ca. 300 plant samples have been analysed so far but the plant diversity on the African continent is much higher. In general, the results confirm the hypothesis that mean values remain stable whether calculated with the arithmetic average or the median. This confirms the *n*-alkane parameters to be valuable tools for vegetation reconstructions.

### 2.5.3. Continental plant transect

In Fig. 2.4a, the *n*-alkane data for all plants analysed by Rommerskirchen et al. (2006b), Vogts et al. (2009) and in this study are grouped according to their vegetation zones (cf. Fig. 2.1a; Mayaux et al., 2004). Vogts et al. (2009) analysed $C_3$ plants from the rain forest and the savannah. This study deals with $C_3$ and $C_4$ plants from the wood- and shrubland and the study of Rommerskirchen et al. (2006b) with $C_4$ grasses from the savannah. The plant samples from Australia and Peru analysed by Rommerskirchen et al. (2006b) are excluded here. Altogether, the plant data span a continental transect from the equator via Angola to South Africa, mostly southwestern Africa. In the following, only the arithmetic average is regarded since the results calculated by the arithmetic average and the median have been shown before to be fairly similar.

#### *2.5.3.1. Carbon isotopic composition*

When the vegetation zones are compared, the differences in isotopic composition between $C_3$ and $C_4$ plants are >10‰ (Fig. 2.4a). In contrast to this, the largest

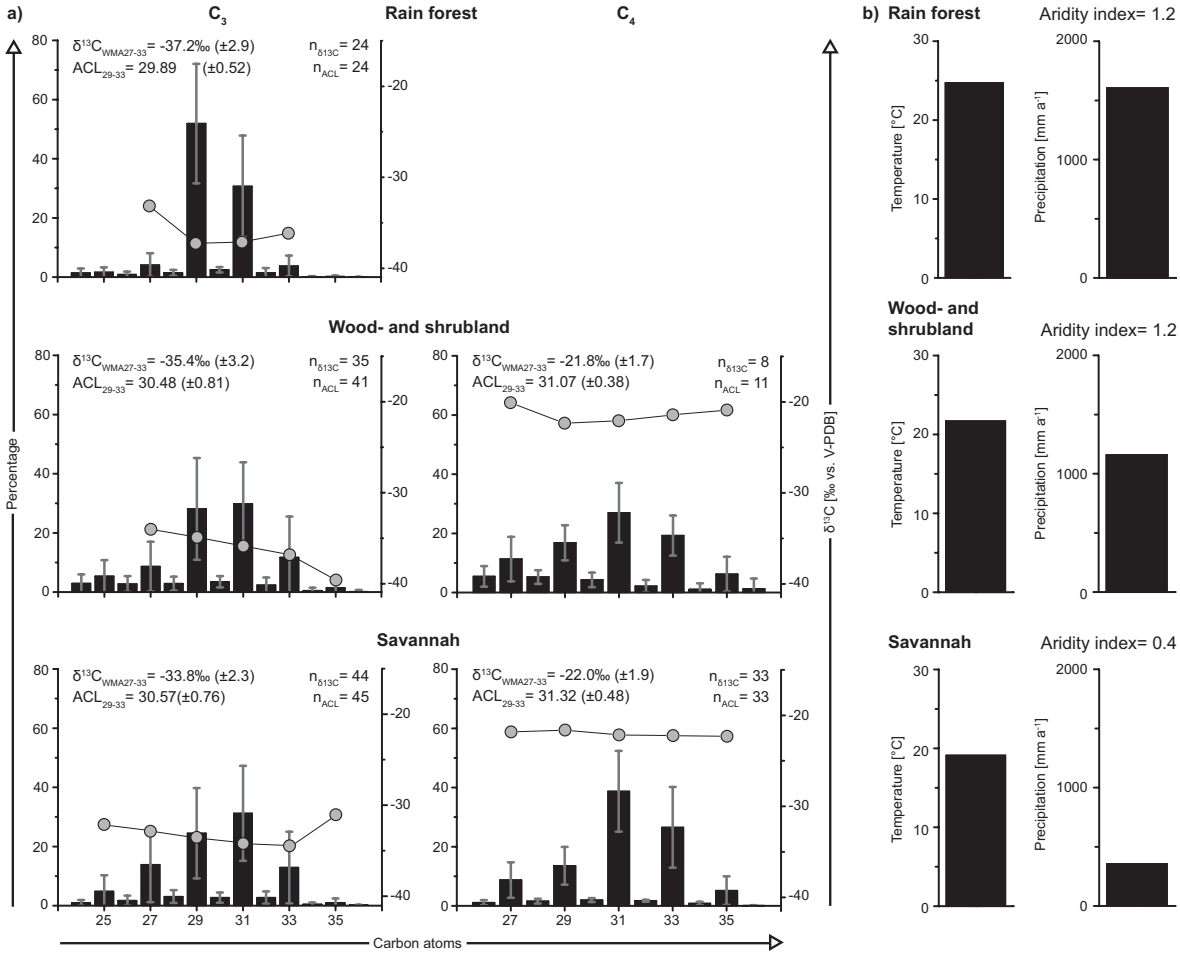


**Fig. 2.4:** *n*-Alkane distribution and carbon isotopic composition for $C_3$ and $C_4$ plants of the different vegetation zones (a) and the correspondent mean annual temperature and precipitation as well as aridity indices (b); $ACL_{29\text{-}33}$: mean average chain length of odd-numbered *n*-alkanes ($C_{29}$ to $C_{33}$) and $\delta^{13}C_{WMA27\text{-}33}$: weighted mean average of $\delta^{13}C$ values of odd-numbered $C_{27}$ to $C_{33}$ *n*-alkanes (including standard deviation in parentheses); n: number of species for the averaged parameters; data from rain forest and savannah are adopted from Vogts et al. (2009) and Rommerskirchen et al. (2006b); ACL after Poynter (1989); mean temperature and precipitation values for the sampling locations calculated according to Matsuura et al. (2009); aridity index calculated according to UNEP (1997).

differences within a photosynthetic pathway are up to 4‰. Within the $C_3$ plants, the $C_{29}$ and $C_{31}$ *n*-alkanes dominate in every vegetation zone and their $\delta^{13}C$ values become heavier towards the south (for $C_{29}$ about 4‰ and for $C_{31}$ ca. 3‰). The trend to a more positive carbon isotopic composition is also reflected by the $\delta^{13}C_{WMA27\text{-}33}$ parameter which increases by about 3‰ towards the south. The stable carbon isotope ratio of the $C_{27}$ and $C_{33}$ *n*-alkanes also becomes more positive towards the south (1 to 2‰). Due to their low abundance in some samples, their average consists of only three ($C_{27}$) or six ($C_{33}$) values for the rainforest and seven ($C_{27}$) or twelve ($C_{33}$) values for the wood- and shrubland. For the savannah plants, at least

30 different values are available. Therefore, only in this vegetation zone assumptions about a general $\delta^{13}C$ pattern are valid for the $C_{27}$ and the $C_{33}$ *n*-alkanes.

The $C_4$ plants do not show a consistent trend towards the south (Fig. 2.4a). Only small changes were observed with a tendency to more negative values towards the south. However, for the wood- and shrubland only up to eight values for single *n*-alkanes are available. Thus, the number of *n*-alkane values is too small to infer a significant trend towards the south.

The potential reasons for an increase of $\delta^{13}C$ values for $C_3$ plants towards the south were summarised by Arens et al. (2000). Among these, the most stringent factors are higher water stress, less recycled material and higher light intensity. Towards the south, the climate becomes more arid (Fig. 2.4b). To maintain a high water use efficiency and to prevent water loss, the $C_3$ plants close their stomata. Thus, less $CO_2$ enters the plant cell which causes less discrimination of the $^{13}C$ isotope and the higher $\delta^{13}C$ values of the plant material. The change in $\delta^{13}C$ is estimated to be about 3 to 6‰ (Brodribb, 1996; Arens et al., 2000; Macková et al., 2013). In addition, the vegetation changes from dense formations to open land cover towards the south (White, 1983). Under canopies, the $\delta^{13}C$ value of $CO_2$ is more negative compared to atmospheric $CO_2$. The lower values are a result of the decomposition of organic material on the ground. The plants near the ground incorporate the lighter $CO_2$ yielding more negative $\delta^{13}C$ values by 1 to 5‰ compared to plants growing in open lands (Medina et al., 1986; Arens et al., 2000). Due to the closed vegetation, the plants towards the equator also receive increasing less light. Under a canopy, the concentration of $CO_2$ inside the cell is higher compared to high light intensity conditions. This leads to lower $\delta^{13}C$ values of the plant material by about 5 to 6‰ (Farquhar et al., 1989; Zimmerman and Ehleringer, 1990; Arens et al., 2000). The factors described should lead to larger changes in the isotopic composition than indicated by the measured $\delta^{13}C$ values of the individual *n*-alkanes. However, several other factors, such as plant age or nutrient availability, may counteract the described effects leading to a less pronounced trend to heavier *n*-alkanes towards the south.

#### *2.5.3.2. Chain length distribution*

The *n*-alkane chain length increases towards the south for both the $C_3$ and $C_4$ plants (Fig. 2.4a). For the $C_3$ plants, $C_{29}$ dominates in the rain forest, whereas $C_{29}$ and $C_{31}$ are similarly abundant in the wood- and shrubland and $C_{31}$ prevails in the distribution patterns of the savannah. In addition, the distribution patterns become broader from the equator towards the south. The abundances of $C_{27}$ and

**Table 2.2:** Mean $ACL_{27-33}$ values for rain forest (number of analysed species (n): $n_{C3}$= 24, Vogts et al., 2009), wood- and shrubland ($n_{C3}$= 41, $n_{C4}$= 11, this study) and savannah ($n_{C3}$= 46, $C_3$ plants analysed by Vogts et al., 2009; $n_{C4}$= 33, $C_4$ plants analysed by Rommerskirchen et al., 2006b); ACL after Poynter (1989).

| | $ACL_{27-33}$ | |
|---|---|---|
| | $C_3$ plants | $C_4$ plants |
| Rain forest | 29.76 | - |
| Wood- and shrubland | 30.12 | 30.49 |
| Savannah | 30.01 | 30.89 |

$C_{33}$ increase, accompanied by a decrease of the $C_{29}$ percentage. In contrast, the abundance of $C_{31}$ remains constant (ca. 30%) in all vegetation zones.

In the literature, mainly broad ranges are used to calculate ACL values (e.g., Rommerskirchen et al., 2006b; Vogts et al., 2009; Carr et al., 2014). We therefore, initially applied an $ACL_{27-33}$ parameter (Table 2.2), which, however, only partly reflects the change in chain length. The $ACL_{27-33}$ values consistently increase from the rain forest to the wood- and shrubland (about 0.4). From the wood- and shrubland towards the savannah, however, the histograms indicate an increase in the chain length, although the $ACL_{27-33}$ values slightly decrease (0.1). This is due to the broadening of the distribution pattern where $C_{29}$ decreases more strongly than $C_{33}$ increases. If, however, a narrower ACL range is used (e.g., $C_{29}$ to $C_{33}$; Fig. 2.4a) the values reflect the increase in chain length as visually observed in the distribution patterns.

In the $C_4$ plants, $C_{31}$ dominates in both vegetation zones but this is more pronounced in the savannah than in the wood- and shrubland (39 and 27%, respectively; Fig. 2.4a). Towards the south, the abundance of $C_{33}$ increases (from 19 to 27%). The longer chain length is reflected by higher $ACL_{27-33}$ and $ACL_{29-33}$ values in the savannah (increase of 0.40 and 0.25, respectively; Table 2.2, Fig. 2.4a).

In sediment studies, ACL has been employed to deduce the $C_4$ abundance in the vegetation on the adjacent continent (e.g., Vogts et al., 2012). Our results do not show a direct relation between ACL and the photosynthetic pathway. If ACL was connected directly to the photosynthetic pathway the chain length would possibly be similar for all vegetation zones. Differences would only be visible in the comparison of $C_3$ and $C_4$ plants. Vogts et al. (2012) suggested that the local environmental conditions determine the chain length leading to an indirect relationship between ACL and the photosynthetic pathway.

To evaluate the potential relationship between ACL and the environmental conditions, we determined the temperature, precipitation and the aridity index for each

sampling area (Fig. 2.4b). This approach is limited because the distribution and growth of a plant depend on several interacting, local parameters (e.g., light intensity, soil salinity; Sage, 2001) whose values are largely unknown. We used the Web-WIMP modeling program (Matsuura et al., 2009) to calculate the annual mean temperature, the annual mean precipitation and the potential evaporation. The aridity indices were calculated as the quotient of the mean annual precipitation and the potential evaporation according to UNEP (1997). Within a given vegetation zone, the environmental conditions are fairly uniform. Hence, the plant samples for which the exact sampling location is unknown were also considered in the averaged ACL values.

Temperature and precipitation decrease towards the south from 25°C to 19°C and from 1600 mm $a^{-1}$ to 350 mm $a^{-1}$, respectively (Fig. 2.4b). The aridity indices indicate a humid climate for the rain forest as well as for the wood- and shrubland and a semiarid climate for the savannah. The chain length and $ACL_{29\text{-}33}$ increase for $C_3$ and $C_4$ plants towards the south. Also, the temperature decreases steadily while precipitation and aridity index show the most distinct changes from the wood- and shrubland towards the savannah. In contrast, the changes in the $C_3$ chain length are higher from the rain forest towards the wood- and shrubland and less distinct from the wood- and shrubland towards the savannah. Thus, the dataset points to a potential connection between the climatic parameters and the chain length but provides no distinct relations.

Carr et al. (2014) investigated the *n*-alkane distribution of succulent plants (mainly CAM) and found only a weak connection between ACL and aridity. In addition, two different plant species show opposite trends in the chain length with increasing aridity in Australia (Hoffmann et al., 2013). In contrast, individual plants are able to react to water stress with a shift to longer chain length (Macková et al., 2013). However, the effects of individual plants may counteract each other within a vegetation zone. Therefore, individual plant studies may not allow conclusions on the complex interactions in a vegetation zone.

The mean annual temperature may not reflect the temperature relevant for leaf wax synthesis. Another influence on ACL may be the leaf temperature which has been discussed by Rommerskirchen et al. (2006b) and Vogts et al. (2009 and references therein). In short, it is suggested that the plants increase the *n*-alkane chain length to maintain the hardness of their leaf surface. For instance, an ACL increase by two raises the *n*-alkane melting point by ca. 4°C (Rommerskirchen et al., 2006b). In a vertical temperature gradient, the temperatures are higher at the bottom of a plant and decrease with height above the ground. This effect is more pronounced for

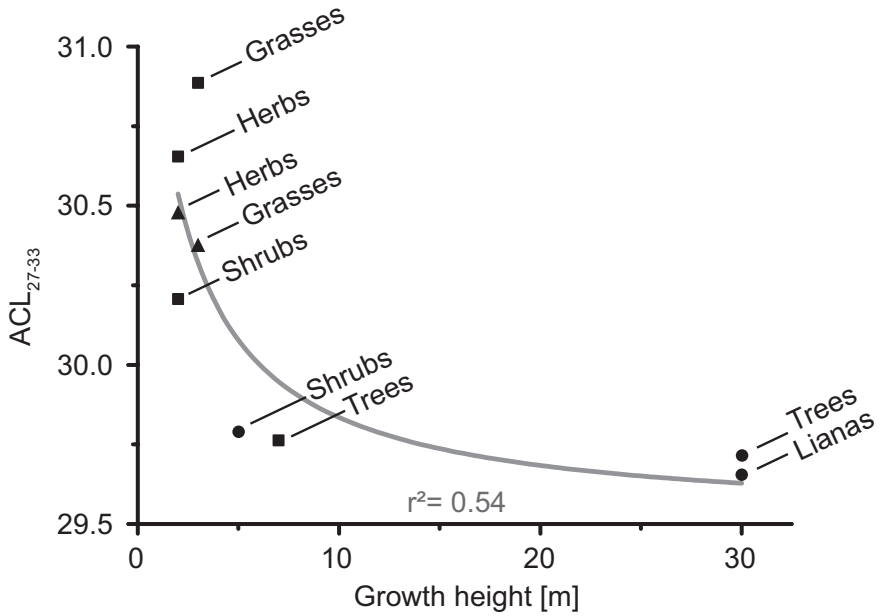


**Fig. 2.5:** Mean $ACL_{27\text{-}33}$ values plotted against the growth height of different plant types from different vegetation zones (circles: rain forest, triangles: wood- and shrubland, rectangles: savannah); data from rain forest and from trees, shrubs and herbs from savannah by Vogts et al. (2009) and data for savannah grasses by Rommerskirchen et al. (2006b); determination of the growth height after White (1983); correlation calculated with Eq. 2.1 according to Ratkowski (1990).

plants in open areas, like savannahs. Vogts et al. (2009) attributed this temperature gradient to be a driving factor in the changes of ACL.

With the additional data of plants from the wood- and shrubland, we present a first approach to evaluate the influence of a vertical temperature gradient for plants of different height. As a first approximation, we use the plant heights described for the different growth forms (tree, grass, liana, shrub, herb) in different habitats (rain forest, wood- and shrubland, savannah; White, 1983). We further assume that lianas are as high as trees in the rain forest and herbs as high as shrubs in the savannah (Fig. 2.5). The classification of the growth form of a given plant is according either to the description given of the authors of previous studies (Rommerskirchen et al., 2006b; Vogts et al., 2009) or, for the plants of the wood- and shrubland, to the collectors and Stevens (2001, Supplementary Table 2.S1). Only those growth forms are included into the calculations where *n*-alkane data for at least seven plants are available.

For every growth height, the $ACL_{27\text{-}33}$ values scatter but to estimate an average trend, we calculated average $ACL_{27\text{-}33}$ values for each plant group in each habitat (Fig. 2.5). The mean values of $ACL_{27\text{-}33}$ decrease with the growth height. To

determine a correlation, we used a three-parameter exponential function (Eq. 2.1),

$$y = a \times \exp^{\left(\frac{b}{x + c}\right)} \qquad \textbf{Equation 2.1}$$

where a is the asymptote for $x \rightarrow \infty$, b is the difference between a and the y-axis intercept (if x=0) and c is the rate for the change of the y-value from its original value at x=0 (Ratkowski, 1990). This function describes a correlation between the mean $ACL_{27\text{-}33}$ values and the growth height ($r^2$= 0.54) in spite of the many assumptions (Fig. 2.5). For $ACL_{29\text{-}33}$, a similar correlation is obtained. However, this limited approach needs further verification on more data especially for growth heights between 10 and 30 m as well as samples from plants with known growth heights.

Furthermore, Fig. 2.5 shows that the mean $ACL_{27\text{-}33}$ values of trees in different vegetation zones are nearly equally low. The mean $ACL_{27\text{-}33}$ value of grasses in the savannah is the highest and the values for herbs and the shrubs are in between the values for trees and savannah grasses. The similarity of the $ACL_{27\text{-}33}$ values of trees may eventually be used in palaeoenvironmental studies to reconstruct the tree abundance. To evaluate this hypothesis, we calculated tree abundance using a binary mixing equation. This equation is similar to that applied for $\%C_4$ calculation from the mean end member $ACL_{27\text{-}33}$ values (29.74 and 30.79, respectively) for trees (averaged rain forest, wood- and shrubland and savannah) and for grasses (averaged wood- and shrubland and savannah). To apply the tree abundance approach, we used the $ACL_{27\text{-}33}$ values of the sedimentary *n*-alkane study off southwest Africa by Vogts et al. (2012). This approach is similar to that of Bush and McInerney (2013) who used a given amount of $C_{29}$ and $C_{31}$ *n*-alkanes to conclude on either a woody plant or a grass origin.

In the northern part of the transect, the tree abundance is high (Fig. 2.3d, >60%, locations 1-6) and decreases towards the south to 1% (location 13). This trend roughly concurs with the tree distribution in the postulated catchment areas (Mayaux et al., 2004). The transport of plant material from the continent to the sediments occurs on nearly longitudinal pathways from the continent to the sediments via wind and rivers (Dupont and Wyputta, 2003; Vogts et al., 2012). However, in the northern part of the transect, the calculated tree abundance appears to be too small compared to the vegetation on the adjacent continent. This might be due to the transport of plant material from north-central Africa by, e.g., Harmattan winds (Schefuß et al., 2003a; Vogts et al., 2012). However, this first approach should be further verified as other factors (e.g., sampling season) may influence the chain length distribution of the *n*-alkanes.

## 2.6. Conclusions

We analysed 41 $C_3$ plants and 11 $C_4$ plants from the wood- and shrubland in Angola for wax *n*-alkane distribution and the molecular carbon isotopic composition of these compounds. We have expanded the plant database for African $C_3$ and $C_4$ species, but the end member data remain fairly uniform even if calculated by different averaging methods (arithmetic average, median). This result confirms the *n*-alkane parameters to be valuable tools for the assessment of palaeovegetation and -climate.

In contrast to the $C_4$ plants, the stable carbon isotopes of the *n*-alkanes of the $C_3$ plants become slightly heavier from the rain forest through the wood- and shrubland towards the savannah. This is probably due to the influence of different environmental conditions on the $C_3$ plants (e.g., water stress, light intensity or incorporation of $CO_2$ from decayed plants). For $C_3$ and $C_4$ plants, the chain length increases towards the south which is best reflected by an ACL in a small range ($C_{29}$ to $C_{33}$). For palaeoenvironmental studies, ACL is not a direct indicator for the $C_3/C_4$ distribution of past vegetation. But the $ACL_{27\text{-}33}$ may indicate the growth height of the plants and/or the tree abundance.

## 2.7. Acknowledgements

We thank W. Lobin (University of Bonn) for providing the plant material and valuable information regarding their sampling and storage. We are grateful to B. Kopke for help and advice during carbon isotope analysis and to D. Lorenz as well as K. Bengard (all ICBM) for their support during sample workup. F. Rommerskirchen (University of Bremen) is gratefully acknowledged for valuable remarks regarding the data interpretation.

**Supplementary Table 2.S1:** Sample information: Analysed plant families, species and photosynthetic pathway (PP), consecutive number for species per family, plant growth form, month and year of collection and location of collection; growth form according to Steven (2001) or the collectors (*); n.d. - not determined.

| PP/ Family | No. | Species | Growth form | Collected | Latitude (°S) | Longitude (°E) |
|---|---|---|---|---|---|---|
| **$C_3$ plants** | | | | | | |
| Apiaceae | I | n.d. | n.d. | 06.2007 | 12°29.910' | 16°46.541' |
| Asteraceae | I | n.d. | n.d. | 06.2007 | 12°30.269' | 17°12.681' |
| Asteraceae | II | n.d. | n.d. | 06.2007 | 11°51' | 15°03' |
| Asteraceae | III | n.d. | n.d. | 06.2007 | 12°29.910' | 16°46.541' |
| Asteraceae | IV | *Vernonia colorata* | n.d. | 08.-09.2006 | 9°44.301' | 13°59.145' |
| Asteraceae | V | *Vernonia* sp. | n.d. | 08.-09.2006 | 9°44.301' | 13°59.145' |
| Capparaceae | I | *Cleome* sp. | n.d. | 06.2007 | 12°29.910' | 16°46.541' |
| Combretaceae | I | n.d. | n.d. | 08.-09.2006 | 9°21.267' | 13°32.653' |
| Combretaceae | II | *Combretum paniculatum* | n.d. | 06.2007 | n.d. | n.d. |
| Combretaceae | III | *Terminalia brachystemma* | n.d. | 06.2007 | n.d. | n.d. |
| Commelinaceae | I | n.d. | n.d. | 06.2007 | 12°29.910' | 16°46.541' |
| Crassulaceae | I | *Crassula vaginata* | n.d. | 06.2007 | 11°51' | 15°03' |
| Euphorbiaceae | I | *Acalypha* sp. | Herb | 06.2007 | 12°28.922' | 17°06.316' |
| Euphorbiaceae | II | *Croton gratissimus* | Herb | 08.-09.2006 | 9°44.200' | 13°59.145' |
| Euphorbiaceae | III | *Uapaca sansibarica* | Herb | 06.2007 | 11°50' | 14°58' |
| Fabaceae | I | n.d. | n.d. | 06.2007 | 12°29.910' | 16°46.541' |
| Fabaceae | II | n.d. | n.d. | 06.2007 | 12°28.922' | 17°06.316' |
| Fabaceae | III | n.d. | n.d. | 06.2007 | 12°27.917' | 17°02.219' |
| Fabaceae | IV | n.d. | n.d. | 06.2007 | 12°30' | 16°54' |
| Fabaceae | V | n.d. | n.d. | 06.2007 | 12°30.269' | 17°12.681' |
| Fabaceae | VI | n.d. | Shrub* | 06.2007 | 12°10' | 16°54' |
| Fabaceae | VII | n.d. | n.d. | 06.2007 | 11°51' | 15°03' |

**Supplementary Table 2.S1** (continued)

| PP/ Family | No. | Species | Growth form | Collected | Latitude (°S) | Longitude (°E) |
|---|---|---|---|---|---|---|
| Fabaceae | VIII | n.d. | n.d. | 06.2007 | 9°04’ | 16°00’ |
| Fabaceae | IX | n.d. | n.d. | 06.2007 | 9°04’ | 16°37’ |
| Fabaceae | X | *Brachystegia* sp. | n.d. | 08.-09.2006 | 11°46.959’ | 14°53.026’ |
| Fabaceae | XI | *Brachystegia wangermeeana* | n.d. | 08.-09.2006 | 12°30.269’ | 17°12.681’ |
| Fabaceae | XII | *Pterocarpus tinctoria* | Herb | 08.-09.2006 | 9°44.200’ | 13°44.551’ |
| Fabaceae | XIII | *Rhynchosia* sp. | n.d. | 06.2007 | 12°29.910’ | 16°46.541’ |
| Fabaceae | XIV | *Tessmannia* sp. | n.d. | 08.-09.2006 | 9°45.357’ | 13°50.751’ |
| Melastomataceae | I | *Dissotis* sp. | n.d. | 06.2007 | 12°28.922’ | 17°06.316’ |
| Melastomataceae | II | *Dissotis* sp. | n.d. | 06.2007 | 11°52.958’ | 15°13.720’ |
| Pedaliaceae | I | *Sesamum* sp. | Herb | 08.-09.2006 | 9°23.197’ | 13°10.937’ |
| Plumbaginaceae | I | n.d. | n.d. | 06.2007 | 11°52.958’ | 15°13.720’ |
| Proteaceae | I | *Protea* sp. | n.d. | 06.2007 | 12°29.910’ | 16°46.541’ |
| Proteaceae | II | *Protea* sp. | n.d. | 06.2007 | 9°04’ | 16°37’ |
| Ranunculaceae | I | *Clematis villosa* | n.d. | 06.2007 | 11°43’ | 14°27’ |
| Rubiaceae | I | n.d. | Tree* | 06.2007 | 12°29.910’ | 16°46.541’ |
| Scrophulariaceae | I | *Aptosimum linearis* | n.d. | 08.2006 | 9°44.200’ | 13°59.145’ |
| Thymelaeaceae | I | *Gnidia chrysantha* | n.d. | 06.2007 | 12°27.917’ | 17°02.219’ |
| Verbenaceae | I | *Clerodendrum* sp. | n.d. | 08.-09.2006 | 9°23.197’ | 13°10.937’ |
| Verbenaceae | II | *Stachytarpheta elegans* | n.d. | 08.-09.2006 | 9°23.197’ | 13°10.937’ |
| **$C_4$ plants** | | | | | | |
| Cyperaceae | I | n.d. | Herb | 06.2007 | 12°28.922’ | 17°06.316’ |
| Cyperaceae | II | n.d. | Herb | 06.2007 | 12°28.922’ | 17°06.316’ |
| Cyperaceae | III | n.d. | Herb | 06.2007 | 9°04’ | 16°00’ |
| Poaceae | I | n.d. | Grass | 06.2007 | 12°28.922’ | 17°06.316’ |
| Poaceae | II | n.d. | Grass | 06.2007 | 12°28.922’ | 17°06.316’ |

**Supplementary Table 2.S1** (continued)

| PP/ Family | No. | Species | Growth form | Collected | Latitude (°S) | Longitude (°E) |
|---|---|---|---|---|---|---|
| Poaceae | III | n.d. | Grass | 06.2007 | 12°28.922’ | 17°06.316’ |
| Poaceae | IV | n.d. | Grass | 06.2007 | 12°30.269’ | 17°12.681’ |
| Poaceae | V | n.d. | Grass | 06.2007 | 11°51’ | 15°03’ |
| Poaceae | VI | n.d. | Grass | 06.2007 | 11°51’ | 15°03’ |
| Poaceae | VII | n.d. | Grass | 06.2007 | 11°43’ | 14°27’ |
| Poaceae | VIII | n.d. | Grass | 06.2007 | 12°29.910’ | 16°46.541’ |

**Supplementary Table 2.S2:** $\delta^{13}C$ values and $\delta^{13}C_{WMA}$: Analysed plant families and photosynthetic pathway (PP), consecutive number for species per family (see Supplementary Table 2.S1) and $\delta^{13}C$ values of plant material (PM), odd-numbered *n*-alkanes from $C_{27}$ to $C_{35}$ and weighted mean average (WMA) for different ranges as well as arithmetic average (arithm. average), median, standard deviation (SD) and median absolute deviation (MAD) of the plant species analysed here and total analysed African plant samples (mean $C_3$ or mean $C_4$ plants) compiled by Rommerskirchen et al. (2006b) and Vogts et al. (2009); n.d. - not determined.

| PP/ Family | No. | $\delta^{13}C$ of the plant material and the *n*-alkanes (‰ vs. V-PDB) | | | | | | | | | |
|---|---|---|---|---|---|---|---|---|---|---|---|
| | | $\delta^{13}C_{PM}$ | $C_{27}$ | $C_{29}$ | $C_{31}$ | $C_{33}$ | $C_{35}$ | $\delta^{13}C_{WMA25-35}$ | $\delta^{13}C_{WMA29-33}$ | $\delta^{13}C_{WMA27-33}$ | $\delta^{13}C_{WMA27-35}$ |
| **$C_3$ plants** | | | | | | | | | | | |
| Apiaceae | I | -28.4 | n.d. | n.d. | n.d. | n.d. | n.d. | n.d. | n.d. | n.d. | n.d. |
| Asteraceae | I | -30.6 | n.d. | n.d. | -37.6 | -37.7 | -37.7 | -37.7 | -37.7 | -37.7 | -37.7 |
| Asteraceae | II | -27.6 | -34.1 | -34.2 | -34.6 | n.d. | n.d. | -34.4 | -34.4 | -34.4 | -34.4 |
| Asteraceae | III | -31.5 | n.d. | n.d. | n.d. | n.d. | n.d. | n.d. | n.d. | n.d. | n.d. |
| Asteraceae | IV | -29.0 | n.d. | -35.2 | -35.2 | n.d. | n.d. | -31.5 | -35.2 | -31.5 | -31.5 |
| Asteraceae | V | -28.4 | n.d. | -36.6 | n.d. | n.d. | n.d. | -36.6 | -36.6 | -36.6 | -36.6 |
| Capparaceae | I | -28.2 | n.d. | n.d. | -37.7 | -37.5 | n.d. | -37.6 | -37.6 | -37.6 | -37.6 |
| Combretaceae | I | -28.4 | n.d. | -36.3 | -36.2 | n.d. | n.d. | -34.7 | -36.3 | -34.7 | -34.7 |
| Combretaceae | II | -26.4 | n.d. | n.d. | -35.7 | -35.8 | n.d. | -35.7 | -35.7 | -35.7 | -35.7 |
| Combretaceae | III | -26.0 | -32.8 | -31.1 | -29.3 | n.d. | n.d. | -31.1 | -30.9 | -31.1 | -31.1 |
| Commelinaceae | I | -26.9 | n.d. | n.d. | -38.3 | -39.2 | n.d. | -38.5 | -38.5 | -38.5 | -38.5 |
| Crassulaceae | I | -29.7 | n.d. | n.d. | -42.1 | -43.2 | -43.5 | -43.0 | -42.9 | -42.9 | -43.0 |
| Euphorbiaceae | I | -28.5 | n.d. | -37.2 | -38.1 | n.d. | n.d. | -37.8 | -37.8 | -37.8 | -37.8 |
| Euphorbiaceae | II | -27.3 | n.d. | -35.4 | -35.3 | n.d. | n.d. | -35.4 | -35.4 | -35.4 | -35.4 |
| Euphorbiaceae | III | -29.1 | n.d. | -36.6 | -36.6 | n.d. | n.d. | -36.6 | -36.6 | -36.6 | -36.6 |
| Fabaceae | I | -27.4 | n.d. | -34.2 | -34.3 | n.d. | n.d. | -34.2 | -34.2 | -34.2 | -34.2 |
| Fabaceae | II | -30.3 | -36.9 | -37.1 | -37.8 | n.d. | n.d. | -37.4 | -37.6 | -37.4 | -37.4 |
| Fabaceae | III | -28.7 | n.d. | -36.7 | -38.7 | n.d. | n.d. | -37.8 | -37.8 | -37.8 | -37.8 |
| Fabaceae | IV | -26.9 | n.d. | n.d. | n.d. | n.d. | n.d. | n.d. | n.d. | n.d. | n.d. |
| Fabaceae | V | -29.4 | n.d. | n.d. | n.d. | n.d. | n.d. | n.d. | n.d. | n.d. | n.d. |

**Supplementary Table 2.S2** (continued)

| PP/ Family | No. | $\delta^{13}C$ of the plant material and the *n*-alkanes (‰ vs. V-PDB) | | | | | | | | | |
|---|---|---|---|---|---|---|---|---|---|---|---|
| | | $\delta^{13}C_{PM}$ | $C_{27}$ | $C_{29}$ | $C_{31}$ | $C_{33}$ | $C_{35}$ | $\delta^{13}C_{WMA25-35}$ | $\delta^{13}C_{WMA29-33}$ | $\delta^{13}C_{WMA27-33}$ | $\delta^{13}C_{WMA27-35}$ |
| Fabaceae | VI | -29.1 | n.d. | -38.5 | -39.1 | n.d. | n.d. | -39.0 | -39.0 | -39.0 | -39.0 |
| Fabaceae | VII | -31.8 | n.d. | -42.3 | n.d. | n.d. | n.d. | -42.3 | -42.3 | -42.3 | -42.3 |
| Fabaceae | VIII | -28.0* | n.d. | -34.7 | -34.1 | n.d. | n.d. | -34.4 | -34.4 | -34.4 | -34.4 |
| Fabaceae | IX | -27.4* | n.d. | -35.6 | -35.0 | n.d. | n.d. | -35.4 | -35.4 | -35.4 | -35.4 |
| Fabaceae | X | -25.1 | -31.4 | -30.4 | n.d. | n.d. | n.d. | -26.3 | -30.4 | -26.3 | -26.3 |
| Fabaceae | XI | -26.5 | n.d. | -30.6 | -33.8 | n.d. | n.d. | -31.3 | -31.3 | -31.3 | -31.3 |
| Fabaceae | XII | -25.5 | n.d. | -31.6 | -31.7 | n.d. | n.d. | -31.6 | -31.6 | -31.6 | -31.6 |
| Fabaceae | XIII | -29.6 | n.d. | -35.4 | -36.3 | n.d. | n.d. | -35.9 | -35.9 | -35.9 | -35.9 |
| Fabaceae | XIV | -24.9 | n.d. | -32.6 | n.d. | n.d. | n.d. | -32.6 | -32.6 | -32.6 | -32.6 |
| Melastomataceae | I | -27.0 | n.d. | -34.1 | -34.2 | -33.8 | n.d. | -34.0 | -34.0 | -34.0 | -34.0 |
| Melastomataceae | II | -30.1 | n.d. | -36.2 | -36.0 | -35.3 | n.d. | -35.7 | -35.7 | -35.7 | -35.7 |
| Pedaliaceae | I | -28.4 | n.d. | -35.4 | -35.4 | -35.2 | n.d. | -35.3 | -35.3 | -35.3 | -35.3 |
| Plumbaginaceae | I | -26.9 | n.d. | -34.2 | -36.6 | -34.4 | n.d. | -35.9 | -35.9 | -35.9 | -35.9 |
| Proteaceae | I | -26.2 | -31.5 | -32.1 | -30.2 | n.d. | n.d. | -31.2 | -31.1 | -31.2 | -31.2 |
| Proteaceae | II | -28.6 | n.d. | -33.4 | n.d. | n.d. | n.d. | -33.4 | -33.4 | -33.4 | -33.4 |
| Ranunculaceae | I | -25.8 | -34.9 | -32.7 | -32.8 | n.d. | n.d. | -33.0 | -32.8 | -33.0 | -33.0 |
| Rubiaceae | I | -28.9 | n.d. | -34.5 | -35.0 | -35.7 | n.d. | -34.9 | -34.9 | -34.9 | -34.9 |
| Scrophulariaceae | I | -29.1 | n.d. | -34.3 | -36.7 | -37.2 | n.d. | -36.3 | -36.3 | -36.3 | -36.3 |
| Thymelaeaceae | I | -28.4 | -36.5 | -38.3 | -38.9 | n.d. | n.d. | -37.9 | -38.6 | -37.9 | -37.9 |
| Verbenaceae | I | -27.8 | n.d. | -34.7 | n.d. | n.d. | n.d. | -34.7 | -34.7 | -34.7 | -34.7 |
| Verbenaceae | II | -29.5 | n.d. | n.d. | -35.6 | -36.7 | -37.5 | -36.5 | -36.4 | -36.4 | -36.5 |
| Arith. aver. | | -28.1 | -34.0 | -34.9 | -35.8 | -36.8 | -39.6 | -35.3 | -35.6 | -35.3 | -35.3 |
| Median | | -28.4 | -34.1 | -34.7 | -35.7 | -36.3 | -37.7 | -35.4 | -35.7 | -35.4 | -35.4 |
| SD | | 1.6 | 2.2 | 2.5 | 2.6 | 2.5 | 3.4 | 3.1 | 2.8 | 3.1 | 3.1 |
| MAD | | 1.1 | 2.4 | 1.9 | 1.7 | 1.1 | 0.2 | 2.0 | 1.6 | 2.0 | 2.0 |

**Supplementary Table 2.S2** (continued)

| PP/ Family | No. | $\delta^{13}C$ of the plant material and the *n*-alkanes (‰ vs. V-PDB) | | | | | | | | | |
|---|---|---|---|---|---|---|---|---|---|---|---|
| | | $\delta^{13}C_{PM}$ | $C_{27}$ | $C_{29}$ | $C_{31}$ | $C_{33}$ | $C_{35}$ | $\delta^{13}C_{WMA25-35}$ | $\delta^{13}C_{WMA29-33}$ | $\delta^{13}C_{WMA27-33}$ | $\delta^{13}C_{WMA27-35}$ |
| **Mean $C_3$ plants** (Vogts et al., 2009, this study) | | | | | | | | | | | |
| Arith. aver. | | -28.0 | -33.1 | -34.9 | -35.3 | -35.3 | -35.3 | -35.1 | -35.3 | -35.1 | -35.1 |
| Median | | -28.1 | -32.9 | -34.7 | -35.5 | -35.4 | -36.5 | -34.9 | -35.3 | -34.9 | -34.9 |
| SD | | 1.8 | 2.2 | 2.9 | 2.9 | 2.5 | 5.7 | 3.0 | 2.9 | 3.0 | 3.0 |
| MAD | | 1.2 | 1.5 | 2.0 | 1.7 | 1.7 | 4.1 | 1.9 | 1.9 | 1.9 | 1.9 |
| **$C_4$ plants** | | | | | | | | | | | |
| Cyperaceae | I | -12.4 | n.d. | n.d. | n.d. | n.d. | n.d. | n.d. | n.d. | n.d. | n.d. |
| Cyperaceae | II | -12.7 | n.d. | n.d. | -22.4 | -21.6 | n.d. | -22.1 | -22.1 | -22.1 | -22.1 |
| Cyperaceae | III | -11.1 | n.d. | n.d. | n.d. | n.d. | n.d. | n.d. | n.d. | n.d. | n.d. |
| Poaceae | I | -12.9 | n.d. | n.d. | n.d. | n.d. | n.d. | n.d. | n.d. | n.d. | n.d. |
| Poaceae | II | -11.5 | n.d. | n.d. | -20.7 | -20.5 | n.d. | -20.6 | -20.6 | -20.6 | -20.6 |
| Poaceae | III | -13.1 | n.d. | -25.8 | -22.6 | -21.9 | n.d. | -23.2 | -23.2 | -23.2 | -23.2 |
| Poaceae | IV | -12.2 | n.d. | -20.4 | -21.3 | -21.2 | -20.9 | -21.0 | -21.0 | -21.0 | -21.0 |
| Poaceae | V | -12.0 | n.d. | -26.2 | -24.8 | n.d. | n.d. | -25.3 | -25.3 | -25.3 | -25.3 |
| Poaceae | VI | -11.2 | n.d. | -20.0 | -19.9 | -23.2 | n.d. | -20.5 | -20.5 | -20.5 | -20.5 |
| Poaceae | VII | -11.1 | n.d. | -19.7 | -20.1 | -20.0 | n.d. | -20.0 | -20.0 | -20.0 | -20.0 |
| Poaceae | VIII | -12.7 | -20.1 | -21.9 | -24.7 | n.d. | n.d. | -21.8 | -22.9 | -21.8 | -21.8 |
| Arith. aver. | | -12.1 | -20.1 | -22.3 | -22.1 | -21.4 | -20.9 | -21.8 | -21.9 | -21.8 | -21.8 |
| Median | | -12.2 | -20.1 | -21.2 | -21.8 | -21.4 | -20.9 | -21.4 | -21.5 | -21.4 | -21.4 |
| SD | | 0.8 | n.d. | 2.9 | 1.9 | 1.1 | n.d. | 1.7 | 1.8 | 1.7 | 1.7 |
| MAD | | 0.7 | n.d. | 1.3 | 1.5 | 0.7 | n.d. | 0.8 | 1.2 | 0.8 | 0.8 |

**Supplementary Table 2.S2** (continued)

| | $\delta^{13}C$ of the plant material and the *n*-alkanes (‰ vs. V-PDB) | | | | | | | | | |
|---|---|---|---|---|---|---|---|---|---|---|
| | $\delta^{13}C_{PM}$ | $C_{27}$ | $C_{29}$ | $C_{31}$ | $C_{33}$ | $C_{35}$ | $\delta^{13}C_{WMA25-35}$ | $\delta^{13}C_{WMA29-33}$ | $\delta^{13}C_{WMA27-33}$ | $\delta^{13}C_{WMA27-35}$ |
| **Mean $C_4$ plants** (Rommerskirchen et al., 2006b, this study) | | | | | | | | | | |
| Arith. aver. | -12.07 | -21.5 | -21.5 | -21.8 | -21.8 | -21.9 | -21.9 | -22.0 | -22.0 | -22.0 |
| Median | -12.17 | -21.0 | -21.6 | -21.8 | -22.0 | -21.8 | -21.7 | -22.1 | -21.8 | -21.8 |
| SD | 0.9 | 2.5 | 2.2 | 2.2 | 1.8 | 1.8 | 1.9 | 1.9 | 1.9 | 1.9 |
| MAD | 0.6 | 1.4 | 1.5 | 1.8 | 1.5 | 1.2 | 1.3 | 1.6 | 1.4 | 1.3 |

* only one value available

**Supplementary Table 2.S3:** CPI and ACL values of different ranges, arithmetic average (arithm. average) and median for $C_3$ and $C_4$ plants, standard deviation (SD) and median absolute deviation (MAD) of the plant species analysed here as well as total analysed African plant samples (mean $C_3$ or mean $C_4$ plants) compiled by Rommerskirchen et al. (2006b) and Vogts et al. (2009); CPI after Marzi et al. (1993), ACL after Poynter (1989); n.d. - not determined.

| PP/ Family | No. | $CPI_{25-35}$ | $ACL_{27-33}$ | $ACL_{29-33}$ | $ACL_{25-35}$ | $ACL_{27-35}$ |
|---|---|---|---|---|---|---|
| **$C_3$ plants** | | | | | | |
| Apiaceae | I | n.d. | 27.96 | 29.00 | 27.37 | 28.54 |
| Asteraceae | I | 8.5 | 31.78 | 31.89 | 32.45 | 32.51 |
| Asteraceae | II | 10.5 | 29.48 | 29.97 | 29.36 | 29.52 |
| Asteraceae | III | 10.6 | 30.55 | 31.00 | 30.55 | 30.55 |
| Asteraceae | IV | 7.6 | 30.16 | 30.36 | 30.05 | 30.22 |
| Asteraceae | V | 4.0 | 30.77 | 30.89 | 30.91 | 30.91 |
| Capparaceae | I | 7.7 | 30.99 | 31.31 | 30.49 | 30.99 |
| Combretaceae | I | 14.2 | 29.81 | 29.85 | 29.81 | 29.83 |
| Combretaceae | II | 13.7 | 29.96 | 30.04 | 29.89 | 29.98 |
| Combretaceae | III | 23.9 | 29.03 | 29.26 | 28.96 | 29.03 |
| Commelinaceae | I | 4.5 | 30.93 | 31.23 | 30.79 | 31.06 |
| Crassulaceae | I | 8.0 | 32.26 | 32.34 | 32.54 | 32.62 |
| Euphorbiaceae | I | 3.6 | 30.40 | 30.67 | 30.07 | 30.40 |
| Euphorbiaceae | II | 4.5 | 29.80 | 30.16 | 29.48 | 29.93 |
| Euphorbiaceae | III | 10.1 | 30.05 | 30.07 | 30.04 | 30.06 |
| Fabaceae | I | 5.3 | 30.27 | 30.63 | 29.84 | 30.33 |
| Fabaceae | II | 5.7 | 30.12 | 30.77 | 29.59 | 30.12 |
| Fabaceae | III | 2.1 | 30.36 | 30.36 | 29.25 | 30.14 |
| Fabaceae | IV | 2.8 | 30.14 | 30.53 | 30.15 | 30.60 |
| Fabaceae | V | 4.5 | 29.27 | 30.08 | 28.80 | 29.37 |
| Fabaceae | VI | 13.1 | 30.46 | 30.68 | 30.23 | 30.46 |
| Fabaceae | VII | 8.2 | 28.96 | 29.50 | 28.54 | 29.17 |
| Fabaceae | VIII | 4.8 | 29.88 | 30.27 | 29.16 | 30.03 |
| Fabaceae | IX | 16.4 | 29.66 | 29.70 | 29.64 | 29.68 |
| Fabaceae | X | 8.0 | 28.77 | 29.31 | 28.55 | 28.95 |
| Fabaceae | XI | 4.4 | 29.04 | 29.62 | 28.81 | 29.09 |
| Fabaceae | XII | 14.3 | 30.17 | 30.40 | 30.17 | 30.17 |
| Fabaceae | XIII | 6.7 | 30.37 | 30.62 | 29.95 | 30.37 |
| Fabaceae | XIV | 4.8 | 29.33 | 29.56 | 29.22 | 29.40 |
| Melastomataceae | I | 7.5 | 31.68 | 31.75 | 31.67 | 31.71 |
| Melastomataceae | II | 8.9 | 31.52 | 31.63 | 31.41 | 31.53 |
| Pedaliaceae | I | 6.1 | 30.99 | 31.18 | 31.15 | 31.18 |
| Plumbaginaceae | I | 6.4 | 30.82 | 31.03 | 30.45 | 30.90 |
| Proteaceae | I | 5.4 | 29.06 | 30.44 | 28.05 | 29.06 |
| Proteaceae | II | 3.5 | 28.93 | 29.93 | 27.87 | 29.22 |
| Ranunculaceae | I | 14.6 | 30.02 | 30.43 | 29.72 | 30.04 |

**Supplementary Table 2.S3** (continued)

| PP/ Family | No. | $CPI_{25-35}$ | $ACL_{27-33}$ | $ACL_{29-33}$ | $ACL_{25-35}$ | $ACL_{27-35}$ |
|---|---|---|---|---|---|---|
| Rubiaceae | I | 39.6 | 30.51 | 30.57 | 30.53 | 30.54 |
| Scrophulariaceae | I | 4.4 | 30.70 | 31.08 | 30.34 | 30.76 |
| Thymelaeaceae | I | 9.8 | 29.10 | 30.01 | 28.53 | 29.33 |
| Verbenaceae | I | 5.9 | 28.87 | 29.30 | 28.38 | 28.96 |
| Verbenaceae | II | 8.7 | 32.21 | 32.25 | 32.32 | 32.41 |
| Arith. aver. | | 8.8 | 30.12 | 30.48 | 29.88 | 30.24 |
| Median | | 7.5 | 30.14 | 30.43 | 29.89 | 30.14 |
| SD | | 6.7 | 0.97 | 0.81 | 1.20 | 0.99 |
| MAD | | 1.8 | 0.65 | 0.50 | 0.66 | 0.69 |
| **Mean $C_3$ plants** (Vogts et al., 2009, this study) | | | | | | |
| Arith. aver. | | 10.7 | 30.00 | 30.39 | 29.81 | 30.06 |
| Median | | 8.7 | 29.97 | 30.36 | 29.85 | 30.04 |
| SD | | 7.1 | 0.9 | 0.8 | 1.1 | 0.9 |
| MAD | | 4.5 | 0.6 | 0.5 | 0.7 | 0.7 |
| **$C_4$ plants** | | | | | | |
| Cyperaceae | I | 2.7 | 31.15 | 31.54 | 31.29 | 31.82 |
| Cyperaceae | II | 4.4 | 30.70 | 31.30 | 29.73 | 30.70 |
| Cyperaceae | III | 2.7 | 30.50 | 31.17 | 30.66 | 31.39 |
| Poaceae | I | 3.8 | 29.87 | 30.79 | 29.25 | 29.87 |
| Poaceae | II | 4.7 | 30.99 | 31.29 | 30.95 | 31.36 |
| Poaceae | III | 4.8 | 30.72 | 31.04 | 31.20 | 31.20 |
| Poaceae | IV | 8.7 | 30.99 | 31.49 | 31.13 | 31.65 |
| Poaceae | V | 2.7 | 30.30 | 31.05 | 29.45 | 30.58 |
| Poaceae | VI | 5.7 | 30.46 | 30.85 | 30.44 | 30.60 |
| Poaceae | VII | 10.6 | 30.57 | 31.03 | 30.74 | 30.97 |
| Poaceae | VIII | 6.4 | 29.11 | 30.27 | 28.96 | 29.16 |
| Arith. aver. | | 5.2 | 30.49 | 31.07 | 30.35 | 30.85 |
| Median | | 4.7 | 30.57 | 31.05 | 30.66 | 30.97 |
| SD | | 2.5 | 0.6 | 0.4 | 0.8 | 0.8 |
| MAD | | 1.5 | 0.3 | 0.2 | 0.5 | 0.4 |
| **Mean $C_4$ plants** (Rommerskirchen et al., 2006b, this study) | | | | | | |
| Arith. aver. | | 11.8 | 30.62 | 31.16 | 30.69 | 30.75 |
| Median | | 9.4 | 30.76 | 31.16 | 30.83 | 30.85 |
| SD | | 8.9 | 0.8 | 0.5 | 0.9 | 0.9 |
| MAD | | 4.3 | 0.4 | 0.3 | 0.5 | 0.5 |

**Supplementary Table 2.S4:** *n*-Alkane content: Analysed plant families and photosynthetic pathway (PP), consecutive number for species per family (see Supplementary Table 2.S1) and content or relative abundance of $C_{24}$ to $C_{36}$ *n*-alkanes as well as arithmetic average (arithm. average), median, standard deviation (SD) and median absolute deviation (MAD) of the plant species analysed here ($C_3$ and $C_4$ plants) and total analysed African plant samples (mean $C_3$ or mean $C_4$ plants) compiled by Rommerskirchen et al. (2006b) and Vogts et al. (2009); DM - dry matter; n.d. - not determined.

| PP/ Family | No. | *n*-Alkane content (µg $g^{-1}$ DM) | | | | | | | | | | | | |
|---|---|---|---|---|---|---|---|---|---|---|---|---|---|---|
| | | $C_{24}$ | $C_{25}$ | $C_{26}$ | $C_{27}$ | $C_{28}$ | $C_{29}$ | $C_{30}$ | $C_{31}$ | $C_{32}$ | $C_{33}$ | $C_{34}$ | $C_{35}$ | $C_{36}$ |
| **$C_3$ plants** | | | | | | | | | | | | | | |
| Apiaceae | I | n.d. | 3.7 | n.d. | 7.8 | n.d. | 7.2 | n.d. | n.d. | n.d. | n.d. | n.d. | n.d. | n.d. |
| Asteraceae | I | 5.1 | 5.9 | 8.8 | 13.2 | 8.4 | 36.0 | 15.7 | 264.8 | 28.7 | 303.4 | 21.7 | 179.4 | 9.9 |
| Asteraceae | II | 1.9 | 4.1 | 2.1 | 23.6 | 5.3 | 68.3 | 4.7 | 44.0 | 1.7 | 7.1 | n.d. | n.d. | n.d. |
| Asteraceae | III | n.d. | n.d. | n.d. | 33.5 | n.d. | 80.3 | 28.1 | 101.6 | n.d. | 80.7 | n.d. | n.d. | n.d. |
| Asteraceae | IV | 5.2 | 6.6 | 4.1 | 10.8 | 5.3 | 66.0 | 11.7 | 102.3 | 4.4 | 9.0 | n.d. | 2.3 | n.d. |
| Asteraceae | V | n.d. | n.d. | 12.2 | 10.7 | 12.0 | 65.6 | 24.9 | 210.8 | 35.8 | 47.9 | n.d. | 11.7 | n.d. |
| Capparaceae | I | 3.8 | 9.6 | 3.8 | 7.9 | n.d. | 13.1 | 4.2 | 56.5 | 6.4 | 28.4 | n.d. | n.d. | n.d. |
| Combretaceae | I | 3.4 | 3.8 | 3.2 | 16.0 | 15.4 | 769.4 | 50.4 | 453.7 | 19.0 | 40.2 | 2.3 | 4.7 | n.d. |
| Combretaceae | II | 5.0 | 4.9 | 3.8 | 8.7 | 7.7 | 174.2 | 9.7 | 143.7 | 3.9 | 14.6 | n.d. | n.d. | n.d. |
| Combretaceae | III | 2.4 | 5.1 | 2.0 | 32.7 | 7.3 | 244.0 | 3.3 | 34.8 | 0.6 | 1.0 | n.d. | n.d. | n.d. |
| Commelinaceae | I | 16.0 | 20.3 | 8.3 | 29.7 | 14.3 | 58.3 | 31.8 | 222.9 | 41.0 | 102.5 | n.d. | 14.2 | n.d. |
| Crassulaceae | I | 4.4 | 3.3 | 1.8 | 4.3 | 2.6 | 9.6 | 3.9 | 71.6 | 17.2 | 194.8 | 12.5 | 42.5 | 1.8 |
| Euphorbiaceae | I | 0.6 | 0.5 | 0.6 | 0.6 | 0.6 | 2.3 | 0.7 | 4.5 | 0.5 | 1.0 | n.d. | n.d. | n.d. |
| Euphorbiaceae | II | 9.9 | 12.6 | 7.2 | 13.8 | 7.2 | 54.7 | 8.8 | 42.7 | 5.5 | 9.6 | n.d. | 3.3 | n.d. |
| Euphorbiaceae | III | 2.9 | 3.7 | 2.1 | 8.3 | 13.9 | 589.5 | 79.9 | 541.4 | 21.2 | 45.3 | n.d. | n.d. | n.d. |
| Fabaceae | I | 3.0 | 3.9 | 2.8 | 4.4 | 2.9 | 15.2 | 3.0 | 16.5 | n.d. | 7.9 | n.d. | n.d. | n.d. |
| Fabaceae | II | 4.8 | 10.5 | 6.3 | 15.7 | 5.6 | 21.9 | 4.8 | 40.2 | n.d. | 13.2 | n.d. | n.d. | n.d. |
| Fabaceae | III | 2.5 | 4.8 | 3.1 | n.d. | 2.7 | 7.5 | 2.2 | 9.2 | 2.1 | 1.6 | n.d. | n.d. | n.d. |
| Fabaceae | IV | 5.3 | 6.6 | 5.7 | 7.6 | 4.8 | 23.3 | 5.9 | 28.5 | 6.1 | 9.0 | 4.1 | 7.3 | 3.6 |
| Fabaceae | V | 7.2 | 11.8 | 8.9 | 25.1 | 7.7 | 38.4 | 6.0 | 26.2 | n.d. | 6.0 | n.d. | n.d. | n.d. |

**Supplementary Table 2.S4** (continued)

| PP/ Family | No. | *n*-Alkane content (µg $g^{-1}$ DM) | | | | | | | | | | | | |
|---|---|---|---|---|---|---|---|---|---|---|---|---|---|---|
| | | $C_{24}$ | $C_{25}$ | $C_{26}$ | $C_{27}$ | $C_{28}$ | $C_{29}$ | $C_{30}$ | $C_{31}$ | $C_{32}$ | $C_{33}$ | $C_{34}$ | $C_{35}$ | $C_{36}$ |
| Fabaceae | VI | 1.8 | 2.3 | n.d. | 3.1 | 1.9 | 13.2 | 2.1 | 29.6 | n.d. | 5.4 | n.d. | n.d. | n.d. |
| Fabaceae | VII | n.d. | 10.3 | n.d. | 18.6 | 11.2 | 51.3 | n.d. | 17.1 | n.d. | n.d. | n.d. | n.d. | n.d. |
| Fabaceae | VIII | 5.6 | 5.8 | 3.1 | 4.0 | 2.1 | 13.8 | 2.3 | 12.4 | n.d. | 3.1 | n.d. | n.d. | n.d. |
| Fabaceae | IX | 7.3 | 7.9 | 5.7 | 15.6 | 13.1 | 664.9 | 27.4 | 295.9 | 11.9 | 24.4 | 3.4 | 4.4 | 2.1 |
| Fabaceae | X | 7.3 | 10.0 | 6.3 | 36.7 | 7.6 | 101.8 | 6.3 | 18.9 | n.d. | n.d. | n.d. | n.d. | n.d. |
| Fabaceae | XI | 14.5 | 26.3 | 31.0 | 95.6 | 36.5 | 249.2 | 21.5 | 69.6 | 11.3 | 17.0 | n.d. | n.d. | n.d. |
| Fabaceae | XII | n.d. | n.d. | n.d. | 17.6 | 3.1 | 90.8 | 8.1 | 131.3 | 6.8 | 19.0 | n.d. | n.d. | n.d. |
| Fabaceae | XIII | 10.1 | 11.0 | 7.4 | 8.9 | 5.9 | 38.8 | 6.8 | 66.9 | n.d. | 15.5 | n.d. | n.d. | n.d. |
| Fabaceae | XIV | 4.2 | 5.9 | 5.2 | 20.7 | 17.1 | 156.7 | 15.0 | 45.8 | 7.4 | 6.2 | 4.0 | n.d. | 4.7 |
| Melastomataceae | I | 3.0 | 5.7 | 1.6 | 11.8 | 5.6 | 63.2 | 21.2 | 379.4 | 68.8 | 365.4 | 13.0 | 8.0 | n.d. |
| Melastomataceae | II | 12.9 | 26.7 | 8.1 | 31.0 | 14.1 | 85.8 | 32.9 | 762.1 | 90.5 | 513.1 | 12.7 | 3.7 | n.d. |
| Pedaliaceae | I | n.d. | 7.8 | 8.1 | 81.1 | 38.0 | 440.9 | 80.0 | 654.5 | 116.3 | 593.2 | 57.0 | 87.7 | n.d. |
| Plumbaginaceae | I | 9.6 | 15.1 | 5.4 | 11.4 | n.d. | 31.5 | 13.7 | 145.9 | 16.9 | 34.1 | n.d. | n.d. | n.d. |
| Proteaceae | I | 1.1 | 3.1 | 1.0 | 3.8 | 0.6 | 2.3 | 0.5 | 2.7 | n.d. | 0.7 | n.d. | n.d. | n.d. |
| Proteaceae | II | 1.9 | 3.1 | 1.4 | 2.9 | 0.8 | 3.6 | 0.7 | 1.3 | n.d. | 0.6 | n.d. | n.d. | n.d. |
| Ranunculaceae | I | 3.6 | 5.1 | 2.2 | 9.8 | 1.6 | 23.3 | 1.9 | 46.0 | n.d. | 2.8 | n.d. | n.d. | n.d. |
| Rubiaceae | I | 3.7 | 10.7 | 2.3 | 66.0 | 16.8 | 1213.4 | 42.8 | 2250.0 | 35.6 | 388.4 | 2.0 | 27.8 | n.d. |
| Scrophulariaceae | I | 9.7 | 14.8 | 13.1 | 20.3 | 10.1 | 46.6 | 14.7 | 97.4 | 13.5 | 54.7 | n.d. | n.d. | n.d. |
| Thymelaeaceae | I | n.d. | 14.1 | 9.7 | 26.9 | n.d. | 30.8 | n.d. | 31.1 | n.d. | n.d. | n.d. | n.d. | n.d. |
| Verbenaceae | I | 6.0 | 6.1 | 3.2 | 7.9 | 3.0 | 30.6 | 1.6 | 3.2 | n.d. | 1.0 | n.d. | n.d. | n.d. |
| Verbenaceae | II | 8.0 | 9.8 | 5.2 | 7.1 | 3.8 | 47.7 | 11.5 | 204.5 | 44.4 | 549.1 | 31.8 | 62.4 | 1.4 |
| Arith. aver. | | 5.7 | 8.5 | 5.7 | 19.4 | 8.8 | 140.1 | 16.1 | 192.0 | 23.7 | 95.1 | 15.0 | 32.8 | 3.9 |
| Median | | 4.9 | 6.3 | 4.6 | 12.5 | 6.5 | 47.7 | 8.4 | 61.7 | 12.7 | 15.5 | 12.5 | 9.9 | 2.9 |
| SD | | 3.8 | 6.0 | 5.4 | 20.3 | 8.5 | 249.6 | 19.6 | 380.8 | 28.9 | 168.9 | 16.8 | 49.5 | 3.2 |
| MAD | | 2.3 | 3.1 | 2.5 | 7.0 | 3.9 | 33.9 | 6.3 | 47.2 | 8.7 | 14.5 | 9.1 | 6.4 | 1.3 |

**Supplementary Table 2.S4** (continued)

| PP/ Family | No. | *n*-Alkane content (µg $g^{-1}$ DM) | | | | | | | | | | | | |
|---|---|---|---|---|---|---|---|---|---|---|---|---|---|---|
| | | $C_{24}$ | $C_{25}$ | $C_{26}$ | $C_{27}$ | $C_{28}$ | $C_{29}$ | $C_{30}$ | $C_{31}$ | $C_{32}$ | $C_{33}$ | $C_{34}$ | $C_{35}$ | $C_{36}$ |
| **Mean $C_3$ plants** (Vogts et al., 2009, this study) | | | | | | | | | | | | | | |
| | | Relative *n*-alkane abundance (%) | | | | | | | | | | | | |
| | | $C_{24}$ | $C_{25}$ | $C_{26}$ | $C_{27}$ | $C_{28}$ | $C_{29}$ | $C_{30}$ | $C_{31}$ | $C_{32}$ | $C_{33}$ | $C_{34}$ | $C_{35}$ | $C_{36}$ |
| Arith. aver. | | 2.0 | 4.2 | 2.1 | 9.5 | 2.8 | 31.3 | 3.0 | 30.3 | 2.6 | 10.4 | 0.5 | 1.1 | 0.2 |
| Median | | 1.1 | 2.8 | 1.2 | 6.9 | 2.3 | 24.3 | 2.7 | 29.7 | 2.2 | 5.5 | 0.2 | 0.3 | 0.0 |
| SD | | 2.3 | 4.7 | 2.1 | 9.9 | 2.1 | 20.1 | 1.6 | 15.3 | 2.0 | 11.9 | 0.8 | 2.5 | 0.5 |
| MAD | | 0.8 | 2.1 | 0.9 | 4.7 | 1.4 | 12.3 | 1.0 | 11.8 | 1.1 | 3.6 | 0.2 | 0.3 | 0.0 |
| **$C_4$ plants** | | | | | | | | | | | | | | |
| Cyperaceae | I | 22.1 | 19.2 | 17.5 | 16.2 | 16.2 | 29.3 | 16.5 | 67.3 | 18.9 | 75.6 | 11.5 | 39.8 | 8.8 |
| Cyperaceae | II | 12.2 | 11.7 | 8.3 | 7.9 | 5.8 | 9.8 | n.d. | 22.2 | n.d. | 17.0 | n.d. | n.d. | n.d. |
| Cyperaceae | III | 11.3 | 17.6 | 7.3 | 17.5 | 7.9 | 28.7 | 9.7 | 26.8 | 10.4 | 36.2 | 12.8 | 27.0 | 23.7 |
| Poaceae | I | 13.0 | 15.7 | 13.2 | 26.2 | 10.8 | 26.9 | 6.7 | 36.9 | n.d. | 18.2 | n.d. | n.d. | n.d. |
| Poaceae | II | 5.2 | 6.9 | 5.0 | 6.2 | 5.6 | 11.7 | 6.3 | 48.4 | 3.8 | 23.8 | n.d. | 9.1 | n.d. |
| Poaceae | III | n.d. | n.d. | 7.6 | 12.1 | 8.8 | 33.4 | 10.8 | 73.1 | 7.5 | 36.2 | n.d. | 19.5 | n.d. |
| Poaceae | IV | 7.5 | 43.0 | 8.9 | 47.4 | 12.1 | 97.7 | 13.0 | 88.3 | 11.2 | 190.8 | 11.0 | 83.9 | n.d. |
| Poaceae | V | 5.3 | 8.2 | 6.2 | 7.9 | 5.4 | 9.1 | 5.7 | 16.0 | n.d. | 9.9 | n.d. | n.d. | n.d. |
| Poaceae | VI | 4.8 | 6.8 | 7.1 | 22.9 | 12.3 | 50.1 | 15.3 | 119.3 | 6.4 | 34.9 | n.d. | 7.2 | n.d. |
| Poaceae | VII | 6.2 | 8.7 | 5.6 | 23.1 | 5.2 | 54.2 | 5.1 | 67.3 | 4.5 | 56.9 | n.d. | 20.1 | n.d. |
| Poaceae | VIII | 4.2 | 3.9 | 6.0 | 36.9 | 7.5 | 36.5 | 3.1 | 19.0 | n.d. | 11.8 | n.d. | n.d. | n.d. |
| Arith. aver. | | 9.2 | 14.2 | 8.4 | 20.4 | 8.9 | 35.2 | 9.2 | 53.1 | 9.0 | 46.5 | 11.8 | 29.5 | 16.2 |
| Median | | 6.8 | 10.2 | 7.3 | 17.5 | 7.9 | 29.3 | 8.2 | 48.4 | 7.5 | 34.9 | 11.5 | 20.1 | 16.2 |
| SD | | 5.6 | 11.3 | 3.7 | 12.9 | 3.6 | 25.5 | 4.6 | 33.0 | 5.2 | 51.8 | 0.9 | 26.4 | 10.6 |
| MAD | | 2.3 | 4.4 | 1.3 | 8.8 | 2.4 | 17.7 | 2.8 | 24.7 | 2.9 | 17.8 | 0.5 | 10.9 | 7.5 |

**Supplementary Table 2.S4** (continued)

| | *n*-Alkane content (µg $g^{-1}$ DM) | | | | | | | | | | | | |
|---|---|---|---|---|---|---|---|---|---|---|---|---|---|
| | $C_{24}$ | $C_{25}$ | $C_{26}$ | $C_{27}$ | $C_{28}$ | $C_{29}$ | $C_{30}$ | $C_{31}$ | $C_{32}$ | $C_{33}$ | $C_{34}$ | $C_{35}$ | $C_{36}$ |
| **Mean $C_4$ plants** (Rommerskirchen et al., 2006b, this study) | | | | | | | | | | | | | |
| | Relative *n*-alkane abundance (%) | | | | | | | | | | | | |
| | $C_{24}$ | $C_{25}$ | $C_{26}$ | $C_{27}$ | $C_{28}$ | $C_{29}$ | $C_{30}$ | $C_{31}$ | $C_{32}$ | $C_{33}$ | $C_{34}$ | $C_{35}$ | $C_{36}$ |
| Arith. aver. | n.d. | n.d. | 0.9 | 12.6 | 1.3 | 17.5 | 1.6 | 35.3 | 1.2 | 25.3 | 0.7 | 5.9 | 0.5 |
| Median | n.d. | n.d. | 0.0 | 9.6 | 0.0 | 16.5 | 0.0 | 34.2 | 0.0 | 23.8 | 0.0 | 4.1 | 0.0 |
| SD | n.d. | n.d. | 1.7 | 10.6 | 1.9 | 8.3 | 2.3 | 12.7 | 2.0 | 14.1 | 1.8 | 5.8 | 1.7 |
| MAD | n.d. | n.d. | 0.0 | 4.5 | 0.0 | 5.0 | 0.0 | 7.8 | 0.0 | 10.4 | 0.0 | 3.6 | 0.0 |

# 3. *n*-Alkane parameters from a deep sea sediment transect off southwest Africa reflect continental vegetation and climate conditions

Angela Vogts [a,1]*, Enno Schefuß [b], Tanja Badewien [a], Jürgen Rullkötter [a]

[a] Institute for Chemistry and Biology of the Marine Environment (ICBM), Carl von Ossietzky University of Oldenburg, Germany
[b] Marum, Center for Marine Environmental Sciences, University of Bremen, Germany
[1] Present address: Leibniz Institute for Baltic Sea Research Warnemünde, Seestraße 15, D-18119 Warnemünde, Germany

* Corresponding author. Tel.: +49 381 5197 353; Fax: +49-381-5197 440.
E-mail address: angela.vogts@io-warnemuende.de (Angela Vogts).

This chapter is published in Organic Geochemistry 47, 109-119 (2012).

## 3.1. Abstract

An isobathic transect of marine surface sediments from 1°N to 28°S off southwest Africa was used to further evaluate the potential of the chain length distribution and carbon stable isotope composition of higher plant *n*-alkanes as proxies for continental vegetation and climate conditions. We found a strong increase in the *n*-$C_{29-33}$ weighted mean average $\delta^{13}C$ values from -33‰ near the equator to around -26‰ further south. Additionally, $C_{25-35}$ *n*-alkanes reveal a southward trend of increasing average chain length from 30.0 to 30.5. The data reflect the changing contribution of plants employing different photosynthetic pathways ($C_3$ and $C_4$) and/or being differently influenced by the environmental conditions of their habitat. The $C_4$ plant proportions calculated from the data (ca. 20% for rivers draining the rain forest, to ca. 70% at higher latitude) correspond to the $C_4$ plant abundance in continental catchment areas postulated by considering prevailing wind systems and river outflows. Furthermore, the $C_4$ plant contribution to the sediments correlates with the mean annual precipitation and aridity at selected continental locations in the postulated

catchment areas, suggesting that the $C_4$ plant fraction in marine sediments can be used to assess these environmental parameters.

## 3.2. Introduction

Land plant biomarkers in undisturbed sedimentary archives of ocean margins provide useful information about past vegetation and its climate-dependent variation on the adjacent continent. In previous studies, constituents of epicuticular waxes and their isotopic signatures were employed to unravel the influence of climate change on continental vegetation (e.g. Rommerskirchen et al., 2003, 2006a; Schefuß et al., 2003a, 2005; Zhao et al., 2003; McDuffee et al., 2004; Feakins et al., 2005; Weijers et al., 2007; Niedermeyer et al., 2010; Tierney et al., 2010a,b). Epicuticular wax covers all aerially exposed organs of higher land plants, and in virtually all cases they contain long chain *n*-alkanes, which are the focus of this study. After plant decay, the *n*-alkanes can persist in soil or are, mainly in association with particulate matter, transported by wind and rivers to ocean sediments.

Higher plant *n*-alkanes occur typically in the $C_{25}$-$C_{35}$ range (Chibnall et al., 1934) with an odd/even carbon number predominance (Eglinton and Hamilton, 1967). It was suggested that plants in arid tropical and subtropical climates biosynthesise longer chain wax components than those in habitats of temperate regions (Gagosian and Peltzer, 1986); this would make their chain length distribution a potentially useful proxy parameter for climatedependent vegetation change.

The carbon stable isotope composition of *n*-alkanes is a specific feature related to $CO_2$ fixation pathway. Nearly 90% of the estimated 250,000 land plant species, i.e. almost all woody species of temperate and wet tropical regions (Sage, 2001), use the $C_3$ pathway (Calvin-Benson-Bassham Cycle; Bassham et al., 1954). The $C_4$ metabolism (Hatch-Slack-Cycle; Hatch and Slack, 1966) is an elaboration of the Calvin-Benson-Bassham Cycle and pre-concentrates $CO_2$ by way of a complex biochemical process (Hatch, 1987). This $CO_2$ concentrating mechanism prevents ineffective photorespiration and improves water use efficiency under environmental stress, notably high temperature, light intensity or salinity, limited water supply and/or low $CO_2$ concentration (Downes, 1969; Björkmann, 1976). Since extra energy is needed for the two-step process, $C_4$ plants successfully outcompete $C_3$ plants only in areas such as sunny subtropical and tropical savannas (Sage, 2004). The different $CO_2$ fixation pathways cause characteristic differences in the carbon stable isotope composition of leaf wax lipids of -29‰ to -39‰ in $C_3$ and -14‰ to -26‰ in $C_4$ plants, respectively (Bi et al., 2005 and references therein).

Crassulacean acid metabolism (CAM) is a less common elaboration of the

$C_3$ pathway (Winter et al., 2005) and is mostly used by plants populating environmental niches, e.g. desert succulents and tropical epiphytes (Keeley and Rundel, 2003). As this pathway is generally a strategy for stress survival and not for high productivity, the contribution of CAM plants to biomass production is low (Lüttge, 2004).

This study elucidates *n*-alkane characteristics in modern southeast Atlantic Ocean margin sediments reflecting the contribution of $C_3$ and $C_4$ plants from the adjacent African continent. Furthermore, we evaluate if the $C_4$ plant abundance can be correlated with major climatic parameters (mean annual precipitation and aridity). The information is essential for reconstruction of palaeovegetation and palaeoclimatic change. To reach this goal, we analysed a transect of sediments off southwest Africa (1°N to 28°S) for their *n*-alkane distribution patterns and the molecular carbon stable isotope composition of these biomarkers. Based on experiences from previous transect studies (Rommerskirchen et al., 2003), only surface sediments from similar

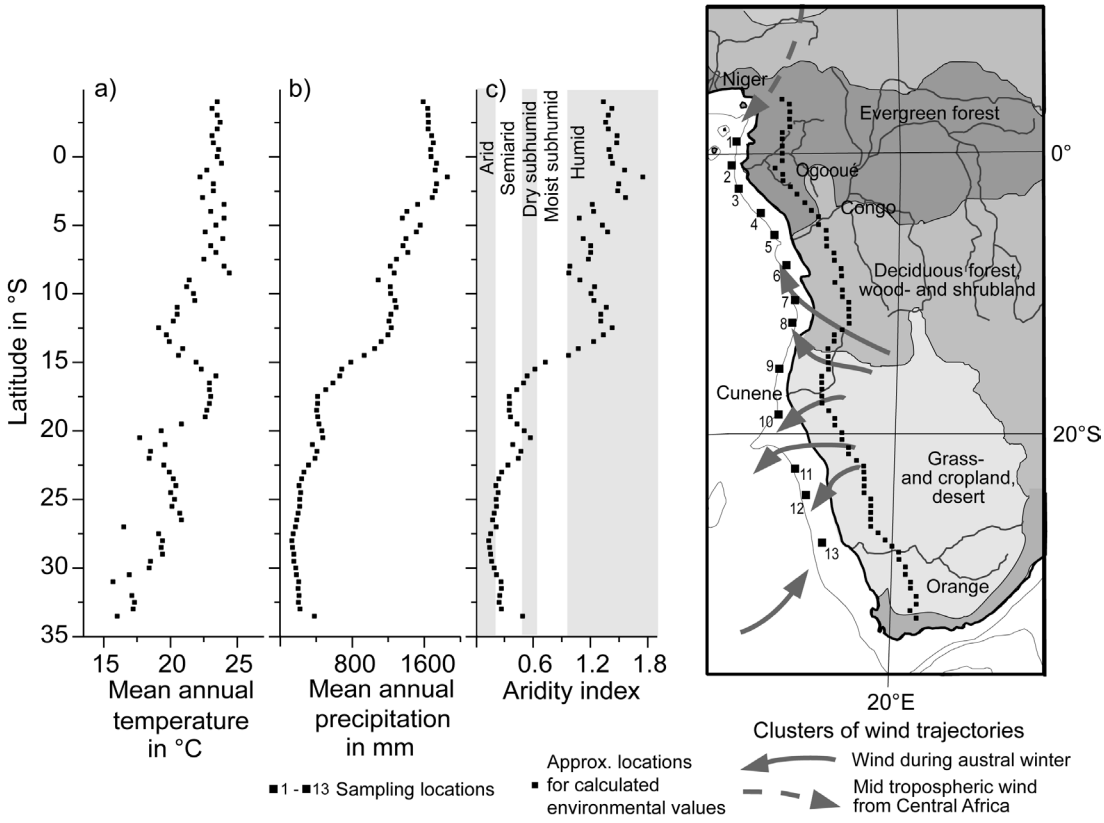


**Fig. 3.1:** Simplified present-day land cover based on map of Mayaux et al. (2004), with generalised wind directions (Dupont and Wyputta, 2003) and sampling locations, as well as continental environmental conditions with (a) mean annual precipitation, (b) mean annual temperature and (c) aridity index calculated as quotient of mean annual precipitation and potential evapotranspiration according to UNEP (1992). All environmental parameters were calculated for locations with ca. 350 km distance to the coast using the WebWIMP modeling program (Matsuura et al., 2009). Exact locations and values: Supplementary Table 3.S1.

water depth were used to minimise possible effects of different transport distances from the continent or water column height on organic matter (OM) alteration.

## 3.3. Material and methods

### 3.3.1. Sediment material

We analysed 13 marine surface sediment samples that constitute an isobathic (ca. 1300 m water depth) north to south transect (1°N to 28°S) along the south-western African continental margin. The samples were retrieved during cruises M34/2 and M41/1 of the German research vessel Meteor in 1996 and 1998, respectively, and recovered by way of multi-corer to obtain undisturbed sediment surfaces. Sampling locations are displayed in Fig. 3.1 and general sample information is in Table 3.1. The multicores were separated into depth intervals, sealed in polyethylene bags and stored at -20°C on board and afterwards at the University of Bremen. Material from the topmost available sediment layers (up to 3.5 cm depth; Table 3.1) was freeze dried and finely ground prior to analysis.

### 3.3.2. Analytical methods

#### *3.3.2.1. Bulk parameters*

Total organic carbon (TOC) content was determined as the difference between total C measured with a Vario EL Cube combustion instrument and inorganic C analysed via a UIC $CO_2$-coulometer. For C stable isotope analysis of bulk OM, carbonate was dissolved by repeated addition of HCl (2 mol $l^{-1}$) and drying of the samples at 50°C without washing, because washing has been reported to alter the carbon stable isotope ratio of sedimentary OM (Schubert and Nielsen, 2000). For analysis, a Carlo Erba Elemental Analyser 1108 was coupled to a Finnigan MAT 252 isotope ratio mass spectrometer. Isotope composition is expressed as $\delta^{13}C$ values in ‰ relative to Vienna-Pee Dee Belemnite (V-PDB). Calibration was performed by injecting several pulses of $CO_2$ reference gas at the beginning and the end of each run. The carbon stable isotope composition of the reference gas was calibrated from measurements of certified standard material (IVA, high OC sediment standard, -26.1‰). This certified standard was also measured between sample runs for quality control with a result of -26.1 ± 0.2‰ (n= 12). Samples were run at least in duplicate. Results for bulk parameters are given in Table 3.1 for information.

**Table 3.1:** Sample information and analytical data for bulk material with standard deviation (1σ).

| No. | GeoB No. | Latitude | Longitude | Water depth (m) | Cruise | Interval (cm bsf)[a] | TOC (%) | TIC (%) | $\delta^{13}C_{OM}$ (‰) |
|---|---|---|---|---|---|---|---|---|---|
| 1 | 4904-6 | 0.962°N | 8.88°E | 1349 | M41/1 | 0.5 - 2 | 2.65 ± 0.02 | 0.91 ± 0.01 | -20.3 ± 0.3 |
| 2 | 4906-4 | 0.69°S | 8.378°E | 1272 | M41/1 | 1 - 2 | 3.04 ± 0.04 | 0.34 ± 0.04 | -22.0 ± 0.2 |
| 3 | 4909-3 | 2.068°S | 8.625°E | 1305 | M41/1 | 0 - 1.5 | 2.27 ± 0.07 | 1.53 ± 0.03 | -20.5 ± 0.2 |
| 4 | 4912-3 | 3.73°S | 09.785°E | 1298 | M41/1 | 0 - 1 | 2.33 ± 0.02 | 1.39 ± 0.02 | -20.3 ± 0.2 |
| 5 | 4913-3 | 5.503°S | 11.072°E | 1296 | M41/1 | 0 - 2.5 | 3.33 ± 0.01 | 0.02 ± 0.01 | -22.4 ± 0.2 |
| 6 | 4915-2 | 7.75°S | 11.873°E | 1306 | M41/1 | 0.5 - 2 | 2.94 ± 0.04 | 0.11 ± 0.02 | -20.8 ± 0.1 |
| 7 | 4916-3 | 10.173°S | 12.687°E | 1294 | M41/1 | 0 - 1 | 4.08 ± 0.02 | 0.21 ± 0.02 | -20.8 ± 0.2 |
| 8 | 4917-4 | 11.903°S | 13.073°E | 1300 | M41/1 | 0.5 - 2.5 | 3.85 ± 0.00 | 0.39 ± 0.00 | -20.6 ± 0.2 |
| 9 | 3713-1 | 15.628°S | 11.58°E | 1330 | M34/2 | 1.5 - 2.5 | 1.51 ± 0.03 | 0.55 ± 0.02 | -19.6 ± 0.2 |
| 10 | 3715-2 | 18.955°S | 11.057°E | 1203 | M34/2 | 1 - 3.5 | 4.52 ± 0.05 | 3.12 ± 0.03 | -19.7 ± 0.1 |
| 11 | 3706-3 | 22.717°S | 12.602°E | 1313 | M34/2 | 0.5 - 1.5 | 4.05 ± 0.05 | 8.02 ± 0.03 | -20.5 ± 0.3 |
| 12 | 3705-3 | 24.303°S | 12.997°E | 1308 | M34/2 | 0.5 - 2 | 4.24 ± 0.10 | 8.40 ± 0.07 | -20.9 ± 0.3 |
| 13 | 3701-1 | 27.952°S | 14.003°E | 1488 | M34/2 | 0.5 - 1.5 | 1.13 ± 0.10 | 9.38 ± 0.10 | -19.5 ± 0.3 |

[a] Sediment interval in cm below sea floor (bsf).

#### *3.3.2.2. Sample extraction and compound isolation*

Sediment (9-23 g, depending on TOC content) was extracted with $CH_2Cl_2$ and MeOH (9/1, v/v; 3 x 5 min, 70 bar, 100°C) using an accelerated solvent extractor (ASE 200, Dionex). Completeness of extraction was checked on random samples by way of repeated extraction. Squalane was added to the extracts as an internal standard. After removal of solvent, the extracts were re-dissolved in *n*-hexane and insoluble components removed by filtration over $NaSO_4$. The aliphatic/alicyclic hydrocarbons were separated from the *n*-hexane-soluble fraction using medium pressure liquid chromatography (Radke et al., 1980). Prior to analysis, methyl docosanate was added to the hydrocarbon fraction as injection standard.

#### *3.3.2.3. Gas chromatography (GC)*

The hydrocarbon fractions were analysed using GC with an Agilent 6890 instrument equipped with a cold injection system (Gerstel KAS 4), a high-temperature column (J&W, DB-5HT, 30 m x 0.25 mm i.d., 0.1 µm film thickness) and a flame ionisation detector (FID). The injector temperature was programmed from 60°C (held 5 s) to 350°C (held 60 s) at 10°C $s^{-1}$. He was used as carrier gas, and the GC oven was programmed from 60 °C (held 2 min) to 350°C (held 15 min) at 3°C $min^{-1}$. The *n*-alkanes were identified by comparison of relative retention times with standard mixtures, and abundances were calculated as µg $g^{-1}$ sediment dry wt. on the basis of signal intensity relative to that of the internal standard (squalane) in the GC-FID traces. Recovery was 85% or better. The difference in response between homologues of different chain length and internal standard was negligible (coefficient of variation <6%), and no trend in response factors with chain length was observed.

#### *3.3.2.4. Carbon stable isotope composition*

The *n*-alkanes were separated from the branched and cyclic saturated hydrocarbons using urea adduction (Rommerskirchen et al., 2006b). Carbon stable isotope compositions were determined using a gas chromatograph (HP 5990) coupled to a Finnigan MAT 252 isotope ratio mass spectrometer via a combustion interface (GCC-II). The GC conditions were similar to those for quantification with the exception that the injector temperature was programmed from 60°C (held 5 s) to 325°C (held 120 s) at 10°C $s^{-1}$ and the GC oven from 60°C (held 2 min) to 325°C (held 41 min) at 3°C $min^{-1}$.

Calibration was performed by injecting several pulses of $CO_2$ reference gas at the beginning and the end of each run. The carbon stable isotope composition

of the reference gas was calibrated by measurements of certified standard mixtures. For quality control certified and lab standards (long chain alkanes and methyl alkanoates) were measured between sample runs. Additionally, the lab standard methyl docosanate of known carbon stable isotope composition (-30‰) was added to the samples and used for quality control ($\delta^{13}C$ of -29.8‰ ± 0.5‰, n= 40). Samples were run at least in duplicate.

### 3.3.3. Models and maps employed

#### *3.3.3.1. WebWIMP modeling program for climatic parameters*

The WebWIMP modeling program (Matsuura et al., 2009) was used to calculate annual mean temperature, precipitation and potential evapotranspiration. It calculates climatically averaged monthly water balance for continental locations at nodes of a one half of a degree of latitude by one half of a degree of longitude grid. Average monthly air temperature and precipitation data for weather stations are interpolated to the grid nodes and the grid point water balance is calculated with a modified Thornthwaite procedure. A limitation of the model may be the uneven spatial distribution of weather stations, especially in Africa. Furthermore, the weather records partly cover different years and different time spans (Willmott et al., 1985).

#### *3.3.3.2. Map of $C_4$ plant abundance on the continent*

The map with 1 km resolution displaying the $C_4$ plant abundance on the continent (Still and Powell, 2010) is based on a pattern of regions favourable for $C_4$ vegetation and satellite-based growth from fields, estimating the annual % cover by (i) small species, (ii) trees higher than 5 m ($C_3$ cover) and (iii) bare soil. Plants smaller than 5 m were further differentiated into a shrub layer ($C_3$ cover) and herbaceous species including grass ($C_4$ species) with the aid of a satellite-derived land cover map (Mayaux et al., 2004). A limitation of the approach is its slight overestimation of the $C_4$ plant abundance in some regions because it does not differentiate between herbaceous $C_4$ and $C_3$ species. Furthermore, it does not take into account the amount of biomass produced.

## 3.4. Regional setting

### 3.4.1. Environmental conditions in southwest Africa

Southwest Africa is characterised by a distinct topography. From the equatorial Congo Basin (usually <500 m) the elevation increases towards the South African

Plateau, reaching an average of 1000 m at about 10°S. Lower elevation occurs in a narrow strip along the coast separated from the plateau by a steep slope.

In order to depict the climatic conditions in the study area, the WebWIMP modeling program (Matsuura et al., 2009) was employed for locations from 4°N to 33.5°S (0.5° steps) at ca. 350 km distance to the coast (data compiled in Supplementary Table 3.S1). This distance was chosen to avoid an influence of coastal climate, such as cold coastal temperatures in regions of coastal upwelling. On a large scale, mean annual temperature, precipitation and aridity index (calculated according to UNEP, 1992) decrease from the equator to the south (Fig. 3.1a-c). Based on the aridity indices the climate is defined as being humid in central Africa. South of ca. 14°S the climate becomes drier and spans dry sub-humid and semiarid to arid locations. Only in the southernmost part of the continent does one see increases in the temperature, precipitation and aridity indices again.

### 3.4.2. Vegetation in southwest Africa

The central African rain forest vegetation is characterised by woody $C_3$ plants as the major representatives of the flora (Richards, 1996). This evergreen rain forest extends to about 9°S and is increasingly confined to river valleys towards its limits. Dry evergreen forests and, further south, forests with deciduous plants then gain importance. The closed forest (no grass cover) often abruptly passes into a wide zone of savanna, wood- and shrubland (Richards, 1996). In the savannas, deciduous woody species can cover up to 60% of the area (Cole, 1986), but the amount of woody $C_3$ vegetation decreases with increasing aridity at the expense of increasing $C_4$ grass abundance. In the semi-deserts on the African Plateau (Kalahari and Nama Karoo) $C_4$ grass dominates the vegetation, while in the dry coastal Namib Desert, the vegetation is very sparse and in the Succulent Karoo succulent plants dominate. Towards the Cape region woody $C_3$ vegetation becomes abundant again.

### 3.4.3. Transport pathways for plant wax lipids

#### *3.4.3.1. Aeolian transport*

Aeolian transport pathways of terrestrial components were calculated by Dupont and Wyputta (2003) for wind borne material reaching sediments off southwest Africa (6°S to 30°S; implemented in Fig. 3.1). They estimated the origin of the transported material by backwards modelled trajectories and found a good correspondence between the distribution patterns of pollen in marine surface sediments and the occurrence of the source plants on the continent. During austral summer, winds

blow from the Atlantic towards the continent or parallel to the coast. Thus, there is little transport of terrestrial material to the ocean during this season. Only for the equatorial sites is there some mid-tropospheric transport by Harmattan winds from north-central Africa. The main seaward transport from the continent occurs during austral fall and winter when easterly and southeasterly winds prevail. South of 25°S, winds blow mostly from the west and southwest, so the aeolian supply of terrigenous material is very low. There may be some potential for long-range transport from South America but neither mid- nor low-tropospheric trajectories calculated by Dupont and Wyputta (2003) pass over parts of the South American continent.

#### *3.4.3.2. Riverine transport*

In contrast to the coverage of wide ocean areas by wind, most of the fluvially transported material is deposited near river mouths (Burdige, 2005). Rivers transport large amounts of dissolved and particulate organic matter to the oceans, and it has been shown that *n*-alkanes in marine sediments off rivers reflect the vegetation in their catchment areas (Bird et al., 1995; Schefuß et al., 2004; Weijers et al., 2009). In the study area, the Congo River system is the largest and the second biggest in the world regarding the outflow at the mouth (Dai and Trenbeth, 2002). The outflow of other rivers in the study area is lower by a factor of ca. 10 for the Ogooué (ca. 1°S) and the Orange (28.5°S) and by a factor of ≥50 for other rivers (e.g. Kunene, 17°S; Heyns, 2003; Nilsson et al., 2005). However, the river outflow data reflect only the quantity of water and not the amount of *n*-alkanes. Directly determined quantitative data for *n*-alkane discharge to ocean sediments by these rivers are not available.

## 3.5. Results and discussion

### 3.5.1. *n*-Alkane composition

#### *3.5.1.1. Absolute abundance*

Long chain *n*-alkanes in the range $C_{25}$-$C_{35}$ had a summed abundance between 0.9 and 4.7 mg $kg^{-1}$ sediment dry wt. (Table 3.2). The lowest abundance was determined for the southernmost site, likely a result of the low offshore transport of terrestrial material due to the prevailing westerly winds, in agreement with findings by Rommerskirchen et al. (2003). The abundances were highest off the Ogooué and Congo River mouths, reflecting the massive transport of terrestrial material by these river systems, as also observed by Schefuß et al. (2004).

**Table 3.2:** Data for major terrestrial *n*-alkanes.

| No. | *n*-Alkane content (µg $kg^{-1}$ dry wt.) [a] | | | | | | | | | | | $\Sigma_{25\text{-}35}$ (mg $kg^{-1}$ dry wt.) | $CPI_{27\text{-}33}$ [b] | $ACL_{25\text{-}33}$ [c] | $ACL_{25\text{-}35}$ [c] |
|---|---|---|---|---|---|---|---|---|---|---|---|---|---|---|---|
| | 25 | 26 | 27 | 28 | 29 | 30 | 31 | 32 | 33 | 34 | 35 | | | | |
| 1 | 142 | 109 | 296 | 159 | **1030** | 188 | 939 | 138 | 452 | 54.9 | 120 | 3.63 | 4.81 | 29.8 | 30.0 |
| 2 | 161 | 114 | 337 | 203 | **1440** | 266 | 1230 | 210 | 510 | 94.4 | 161 | 4.73 | 4.49 | 29.8 | 30.1 |
| 3 | 99.4 | 74.2 | 193 | 115 | **775** | 140 | 673 | 108 | 302 | 48.2 | 94.9 | 2.62 | 4.58 | 29.8 | 30.0 |
| 4 | 85.0 | 66 | 170 | 106 | **606** | 123 | 546 | 96.4 | 272 | 42.3 | 85.9 | 2.20 | 4.21 | 29.8 | 30.1 |
| 5 | 229 | 145 | 370 | 213 | **1170** | 245 | 1010 | 186 | 486 | 66.8 | 169 | 4.29 | 4.06 | 29.7 | 29.9 |
| 6 | 128 | 95.7 | 227 | 145 | **686** | 142 | 575 | 102 | 292 | 37.3 | 96.3 | 2.53 | 3.92 | 29.6 | 29.8 |
| 7 | 148 | 88.9 | 265 | 133 | **843** | 145 | 766 | 119 | 441 | 47.7 | 153 | 3.15 | 4.98 | 29.8 | 30.1 |
| 8 | 114 | 63.8 | 203 | 90.7 | **621** | 92.9 | 596 | 84.9 | 377 | 36.9 | 123 | 2.40 | 5.64 | 29.9 | 30.2 |
| 9 | 74.6 | 42.6 | 133 | 55.3 | 340 | 55.0 | **524** | 57.3 | 356 | 23.9 | 87.0 | 1.75 | 6.75 | 30.2 | 30.5 |
| 10 | 125 | 61.1 | 210 | 85.5 | 504 | 96.3 | **915** | 92.3 | 568 | 38.1 | 125 | 2.82 | 6.79 | 30.2 | 30.5 |
| 11 | 68.3 | 41.8 | 93.8 | 43.5 | 231 | 50.0 | **494** | 46.6 | 278 | 23.3 | 62.5 | 1.43 | 6.38 | 30.2 | 30.5 |
| 12 | 75.7 | 47.2 | 101 | 56.9 | 254 | 59.8 | **575** | 56.5 | 310 | 26.4 | 66.8 | 1.63 | 5.93 | 30.3 | 30.5 |
| 13 | 46.8 | 28.6 | 57.1 | 35.0 | 119 | 39.1 | **327** | 37.1 | 159 | 25.7 | 40.0 | 0.91 | 4.79 | 30.2 | 30.5 |

[a] Bold values for individual *n*-alkanes refer to distribution pattern maxima.

[b] $CPI_{27\text{-}33} = 0.5*\Sigma(X_{27}\text{-}X_{33})/(X_{26}\text{-}X_{32})+0.5*\Sigma(X_{27}\text{-}X_{33})/(X_{28}\text{-}X_{34})$, where X is abundance.

[c] $ACL_{n\text{-}m} = \Sigma(i*Xi)/\ \Sigma Xi$, where X is abundance and i ranges from n to m.

### *3.5.1.2. Carbon preference index (CPI)*

The $C_{27}$-$C_{33}$ *n*-alkanes showed a strong odd/even predominance of >3.9 (carbon preference index, $CPI_{27\text{-}33}$; Table 3.2; note: range selected to match that of the other studies referred to) typical for their origin from higher land plant wax and similar to the values found by Rommerskirchen et al. (2003) and Schefuß et al. (2004) for the same area. In contrast, McDuffee et al. (2004) reported lower $CPI_{27\text{-}33}$ values of 1.3-2.7 for *n*-alkanes in sediments from the same or very similar locations and water depth. But McDuffee et al. (2004) employed a different work-up procedure, including saponification of the sediment, isolation of the *n*-alkanes with molecular sieve (subsequently liberated by HF digestion), and removal of unsaturated hydrocarbons by oxidation with $RuO_4$, although none of these steps should influence the CPI of alkanes. Our analytical protocol did not include removal of unsaturated hydrocarbons but in our samples *n*-alkenes were not abundant and do not co-elute with the *n*-alkanes under the GC conditions employed.

A distinct trend in CPI values from ca. 4 in the north to values near 7 off savannah regions was observed (Fig. 3.2a). A changing contamination with natural petroleum or refinery products, contributing homologous series of *n*-alkanes with low

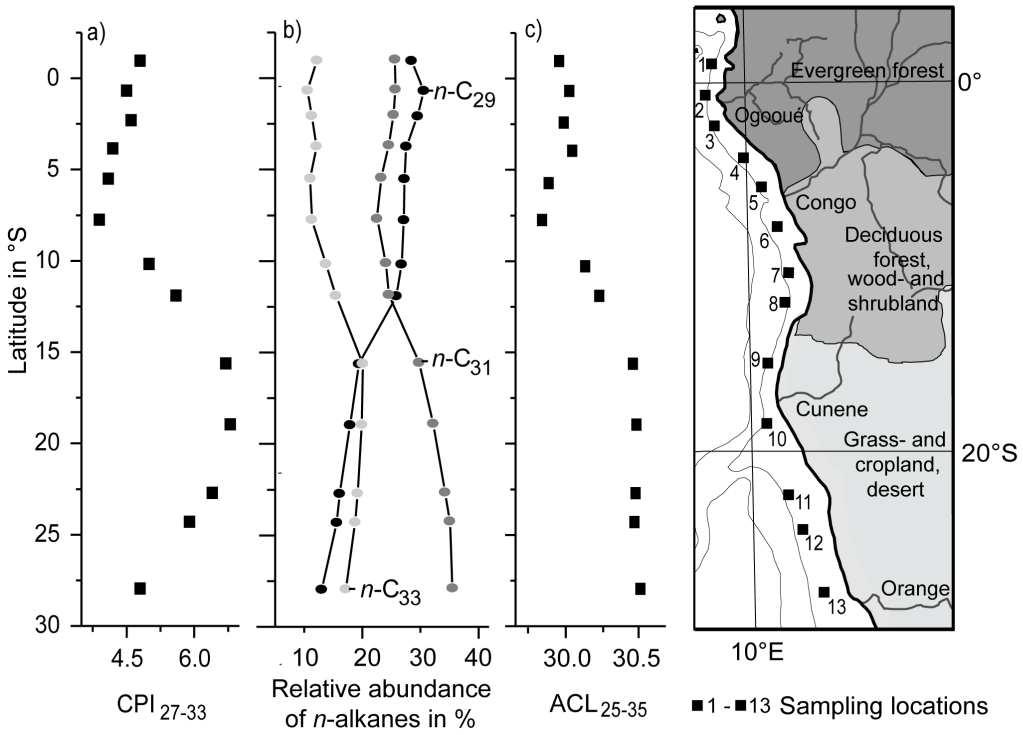


**Fig. 3.2:** Simplified present-day land cover based on Mayaux et al. (2004) with sampling locations of the north to south transect and graphs of sediment analysis results with (a) CPI for *n*-alkanes with 27-33 carbon atoms ($CPI_{27\text{-}33}$), (b) relative abundance of individual *n*-alkanes and (c) ACL for *n*-$C_{25}$ to *n*-$C_{35}$ alkanes ($ACL_{25\text{-}35}$).

CPI values (ca. 1) could explain the trend. But even though mass spectral analysis showed the presence of minor amounts of 17α-hopanes, indicating fossil material, the 17α-hopane abundance was similar for the samples with lowest and highest CPI values. Moreover, the occurrence of small amounts of mature polycyclic saturated hydrocarbon biomarkers in ocean surface sediments without corresponding oil-like *n*-alkanes is quite common and has been attributed to an admixture of eroded material from land (e.g. Rullkötter et al., 1984). The contribution of *n*-alkanes from eroded older terrestrial material is assumed to be low because previous studies showed that dust and sediment samples off southwest Africa predominantly mirrored recent continental vegetation (Rommerskirchen et al., 2003; Schefuß et al., 2003b, 2004). Furthermore, the leaf wax signal of present vegetation or OM of contemporary soils can be assumed to rapidly overprint contributions from older sediments or soils or from anthropogenic components (Simoneit et al., 1988; Simoneit, 1997; Schefuß et al., 2003b).

Alternatively, the trend in CPI values may be caused by plants exhibiting different *n*-alkane CPI values. Analysis of rain forest and savannah $C_3$ plants did not, however, reveal statistically significant differences in *n*-alkane CPI ratio (Vogts et al., 2009). Thus, the most likely cause for the trend in CPI values is the extent of degradation taking place after the decay of plants and/or their wax-containing parts. In eastern China, Rao et al. (2009) observed higher *n*-alkane CPI values in colder and drier areas vs. wetter and warmer tropical soils, i.e. moisture – not unexpectedly – appears to be required for rapid (microbial) degradation. This corresponds to our observation that higher values were observed off drier regions than off the moist rain forests. There may be an additional effect on CPI due to transport pathways. In particular, the southern sites receive mainly aeolian material presumably removed directly from the plant by sand blasting during storms (Cleugh et al., 1998) or by evaporation during forest fires (Simoneit et al., 1977). The *n*-alkane distributions in these cases are assumed to remain relatively unchanged, i.e. close to the plant wax composition.

#### *3.5.1.3. Chain length distribution*

The $C_{29}$, $C_{31}$ and $C_{33}$ *n*-alkanes had the highest abundance in all transect samples. Distinct trends in their relative abundance are displayed in Fig. 3.2b. The abundance of shorter chain alkanes, common in the wax layers of submerged plants (Ficken et al., 2000), was low (Table 3.2) indicating that submerged plants contribute little to the sedimentary alkanes and do not affect the interpretation regarding land plants. Near the equator, $C_{29}$ dominates the distributions; this corresponds

well with lipid data for rain forest plants, in which it is the most abundant homologue (Vogts et al., 2009). Southwards, its relative abundance decreases, and at 12°S the abundance of $C_{29}$ and $C_{31}$ is almost identical. The increasing amount of $C_{31}$ mirrors the continental transition from closed forest to open woodland because $C_{31}$ is the dominant homologue of plant wax in open savanna regions (Rommerskirchen et al., 2006b; Vogts et al., 2009). At 15°S and further south, $C_{33}$ is the second-most abundant homologue, while the abundance of $C_{29}$ further declines. This is consistent with the decreasing importance of woody vegetation and the increase in $C_4$ grass, in which $C_{33}$ is particularly abundant (Rommerskirchen et al., 2006b; Vogts et al., 2009).

The changing abundance of individual *n*-alkanes is numerically displayed by the average chain length (ACL). Near the equator, $ACL_{25\text{-}35}$ was around 30.1 (Table 3.2; Fig. 3.2c). At 10°S, the ratio started to increase and reached values of 30.5 in the south. $ACL_{25\text{-}35}$ ratios for Holocene sediments of this region calculated from Rommerskirchen et al. (2003) are in the same range but dust samples exhibited lower $ACL_{25\text{-}35}$ values of 26-29 (Schefuß et al., 2003b). McDuffee et al. (2004) employed a slightly different chain length interval and used the $ACL_{25\text{-}33}$ value, which we also calculated for our samples (Table 3.2). Even though both studies employed samples from similar sampling locations the $ACL_{25\text{-}33}$ values of McDuffee et al. (2004) were 0.8-1.6 lower than those in this study. Above this, the trend to higher values for the southern samples was less pronounced in the study of McDuffee et al. (2004). As mentioned before, the cause of this is unknown.

$ACL_{25\text{-}35}$ values for the northern sediments in this study were higher than those calculated for $C_3$ rain forest plant material analysed by Vogts et al. (2009). The discrepancy may be due to the limited plant database but some contribution of $C_4$ grass wax with longer chain *n*-alkanes to the northern sites also appears possible. As postulated in previous studies (Rommerskirchen et al., 2003, 2006a; Schefuß et al., 2004) such $C_4$ plant material can reach the northern sites via long-range aeolian transport from north-central Africa or may originate from rain forest swamps where $C_4$ grass dominates, e.g. those of the genus Cyperus (like papyrus). However, since the overall *n*-alkane characteristics of tropical swamp $C_4$ grass are unknown, their influence on the ACL remains speculative. At the southern sampling sites, the sedimentary $ACL_{25\text{-}35}$ values are higher than in the north but do not resemble those of $C_4$ grass calculated from the dataset presented by Rommerskirchen et al. (2006b), indicating a strong but not exclusive $C_4$ plant contribution.

**Table 3.3:** Stable carbon isotope composition of major terrestrial *n*-alkanes with standard deviation (1σ) of measurements as well as weighted mean average (WMA).

| No. | $\delta^{13}C_{29}$ | $\delta^{13}C_{31}$ | $\delta^{13}C_{33}$ | $\delta^{13}C_{WMA29-33}$ |
|---|---|---|---|---|
| 1 | -31.6 ± 0.2 | -30.2 ± 0.0 | -27.6 ± 0.1 | -30.3 ± 0.1 |
| 2 | -34.1 ± 0.4 | -33.2 ± 0.2 | -30.6 ± 0.2 | -33.2 ± 0.3 |
| 3 | -32.3 ± 0.1 | -31.6 ± 0.1 | -28.9 ± 0.2 | -31.4 ± 0.1 |
| 4 | -32.0 ± 0.3 | -30.6 ± 0.2 | -27.9 ± 0.3 | -30.7 ± 0.3 |
| 5 | -33.0 ± 0.0 | -32.3 ± 0.2 | -29.6 ± 0.4 | -32.1 ± 0.2 |
| 6 | -31.8 ± 0.2 | -31.2 ± 0.3 | -27.7 ± 0.3 | -30.8 ± 0.2 |
| 7 | -30.8 ± 0.1 | -29.8 ± 0.1 | -26.3 ± 0.2 | -29.4 ± 0.1 |
| 8 | -29.6 ± 0.2 | -28.3 ± 0.1 | -26.0 ± 0.1 | -28.3 ± 0.2 |
| 9 | -27.9 ± 0.2 | -27.0 ± 0.2 | -25.6 ± 0.3 | -26.9 ± 0.2 |
| 10 | -28.2 ± 0.1 | -26.8 ± 0.3 | -25.8 ± 0.2 | -26.9 ± 0.2 |
| 11 | -27.1 ± 0.2 | -25.2 ± 0.1 | -24.7 ± 0.2 | -25.5 ± 0.2 |
| 12 | -28.2 ± 0.3 | -25.6 ± 0.1 | -24.9 ± 0.2 | -26.0 ± 0.1 |
| 13 | -28.6 ± 0.0 | -26.1 ± 0.1 | -24.9 ± 0.2 | -26.3 ± 0.1 |

### 3.5.2. Carbon stable isotope composition

The dominant *n*-alkanes have carbon stable isotope ratio values from -34‰ to -25‰ (Table 3.3), i.e. in the range of values determined in other studies (Huang et al., 2000; Rommerskirchen et al., 2003; McDuffee et al., 2004; Schefuß et al., 2004). As these long chain alkanes are not common in marine organisms (Chikaraishi and Naraoka, 2003; Mead et al., 2005) and hopane and CPI analysis indicated only a very minor contamination with petroleum *n*-alkanes, if at all, we are confident that the observed trends of the *n*-alkane carbon stable isotope composition are related to the terrestrial plant origin of these compounds.

Most obvious is a trend to less negative $\delta^{13}C$ values from north to south, virtually parallel for the three individual *n*-alkanes depicted in Fig. 3.3a. This is caused by a dominance of $C_3$ plant material from woody vegetation in the northern part of the transect and an increasing contribution of $C_4$ grass further south. The most negative values were observed off the Ogooué and Congo River mouths, with values on average 2‰ lower than at other locations off the rain forest. These low values may be related to either one or a combination of the following phenomena: First, there may be a more pronounced dominance of $C_3$ plant discharge at the river mouths, reflecting the vegetation in the catchment area. For the other locations off the rain forest, the $C_3$ plant signal may be slightly overprinted by an aeolian $C_4$ plant signal from more distant savanna regions. A second possible explanation may be the heterogeneity in carbon stable isotope signature of rain forest plants. Plant parts growing under the canopy show more negative $\delta^{13}C$ values than those of the tree crowns

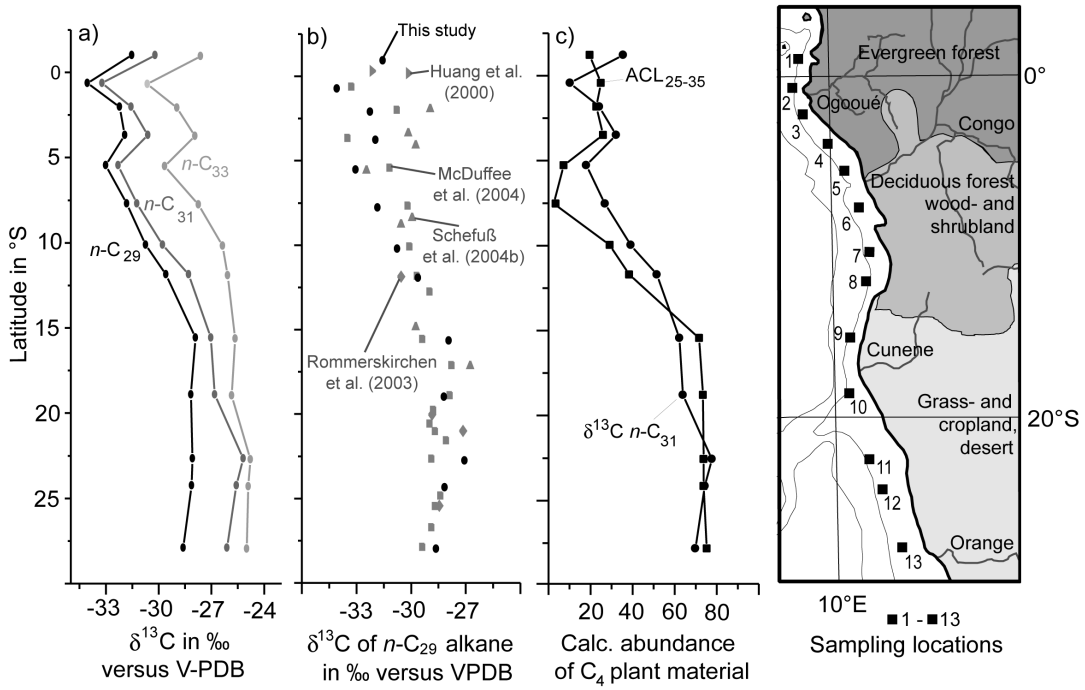


**Fig. 3.3:** Simplified present-day land cover based on Mayaux et al. (2004) with sampling locations of the north to south transect and graphs of sediment analysis results with (a) stable carbon isotope composition of dominating *n*-alkanes (‰), (b) comparison of results for the stable carbon isotope composition of the *n*-$C_{29}$ alkane for our study (black circles) and with literature data (grey symbols) and (c) calculated $C_4$ plant abundance based on ACL of *n*-$C_{25}$ to *n*-$C_{35}$ alkanes ($ACL_{25\text{-}35}$, black squares) as well as on stable carbon isotope composition of the *n*-$C_{31}$ alkane (black circles).

(Medina and Minchin, 1980). Thus, rivers may predominantly transport the more negative signal of the understory rain forest even though parts of the upper canopy also reach the rivers. In contrast, the wind load reflects the abrasion of isotopically less negative plant constituents solely from the upper canopy. The assumed $C_3$ "river signal" in the carbon stable isotope composition is, however, not paralleled by the ACL values. The reason for this discrepancy is unknown.

At all locations, the $\delta^{13}C$ values increase from $C_{29}$ to the higher homologues, because $C_4$ plants produce higher proportions of longer chain *n*-alkanes than $C_3$ species (Rommerskirchen et al., 2006b; Vogts et al., 2009). At the northern sites, the $\delta^{13}C$ values of $C_{31}$ are closer to those of $C_{29}$, whereas they resemble more the values of $C_{33}$ at the southern sites (Fig. 3.3a). This shift relative to the other homologues reflects the predominant $C_3$ plant origin at the northern sites and the increasing contribution of $C_4$ plant material in the south. Thus, the trend to less negative

values from equatorial to southern sites is more pronounced for $C_{31}$.

A combined plot of our results for *n*-$C_{29}$ alkane together with literature data from the same region (Huang et al., 2000; Rommerskirchen et al., 2003; McDuffee et al., 2004; Schefuß et al., 2004) is shown in Fig. 3.3b. The comparison is restricted to sediments derived from a water depth between 500 and 2500 m in order to limit possible effects of water column height or increasing offshore transport distance on OM transformation. Even though there is some variation in the combined dataset, the general trend to less negative values from the equator to the south is recognisable and mirrors the increasing extension of $C_4$ plant-dominated grassland on the continent. The largest variation in $\delta^{13}C_{29}$ values were observed for the northern part of the study area. This is attributed to the different distances of the sampling locations to the river mouths and river plumes, where the amounts of riverine and aeolian material (and accordingly the abundance of $C_4$ plant-derived wax alkanes) may vary significantly over short distances.

## 3.6. Reconstructing $C_4$ plant contribution

On the basis of *n*-alkane parameters, a binary mixing equation was used to calculate the abundance (%) of $C_4$ plant material in sediments. The equation used is:

$$\%C_4 = \frac{X_S - X_{C3}}{X_{C4} - X_{C3}} \qquad \textbf{Equation 3.1}$$

where X is the ratio of *n*-alkanes (ACL or $\delta^{13}C$) extracted from the sediment (S) or from the leaf wax of the $C_3$ or $C_4$ plants, respectively. Crucial for such calculations is the availability of suitable plant end member data. While Rommerskirchen et al. (2006b) presented such data for $C_4$ grasses, $C_3$ plant values are more heterogeneous. As an approximation, the mean values of two datasets for African rain forest and savanna plants (Vogts et al., 2009) were averaged. The averaged $\delta^{13}C$ values

**Table 3.4:** End member data and results with standard deviations. The standard deviations display the variation width within the dataset and do not represent the analytical error.

| End member data for | $\delta^{13}C_{29}$ | $\delta^{13}C_{31}$ | $\delta^{13}C_{33}$ | $\delta^{13}C_{WMA29-33}$ | $ACL_{25-35}$ |
|---|---|---|---|---|---|
| $C_3$ plants [a] | -35.4±2.6 | -35.7±2.8 | -35.3±1.9 | -35.6±2.6 | 29.7±1.0 |
| $C_4$ grass [b] | -21.6±2.0 | -22.1±2.1 | -22.2±1.8 | -22.0±1.9 | 30.8±0.9 |

[a] Data for $C_3$ plants: Mean of two averaged datasets for 24 rain forest and 44/45 savannah $C_3$ plants analysed by Vogts et al. (2009); number of plants for averaging: 68 for $\delta^{13}C$ and 69 for $ACL_{25-35}$, respectively.

[b] Data for $C_4$ plants from Rommerskirchen et al. (2006b); number of plants for averaging: 33 for $\delta^{13}C$ and 178 for $ACL_{25-35}$ ratios, respectively.

fall between values employed in other studies (Rommerskirchen et al., 2003; Schefuß et al., 2004); ACL values were not used in these studies. The end member values for calculating the mixing ratios are compiled in Table 3.4.

The binary mixture calculations ignore CAM plants. In the study area CAM plants are only abundant in the Succulent Karroo, a ca. 250 km wide strip along the coast from ca. 27°S to 34°S (Milton et al., 1997). From this region aeolian offshore transport is low and the main contribution to the sediments is assumed to derive from the Orange River which transports mainly river bank material lean in CAM plants. Above this, the contribution of CAM-utilising plants to biomass production is low (Lüttge, 2004). Thus, neglecting CAM plants in our attempt to assess gross continental vegetation patterns from a continental margin geological archive appears justified.

### 3.6.1. Calculations based on $\delta^{13}C$ values

The carbon stable isotope composition used for the calculation of $C_4$ plant abundance is a parameter directly linked to the metabolic pathway of the plants. The results of our calculations of $C_4$ plant proportion based on the dominant *n*-alkanes depend largely on the homologues used (Table 3.5). For instance, using $C_{29}$ and $C_{31}$ gives differences of up to 22%. But if the results for the two most abundant homologues in a particular sample are compared (bold values in Table 3.5) the

**Table 3.5:** Calculations of abundance of $C_4$ plant-derived material at the sample locations based on different *n*-alkane-based parameters.

| No. | Calculated $C_4$ plant contribution to sediments (%) based on | | | | |
|---|---|---|---|---|---|
| | $\delta^{13}C_{29}$ [a,b] | $\delta^{13}C_{31}$ [a,b] | $\delta^{13}C_{33}$ [a,b] | $\delta^{13}C_{WMA29-33}$ [b] | $ACL_{25-35}$ |
| 1 | **28±2** | **40±0** | 59±1 | 39±1 | 26 |
| 2 | **10±3** | **18±2** | 36±1 | 18±2 | 31 |
| 3 | **23±1** | **30±0** | 49±1 | 31±1 | 29 |
| 4 | **25±2** | **37±1** | 57±3 | 36±2 | 32 |
| 5 | **17±0** | **25±2** | 43±3 | 26±1 | 15 |
| 6 | **26±1** | **33±2** | 58±2 | 35±2 | 11 |
| 7 | **34±1** | **44±1** | 69±2 | 45±1 | 35 |
| 8 | **42±2** | **54±1** | 71±1 | 54±1 | 43 |
| 9 | 54±1 | **64±1** | **74±2** | 64±2 | 72 |
| 10 | 52±1 | **65±2** | **73±1** | 64±2 | 74 |
| 11 | 60±1 | **77±1** | **81±1** | 74±1 | 74 |
| 12 | 53±2 | **75±0** | **80±1** | 71±1 | 74 |
| 13 | 49±0 | **71±0** | **79±1** | 69±1 | 75 |

[a] **Bold values** refer to two most abundant homologues.

[b] Standard deviation (1σ) calculated from standard deviation of sediment analyses.

differences in $C_4$ plant proportion do not exceed 12%. Despite these variations, our results derived from carbon stable isotope data are in the range of those based on pollen abundance and $\delta^{13}C$ values of *n*-alkanes and *n*-alkan-1-ols presented by Rommerskirchen et al. (2003) and Schefuß et al. (2004).

Based on *n*-$C_{31}$, a $C_4$ contribution of ca. 30% was calculated for the equatorial locations, with a lower $C_4$ plant contribution (20%) off the major rivers (Fig. 3.3c). This means that an exclusive $C_3$ signal was not observed at any of the sediment sampling locations and that $C_4$ plant material was transported to all the sites, either by wind from larger distances or by rivers from $C_4$ plants growing in the rain forest (e.g. swamps with papyrus). For the southern sites, a $C_4$ plant abundance of ca. 70% was calculated (Fig. 3.3c).

Some studies have employed weighted mean averages of carbon stable isotope ratio values for the calculation of $C_4$ plant abundance. Applying this method to the *n*-$C_{27}$ to *n*-$C_{35}$ (not displayed) and the *n*-$C_{29}$ to *n*-$C_{33}$ alkanes (Table 3.5) yielded results closely resembling those based on *n*-$C_{31}$ alone. Thus, at least for the present dataset there was no benefit from using weighted mean averages.

### 3.6.2. Calculations based on ACL

Other than carbon isotopes, the chain lengths of wax alkanes are not directly related to the photosynthetic pathway of the plants. It is more likely that the environmental conditions, under which the different plants types thrive, determine the alkane chain length and, since $C_3$ and $C_4$ plants have different abundances in certain habitats, provide an indirect empirical relationship between plant type and wax composition. Studies of the *n*-alkane characteristics of African plants have at least shown that not only $\delta^{13}C$ values but also $ACL_{25\text{-}35}$ values differ between $C_3$ and $C_4$ plants (Rommerskirchen et al., 2006b; Vogts et al., 2009). Employing the ACL parameter to the calculation of $C_4$ plant abundance shows that the results roughly match those based upon the carbon stable isotope composition (Table 3.5, Fig. 3.3c).

The slight discrepancies may partly be caused by limitations of the end member values used in the calculations. The plant database mainly comprises one sample per species and does not take into account potential variation in the *n*-alkane distribution patterns due to different growth conditions. Also, the database for $C_3$ plants may not fully represent the actual transfer of wax components to the geological archives. In particular, the average was calculated from non-weighted single species data and neglects the possibility that certain species with a distinct distribution pattern may dominate the vegetation in a given region and thus also the transfer of wax *n*-alkanes into the continental margin sediments.

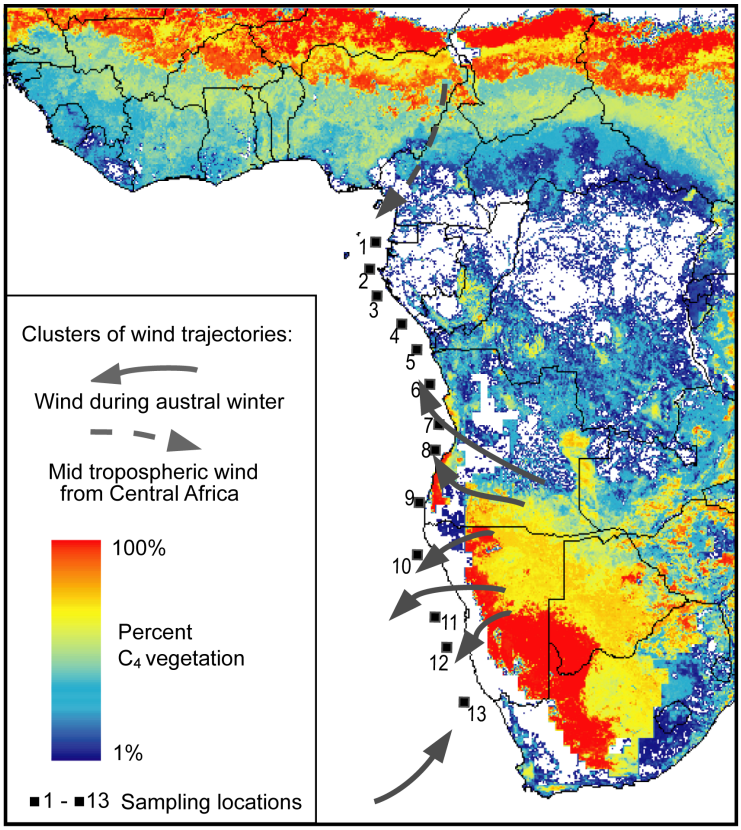


**Fig. 3.4:** Colour-coded map of proportion (%) of continental vegetation using the $C_4$ pathway (Still and Powell, 2010), with wind trajectories (Dupont and Wyputta, 2003) and sampling locations. White areas represent either 100% $C_3$ vegetation (e.g. central African rain forest) or absence of vegetation (e.g. Namib Desert).

### 3.6.3. Significance of calculated $C_4$ plant contribution

The contribution of $C_4$ plant material in the sediments calculated from the carbon isotope composition of $C_{31}$ was compared with a map showing the proportion (%) of plants that use the $C_4$ metabolic pathway (Still and Powell, 2010; Fig. 3.4). Postulated transport scenarios and resulting relative abundances are explained below and compiled in Table 3.6.

$C_4$ plant proportion of 18-40% calculated for sediment locations 1-4 does not reflect the $C_4$ plant abundance in the rain forest at the same latitude (maximum 10% along the equator, increasing to 20% further south). Thus, additional long-range transport of aeolian material by, e.g. Harmattan winds from north-central Africa (Schefuß et al., 2003b) carrying material with ca. 80% $C_4$ signature probably contributes to these sediments. This effect should be highest for the northern site (40% $C_4$), decrease further south (20%) and be of low significance off the Ogooué river (10%), where the fluvial signal dominates the sediment material.

**Table 3.6:** Postulated contribution scenarios explaining the abundance of $C_4$ plant material in the sediments based on river discharge and wind trajectories (Dupont and Wyputta. 2003) and a map of the proportion (%) of continental vegetation using the $C_4$ pathway (Still and Powell, 2010; Fig. 3.4).

| No. | Observed [a] | Scenario-based [b] | Postulated contribution scenarios and estimated amount of $C_4$ material transported |
|---|---|---|---|
| 1 | 40 | 38 | 60% zonal wind transport from rain forest areas (10% $C_4$) and 40% long range wind transport from north central Africa (80% $C_4$) |
| 2 | 18 | 17 | 90% Ogooué river outflow from rain forest areas (10% $C_4$) and 10% long range wind transport from north central Africa (80% $C_4$) |
| 3 | 30 | 32 | 80% zonal wind transport from rain forest areas (20% $C_4$) and 20% long range transport from north central Africa (80% $C_4$) |
| 4 | 37 | 32 | 80% zonal wind transport from rain forest areas (20% $C_4$) and 20% long range transport from north central Africa (80% $C_4$) |
| 5 | 25 | 20 | 100% from Congo river outflow (20% $C_4$) |
| 6 | 33 | 30 | 20% ESE wind transport from areas with high $C_4$ plant abundance (70% $C_4$) and 80% ESE wind transport from areas with low $C_4$ plant abundance (20% $C_4$) |
| 7 | 44 | 40 | 40% ESE wind transport from areas with high $C_4$ plant abundance (70% $C_4$) and 60% ESE wind transport from areas with low $C_4$ plant abundance (20% $C_4$) |
| 8 | 54 | 50 | 100% ESE wind transport from $C_3/C_4$ transition zone (50% $C_4$) |
| 9 | 64 | 68 | 80% E wind transport from areas with high $C_4$ plant abundance (80% $C_4$) and 20% E wind transport from coastal areas with low $C_4$ plant abundance (20% $C_4$) |
| 10 | 65 | 68 | 80% E wind transport from areas with high $C_4$ plant abundance (80% $C_4$) and 20% E wind transport from coastal areas with low $C_4$ plant abundance (20% $C_4$) |
| 11 | 77 | 80 | 100% E wind transport from areas with high $C_4$ plant abundance (80% $C_4$) |
| 12 | 75 | 80 | 100% E wind transport from areas with high $C_4$ plant abundance (80% $C_4$) |
| 13 | 71 | 67 | 30% ENE wind transport from cape flora and grasslands (60% $C_4$) and 70% from Orange river outflow |

[a] Amount of $C_4$ material in sediments (%). Calculation based on $\delta^{13}C_{31}$.

[b] Amount of $C_4$ material (%) contributed to sediments according to scenarios in this Table.

The $C_4$ abundance calculated from the sediment at location 5 off the Congo River (25%) roughly corresponds to the $C_4$ plant abundance in the catchment area (20%). Apparently, the intense river drainage overprints any contribution of windblown material of different origin.

For locations 6-8 the calculated $C_4$ plant proportion (30-50%) does not match the continental abundance of $C_4$ plants at the same latitude (up to 20%). However, wind trajectories contributing to these sediments originate from an east-southeast direction (Dupont and Wyputta, 2003). This may explain the values calculated for the sediments, as winds from east-southeast partly pass over areas with higher $C_4$ plant abundance. Further south, adjacent to ocean margin sites 9 and 10, continental vegetation is divided into a more $C_3$ dominated region closer to the coast and an area with high $C_4$ plant abundance further inland. Obviously, the zonal wind transports this mixture of plant material to the sediments, leading to the calculated values of about 60% $C_4$ plant material.

Locations 11-13 revealed the highest proportion of $C_4$ material in the sediments (>65%) reflecting the high abundance of $C_4$ plant wax transported offshore by nearly zonal winds at location 11 and east-northeasterly winds at location 12. The Orange River may transport most of the terrigenous material to the sediments at the southernmost site 13 because winds blow mainly parallel to the coast or towards the continent in this area (Dupont and Wyputta, 2003).

### 3.6.4. Correlation of environmental parameters with $C_4$ plant abundance

The rough estimate of scenarios presented above is able to explain the abundance of $C_4$ plant material in the sediment samples (Table 3.6), which enables the application of the postulated transport pathways to infer the environmental conditions in the catchment area. Sampling sites 1-4 were discounted in the assessment because they potentially received a significant amount of aeolian material from distant locations in the north with unconstrained climatic conditions. For the other sampling locations mean annual precipitation and potential annual evapotranspiration along the postulated transport pathways were calculated with the WebWIMP modeling program (Matsuura et al., 2009). The aridity index was calculated according to UNEP (1992) as a quotient of mean annual precipitation and potential annual evapotranspiration in order to elucidate not only the actual precipitation but the dryness the plants have to tolerate. Other parameters influencing $C_4$ plant abundance such as temperature and light, the primary needs of $C_4$ plants (Sage, 2001), are not limiting factors in this region. Secondary aspects like seasonality of rainfall, edaphic characteristics, fire and grazing stress are important as well but these more local

**Table 3.7:** Pearson correlation coefficients (r) of $C_4$ material abundance in sediments calculated from the stable carbon isotope composition of the *n*-$C_{31}$ alkane with mean annual precipitation and aridity index for postulated punctual catchment areas along the transect at given distances to the coast.[a]

| | Distance to coast | | | | | |
|---|---|---|---|---|---|---|
| | 150 km | 200 km | 250 km | 300 km | 350 km | 400 km |
| Mean annual precipitation | **-0.81** | **-0.85** | **-0.89** | **-0.90** | **-0.95** | **-0.95** |
| Aridity index [b] | -0.61 | -0.71 | **-0.78** | **-0.82** | **-0.92** | **-0.91** |

[a] **Bold values** significant at 99% level ($p < 0.01$).

[b] Calculated as quotient of mean annual precipitation and potential evapotranspiration according to UNEP (1992).

aspects are not addressed in this continent-wide study.

The continental locations selected for calculation of environmental parameters were at the same latitude as the sampling locations for sampling sites 5, 9 -11 and 13. For sites 6-8 locations were in an east-southeast and for site 12 in an east-northeast direction. Climatic parameters were calculated for locations of ca. 150-400 km inland (every 50 km; values are provided as Supplementary Table 3.S2). A minimum distance inshore of 150 km was employed to avoid the influence of coastal climate, such as low precipitation due to cold temperatures in coastal upwelling regions.

Pearson correlation factors from these calculations are compiled in Table 3.7. Locations ca. 350 km from the coast gave the highest correlation coefficients (Fig. 3.5). For mean annual precipitation high negative correlation factors (99% significance) were obtained for all distance intervals (Table 3.7). For the aridity indices

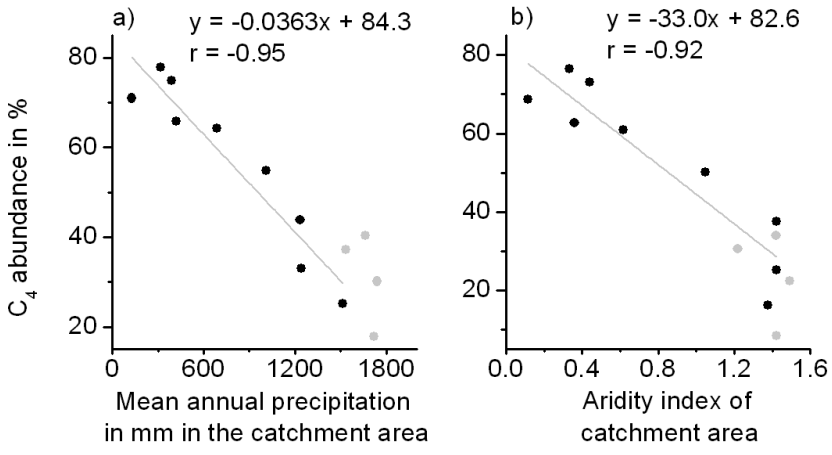


**Fig. 3.5:** Correlation of contribution of $C_4$ plant material calculated from stable carbon isotope composition of the *n*-$C_{31}$ alkane with (a) mean annual precipitation and (b) aridity index of locations in the potential catchment area. Climatic parameters are based on calculations for continental locations of ca. 350 km distance to the coast using the WebWIMP modeling program (Matsuura et al., 2009). Correlations are significant at 99% level ($p < 0.01$). Grey symbols present values for locations 1-4, which were not taken into account for the correlation calculations.

correlation of similar significance were obtained for distances of 200-400 km from the coast (Table 3.7). The significance of the correlations suggests that, at least in this region, precipitation and aridity are major factors influencing the $C_3/C_4$ plant distribution reflected in the sediment record. This corresponds to satellite-based analyses by Still and Powell (2010), who showed a strong relationship between mean annual precipitation and the carbon isotopic composition of continental vegetation in Africa.

We cannot exclude the possibility that other parameters (seasonality of rain fall, fire intensity, edaphic characteristics, grazing) may affect the correlation. Over geological timescales changes in irradiation, temperature, wind systems and $CO_2$ concentration may also have an influence. In order to verify the robustness of these correlations more detailed information and/or independent proxies about the plant end members, vegetation composition, erosion processes, transport pathways and source regions is needed.

## 3.7. Conclusions

This study corroborates the potential of long chain *n*-alkanes for the reconstruction of continental vegetation. From the equator to the south, characteristic trends to longer chain length and less negative carbon stable isotope ratio values were observed in ocean margin sediments along the southwest African continent. Both characteristics can be used to assess the contribution of $C_4$ material to the sediments because carbon stable isotope composition, as well as chain length distinguishes $C_3$ from $C_4$ plant wax *n*-alkanes. The calculated values for the proportion of $C_4$ plant material in the sediments exhibit strong correlation with $C_4$ abundance in continental catchment areas postulated with respect to wind trajectories and river systems. The $C_4$ contribution to the sediments correlates significantly with the mean annual precipitation and the aridity indices in selected catchment areas.

## 3.8. Acknowledgements

We gratefully appreciate the efforts of organisers and participants of RV Meteor cruises M34/2 and M41/1. We are also indebted to M. Zabel (University of Bremen) for helpful advice during sample retrieval. We thank C. Still (University of California at Santa Barbara) and R. Powell (University of Denver) for providing a map of $C_4$ plant distribution in Africa. F. Rommerskirchen (University of Bremen) is gratefully acknowledged for providing figure drafts. We are also indebted to G. Eglinton (University of Bristol) for helpful discussions and remarks regarding the interpretation of the results. Special thanks are given to H. Haase for support during urea adduction

and bulk inorganic carbon analysis, C. Versteegen for help with elemental analysis and B. Kopke (all ICBM) for support during carbon stable isotope analysis. M. Teece (State University of New York) and an anonymous referee are gratefully acknowledged for their constructive reviews. The study was financially supported by Deutsche Forschungsgemeinschaft (DFG, grants no. Ru 485/35 and Ru 485/40).

## 3.9. Supplementary Tables

**Supplementary Table 3.S1:** Locations employed for calculations of continental environmental conditions with the WebWIMP Modelling program and values obtained as displayed in Fig. 3.1.

| Latitude | Longitude at ca. 350 km distance to coast (°E) | Mean annual temperature (°C) | Mean annual precipitation (mm) | Potential evapotranspiration (mm) | Aridity index |
|---|---|---|---|---|---|
| 4.0°N | 12.5 | 23.5 | 1585 | 1188 | 1.33 |
| 3.5°N | 13.0 | 23.1 | 1634 | 1148 | 1.42 |
| 3.0°N | 13.0 | 23.5 | 1640 | 1183 | 1.39 |
| 2.5°N | 13.0 | 23.7 | 1642 | 1209 | 1.36 |
| 2.0°N | 13.0 | 23.5 | 1639 | 1184 | 1.38 |
| 1.5°N | 12.5 | 23.1 | 1680 | 1138 | 1.48 |
| 1.0°N | 12.5 | 23.2 | 1696 | 1150 | 1.47 |
| 0.5°N | 12.5 | 23.6 | 1668 | 1198 | 1.39 |
| 0.0° | 12.5 | 23.5 | 1672 | 1188 | 1.41 |
| 0.5°S | 12.5 | 23.8 | 1733 | 1213 | 1.43 |
| 1.0°S | 12.0 | 22.7 | 1720 | 1106 | 1.56 |
| 1.5°S | 12.5 | 22.2 | 1851 | 1059 | 1.75 |
| 2.0°S | 12.5 | 23.2 | 1732 | 1160 | 1.49 |
| 2.5°S | 13.0 | 23.2 | 1717 | 1158 | 1.48 |
| 3.0°S | 13.5 | 22.4 | 1686 | 1078 | 1.56 |
| 3.5°S | 14.0 | 24.0 | 1525 | 1251 | 1.22 |
| 4.0°S | 14.5 | 23.0 | 1405 | 1140 | 1.23 |
| 4.5°S | 15.0 | 24.0 | 1353 | 1250 | 1.08 |
| 5.0°S | 15.0 | 23.4 | 1553 | 1173 | 1.32 |
| 5.5°S | 15.5 | 22.6 | 1510 | 1096 | 1.38 |
| 6.0°S | 15.5 | 23.9 | 1393 | 1240 | 1.12 |
| 6.5°S | 15.5 | 23.0 | 1361 | 1134 | 1.20 |
| 7.0°S | 16.0 | 23.4 | 1416 | 1178 | 1.20 |
| 7.5°S | 16.0 | 22.5 | 1288 | 1095 | 1.18 |
| 8.0°S | 16.5 | 24.0 | 1221 | 1241 | 0.98 |
| 8.5°S | 16.5 | 24.4 | 1263 | 1300 | 0.97 |
| 9.0°S | 16.0 | 21.4 | 1088 | 1001 | 1.09 |
| 9.5°S | 16.5 | 21.2 | 1220 | 982 | 1.24 |
| 10.0°S | 16.5 | 21.7 | 1225 | 1017 | 1.20 |
| 10.5°S | 17.0 | 21.8 | 1269 | 1028 | 1.23 |
| 11.0°S | 17.0 | 20.5 | 1284 | 941 | 1.36 |
| 11.5°S | 17.0 | 20.5 | 1228 | 939 | 1.31 |
| 12.0°S | 17.0 | 20.2 | 1207 | 923 | 1.31 |
| 12.5°S | 16.5 | 19.1 | 1232 | 865 | 1.42 |
| 13.0°S | 16.0 | 19.7 | 1196 | 896 | 1.33 |
| 13.5°S | 16.0 | 19.9 | 1118 | 907 | 1.23 |
| 14.0°S | 15.5 | 20.9 | 1048 | 978 | 1.07 |

**Supplementary Table 3.S1** (continued)

| Latitude | Longitude at ca. 350 km distance to coast (°E) | Mean annual temperature (°C) | Mean annual precipitation (mm) | Potential evap-otranspiration (mm) | Aridity index |
|---|---|---|---|---|---|
| 14.5°S | 15.5 | 20.6 | 930 | 960 | 0.97 |
| 15.0°S | 15.5 | 21.9 | 782 | 1075 | 0.73 |
| 15.5°S | 15.5 | 22.3 | 681 | 1106 | 0.62 |
| 16.0°S | 15.0 | 23.4 | 662 | 1233 | 0.54 |
| 16.5°S | 15.0 | 22.9 | 586 | 1179 | 0.50 |
| 17.0°S | 15.0 | 22.9 | 504 | 1182 | 0.43 |
| 17.5°S | 15.0 | 23.0 | 416 | 1196 | 0.35 |
| 18.0°S | 15.0 | 22.9 | 415 | 1186 | 0.35 |
| 18.5°S | 15.5 | 22.7 | 406 | 1167 | 0.35 |
| 19.0°S | 16.0 | 22.6 | 418 | 1158 | 0.36 |
| 19.5°S | 16.0 | 20.8 | 430 | 999 | 0.43 |
| 20.0°S | 16.5 | 19.3 | 461 | 911 | 0.51 |
| 20.5°S | 16.5 | 17.7 | 474 | 831 | 0.57 |
| 21.0°S | 17.0 | 19.6 | 358 | 932 | 0.38 |
| 21.5°S | 17.0 | 18.5 | 408 | 870 | 0.47 |
| 22.0°S | 17.5 | 18.4 | 387 | 874 | 0.44 |
| 22.5°S | 18.0 | 19.5 | 315 | 943 | 0.33 |
| 23.0°S | 18.0 | 19.9 | 262 | 971 | 0.27 |
| 23.5°S | 18.0 | 20.2 | 237 | 989 | 0.24 |
| 24.0°S | 18v | 20.4 | 211 | 1011 | 0.21 |
| 24.5°S | 18.0 | 20.0 | 229 | 989 | 0.23 |
| 25.0°S | 18.5 | 20.3 | 216 | 1018 | 0.21 |
| 25.5°S | 18.5 | 20.1 | 216 | 1005 | 0.21 |
| 26.0°S | 18.5 | 20.7 | 198 | 1045 | 0.19 |
| 26.5°S | 18.5 | 20.8 | 184 | 1054 | 0.17 |
| 27.0°S | 18.5 | 16.5 | 170 | 806 | 0.21 |
| 27.5°S | 19.0 | 19.1 | 144 | 948 | 0.15 |
| 28.0°S | 19.5 | 19.4 | 129 | 974 | 0.13 |
| 28.5°S | 20.0 | 19.3 | 137 | 966 | 0.14 |
| 29.0°S | 20.5 | 19.4 | 150 | 983 | 0.15 |
| 29.5°S | 20.5 | 18.5 | 152 | 927 | 0.16 |
| 30.0°S | 21.0 | 18.4 | 175 | 921 | 0.19 |
| 30.5°S | 21.0 | 16.9 | 181 | 842 | 0.21 |
| 31.0°S | 21.5 | 15.7 | 206 | 789 | 0.26 |
| 31.5°S | 21.5 | 14.9 | 200 | 755 | 0.26 |
| 32.0°S | 22.0 | 17.1 | 208 | 834 | 0.25 |
| 32.5°S | 22.0 | 17.3 | 201 | 836 | 0.24 |
| 33.0°S | 21.5 | 17.2 | 219 | 828 | 0.26 |
| 33.5°S | 22.0 | 16.0 | 378 | 774 | 0.49 |

**Supplementary Table 3.S2:** Data of locations employed as representatives of potential catchment areas. Values were used for the calculation of correlation coefficients (Table 3.7). Data of environmental conditions were derived from the WebWIMP modeling program (Matsuura et al., 2009). Aridity index calculated according to UNEP (1992).

| | Distance to coast (km) | | | | | |
|---|---|---|---|---|---|---|
| | 150 km | 200 km | 250 km | 300 km | 350 km | 400 km |
| Latitude (°N) | 1 | 1 | 1 | 1 | 1 | 1 |
| Longitude (°E) | 11.0 | 11.5 | 12.0 | 12.5 | 13.0 | 13.5 |
| Mean annual temperature (°C) | 23.5 | 24.4 | 24.5 | 23.6 | 23.3 | 23.4 |
| Mean annual precipitation (mm) | 2101.1 | 1835.2 | 1647.8 | 1665.9 | 1653 | 1591 |
| Potential evapotranspiration (mm) | 1292 | 1305 | 1198 | 1150 | 1164 | 1177 |
| Aridity index | 1.6 | 1.4 | 1.4 | 1.4 | 1.4 | 1.4 |
| Latitude (°S) | 0.5 | 0.5 | 0.5 | 0.5 | 0.5 | 0.5 |
| Longitude (°E) | 10.0 | 10.5 | 11.0 | 11.5 | 12.0 | 12.5 |
| Mean annual temperature (°C) | 25.9 | 25.8 | 25.8 | 25.8 | 23.6 | 23.8 |
| Mean annual precipitation (mm) | 1971.6 | 2027.5 | 2027.5 | 2027.5 | 1708.2 | 1734.6 |
| Potential evapotranspiration (mm) | 1512 | 1500 | 1222 | 1130 | 1200 | 1213 |
| Aridity index | 1.3 | 1.4 | 1.7 | 1.8 | 1.4 | 1.4 |
| Latitude (°S) | 2 | 2 | 2 | 2 | 2 | 2 |
| Longitude (°E) | 10.5 | 11.0 | 11.5 | 12.0 | 12.5 | 13.0 |
| Mean annual temperature (°C) | 25.6 | 24.3 | 23.3 | 24.2 | 23.2 | 22.9 |
| Mean annual precipitation (mm) | 1890.6 | 1872 | 1837.9 | 1738.9 | 1730.6 | 1816.4 |
| Potential evapotranspiration (mm) | 1481 | 1290 | 1171 | 1276 | 1160 | 1129 |
| Aridity index | 1.3 | 1.5 | 1.6 | 1.4 | 1.5 | 1.6 |
| Latitude (°S) | 3.5 | 3.5 | 3.5 | 3.5 | 3.5 | 3.5 |
| Longitude (°E) | 12.0 | 12.5 | 13.0 | 13.5 | 14.0 | 14.5 |
| Mean annual temperature (°C) | 25.5 | 25.4 | 23.6 | 22.1 | 24.0 | 22.8 |
| Mean annual precipitation (mm) | 1224.1 | 1261.2 | 1455.9 | 1416.8 | 1525.3 | 1697.6 |
| Potential evapotranspiration (mm) | 1457 | 1439 | 1208 | 1056 | 1251 | 1115 |
| Aridity index | 0.8 | 0.9 | 1.2 | 1.3 | 1.2 | 1.5 |
| Latitude (°S) | 5.5 | 5.5 | 5.5 | 5.5 | 5.5 | 5.5 |
| Longitude (°E) | 13.5 | 14.0 | 14.5 | 15.0 | 15.5 | 16.0 |
| Mean annual temperature (°C) | 23.8 | 23.9 | 24.3 | 23.0 | 22.6 | 23.4 |
| Mean annual precipitation (mm) | 1096.2 | 1222.6 | 1297.8 | 1311.4 | 1509.7 | 1531.9 |
| Potential evapotranspiration (mm) | 1233 | 1240 | 1289 | 1140 | 1096 | 1181 |
| Aridity index | 0.9 | 1.0 | 1.0 | 1.2 | 1.4 | 1.3 |
| Latitude (°S) | 9.5 | 9.5 | 10 | 10 | 10.5 | 10.5 |
| Longitude (°E) | 14.5 | 15.0 | 15.5 | 16.0 | 16.0 | 16.5 |
| Mean annual temperature (°C) | 24.8 | 22.9 | 20.7 | 21.5 | 19.2 | 22.0 |
| Mean annual precipitation (mm) | 948.2 | 1035.8 | 1126.7 | 1175.4 | 1236.8 | 1266.9 |
| Potential evapotranspiration (mm) | 1432 | 1218 | 1126 | 1083 | 1242 | 1189 |
| Aridity index | 0.7 | 0.9 | 1.2 | 1.2 | 1.4 | 1.2 |

**Supplementary Table 3.S2** (continued)

| | Distance to coast (km) | | | | | |
|---|---|---|---|---|---|---|
| | 150 km | 200 km | 250 km | 300 km | 350 km | 400 km |
| Latitude (°S) | 11.5 | 11.5 | 12 | 12 | 12.5 | 12.5 |
| Longitude (°E) | 15.0 | 15.5 | 16.0 | 16.0 | 16.5 | 17.0 |
| Mean annual temperature (°C) | 21.0 | 20.7 | 21.5 | 21.7 | 19.1 | 20.7 |
| Mean annual precipitation (mm) | 1218.9 | 1256.3 | 1256.6 | 1256.6 | 1229.9 | 1228.4 |
| Potential evapotranspiration (mm) | 969 | 952 | 1005 | 1017 | 985 | 950 |
| Aridity index | 1.3 | 1.3 | 1.5 | 1.5 | 1.4 | 1.3 |
| Latitude (°S) | 13 | 13 | 13.5 | 13.5 | 14 | 14 |
| Longitude (°E) | 13.0 | 13.0 | 13.5 | 13.5 | 14.0 | 14.0 |
| Mean annual temperature (°C) | 19.4 | 19.4 | 20.0 | 19.9 | 20.6 | 20.4 |
| Mean annual precipitation (mm) | 1210.8 | 1210.8 | 1147.8 | 1116.8 | 1006.9 | 1017.6 |
| Potential evapotranspiration (mm) | 917 | 975 | 866 | 861 | 923 | 994 |
| Aridity index | 1.4 | 1.4 | 1.3 | 1.2 | 1.0 | 1.1 |
| Latitude (°S) | 15.5 | 15.5 | 15.5 | 15.5 | 15.5 | 15.5 |
| Longitude (°E) | 13.5 | 14.0 | 14.5 | 15.0 | 15.5 | 16.0 |
| Mean annual temperature (°C) | 20.3 | 20.7 | 22.1 | 22.7 | 22.3 | 21.8 |
| Mean annual precipitation (mm) | 717.1 | 700.1 | 688.3 | 675.6 | 682.5 | 713.3 |
| Potential evapotranspiration (mm) | 939 | 967 | 1085 | 1146 | 1106 | 1062 |
| Aridity index | 0.8 | 0.7 | 0.6 | 0.6 | 0.6 | 0.7 |
| Latitude (°S) | 19.0 | 19.0 | 19.0 | 19.0 | 19.0 | 19.0 |
| Longitude (°E) | 14.0 | 14.5 | 15.0 | 15.5 | 16.0 | 16.5 |
| Mean annual temperature (°C) | 16.8 | 19.1 | 21.1 | 22.0 | 22.6 | 22.7 |
| Mean annual precipitation (mm) | 284.3 | 313 | 331.5 | 373.7 | 417.5 | 483.8 |
| Potential evapotranspiration (mm) | 774 | 884 | 1021 | 1103 | 1158 | 1180 |
| Aridity index | 0.4 | 0.4 | 0.3 | 0.3 | 0.4 | 0.4 |
| Latitude (°S) | 22.5 | 22.5 | 22.5 | 22.5 | 22.5 | 22.5 |
| Longitude (°E) | 16.0 | 16.5 | 17.0 | 17.5 | 18.0 | 18.5 |
| Mean annual temperature (°C) | 15.5 | 17.7 | 17.9 | 19.1 | 19.5 | 19.7 |
| Mean annual precipitation (mm) | 236.3 | 268.8 | 357.5 | 329.8 | 313.8 | 333 |
| Potential evapotranspiration (mm) | 740 | 829 | 843 | 911 | 943 | 959 |
| Aridity index | 0.3 | 0.3 | 0.4 | 0.4 | 0.3 | 0.3 |
| Latitude (°S) | 23 | 22.5 | 22.5 | 22 | 22 | 21.5 |
| Longitude (°E) | 15.5 | 16.0 | 16.5 | 17.0 | 17.5 | 18.0 |
| Mean annual temperature (°C) | 15.4 | 15.5 | 17.7 | 17.8 | 18.4 | 18.4 |
| Mean annual precipitation (mm) | 176.4 | 236.3 | 268.8 | 384.3 | 384.5 | 394.3 |
| Potential evapotranspiration (mm) | 657 | 803 | 894 | 1023 | 989 | 1026 |
| Aridity index | 0.2 | 0.3 | 0.3 | 0.5 | 0.4 | 0.5 |

**Supplementary Table 3.S2** (continued)

| | Distance to coast (km) | | | | | |
|---|---|---|---|---|---|---|
| | 150 km | 200 km | 250 km | 300 km | 350 km | 400 km |
| Latitude (°S) | 28 | 28 | 28 | 28 | 28 | 28 |
| Longitude (°E) | 17.0 | 17.5 | 18.0 | 18.5 | 19.0 | 19.5 |
| Mean annual temperature (°C) | 19.5 | 19.0 | 19.6 | 20.2 | 20.6 | 19.4 |
| Mean annual precipitation (mm) | 92.3 | 112.5 | 116 | 116.3 | 122.8 | 129 |
| Potential evapotranspiration (mm) | 922 | 914 | 971 | 1024 | 1053 | 974 |
| Aridity index | 0.1 | 0.1 | 0.1 | 0.1 | 0.1 | 0.1 |

# 4. Stable hydrogen isotopic composition of continental precipitation is reflected by δD ratios of land plant-derived *n*-alkanes in marine sediments off southwest Africa

Angela Vogts[a,b,*], Tanja Badewien[a], Jürgen Rullkötter[a], Enno Schefuß[c]

[a] Institute for Chemistry and Biology of the Marine Environment (ICBM), Carl von Ossietzky University of Oldenburg, P.O. Box 2503, D-26111 Oldenburg, Germany
[b] Current address: Leibniz Institute for Baltic Sea Research, Seestraße 15, D-18119 Warnemünde, Germany
[c] MARUM - Center for Marine Environmental Sciences, University of Bremen, Leobener Straße, D-28359 Bremen, Germany

* Corresponding author. Tel.: +49 (0) 381 5197 353; fax: +49 (0) 381 5197 440
E-mail address: angela.vogts@io-warnemuende.de (A. Vogts).

This chapter is in preparation for submission to Organic Geochemistry.

## 4.1. Abstract

A transect of marine surface sediment samples from 1°N to 28°S off southwest Africa was analysed to explore the potential of the hydrogen isotope compositions of terrestrial plant-wax *n*-alkanes preserved in ocean sediments as proxies for continental hydrological conditions. The conditions on the adjacent continent range from humid evergreen forest over deciduous forest, wood- and shrubland to arid grassland and desert. The hydrogen isotope ratios of the dominant *n*-alkane homologues ($C_{29}$, $C_{31}$ and $C_{33}$) vary from -123 to -141‰ V-SMOW and correlate with the modelled hydrogen isotope composition of mean annual and growing-season precipitation of continental source areas along postulated transport pathways (r up to 0.8, $p < 0.01$). The apparent fractionation between the hydrogen isotope compositions of alkanes and mean annual precipitation is remarkably uniform (-109‰ on average, $\sigma \leq 5$‰). Potentially, effects of aridity on the apparent hydrogen isotope fractionation are concealed by the contribution of different plant types (trees vs. grasses). Thus, isotope ratios of leaf wax *n*-alkanes preserved in ocean margin sediments along

SW Africa may be directly converted to δD ratios of ancient precipitation. This facilitates the deduction of, e.g., the amount-dependent hydrogen isotope composition changes of precipitation from sediment records and enables inferences about palaeoclimatic conditions.

## 4.2. Introduction

Ocean margin sediments are valuable archives for palaeoclimatic studies as they can provide long, undisturbed records of climate-dependent changes in sediment characteristics like, e.g., the molecular and isotopic composition of their constituents. But before ancient climate conditions can be assessed from sediment cores, it needs to be evaluated how present-day conditions are reflected in recent sediments. Reliable and ubiquitous molecular biomarkers with a high potential for palaeoenvironmental studies are land plant-derived wax constituents. Plant waxes cover all aerially exposed organs of higher land plants, and in virtually all plant waxes *n*-alkanes, which are the focus of this study, are abundant (Tulloch, 1976). After the decay of plants, the wax components can be stored in intermediate reservoirs or are directly transported by wind and rivers to lake or ocean sediments. In these archives, the *n*-alkanes can be preserved over geological time scales and constitute an integrated signal of the plant wax composition in the terrestrial catchment area.

The hydrogen isotope ratios of biomarkers from land plant waxes have been considered a proxy for the corresponding composition of precipitation and the hydrologic conditions (e.g., Sachse et al., 2012 and references therein). This includes plant wax archives of geological timescales because the hydrogen isotope composition of fossil *n*-alkanes remains unaltered over long periods of time (Schimmelmann et al., 2006; Wang et al., 2009). Hydrogen atoms introduced to plant biomass during photosynthesis derive from plant water and plant water in turn is controlled by soil water, which is the only water source for most plants and originates from precipitation. The hydrogen isotope signature of soil and plant water is influenced by evaporation and evapotranspiration (Sternberg, 1988; Kahmen et al. 2013a,b). It has also been inferred that the δD values of plant water can be influenced to different extents by the plant characteristics like ecological life form (tree, shrub, grass; Liu et al., 2006; Liu and Yang, 2008; Sachse et al., 2012) and the photosynthetic carbon fixation pathway ($C_3$/$C_4$/CAM; Chikaraishi and Naraoka, 2003; Bi et al., 2005; Smith and Freeman, 2006; Feakins and Sessions, 2010b). Despite these potentially obscuring effects, the stable hydrogen isotope compositions of plant lipids in lake sediments exhibit a nearly linear relationship with the δD ratios of the source waters. This corroborates the idea that fossil lipids may serve as a direct proxy for source water

hydrogen isotope characteristics (Sachse et al., 2004; Hou et al., 2008, Sachse et al., 2012). The inferred information about source water isotope characteristics can then be used to deduce palaeohydrologic changes such as variations in rainfall intensity.

In order to further explore the potential of the hydrogen isotope composition of *n*-alkanes preserved in ocean margin sediments as a proxy for hydrological conditions on a continental scale, a transect of 13 marine surface sediment samples from 1°N to 28°S off southwest Africa was analysed. The western part of Africa constitutes an ideal test case for such a study due to its distinct latitudinal distribution of vegetation zones and climatic conditions. We evaluate how the hydrogen isotope composition of *n*-alkanes preserved in ocean margin sediments mirrors the corresponding composition of continental precipitation in potential catchment areas. This correlation is essential for reliable reconstructions of the climate-dependent stable isotope composition of ancient precipitation and its climatic control.

## 4.3. Material and methods

### 4.3.1. Sediment material

We analysed 13 marine surface sediment samples that constitute an isobathic (ca. 1300 m) north to south transect (1°N to 28°S) along the south-western African continental margin (Fig. 4.1, Table 4.1). The samples were retrieved during cruises M34/2 and M41/1 of the German research vessel Meteor in 1996 and 1998, respectively, and recovered by multi-corer in order to receive the undisturbed surface layers. The multi-cores were separated into depth intervals, the sections sealed in polyethylene bags and stored at -20°C on board and afterwards at the University of Bremen.

### 4.3.2. Analytical methods

The procedures for the isolation of aliphatic/alicyclic hydrocarbons from the marine sediments were described by Vogts et al. (2012). Branched compounds were separated from the straight-chain hydrocarbons by urea adduction (Rommerskirchen et al., 2006). Stable hydrogen isotope compositions of the *n*-alkanes were determined by gas chromatography (GC, Agilent 6890 with Gerstel CIS) coupled to a Thermo Scientific MAT 253 isotope-ratio-mass spectrometer via a high temperature conversion reactor and a GCC-III Interface (all Thermo Scientific, Bremen). The GC instrument was equipped with a 30 m capillary column (J&W, DB-5, 0.25 mm i.d., 0.25 µm film thickness), the injector temperature was programmed from 60°C (5 s) to 305°C

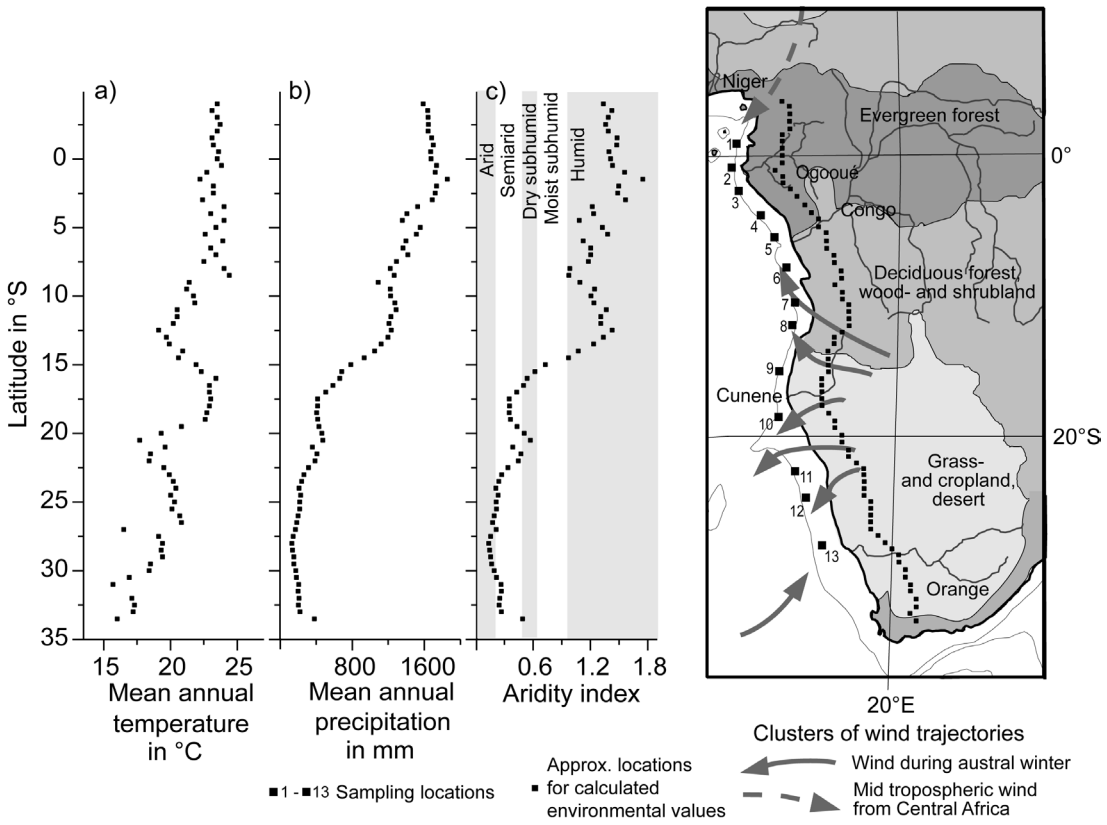


**Fig. 4.1:** Simplified present-day land cover map based on Mayaux et al. (2004) with sampling locations, clusters of wind trajectories based on Dupont and Wyputta (2003), and graphs of environmental parameters calculated for locations at 350 km distance to the coast with the WebWIMP modeling program (Matsuura et al., 2009; aridity index= mean annual precipitation divided by potential evapotranspiration; Supplementary Table 4.S1; UNEP, 1992).

(120 s) at 10°C $s^{-1}$ and the gas chromatographer oven was programmed from 60°C (2 min) to 300°C at a rate of 3°C $min^{-1}$, followed by an isothermal phase of 36 min. Isotope ratios are expressed as δD values in permil (‰) relative to Vienna Standard Mean Ocean Water (V-SMOW).

Calibration of isotope analysis was performed by injecting several pulses of reference gas ($H_2$) at the beginning and at the end of each run. The $H_3$-factor varied from 5.63 to 5.70 over the measuring period (5.66 ±0.03). The δD value of the reference gas was calibrated against the certified B2 reference mixture of *n*-alkanes distributed by the Department of Geological Sciences at Indiana University. A standard mixture containing lab standards and certified standard substances, which together span a range of -50 to -250‰ (vs. V-SMOW), were run repeatedly during each sequence. For eleven standard substances (fatty acid methyl esters and alkanes) in the retention time interval of the target compounds, the precision for replicate analyses expressed as averaged standard deviation was <4‰, and the averaged

**Table 4.1:** Compilation of sample information together with stable hydrogen isotope composition of *n*-alkanes and weighted mean averaged stable hydrogen isotope composition (WMA) with standard deviation (SD, 1σ).

| No. | GeoB No. | Latitude | Longitude | Water depth (m) | Cruise | Interval (cm bsf)[1] | *n*-$C_{29}$ Alkane δD (‰)[2] | SD (‰) | *n*-$C_{31}$ Alkane δD (‰)[2] | SD (‰) | *n*-$C_{33}$ Alkane δD (‰)[2] | SD (‰) | $WMA_{29-33}$ δD (‰) | SD (‰)[3] |
|---|---|---|---|---|---|---|---|---|---|---|---|---|---|---|
| 1 | 4904-6 | 0.962°N | 8.88°E | 1349 | M41/1 | 0.5 - 2 | **-133** | 2 | **-139** | 2 | -140 | 3 | -136 | 2 |
| 2 | 4906-4 | 0.69°S | 8.378°E | 1272 | M41/1 | 1 - 2 | **-127** | 2 | **-134** | 2 | -127 | 3 | -130 | 2 |
| 3 | 4909-3 | 2.068°S | 8.625°E | 1305 | M41/1 | 0 - 1.5 | **-127** | 2 | **-131** | 3 | -128 | 3 | -129 | 2 |
| 4 | 4912-3 | 3.73°S | 09.785°E | 1298 | M41/1 | 0 - 1 | **-127** | 2 | **-132** | 1 | -129 | 1 | -130 | 2 |
| 5 | 4913-3 | 5.503°S | 11.072°E | 1296 | M41/1 | 0 - 2.5 | **-131** | 2 | **-134** | 2 | -132 | 3 | -132 | 2 |
| 6 | 4915-2 | 7.75°S | 11.873°E | 1306 | M41/1 | 0.5 - 2 | **-131** | 2 | **-139** | 1 | -132 | 2 | -134 | 2 |
| 7 | 4916-3 | 10.173°S | 12.687°E | 1294 | M41/1 | 0 - 1 | **-129** | 0 | **-139** | 2 | -139 | 1 | -135 | 1 |
| 8 | 4917-4 | 11.903°S | 13.073°E | 1300 | M41/1 | 0.5 - 2.5 | **-133** | 1 | **-140** | 1 | -139 | 3 | -137 | 2 |
| 9 | 3713-1 | 15.628°S | 11.58°E | 1330 | M34/2 | 1.5 - 2.5 | -133 | 3 | **-133** | 2 | **-135** | 2 | -134 | 2 |
| 10 | 3715-2 | 18.955°S | 11.057°E | 1203 | M34/2 | 1 - 3.5 | -129 | 2 | **-139** | 2 | **-141** | 2 | -137 | 2 |
| 11 | 3706-3 | 22.717°S | 12.602°E | 1313 | M34/2 | 0.5 - 1.5 | -130 | 2 | **-138** | 3 | **-136** | 1 | -135 | 2 |
| 12 | 3705-3 | 24.303°S | 12.997°E | 1308 | M34/2 | 0.5 - 2 | -131 | 2 | **-137** | 1 | **-137** | 3 | -136 | 2 |
| 13 | 3701-1 | 27.952°S | 14.003°E | 1488 | M34/2 | 0.5 - 1.5 | -123 | 2 | **-126** | 2 | **-127** | 3 | -126 | 2 |

[1] Analysed sediment interval in cm below sea floor.

[2] **Boldface values** refer to the two most abundant homologues.

[3] Calculated as weighted mean average from alkane abundances (Vogts et al., 2012).

absolute error was 2‰ (n= 33). Analyses of samples were performed at least in triplicate with standard deviations <4‰ (2‰ on average, n= 60). Eicosanoic acid methyl ester (certified) and docosanoic acid methyl ester (lab standard) of known hydrogen isotope composition were added to the samples and used for quality control, but standard deviations for these internal standards were higher (8‰ and 7‰, respectively). This is attributed to coelution of sample components with the standards.

### 4.3.3. Employed models

#### *4.3.3.1. WebWIMP modeling program for climatic parameters*

The WebWIMP modeling program (Matsuura et al., 2009) was used to calculate annual mean temperature, precipitation and potential evapotranspiration. The WebWIMP modeling program calculates climatically-averaged monthly water balances for continental locations at nodes of half a degree of latitude by half a degree of longitude. Average monthly air temperature and precipitation data of weather stations are interpolated to the grid nodes and the grid-point water balance is calculated by a modified Thornthwaite procedure.

#### *4.3.3.2. OIPC for hydrogen isotope ratios of precipitation*

The online isotopes in precipitation calculator (OIPC) was used to calculate the estimated modern mean annual and monthly hydrogen isotope composition of precipitation ($\delta D_P$) for a set of given longitude, latitude and elevation. Elevation was received from a digital elevation model based on SRTM3 data (Michalak, 2004). Hydrogen isotope ratios of precipitation were calculated from a global data set according to an algorithm developed by Bowen and Wilkinson (2002) and refined by Bowen and Revenaugh (2003) and Bowen et al. (2005). The data used by the OIPC is derived primarily from the International Atomic Energy Association/World Meteorological Organisation Global Network for Isotopes in Precipitation.

#### *4.3.3.3. Limitations*

A limitation for both employed models may be the uneven spatial distribution of weather stations in Africa. Furthermore, the weather records partly cover different years and different time spans and the time span covered by the sediment material may be longer than the time interval covered by the data base for the models.

## 4.4. Regional setting

### 4.4.1. Hydrological conditions in southwest Africa

To depict environmental conditions in the study area, Fig. 4.1 provides values for mean temperature and precipitation (WebWIMP; Matsuura et al., 2009) as well as aridity index (mean annual precipitation divided by potential evapotranspiration; Supplementary Table 4.S1; UNEP, 1992). Along the equator a humid zone with mean annual rainfall of more than 1500 mm prevails (Fig. 4.1b). Further south, mean annual precipitation decreases gradually and the climate exhibits austral summer rain and winter droughts, a result of the seasonal migration of the Intertropical Convergence Zone in response to changes in the latitudinal maximum of solar heating. Subtropical deserts follow where precipitation is scarce. South of 32°S mean annual precipitation increases again due to the equatorward displacement of the mid-latitude Westerlies during austral winter causing highest precipitation during winter and dry summers.

The hydrogen isotope composition of the precipitation varies with moisture source, altitude, temperature, amount of precipitation and degree of continentality (Gat, 1996). The model-based map of δD values of mean annual precipitation ($\delta D_P$) mirrors the interplay of these factors leading to ratios ranging from more positive values in the rain forest region to more negative values south of the Congo River and back to more positive ratios south of 20°S (Fig. 4.2a, Supplementary Table 4.S2; Bowen and Revenaugh, 2003). The $\delta D_P$ in Africa varies with season by up to 60‰ but for the postulated catchment areas relevant to this study extreme $\delta D_P$ values occur mostly in months with negligible precipitation and $\delta D_P$ during the growing season is less variable (Supplementary Table 4.S3).

### 4.4.2. Vegetation of southwest Africa

There is a gradient from dense evergreen biomes to dry open land-cover from the equator to the subtropics, corresponding to the mean annual rainfall gradient (Mayaux et al., 2004). The equatorial rain forest vegetation is characterised by woody $C_3$ plants as major representatives of the flora (Richards, 1996). The evergreen rain forest extends to about 9°S and is increasingly confined to river valleys toward its limits. The closed forest (no grass cover on the ground) often abruptly passes into a wide zone of wood- and shrubland (Richards, 1996). In these regions, deciduous woody species can cover up to 60% of the area (Cole, 1986). The amount of woody $C_3$ vegetation decreases with increasing aridity, accompanied by increasing $C_4$ grass abundance. On the African Plateau, $C_4$ grasses dominate the vegetation

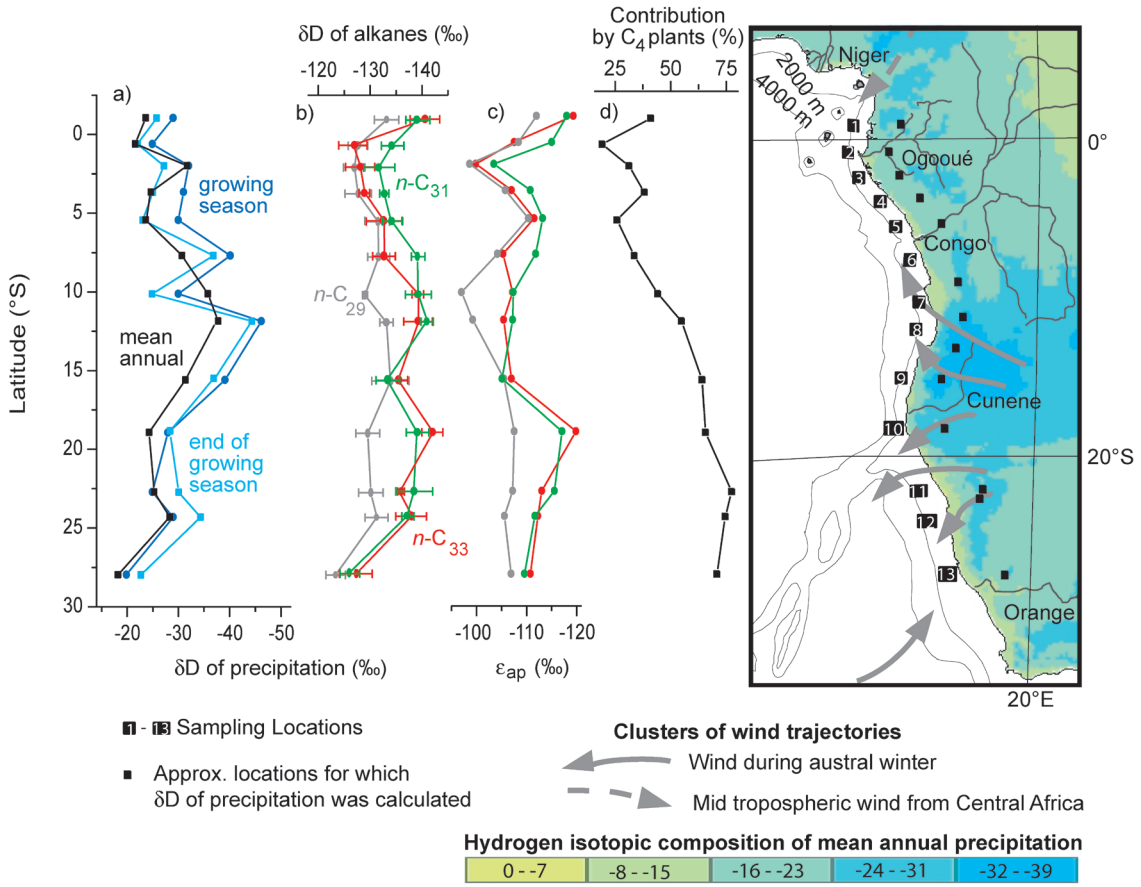


**Fig. 4.2:** Stable hydrogen isotope composition of (a) precipitation at 350 km distance from the coast in postulated catchment areas indicated by black squares in the map (Supplementary Tables 4.S2, 4.S3), (b) *n*-alkanes dominating the aliphatic fraction of the sediment samples as well as (c) apparent fractionation between *n*-alkanes and mean annual precipitation, and (d) contribution by $C_4$ plants to the sediments calculated from the weighted mean averaged stable carbon isotopic composition of *n*-alkanes (Vogts et al., 2012), and map of southwest Africa showing sampling locations as well as hydrogen isotope composition of mean annual precipitation (Bowen and Revenaugh, 2003). Clusters of wind trajectories based on Dupont and Wyputta (2003).

while in the dry coastal Namib Desert the vegetation is very sparse. In the Succulent Karoo, succulent plants employing the Crassulacean Acid Metabolism (CAM) dominate. However, since CAM is generally a strategy for stress survival and not for high productivity (Lüttge, 2004) we assume the contribution of CAM-utilising plants to biomass production, and thus also to geological archives, to be negligible.

### 4.4.3. Transport pathways and catchment areas for plant wax lipids

Vogts et al. (2012) presented potential catchment areas for the sampling locations, which reasonably explain the $C_4$ plant contribution to the sediments. The origin of the material was estimated based on modelled aeolian transport pathways

of terrestrial components (implemented in Figs. 4.1 and 4.2; Dupont and Wyputta, 2003). For the equatorial sites (1-4) mid-tropospheric transport by Harmattan winds from north-central Africa contributes material to the sediments. Therefore, these locations were plotted but not used for correlations by Vogts et al. (2012) and will be treated likewise in this study.

Also, potential riverine contributions were taken into account to explain the $C_3/C_4$ plant contribution to the sediments (Vogts et al., 2012). In the study area, the Congo River system draining toward location 5 is the largest and also the second biggest in the world regarding the outflow at the mouth (Dai and Trenberth, 2002). The outflows of the Ogooué (ca. 1°S, location 2) and the Orange (28.5°S, location 13) are lower by a factor of ca. ten, and the outflow of other rivers is lower by a factor of 50 or more (e.g., Kunene, 17°S; Heyns, 2003; Nilsson et al., 2005). However, the river outflow data only reflect the quantity of water and not the amount of *n*-alkanes transported. Quantitative data on the contribution of *n*-alkanes to deep sea sediments by these rivers are not available.

## 4.5. Results and discussion

### 4.5.1. Hydrogen isotope composition of *n*-alkanes

In all samples, the *n*-$C_{29}$, *n*-$C_{31}$, and *n*-$C_{33}$ alkanes (hereafter abbreviated $C_{29}$, $C_{31}$ and $C_{33}$) are the most abundant homologues (Vogts et al., 2012). The stable hydrogen isotope compositions of these compounds vary from -123 to -141‰ (Table 4.1, Fig. 4.2b). The observed values are slightly more positive than the ratios for $C_{29}$ in core-top material of sediment recovered off the Congo River mouth (ca. -145‰; Schefuß et al., 2005) and Late Holocene samples collected off SW Africa (-138 to -154‰; Collins et al., 2013). As marine organisms do not biosynthesise any significant amounts of these long chain alkanes (Chikaraishi and Naraoka, 2003; Mead et al., 2005) and hopane analyses as well as carbon preference indices indicate the presence of a constant but only very small amount of petroleum-derived *n*-alkanes (Vogts et al., 2012), the observed variations of the *n*-alkane stable hydrogen isotope composition are nearly exclusively related to the source land plants.

The δD ratios of $C_{29}$ ($\delta D_{29}$) vary by 10‰ and the variations of $\delta D_{31}$ and $\delta D_{33}$ are only slightly higher (14‰; Fig. 4.2b). Among the *n*-alkanes of a given sampling location $\delta D_{29}$ is the most positive in the majority of cases and $\delta D_{31}$ is 5‰ more negative on average. $\delta D_{33}$ resembles $\delta D_{31}$ except for locations 2 to 5 where the values are similar to those of $C_{29}$. The averaged hydrogen isotope composition is presented as weighted mean average ($\delta D_{WMA}$; Table 4.1) and shows a variation of 11‰.

**Table 4.2:** Hydrogen isotope composition of mean annual (left) and growing-season (right) precipitation for continental locations in postulated catchment areas together with Pearson correlation coefficients (bottom) for linear correlation with sediment derived *n*-alkane stable hydrogen isotope composition.

| | Distance to coast (km ) | | | | | | | | | | | | | | | | | | | | | |
|---|---|---|---|---|---|---|---|---|---|---|---|---|---|---|---|---|---|---|---|---|---|---|
| | 150 | | 200 | | 250 | | 300 | | 350 | | 400 | | 350 | | 350 | | 350 | | | | | |
| | Hydrogen isotope composition of precipitation and 95% confidence interval (‰)[1] | | | | | | | | | | | | | | | | | | | | | |
| No. | Annual mean | | Annual mean | | Annual mean | | Annual mean | | Annual mean | | Annual mean | | December | | $P_{WMA}$[3] Dec-March | | $P_{WMA}$[3] of 3 months with highest precipitation | | | |
| 5 | -20 | 3 | -18 | 3 | -19 | 3 | -24 | 3 | -23 | 3 | -26 | 3 | -29 | | -22 | | -28 | | | | | |
| 6 | -13 | 3 | -17 | 3 | -26 | 3 | -24 | 3 | -30 | 3 | -25 | 3 | -39 | | -36 | | -34 | | | | | |
| 7 | -30 | 3 | -30 | 3 | -35 | 4 | -35 | 4 | -35 | 5 | -35 | 5 | -29 | | -24 | | -23 | | | | | |
| 8 | -41 | 3 | -41 | 3 | -36 | 3 | -38 | 4 | -37 | 4 | -37 | 4 | -45 | | -43 | | -43 | | | | | |
| 9 | -31 | 3 | -31 | 2 | -32 | 2 | -30 | 2 | -31 | 2 | -33 | 1 | -38 | | -36 | | -36 | | | | | |
| 10 | -27 | 5 | -26 | 5 | -25 | 5 | -24 | 5 | -24 | 5 | -24 | 5 | -27 | | -28 | | -28 | | | | | |
| 11 | -20 | 3 | -25 | 3 | -25 | 3 | -27 | 3 | -25 | 3 | -24 | 3 | -24 | | -29 | | -30 | | | | | |
| 12 | -17 | 4 | -20 | 4 | -25 | 4 | -23 | 4 | -28 | 4 | -26 | 5 | -28 | | -34 | | -34 | | | | | |
| 13 | -15 | 4 | -16 | 4 | -16 | 4 | -19 | 4 | -18 | 4 | -17 | 4 | -19 | | -22 | | -22 | | | | | |
| r (*n*-$C_{29}$ alkane)[2] | 0.45 | | *0.49* | | *0.60* | | *0.52* | | *0.65* | | ***0.68*** | | ***0.80*** | | ***0.71*** | | ***0.79*** | | | | | |
| r (*n*-$C_{31}$ alkane)[2] | 0.41 | | *0.51* | | ***0.66*** | | *0.59* | | ***0.69*** | | *0.58* | | *0.53* | | *0.51* | | 0.47 | | | | | |
| r (*n*-$C_{33}$ alkane)[2] | *0.62* | | *0.65* | | ***0.67*** | | *0.56* | | *0.57* | | *0.58* | | 0.31 | | 0.35 | | 0.31 | | | | | |
| r ($\delta D_{WMA29-33}$)[2] | 0.49 | | *0.57* | | *0.65* | | *0.54* | | *0.63* | | *0.58* | | *0.52* | | *0.56* | | *0.56* | | | | | |

[1] Confidence intervals not available for monthly values.

[2] ***Bold italic numbers:*** Correlation significant at the 99% level. *Italic numbers:* Correlation significant at the 95% level, calculations based on locations 5-13.

[3] $P_{WMA}$= weighted mean average of precipitation

### 4.5.2. Correlation with the δD signal of precipitation

To elucidate possible correlations of the $\delta D_L$ (stable hydrogen isotope composition of lipids) the online isotopes in precipitation calculator (OIPC 2.2; Bowen and Revenaugh, 2003) was employed to determine $\delta D_P$ (Supplementary Table 4.S2). Calculations were made for equidistant locations along postulated main contribution pathways spanning from 150 to 400 km inland from the coast (Vogts et al., 2012).

The range of $\delta D_P$ for the continental locations (max. 28‰; Table 4.2, Fig. 4.2) is broader than the range of hydrogen isotope ratios of sedimentary alkanes (max. 14‰). This may be related to mixing of *n*-alkanes from catchment areas wider than postulated with the effect of averaging out $\delta D_L$ differences to some extent. The $\delta D_P$ values (Table 4.2) were correlated with the sediment-derived $\delta D_L$ values. Except for 150 km distance from the coast, the correlation coefficients are above 0.49 ($p < 0.05$; Table 4.2). The highest correlation coefficients were observed for the distances of 250, 350 and 400 km from the coast (up to 0.69, $p < 0.01$). Previous analyses of the same samples (Vogts et al., 2012) revealed significant correlations (r up to 0.95, $p < 0.01$) of the $C_4$ contribution to the sediments (calculated from the *n*-$C_{31}$ alkane stable carbon isotope composition) with environmental parameters for the same postulated catchment areas (highest correlation with locations at 350 km). Thus, this area may represent a major source region contributing to the sediments.

As the precipitation is unevenly distributed over the year in terms of amount and stable hydrogen isotope composition, monthly $\delta D_P$ values were calculated for locations at approximately 350 km distance from the coast (Supplementary Table 4.S3, OIPC 2.2; Bowen et al., 2005). The best correlations were obtained for $\delta D_{29}$ and December precipitation (r up to 0.80, $p < 0.01$; Table 4.2), a month representing the beginning of the rain season at most locations. This substantiates the hypothesis that most *n*-alkanes are synthesised during leaf formation at the beginning of the growing season (Jetter et al., 2006). For field-grown barley, Sachse et al. (2010) also revealed that $\delta D_L$ reflects leaf water δD at the time of leaf development. However, in our $C_{29}$ alkane dataset the correlations for March are also significant ($r = 0.75$, $p < 0.01$, data not shown). This, in contrast, is more in line with the idea that alkanes are produced during the whole growing phase, which may last from December to March, and consistent with studies indicating the need of continuous replacement of wax components (Richardson et al., 2005) removed by mechanical stress like sand storms. Consequently, the weighted mean average $\delta D_P$ for December to March (Table 4.2) was correlated with $\delta D_L$ and yielded a similarly good correlation (r up to 0.71, $p < 0.01$). However, not all locations receive the main precipitation from December to March. Maximum rainfall at the northern sites occurs either earlier

(November) or later (April). Thus, the weighted mean average $\delta D_P$ for the three months with the highest precipitation was also calculated and yielded a good correlation as well (r up to 0.79, p <0.01; Table 4.2). Thus, this dataset delivers no clear indication about the timing of *n*-alkane synthesis in the plants and reveals no bias of the sedimentary alkane δD signal toward a particular part of the wet season.

As Sachse et al. (2009) found $\delta D_L$ preserved in soils to be representative of the weeks before leaf senescence, we also calculated correlation coefficients for the last month of the growing season but yielded lower Pearson correlation coefficients (data not displayed). In addition, we tested correlations with weighted mean averaged $\delta D_P$ of all months with precipitation above 20 and 150 mm, respectively, as well as for the two or the four months with highest precipitation, but did not obtain better correlations. A limiting factor for this approach may be that the strength of correlation with growing-season precipitation can also be influenced by the seasonality of the prevailing winds which mainly blow toward the ocean during austral winter (Dupont and Wyputta, 2003).

### 4.5.3. Apparent fractionation

To further evaluate influences on the connection between sedimentary alkane composition and continental precipitation, the apparent stable hydrogen isotope fractionation ($\varepsilon_a$) between $\delta D_P$ and $\delta D_L$ was calculated using the following equation:

$$\varepsilon_a = 1000 \times \frac{\delta D_L + 1000}{\delta D_P + 1000} - 1 \qquad \textbf{Equation 4.1}$$

Calculations were based on mean annual $\delta D_P$ at 350 km distance from the coast in postulated catchment areas, because the improvement of correlation by using monthly values was not consistent for all alkanes. The graphical presentation of $\varepsilon_a$ (Fig. 4.2c) exhibits similar general trends for all analysed alkanes with less negative values from sites 5 to 9 and more negative and constant ratios from locations 10-13. The calculated $\varepsilon_a$ values (-109‰ on average; Table 4.3) for this ocean sediment transect are less negative compared to average $\varepsilon_a$ value for $C_4$ monocotyledons and dicotyledonous $C_3$ plants (-134‰ and -113‰, respectively; Sachse et al., 2012). For Cameroonian rainforest locations $\varepsilon_a$ values up to -154‰ (Garcin et al., 2012) were reported employing estimated surface water values. However, we employ modeled precipitation data and our locations 1-4 off the humid rainforest regions also receive material from long range transport from more arid regions which potentially leads to less negative $\varepsilon_a$ values. For locations 5-13, our results are comparable to $\varepsilon_a$ values found for alkanes in lake sediments of the Venezuelan Páramo shrubland (Polissar

**Table 4.3:** Apparent hydrogen isotope fractionation ($\varepsilon_a$) between sediment derived hydrogen isotope composition of *n*-alkanes and calculated mean annual precipitation for continental locations at 350 km distance from the coast in postulated catchment areas.

| No. | $\varepsilon_{aC29}$ (‰) | $\varepsilon_{aC31}$ (‰) | $\varepsilon_{aC33}$ (‰) | $\varepsilon_{aWMA29-33}$ (‰) |
|---|---|---|---|---|
| 1 | **-112** | **-118** | -120 | -116 |
| 2 | **-109** | **-115** | -108 | -111 |
| 3 | **-99** | **-104** | -100 | -101 |
| 4 | **-106** | **-111** | -107 | -108 |
| 5 | **-111** | **-114** | -112 | -112 |
| 6 | **-104** | **-112** | -105 | -107 |
| 7 | **-97** | **-108** | -107 | -103 |
| 8 | **-99** | **-107** | -106 | -104 |
| 9 | -106 | **-105** | **-107** | -106 |
| 10 | -108 | **-117** | **-120** | -116 |
| 11 | -107 | **-116** | **-113** | -113 |
| 12 | -106 | **-112** | **-113** | -111 |
| 13 | -107 | **-110** | **-111** | -110 |

[1] **Boldface values** refer to the two most abundant homologues.

and Freeman, 2010). In some arid environments even smaller values than observed in this study were reported (e.g., -94‰; Feakins and Sessions, 2010a). However, despite the huge gradient in environmental conditions and vegetation in our study area, the standard deviation of $\varepsilon_a$ in our study is fairly constant ($\sigma$ <5‰).

The calculated $\varepsilon_a$ values incorporate the effects of soil evaporation, transpiration and biosynthesis (Fig 4.3a). For the biosynthesis of *n*-alkanes, it was hypothesised that the fractionation of hydrogen is constant (Sessions et al., 1999; Sachse et al., 2004; Feakins and Sessions, 2010a) even though some growth chamber experiments found variations of 65‰ among different plant species (Kahmen et al., 2013a). Data for $\varepsilon_a$ of plants from the study region are presently not available. Thus, we assume that species dependent variation of fractionation during biosynthesis is constant because it is averaged out due to the high number of contributing species. Therefore, evaporation of soil water and evapotranspiration from the plant are the main factors influencing the apparent fractionation.

As vapour-phase water is depleted in the heavy isotopes relative to the liquid from which it is derived, higher evaporation and transpiration at the arid sites should lead to higher δD ratios of the biosynthetic water pool and a less negative $\varepsilon_a$. For instance, Aichner et al. (2010) and Smith and Freeman (2006) found less negative $\varepsilon_a$ values at more arid sites. In addition, under arid conditions surface soils are more affected by evaporation which leads to higher δD ratios of the biosynthetic water pool of shallow rooted species. Both effects should lead to less negative $\varepsilon_a$

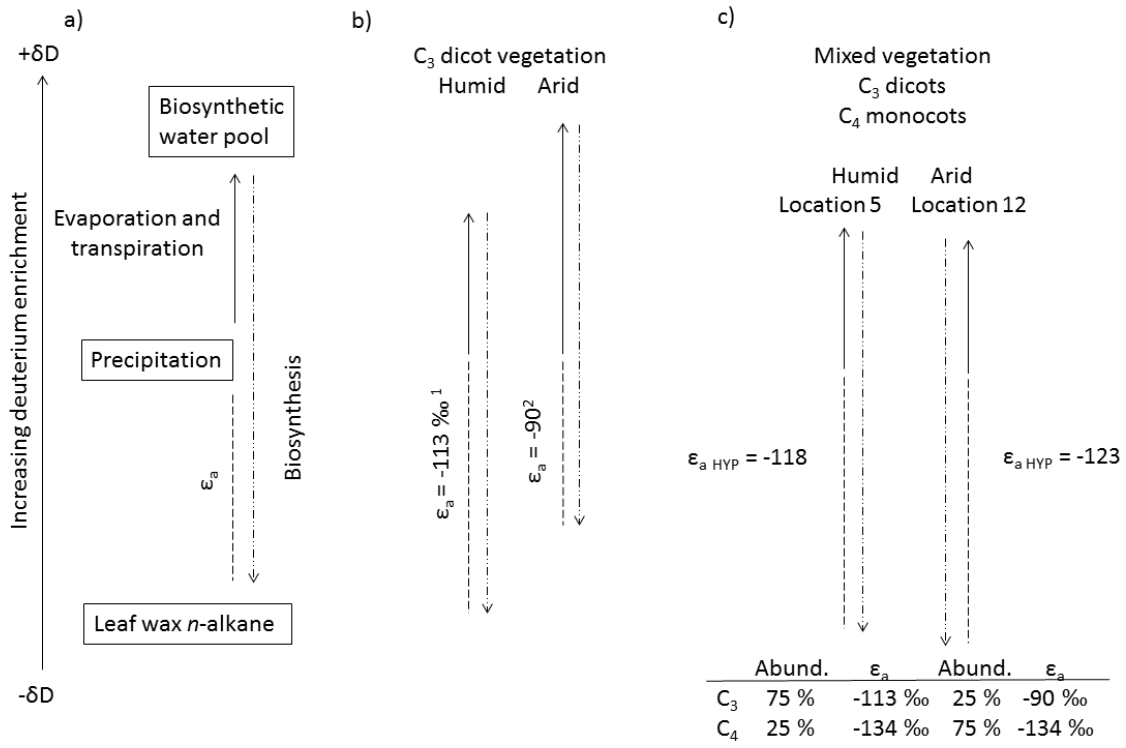


**Fig. 4.3:** Conceptual model explaining the origin of apparent fractionation ($\varepsilon_a$). a) General scheme, b) $\varepsilon_a$ of a dicotyledonous vegetation under humid (Sachse et al., 2012) and arid (Feakins and Sessions, 2010a) conditions, c) hypothetical $\varepsilon_a$ of a mixed $C_3/C_4$ vegetation at continental locations contributing to sample locations 5 and 12 based on binary mixing of data in included table with abundance of monocotyledonous $C_4$ and dicotyledonous $C_3$ plants (Vogts et al 2012) and $\varepsilon_a$ from literature (Feakins and Sessions, 2010a; Sachse et al., 2012).

in arid grasslands compared to humid areas dominated by deep rooted trees. For our samples, however, such a trend is not evident and correlations between $\varepsilon_a$ and environmental parameters (mean annual precipitation, potential evapotranspiration, aridity index) as well as $C_4$ plant abundance (Fig. 4.2d), representing shallow rooted species, do not exceed 0.53 (Table 4.4). Best correlations (r up to 0.53, $p < 0.05$) were obtained for the aridity index, which may best reflect the amount of water available to the plant.

The poor correlation of $\varepsilon_a$ with environmental parameters and $C_4$ grass abundance indicates that other factors may conceal effects of increasing aridity and rooting depth. A potential candidate is the different plant transpiration characteristic of mono- and dicotyledonous vegetation. Data for $\varepsilon_a$ of plants from the study region are presently not available. However, the $\varepsilon_a$ differences observed for mono- and dicotyledonous vegetation of other environments (Liu et al., 2006; Hou et al., 2007, Sachse et al., 2012) may be applicable in Africa, too. Leaves of monocotyledonous species grow and expand at the base of a leaf blade covered by the next older leaf (Kemp,

**Table 4.4:** Pearson correlation coefficients for apparent fractionation and environmental parameters for locations in postulated catchment areas at 350 km distance from the coast (Supplementary Table 4.S2).

| | Mean annual precipitation | Potential evapotranspiration | Aridity index |
|---|---|---|---|
| $\varepsilon_{aC29}$ [1] | 0.29 | -0.39 | 0.40 |
| $\varepsilon_{aC31}$ [1] | 0.23 | -0.23 | 0.30 |
| $\varepsilon_{aC33}$ [1] | *0.51* | -0.09 | *0.53* |
| $\varepsilon_{aWMA29-33}$ [1] | 0.45 | -0.24 | *0.52* |

[1] *Italic numbers:* Correlation significant at the 95% level.

1980) which leads to a low influence of transpiration on the biosynthetic water pool of monocotyledons (Kahmen et al., 2013a). For dicotyledonous plants growth and expansion occur for the whole transpiration enduring leaf after its initial unfolding (Dale, 1988). Thus, dicotyledonous leaf wax synthesis possibly employs more D-enriched leaf water (Kahmen et al, 2013a). In addition, the different evapotranspiration of trees and grasses was assumed to be related to the characteristic differences in leaf morphology, leaf vein pattern and interveinal distance as well as thickset (Smith and Freeman, 2006; Liu and Yang, 2008; Kahmen et al. 2013b). Averaged literature data reflect the described effects: The average $\varepsilon_a$ for alkanes of leaf waxes of $C_3$ monocotyledons including grasses is more negative compared to dicotyledonous $C_3$ plants (-149‰ and -113‰, respectively; Sachse et. al. 2012). The averaged value for $C_4$ monocotyledons including $C_4$ grasses (-134‰) is between those of mono- and dicotyledonous $C_3$ plants indicating that the effects of the metabolic pathway are only of minor relevance for the hydrogen isotope composition of the alkanes.

However, $\varepsilon_a$ is not as constant as the averaged ratios suggest. For subhumid and arid sites in southern California (precipitation <800 mm $a^{-1}$) Feakins and Sessions (2010a) found $\varepsilon_a$ of ca. -90‰ for mixed wood- and shrubland $C_3$ plants, excluding grasses. This points to an influence of aridity on $\varepsilon_a$ of $C_3$ dicotyledons (Fig. 4.3b). In contrast, $\varepsilon_a$ of $C_4$ grasses of the North American Great Plains was still below -140‰ for a location with a fainfall of 360 mm $a^{-1}$ (Smith and Freeman, 2006). McInerney et al. (2011) also did not find a correlation of $\varepsilon_a$ with relative humidity for growth chamber $C_4$ grasses and only a weak correlation for field grown species ($r^2$= 0.35, p <0.05). This difference in response to aridity is consistent with results of Kahmen et al. (2013a), who found that in dicotyledonous plants leaf water on average contributed 96% to the biosynthetic water pool whereas this contribution was only between 18 and 68% in grasses. Thus, transpirational leaf water enrichment may affect dicotyledonous trees much more than monocotyledonous grasses.

For our sedimentary archives, the contribution of trees declines toward the south while their alkanes potentially record less negative $\varepsilon_a$. In parallel, the contribution of $C_4$ grasses with more negative and constant $\varepsilon_a$ increases. This could result in the observed seemingly constant hydrogen isotopic fractionation. To test this hypothesis, we calculated a hypothetical fractionation based on the contribution of different plant groups calculated from the stable carbon isotopic composition of sedimentary alkanes ($C_4$ vs. $C_3$; Vogts et al., 2012) and $\varepsilon_a$ values from literature (Fig. 4.3c). For $C_4$ plants, a fractionation of -134‰ (Sachse et al., 2012) was assumed. For $C_3$ species, we employed an $\varepsilon_a$ of -113‰ for location 5 with the highest precipitation (Sachse et. al., 2012) and -90‰ for location 12 with less than 800 mm $a^{-1}$ precipitation (Feakins and Sessions, 2010a). In this way, we obtained quite similar hypothetical $\varepsilon_a$ values of -118 and -123‰, respectively (Fig. 4.3c). This substantiates that the vegetation shift from $C_3$ dicotyledons to $C_4$ monocotyledons may conceal aridity effects on the apparent fractionation. For North American continental sampling sites it was also hypothesised that the influence of aridity and the associated change in vegetation assembly offset each other reducing the shift in $\varepsilon_a$ (Hou et al., 2008; Gao et al., 2014). This study demonstrates that this hypothesis is also feasible for alkanes derived from marine sediments off tropical areas.

## 4.6. Conclusions

The δD values of leaf wax *n*-alkanes ($C_{29}$, $C_{31}$, and $C_{33}$) in ocean margin sediments off southwest Africa vary from -123 to -141‰. These ratios were compared to the modeled δD ratios for precipitation at continental locations along postulated transport pathways from land to ocean. The highest correlation coefficients were observed for mean annual precipitation values at locations with 350 km distance to the coast. When ratios for the growing season and the end of the growing season are applied, the correlation increases for $C_{29}$, but decreases for $C_{31}$ and $C_{33}$. The apparent fractionations between alkane and precipitation (-109‰ on average) are fairly constant ($\sigma$ <5‰), possibly because the effects of increasing aridity are superimposed on the effect of life form change (trees to grasses). Thus, we conclude that in this region δD ratios of alkanes in ocean margin sediments can directly be related to the isotope composition of continental precipitation by the presented fractionation factors. The feasibility over geological timescales should be best in times of stable or slowly changing vegetation composition. In general, the variations in the abundance of the ecological life forms (trees vs. grasses) should be evaluated in parallel by, e.g., stable carbon isotope or pollen analyses to exclude effects of vegetation change on deductions about continental precipitation changes.

## 4.7. Acknowledgements

We gratefully appreciate the effort of organisers and participants of RV Meteor cruises M34/2 and M41/1. We are indebted to Dr. M. Zabel (University of Bremen) for helpful advice during sample retrieval. Special thanks are given to H. Haase and B. Kopke (both ICBM) for support during urea adduction and help with stable isotope analysis, respectively. Dr. F. Rommerskirchen (University of Bremen) is gratefully acknowledged for providing figure drafts. This study was financially supported by Deutsche Forschungsgemeinschaft (grant no. Ru 458/35).

## 4.8. Supplementary Tables

**Supplementary Table 4.S1:** Locations employed for calculations of continental environmental conditions with the WebWIMP modeling program and values obtained as displayed in Fig. 4.1.

| Latitude | Longitude (°E) | Mean annual temperature (°C) | Mean annual precipitation (mm) | Potential evapotranspiration (mm) | Aridity index |
|---|---|---|---|---|---|
| 4.0°N | 12.5 | 23.5 | 1585 | 1188 | 1.33 |
| 3.5°N | 13 | 23.1 | 1634 | 1148 | 1.42 |
| 3.0°N | 13 | 23.5 | 1640 | 1183 | 1.39 |
| 2.5°N | 13 | 23.7 | 1642 | 1209 | 1.36 |
| 2.0°N | 13 | 23.5 | 1639 | 1184 | 1.38 |
| 1.5°N | 12.5 | 23.1 | 1680 | 1138 | 1.48 |
| 1.0°N | 12.5 | 23.2 | 1696 | 1150 | 1.47 |
| 0.5°N | 12.5 | 23.6 | 1668 | 1198 | 1.39 |
| 0.0° | 12.5 | 23.5 | 1672 | 1188 | 1.41 |
| 0.5°S | 12.5 | 23.8 | 1733 | 1213 | 1.43 |
| 1.0°S | 12 | 22.7 | 1720 | 1106 | 1.56 |
| 1.5°S | 12.5 | 22.2 | 1851 | 1059 | 1.75 |
| 2.0°S | 12.5 | 23.2 | 1732 | 1160 | 1.49 |
| 2.5°S | 13 | 23.2 | 1717 | 1158 | 1.48 |
| 3.0°S | 13.5 | 22.4 | 1686 | 1078 | 1.56 |
| 3.5°S | 14 | 24.0 | 1525 | 1251 | 1.22 |
| 4.0°S | 14.5 | 23.0 | 1405 | 1140 | 1.23 |
| 4.5°S | 15 | 24.0 | 1353 | 1250 | 1.08 |
| 5.0°S | 15 | 23.4 | 1553 | 1173 | 1.32 |
| 5.5°S | 15.5 | 22.6 | 1510 | 1096 | 1.38 |
| 6.0°S | 15.5 | 23.9 | 1393 | 1240 | 1.12 |
| 6.5°S | 15.5 | 23.0 | 1361 | 1134 | 1.2 |
| 7.0°S | 16 | 23.4 | 1416 | 1178 | 1.2 |
| 7.5°S | 16 | 22.5 | 1288 | 1095 | 1.18 |
| 8.0°S | 16.5 | 24.0 | 1221 | 1241 | 0.98 |
| 8.5°S | 16.5 | 24.4 | 1263 | 1300 | 0.97 |
| 9.0°S | 16 | 21.4 | 1088 | 1001 | 1.09 |
| 9.5°S | 16.5 | 21.2 | 1220 | 982 | 1.24 |
| 10.0°S | 16.5 | 21.7 | 1225 | 1017 | 1.2 |
| 10.5°S | 17 | 21.8 | 1269 | 1028 | 1.23 |
| 11.0°S | 17 | 20.5 | 1284 | 941 | 1.36 |
| 11.5°S | 17 | 20.5 | 1228 | 939 | 1.31 |
| 12.0°S | 17 | 20.2 | 1207 | 923 | 1.31 |
| 12.5°S | 16.5 | 19.1 | 1232 | 865 | 1.42 |
| 13.0°S | 16 | 19.7 | 1196 | 896 | 1.33 |
| 13.5°S | 16 | 19.9 | 1118 | 907 | 1.23 |
| 14.0°S | 15.5 | 20.9 | 1048 | 978 | 1.07 |
| 14.5°S | 15.5 | 20.6 | 930 | 960 | 0.97 |

**Supplementary Table 4.S1** (continued)

| Latitude | Longitude (°E) | Mean annual temperature (°C) | Mean annual precipitation (mm) | Potential evapo-transpiration (mm) | Aridity index |
|---|---|---|---|---|---|
| 15.0°S | 15.5 | 21.9 | 782 | 1075 | 0.73 |
| 15.5°S | 15.5 | 22.3 | 681 | 1106 | 0.62 |
| 16.0°S | 15 | 23.4 | 662 | 1233 | 0.54 |
| 16.5°S | 15 | 22.9 | 586 | 1179 | 0.5 |
| 17.0°S | 15 | 22.9 | 504 | 1182 | 0.43 |
| 17.5°S | 15 | 23.0 | 416 | 1196 | 0.35 |
| 18.0°S | 15 | 22.9 | 415 | 1186 | 0.35 |
| 18.5°S | 15.5 | 22.7 | 406 | 1167 | 0.35 |
| 19.0°S | 16 | 22.6 | 418 | 1158 | 0.36 |
| 19.5°S | 16 | 20.8 | 430 | 999 | 0.43 |
| 20.0°S | 16.5 | 19.3 | 461 | 911 | 0.51 |
| 20.5°S | 16.5 | 17.7 | 474 | 831 | 0.57 |
| 21.0°S | 17 | 19.6 | 358 | 932 | 0.38 |
| 21.5°S | 17 | 18.5 | 408 | 870 | 0.47 |
| 22.0°S | 17.5 | 18.4 | 387 | 874 | 0.44 |
| 22.5°S | 18 | 19.5 | 315 | 943 | 0.33 |
| 23.0°S | 18 | 19.9 | 262 | 971 | 0.27 |
| 23.5°S | 18 | 20.2 | 237 | 989 | 0.24 |
| 24.0°S | 18 | 20.4 | 211 | 1011 | 0.21 |
| 24.5°S | 18 | 20.0 | 229 | 989 | 0.23 |
| 25.0°S | 18.5 | 20.3 | 216 | 1018 | 0.21 |
| 25.5°S | 18.5 | 20.1 | 216 | 1005 | 0.21 |
| 26.0°S | 18.5 | 20.7 | 198 | 1045 | 0.19 |
| 26.5°S | 18.5 | 20.8 | 184 | 1054 | 0.17 |
| 27.0°S | 18.5 | 16.5 | 170 | 806 | 0.21 |
| 27.5°S | 19 | 19.1 | 144 | 948 | 0.15 |
| 28.0°S | 19.5 | 19.4 | 129 | 974 | 0.13 |
| 28.5°S | 20 | 19.3 | 137 | 966 | 0.14 |
| 29.0°S | 20.5 | 19.4 | 150 | 983 | 0.15 |
| 29.5°S | 20.5 | 18.5 | 152 | 927 | 0.16 |
| 30.0°S | 21 | 18.4 | 175 | 921 | 0.19 |
| 30.5°S | 21 | 16.9 | 181 | 842 | 0.21 |
| 31.0°S | 21.5 | 15.7 | 206 | 789 | 0.26 |
| 31.5°S | 21.5 | 14.9 | 200 | 755 | 0.26 |
| 32.0°S | 22 | 17.1 | 208 | 834 | 0.25 |
| 32.5°S | 22 | 17.3 | 201 | 836 | 0.24 |
| 33.0°S | 21.5 | 17.2 | 219 | 828 | 0.26 |
| 33.5°S | 22 | 16.0 | 378 | 774 | 0.49 |

**Supplementary Table 4.S2:** Data of locations employed as representatives of potential catchment areas. Data of environmental conditions were derived from the WebWIMP modeling program (Matsuura et al., 2009). Aridity index calculated according to UNEP (1992). Elevations data from digital elevation model based on SRTM3 data (Michalak, 2004). Stable hydrogen composition and its confidence interval derived from online isotopes in precipitation calculator (Bowen and Revenaugh, 2003).

| | Distance to coast (km) | | | | | |
|---|---|---|---|---|---|---|
| | 150 | 200 | 250 | 300 | 350 | 400 |
| Latitude (°N) | 1.0 | 1.0 | 1.0 | 1.0 | 1.0 | 1.0 |
| Longitude (°E) | 11.0 | 11.5 | 12.0 | 12.5 | 13.0 | 13.5 |
| Mean annual temperature (°C) | 23.5 | 24.4 | 24.5 | 23.6 | 23.3 | 23.4 |
| Mean annual precipitation (mm) | 2101 | 1835 | 1648 | 1666 | 1653 | 1591 |
| Potential evapotranspiration (mm) | 1292 | 1305 | 1198 | 1150 | 1164 | 1177 |
| Aridity index | 1.6 | 1.4 | 1.4 | 1.4 | 1.4 | 1.4 |
| Elevation (m) | 505 | 546 | 529 | 500 | 514 | 505 |
| Mean annual $\delta D_P$ (‰) | -23 | -24 | -24 | -23 | -23 | -23 |
| 95% confidence interval (‰) | 4 | 5 | 5 | 5 | 6 | 6 |
| Latitude (°N) | 0.5 | 0.5 | 0.5 | 0.5 | 0.5 | 0.5 |
| Longitude (°E) | 10.0 | 10.5 | 11.0 | 11.5 | 12.0 | 12.5 |
| Mean annual temperature (°C) | 25.9 | 25.8 | 25.8 | 25.8 | 23.6 | 23.8 |
| Mean annual precipitation (mm) | 1972 | 2028 | 2028 | 2028 | 1708 | 1735 |
| Potential evapotranspiration (mm) | 1512 | 1500 | 1222 | 1130 | 1200 | 1213 |
| Aridity index | 1.3 | 1.4 | 1.7 | 1.8 | 1.4 | 1.4 |
| Elevation (m) | 12 | 70 | 560 | 425 | 348 | 351 |
| Mean annual $\delta D_P$ (‰) | -16 | -17 | -24 | -22 | -21 | -21 |
| 95% confidence interval (‰) | 4 | 5 | 5 | 5 | 6 | 6 |
| Latitude (°N) | 2.0 | 2.0 | 2.0 | 2.0 | 2.0 | 2.0 |
| Longitude (°E) | 10.5 | 11.0 | 11.5 | 12.0 | 12.5 | 13.0 |
| Mean annual temperature (°C) | 25.6 | 24.3 | 23.3 | 24.2 | 23.2 | 22.9 |
| Mean annual precipitation (mm) | 1891 | 1872 | 1838 | 1739 | 1731 | 1816 |
| Potential evapotranspiration (mm) | 1481 | 1290 | 1171 | 1276 | 1160 | 1129 |
| Aridity index | 1.3 | 1.5 | 1.6 | 1.4 | 1.5 | 1.6 |
| Elevation (m) | 193 | 116 | 349 | 689 | 751 | 638 |
| Mean annual $\delta D_P$ (‰) | -18 | -17 | -20 | -25 | -26 | -25 |
| 95% confidence interval (‰) | 4 | 4 | 4 | 5 | 5 | 5 |

**Supplementary Table 4.S2** (continued)

| | Distance to coast (km) | | | | | |
|---|---|---|---|---|---|---|
| | 150 | 200 | 250 | 300 | 350 | 400 |
| Latitude (°N) | 3.5 | 3.5 | 3.5 | 3.5 | 3.5 | 3.5 |
| Longitude (°E) | 12.0 | 12.5 | 13.0 | 13.5 | 14.0 | 14.5 |
| Mean annual temperature (°C) | 25.5 | 25.4 | 23.6 | 22.1 | 24.0 | 22.8 |
| Mean annual precipitation (mm) | 1224 | 1261 | 1456 | 1417 | 1525 | 1698 |
| Potential evapotranspiration (mm) | 1457 | 1439 | 1208 | 1056 | 1251 | 1115 |
| Aridity index | 0.8 | 0.9 | 1.2 | 1.3 | 1.2 | 1.5 |
| Elevation (m) | 409 | 69 | 385 | 487 | 627 | 485 |
| Mean annual $\delta D_P$ (‰) | -21 | -16 | -21 | -22 | -24 | -22 |
| 95% confidence interval (‰) | 4 | 4 | 4 | 4 | 4 | 4 |
| Latitude (°N) | 5.5 | 5.5 | 5.5 | 5.5 | 5.5 | 5.5 |
| Longitude (°E) | 13.5 | 14.0 | 14.5 | 15.0 | 15.5 | 16.0 |
| Mean annual temperature (°C) | 23.8 | 23.9 | 24.3 | 23.0 | 22.6 | 23.4 |
| Mean annual precipitation (mm) | 1096 | 1223 | 1298 | 1311 | 1510 | 1532 |
| Potential evapotranspiration (mm) | 1233 | 1240 | 1289 | 1140 | 1096 | 1181 |
| Aridity index | 0.9 | 1.0 | 1.0 | 1.2 | 1.4 | 1.3 |
| Elevation (m) | 437 | 295 | 353 | 698 | 596 | 837 |
| Mean annual $\delta D_P$ (‰) | -20 | -18 | -19 | -24 | -23 | -26 |
| 95% confidence interval (‰) | 3 | 3 | 3 | 3 | 3 | 3 |
| Latitude (°N) | 9.5 | 9.5 | 10.0 | 10.0 | 10.5 | 10.5 |
| Longitude (°E) | 14.5 | 15.0 | 15.5 | 16.0 | 16.0 | 16.5 |
| Mean annual temperature (°C) | 24.8 | 22.9 | 20.7 | 21.5 | 19.2 | 22.0 |
| Mean annual precipitation (mm) | 948 | 1036 | 1127 | 1175 | 1237 | 1267 |
| Potential evapotranspiration (mm) | 1432 | 1218 | 1126 | 1083 | 1242 | 1189 |
| Aridity index | 0.7 | 0.9 | 1.0 | 1.1 | 1.0 | 1.1 |
| Elevation (m) | 215 | 498 | 1186 | 1051 | 1407 | 1078 |
| Mean annual $\delta D_P$ (‰) | -13 | -17 | -26 | -24 | -30 | -25 |
| 95% confidence interval (‰) | 3 | 3 | 3 | 3 | 3 | 3 |
| Latitude (°N) | 11.5 | 11.5 | 12.0 | 12.0 | 12.5 | 12.5 |
| Longitude (°E) | 15.0 | 15.5 | 16.0 | 16.0 | 16.5 | 17.0 |
| Mean annual temperature (°C) | 21.0 | 20.7 | 21.5 | 21.7 | 19.1 | 20.7 |
| Mean annual precipitation (mm) | 1219 | 1256 | 1257 | 1257 | 1230 | 1228 |
| Potential evapotranspiration (mm) | 969 | 952 | 1005 | 1017 | 985 | 950 |
| Aridity index | 1.3 | 1.3 | 1.3 | 1.2 | 1.2 | 1.3 |
| Elevation (m) | 1327 | 1337 | 1630 | 1630 | 1699 | 1715 |
| Mean annual $\delta D_P$ (‰) | -30 | -30 | -35 | -35 | -35 | -35 |
| 95% confidence interval (‰) | 3 | 3 | 4 | 4 | 5 | 5 |

**Supplementary Table 4.S2** (continued)

| | Distance to coast (km) | | | | | |
|---|---|---|---|---|---|---|
| | 150 | 200 | 250 | 300 | 350 | 400 |
| Latitude (°N) | 13.0 | 13.0 | 13.5 | 13.5 | 14.0 | 14.0 |
| Longitude (°E) | 15.0 | 15.0 | 15.5 | 16.0 | 16.5 | 17.0 |
| Mean annual temperature (°C) | 19.4 | 19.4 | 20.0 | 19.9 | 20.6 | 20.4 |
| Mean annual precipitation (mm) | 1211 | 1211 | 1148 | 1117 | 1007 | 1018 |
| Potential evapotranspiration (mm) | 917 | 975 | 866 | 861 | 923 | 994 |
| Aridity index | 1.3 | 1.2 | 1.3 | 1.3 | 1.1 | 1.0 |
| Elevation (m) | 1973 | 1973 | 1613 | 1724 | 1563 | 1553 |
| Mean annual $\delta D_P$ (‰) | -41 | -41 | -36 | -38 | -37 | -37 |
| 95% confidence interval (‰) | 3 | 3 | 3 | 4 | 4 | 4 |
| Latitude (°N) | 15.5 | 15.5 | 15.5 | 15.5 | 15.5 | 15.5 |
| Longitude (°E) | 13.5 | 14.0 | 14.5 | 15.0 | 15.5 | 16.0 |
| Mean annual temperature (°C) | 20.3 | 20.7 | 22.1 | 22.7 | 22.3 | 21.8 |
| Mean annual precipitation (mm) | 717 | 700 | 688 | 676 | 683 | 713 |
| Potential evapotranspiration (mm) | 939 | 967 | 1085 | 1146 | 1106 | 1062 |
| Aridity index | 0.8 | 0.7 | 0.6 | 0.6 | 0.6 | 0.7 |
| Elevation (m) | 1288 | 1277 | 1329 | 1181 | 1174 | 1280 |
| Mean annual $\delta D_P$ (‰) | -31 | -31 | -32 | -30 | -31 | -33 |
| 95% confidence interval (‰) | 5 | 5 | 5 | 5 | 5 | 5 |
| Latitude (°N) | 19.0 | 19.0 | 19.0 | 19.0 | 19.0 | 19.0 |
| Longitude (°E) | 14.0 | 14.5 | 15.0 | 15.5 | 16.0 | 16.5 |
| Mean annual temperature (°C) | 16.8 | 19.1 | 21.1 | 22.0 | 22.6 | 22.7 |
| Mean annual precipitation (mm) | 284 | 313 | 332 | 374 | 418 | 484 |
| Potential evapotranspiration (mm) | 774 | 884 | 1021 | 1103 | 1158 | 1180 |
| Aridity index | 0.4 | 0.4 | 0.3 | 0.3 | 0.4 | 0.4 |
| Elevation (m) | 1335 | 1241 | 1160 | 1113 | 1090 | 1105 |
| Mean annual $\delta D_P$ (‰) | -27 | -26 | -25 | -24 | -24 | -24 |
| 95% confidence interval (‰) | 3 | 3 | 3 | 3 | 3 | 3 |
| Latitude (°N) | 22.5 | 22.5 | 22.5 | 22.5 | 22.5 | 22.5 |
| Longitude (°E) | 16.0 | 16.5 | 17.0 | 17.5 | 18.0 | 18.5 |
| Mean annual temperature (°C) | 15.5 | 17.7 | 17.9 | 19.1 | 19.5 | 19.7 |
| Mean annual precipitation (mm) | 236 | 269 | 358 | 330 | 314 | 333 |
| Potential evapotranspiration (mm) | 740 | 829 | 843 | 911 | 943 | 959 |
| Aridity index | 0.3 | 0.3 | 0.4 | 0.4 | 0.3 | 0.3 |
| Elevation (m) | 1217 | 1529 | 1572 | 1698 | 1521 | 1452 |
| Mean annual $\delta D_P$ (‰) | -20 | -25 | -25 | -27 | -25 | -24 |
| 95% confidence interval (‰) | 4 | 4 | 4 | 4 | 4 | 4 |

**Supplementary Table 4.S2** (continued)

| | Distance to coast (km) | | | | | |
|---|---|---|---|---|---|---|
| | 150 | 200 | 250 | 300 | 350 | 400 |
| Latitude (°N) | 23.0 | 22.5 | 22.5 | 22.0 | 22.0 | 21.5 |
| Longitude (°E) | 15.5 | 16.0 | 16.5 | 17.0 | 17.5 | 18.0 |
| Mean annual temperature (°C) | 15.4 | 15.5 | 17.7 | 17.8 | 18.4 | 18.4 |
| Mean annual precipitation (mm) | 176 | 236 | 269 | 384 | 385 | 394 |
| Potential evapotranspiration (mm) | 657 | 803 | 894 | 1023 | 989 | 1026 |
| Aridity index | 0.3 | 0.3 | 0.3 | 0.4 | 0.4 | 0.4 |
| Elevation (m) | 931 | 1217 | 1529 | 1381 | 1793 | 1607 |
| Mean annual $\delta D_P$ (‰) | -17 | -20 | -25 | -23 | -28 | -26 |
| 95% confidence interval (‰) | 4 | 4 | 4 | 4 | 4 | 5 |
| Latitude (°N) | 28.0 | 28.0 | 28.0 | 28.0 | 28.0 | 28.0 |
| Longitude (°E) | 17.0 | 17.5 | 18.0 | 18.5 | 19.0 | 19.5 |
| Mean annual temperature (°C) | 19.5 | 19.0 | 19.6 | 20.2 | 20.6 | 19.4 |
| Mean annual precipitation (mm) | 92 | 113 | 116 | 116 | 123 | 129 |
| Potential evapotranspiration (mm) | 922 | 914 | 971 | 1024 | 1053 | 974 |
| Aridity index | 0.1 | 0.1 | 0.1 | 0.1 | 0.1 | 0.1 |
| Elevation (m) | 618 | 706 | 716 | 959 | 869 | 807 |
| Mean annual $\delta D_P$ (‰) | -15 | -16 | -16 | -19 | -18 | -17 |
| 95% confidence interval (‰) | 4 | 4 | 4 | 4 | 4 | 4 |

**Supplementary Table 4.S3:** Monthly precipitation characteristics for locations with 350 km distance to the coast. Stable hydrogen composition derived from online isotopes in precipitation calculator (Bowen et al., 2005). Rainfall amount was derived from the WebWIMP modeling program (Matsuura et al., 2009).

| | | Month | | | | | | | | | | | |
|---|---|---|---|---|---|---|---|---|---|---|---|---|---|
| Location | Parameter | 1 | 2 | 3 | 4 | 5 | 6 | 7 | 8 | 9 | 10 | 11 | 12 |
| 1 | $\delta D_P$ in ‰ | -18 | -20 | -29 | -32 | -25 | -12 | -6 | -14 | -13 | -28 | -25 | -28 |
| | Precipitation in mm | 82 | 103 | 198 | 200 | 178 | 63 | 22 | 39 | 149 | 296 | 211 | 113 |
| 2 | $\delta D_P$ in ‰ | -14 | -15 | -28 | -32 | -21 | -9 | 1 | -8 | -8 | -23 | -23 | -24 |
| | Precipitation in mm | 130 | 139 | 207 | 186 | 171 | 30 | 7 | 12 | 90 | 275 | 277 | 186 |
| 3 | $\delta D_P$ in ‰ | -19 | -18 | -36 | -36 | -22 | -12 | 2 | -6 | -7 | -27 | -28 | -31 |
| | Precipitation in mm | 176 | 204 | 225 | 215 | 152 | 16 | 6 | 7 | 43 | 179 | 305 | 204 |
| 4 | $\delta D_P$ in ‰ | -17 | -13 | -34 | -34 | -18 | -12 | 7 | -2 | -2 | -23 | -28 | -30 |
| | Precipitation in mm | 170 | 149 | 189 | 220 | 142 | 6 | 2 | 6 | 31 | 138 | 270 | 202 |
| 5 | $\delta D_P$ in ‰ | -17 | -12 | -29 | -30 | -16 | -9 | 10 | 2 | 1 | -17 | -25 | -29 |
| | Precipitation in mm | 163 | 137 | 153 | 235 | 111 | 9 | 2 | 8 | 68 | 175 | 252 | 197 |
| 6 | $\delta D_P$ in ‰ | -30 | -33 | -40 | -30 | -29 | 2 | 4 | 7 | 1 | -15 | -22 | -39 |
| | Precipitation in mm | 165 | 135 | 207 | 136 | 20 | 1 | 1 | 6 | 44 | 126 | 199 | 198 |
| 7 | $\delta D_P$ in ‰ | -17 | -31 | -21 | -3 | -24 | 0 | -32 | -41 | -28 | -17 | 12 | -29 |
| | Precipitation in mm | 205 | 151 | 209 | 114 | 12 | 1 | 0 | 3 | 22 | 93 | 187 | 235 |
| 8 | $\delta D_P$ in ‰ | -34 | -43 | -52 | -37 | -35 | 9 | 2 | 4 | -1 | -10 | -16 | -45 |
| | Precipitation in mm | 195 | 157 | 194 | 93 | 8 | 1 | 0 | 0 | 9 | 55 | 130 | 167 |
| 9 | $\delta D_P$ in ‰ | -28 | -36 | -42 | -31 | -29 | 14 | 5 | 6 | 2 | -3 | -10 | -38 |
| | Precipitation in mm | 131 | 157 | 150 | 50 | 2 | 0 | 0 | 0 | 1 | 21 | 65 | 104 |
| 10 | $\delta D_P$ in ‰ | -24 | -28 | -32 | -22 | -19 | 23 | 4 | 3 | 2 | 4 | -5 | -27 |
| | Precipitation in mm | 93 | 109 | 81 | 25 | 3 | 1 | 2 | 0 | 2 | 10 | 38 | 54 |
| 11 | $\delta D_P$ in ‰ | -27 | -30 | -34 | -21 | -14 | 24 | -4 | -4 | -3 | 2 | -7 | -24 |
| | Precipitation in mm | 63 | 78 | 58 | 33 | 6 | 2 | 1 | 1 | 4 | 12 | 25 | 32 |
| 12 | $\delta D_P$ in ‰ | -31 | -34 | -39 | -25 | -17 | 23 | -6 | -6 | -4 | -2 | -10 | -28 |
| | Precipitation in mm | 87 | 98 | 70 | 39 | 8 | 2 | 1 | 1 | 4 | 12 | 29 | 36 |
| 13 | $\delta D_P$ in ‰ | -21 | -23 | -23 | -20 | -15 | 3 | -10 | -9 | -5 | -5 | -9 | -19 |
| | Precipitation in mm | 14 | 23 | 29 | 15 | 4 | 4 | 4 | 2 | 3 | 6 | 9 | 11 |

# 5. Influence of Late Pleistocene and Holocene climate on vegetation distributions in southwest Africa elucidated from sedimentary *n*-alkanes - differences between 12°S and 20°S

Tanja Badewien[a,*], Angela Vogts[b], Jürgen Rullkötter[a]

[a] Institute for Chemistry and Biology of the Marine Environment (ICBM), Carl von Ossietzky University of Oldenburg, Germany
[b] Leibniz Institute for Baltic Sea Research, Warnemünde (IOW), Germany

* Corresponding author. Tel.: +49 441 798 3627; fax: +49-441-798 3404.
E-mail address: t.badewien@icbm.de (Tanja Badewien).

This chapter is in revision after review by Quaternary Science Reviews.

## 5.1. Abstract

Global and local climatic forcing, e.g. concentration of atmospheric $CO_2$ or insolation, influence the distribution of $C_3$ and $C_4$ plants in southwest Africa. $C_4$ plants dominate in more arid and warmer areas and are favoured by lower $pCO_2$ levels. Several studies have assessed past and present continental vegetation by the analysis of terrestrial *n*-alkanes in near-coastal deep sea sediments using single samples or a small number of samples from a given climatic stadial. The objectives of this study were to evaluate vegetation changes in southwest Africa with regard to climatic changes during the Late Pleistocene and the Holocene and to elucidate the potential of single sample simplifications. We analysed two sediment cores at high resolution, altogether ca. 250 samples, from the Southeast Atlantic Ocean (20°S and 12°S) covering the time spans of 23 to 2 ka and 73 to 2 ka, respectively. Our results for 20°S showed marginally decreasing $C_4$ domination (of ca. 5%) from the Last Glacial Maximum (LGM) to the present based on average chain length ($ACL_{27\text{-}33}$ values) and carbon isotopic composition of the $C_{31}$ and $C_{33}$ *n*-alkanes. Values for single samples from the LGM and the Holocene overlap and, thus, are not significantly representative of the climatic stadial they derive from. In contrast, at 12°S the *n*-alkane parameters show a clear difference of plant type for the Late

Pleistocene ($C_4$ domination, 66% $C_4$ on average) and the Holocene ($C_3$ domination, 40% $C_4$ on average). During deglaciation, vegetation change highly correlates with the increase in $pCO_2$ ($r^2$= 0.90). Rapidly occurring climatic events like Heinrich Stadials or Antarctic warming periods are not reflected by vegetation changes in the catchment area. Instead, smaller vegetation fluctuations during the Late Pleistocene occur in accordance with local variations of insolation.

## 5.2. Introduction

Climate change, e.g. during glacials and interglacials, may lead to substantial alteration in terrestrial plant zonations. These adaptations of vegetation may involve variations in the distribution of $C_3$ (e.g., trees) and $C_4$ plants (mostly grasses). In order to depict past vegetation changes, *n*-alkanes in aquatic sediments have been proven to be valuable proxies (e.g., Schefuß et al., 2005; Rommerskirchen et al., 2006a; Castañeda et al., 2009; Collins et al., 2011; Sinninghe Damsté et al., 2011; Vogts et al., 2012; Collins et al., 2013). *n*-Alkanes from terrestrial plants (e.g., Eglinton and Hamilton, 1967) are transported to the ocean adjacent to the continent or to lakes by wind or rivers. Upon continuing sedimentation *n*-alkanes form an archive of information on past terrestrial vegetation due to plant specific differences in *n*-alkane composition.

In southwest Africa, $C_4$ plants produce longer chain *n*-alkanes with a heavier stable carbon isotope composition than $C_3$ plants (Rommerskirchen et al., 2006b; Vogts et al., 2009). The difference in their isotopic composition is due to different carbon fixation pathways. While $C_3$ plants assimilate atmospheric $CO_2$ via the Calvin-Bassham-Cycle, $C_4$ plants preconcentrate $CO_2$ before incorporating it into this cycle (Bassham et al., 1954; Hatch, 1987). This initial step leads to higher $CO_2$ concentrations inside the cell as well as higher water use efficiency and avoids photorespiration, which reduces the net $CO_2$ assimilation in $C_3$ plants (Tipple and Pagani, 2007). The differences in carbon fixation lead to advantages for $C_4$ plants, compared to $C_3$ plants, in more arid and warmer areas as well as during glacials, which are characterised by lower concentrations of atmospheric $CO_2$, higher ice volume and cooler global temperatures in comparison to interglacials (e.g., Sage, 2004).

In the past, global climate changed as a result of, e.g., variations in insolation. The amount of solar radiation reaching the upper atmosphere depends on the position of the earth relative to the sun and has lead to the glacial/interglacial cycles throughout the Quaternary (for an overview see, e.g., Pierrehumbert, 2010). Conclusions on past ice volumes are drawn from $\delta^{18}O$ values of benthic foraminifera which are

related to the oxygen isotopic signature of sea water, which depends on the amount of oxygen stored in ice and therefore on the global ice volume (for an overview see, e.g., Hoefs, 2004; Sharp, 2007). In contrast, atmospheric $CO_2$ concentrations are measured directly from air bubbles enclosed in ice cores (Barnola et al., 1987; Petit et al., 1999).

Glacial climate conditions also fluctuated during Heinrich Stadials or Antarctic warming periods. In the Northern Hemisphere, the debris of ice-rafting in sediments is associated with intervals of cooler temperatures (Heinrich Stadials). In the Southern Hemisphere, however, the short-term Heinrich Stadials are marked by warmer conditions and a southward migration of the Intertropical Convergence Zone (Heinrich, 1988; Crowley, 1992; Vellinga and Wood, 2002; Sanchez Goñi and Harrison, 2010). In contrast, the short-term Antarctic warming periods are not reflected in the Northern Hemisphere (Blunier et al., 1998; Blunier and Brook, 2001). The interplay and effects of these climate fluctuations on African vegetation are still a matter of controversial discussion (e.g., Hessler et al., 2010; Schefuß et al., 2011).

Studies investigating vegetation changes have either addressed local changes by analysing long core sections (e.g., Schefuß et al., 2005; Dupont et al., 2008) or targeted longitudinal effects by looking at single or a small number of samples of given climatic stadials from different coring locations (e.g., Rommerskirchen et al., 2006a; Vogts et al., 2012).

Here we present and discuss data for two sediment core locations in the Southeast Atlantic Ocean (12°S, 20°S), which both cover the current interglacial and parts of the last glacial. On the basis of sedimentary *n*-alkanes we evaluate if and how vegetation changes in southwest Africa reflect different climatic parameters (e.g., atmospheric $CO_2$ concentration, insolation changes, Heinrich Stadials or Antarctic warming periods). We further elucidate whether single sample approaches can be representative.

## 5.3. Material and methods

### 5.3.1. Samples and geological setting

We studied sediment cores from two different locations in the Southeast Atlantic Ocean north of and on Walvis Ridge (Fig. 5.1). Cores of the southern and northern location were retrieved during RV Meteor cruises M34/2 and M41/1 in 1996 and 1998, respectively. We collected 73 samples from a multicorer (GeoB 3711-1) and the upper part of a gravity corer (GeoB 3711-3) both recovered at the same location at 19°50´S in 1200 m water depth (Fig. 5.1b; Wefer et al., 1997). From the northern

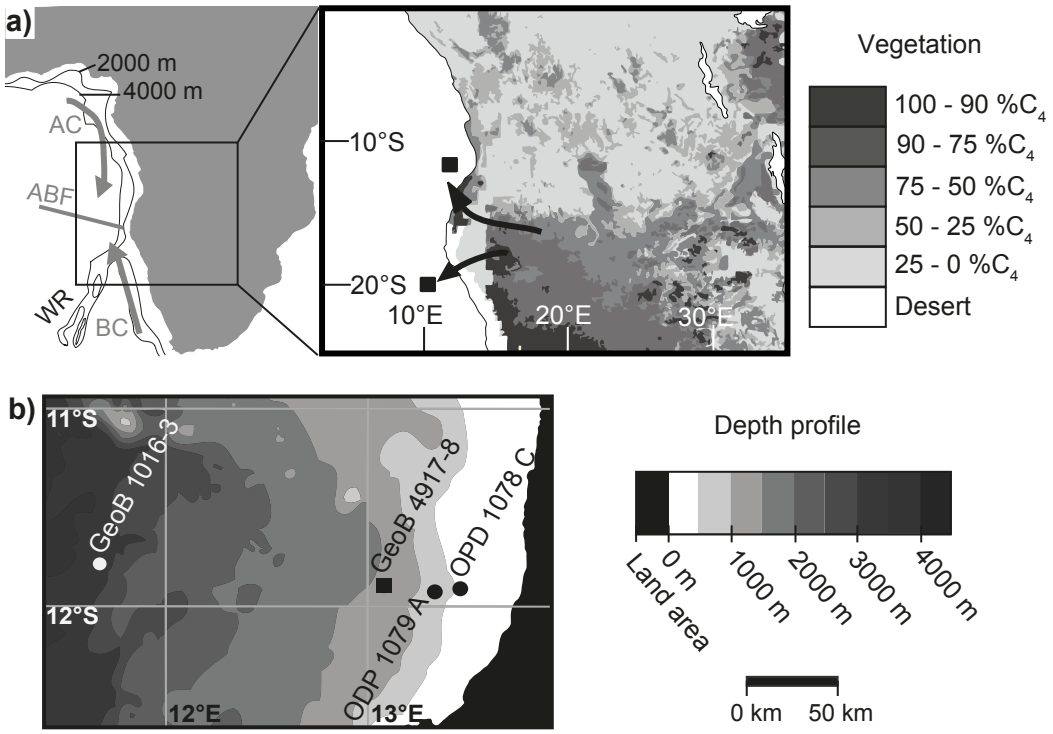


**Fig. 5.1:** Locations of analysed and neighbouring cores, a) Africa with southeastern Atlantic surface currents (grey arrows, AC - Angola Current, BC - Benguela Current, ABF - Angola-Benguela- Front; after Peterson and Stramma, 1991) and Walvis Ridge (WR); magnified map section: investigated core locations (GeoB 4917-8, 12°S, and GeoB 3711-3, 20°S), prevailing winds (black arrows; after Dupont and Wyputta, 2003) and vegetation composition (after Still and Powell, 2010) of the adjacent continent, b) water depth profile and location of investigated (rectangle) and neighbouring cores (circles, GeoB 1016-3 investigated by Rommerskirchen et al., 2003 and Rommerskirchen et al., 2006a; GeoB 4917-3 (same location as GeoB 4917-8) investigated by Vogts et al., 2012; ODP 1079A investigated by Rommerskirchen et al., 2003 and Rommerskirchen et al., 2006a; and ODP 1078C investigated by Dupont et al., 2008, Collins et al., 2011 and Hessler et al., 2012).

gravity core GeoB 4917-8, recovered at 11°54`S in a water depth similar to the southern core (1300 m; Schulz et al., 1999), 184 samples were analysed.

Site GeoB 3711 is located in the cold northward flowing Benguela surface current. Site GeoB 4917 is situated in the Angola Current, a warm-water, surface current flowing southward. Both currents converge between the sample locations and form the Angola-Benguela- Front (Fig. 5.1a; Peterson and Stramma, 1991).

Both coring locations face continental regions presently characterised by different vegetation zones. Adjacent to the southern site the coastal Namib Desert is barely vegetated. Further inland, vegetation changes from exclusively $C_4$ (100 - 90% $C_4$) to $C_4$ plant dominated areas (90 - 50% $C_4$; Fig. 5.1a). Northward, vegetation changes from grassland to woodlands and forest indicating that the northern coring site faces $C_3$ plant dominated areas (Fig. 5.1a; Mayaux et al., 2004; Still and Powell, 2010).

These spatial vegetation differences are a result of the differences in local climate. While at 20°S the climate on the continent is largely arid, precipitation increases northward (White, 1983; Vogts et al., 2012).

### 5.3.2. Analytical procedures

#### *5.3.2.1. Total inorganic carbon*

All sediment samples were freeze dried and ground. Total inorganic carbon (TIC) content was measured according to Eckert et al. (2013) using a CM 5012 coulometer coupled to a CM 5130 acidification module (UIC). The relative standard deviation (RSD) of an in-house standard was better than 1.5%.

#### *5.3.2.2. Radiocarbon dating*

To establish an age model, seven selected samples of core GeoB 4917-8 (12°S) were radiocarbon dated by Accelerator Mass Spectrometry measurement of foraminifera, carried out by Poznań Radiocarbon Laboratory (Poland). The $^{14}C$ ages obtained were converted into calendar ages with the Calib 5.1.0 beta software (Stuiver and Reimer, 1993; http://calib.qub.ac.uk/calib/download/) using the Marine04 calibration curve for the five youngest samples (Hughen et al., 2004). The two remaining samples were out of range of the marine calibration curve and were calibrated using the software of Fairbanks et al. (2005; http://www.radiocarbon.ldeo.columbia.edu/research/radcarbcal.htm). All ages (1000 years BP) are abbreviated as ka.

#### *5.3.2.3. Extraction and liquid chromatography*

The organic matter of 3 to 11 g freeze-dried and ground sediment from cores GeoB 3711-3 and GeoB 4917-8 was extracted using an Accelerated Solvent Extractor (ASE 200, Dionex) with $CH_2Cl_2$ and MeOH (9/1, v/v, 3 x 5 min, 70 bar, 100°C) as solvents. Randomly selected samples were repeatedly extracted in order to verify completeness of the process. Squalane and *n*-nonadecan-10-one were added as internal standards. *n*-Hexane-insoluble compounds were removed by dissolving the extract in *n*-hexane and filtration over dry $NaSO_4$. From the *n*-hexane-soluble compounds the aliphatic/alicyclic hydrocarbon and polar heterocomponent fractions were separated by medium pressure liquid chromatography (Radke et al., 1980). Blank samples of purified sand went through the same procedure and did not show any significant contamination.

#### *5.3.2.4. Gas chromatography*

Long chain alkenones (in the heterocomponent fraction) and *n*-alkanes were analysed by gas chromatography (Agilent 6890) with flame ionisation detector, helium as carrier gas and a high-temperature column (J&W, DB-5ht, 30 m length, 0.25 mm i.d., 0.1 µm film thickness). The temperature of the gas chromatograph (GC) oven was raised from 60°C at a rate of 3°C $min^{-1}$ to 350°C and then held for 5 min.

Before measurement, the heterocomponent fractions were derivatised with N-methyl-N-(trimethylsilyl)-trifluoroacetamide (MSTFA), and *n*-hexadecane was added as injection standard. The ketone unsaturation index ($U^{K'}_{37}$) was calculated by peak area and converted into sea surface temperature (SST) according to the calibration of Prahl and Wakeham (1987). Some values were controlled by repeated measurements. In selected samples the identification of alkenones was verified by gas chromatography-mass spectrometry (Trace GC Ultra coupled to TSQ Quantum, Thermo Fisher Scientific).

*n*-Docosanoic acid methyl ester was added as injection standard to the aliphatic hydrocarbon fraction. Individual *n*-alkanes were identified by comparison of retention times with those of standard mixtures. Based on signal intensity and squalane as internal standard, *n*-alkane abundances were calculated and are reported as µg $g^{-1}$ sediment dry wt. Recovery of internal standard was 73% on average.

#### *5.3.2.5. Stable carbon isotope analysis*

The *n*-alkanes of GeoB 3711-3 were separated from branched and cyclic saturated hydrocarbons by urea adduction prior to carbon isotope analysis (Rommerskirchen et al., 2006b). The stable carbon isotopic composition of *n*-alkanes was determined by two systems, i.e. HP 5890 or Agilent 6890N GC coupled to a Thermo Finnigan MAT 252 or MAT 253 isotope mass spectrometer via combustion interface (GC-II or GC-III), respectively. All gas chromatography conditions were identical to those used for *n*-alkane quantification with the exception of injector and oven temperatures. For HP 5890, the conditions were those described by Vogts et al. (2012). For Agilent 6890, the injector temperature was programmed from 60°C (held 8 s) to 305°C (held 2 min) at a rate of 10°C $min^{-1}$. The GC oven was programmed from 60°C (held 2 min) to 300°C (held 18 min) at a rate of 3°C $min^{-1}$. Where samples had been treated by urea adduction, the final oven temperature was held for 38 min. For each system, calibration was conducted by injection of repeated pulses of $CO_2$ of known carbon isotopic composition at the beginning and at the end of each run. Between sample runs certified and lab standards (*n*-alkanes and fatty acid methyl esters) were measured for quality control. Squalane with known isotopic composition was

used as internal standard. Where squalane had been removed during urea adduction, it was added to the samples prior to isotope analyses. Analysis on both systems lead to the same results. Results were only considered valid if the measured $\delta^{13}C$ values of the standards differed by less than 0.5‰ from those of the known isotopic composition. Samples were run at least in duplicate and yielded values with a difference of less than 0.5‰.

#### *5.3.2.6. X-ray fluorescence analysis*

Extraction residues of sediments from GeoB 3711-1 and -3 were prepared for X-ray fluorescence (XRF) analysis with a Philips PW-2400 WD-XRF spectrometer and measured according to the procedures of Eckert et al. (2013). Possible contamination or alteration due to the extraction process was controlled by XRF measurement of two selected samples prior and after extraction. For interpretation only major element oxides were considered that had not been affected in their concentration by extraction. An in-house standard (Peru 1) was repeatedly measured and RSD for major element oxides was <1%.

## 5.4. Age model

### 5.4.1. Age model for GeoB 3711-3 (20°S)

The age model for GeoB 3711-3 is based on alkenone-derived SST data and sediment loss estimation by comparison of results from GeoB 3711-3 and GeoB 3711-1. A multicorer samples the undisturbed sediment surface while a gravity corer potentially loses surface material during penetration into the sediment. The multicorer and gravity core sediment was recovered from the same location (Schulz et al., 1999).

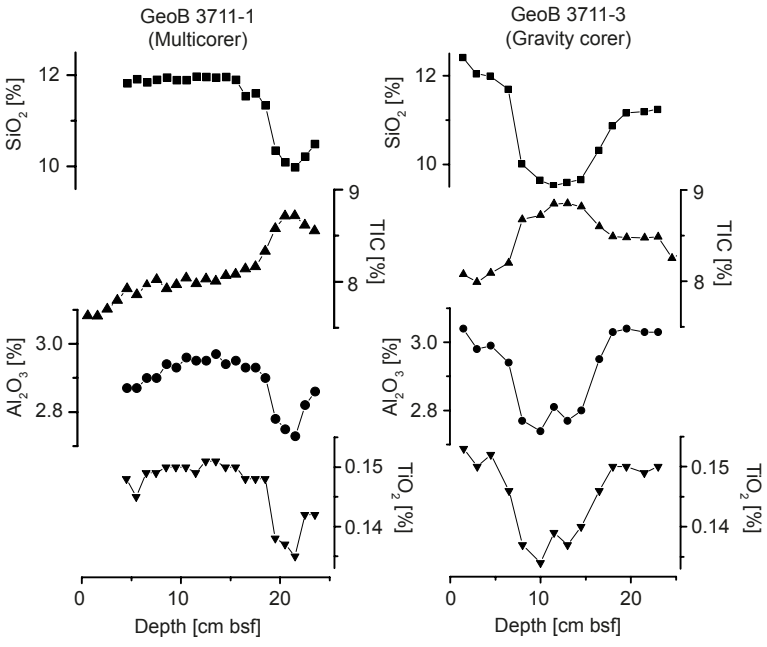


**Fig. 5.2:** Results for GeoB 3711-1 and 3711-3 (20°S): Major element oxides and total inorganic carbon (TIC) for samples retrieved by the multicorer and the gravity corer.

To determine the surface sediment loss of the gravity corer, major element oxide and TIC values were analysed for both cores. Some element oxides (e.g., $SiO_2$, $Al_2O_3$ and $TiO_2$) as well as TIC revealed significant maxima and minima in both cores (Fig. 5.2). For example, the $SiO_2$ content shows a peak in the multicorer between 17 and 24 cm below sea floor (bsf) and in the gravity corer between 6 and 19 cm bsf. We consider these peaks to represent the same event and estimated a sediment loss of 12 cm for the gravity corer. Data for $Al_2O_3$, $TiO_2$ and TIC corroborate this estimation.

To establish an age model, we compared our SST data to alkenone-derived SST values of a nearby core from within the Benguela Current regime and recovered from a similar water depth (ca. 23°S, 1000 m; Kirst et al., 1999). Kirst et al. (1999) based their age model on oxygen isotope analysis of planktonic foraminifera and correlated their results to a radiocarbon-dated core described by Summerhayes et al. (1995). In the study of Kirst et al. (1999), SST increased from 14°C to 19°C between 50 and 10 ka and remained largely uniform during the Holocene. This trend resembles that observed in our study. Here, SST increases from 16°C in the lower part of the core to a largely uniform average of around 18.5°C above 38 cm bsf (Fig. 5.3). Based on comparison with the data of Kirst et al. (1999) we assigned an age of 10 ka to the sample at 38 cm bsf. The resulting sedimentation rate of

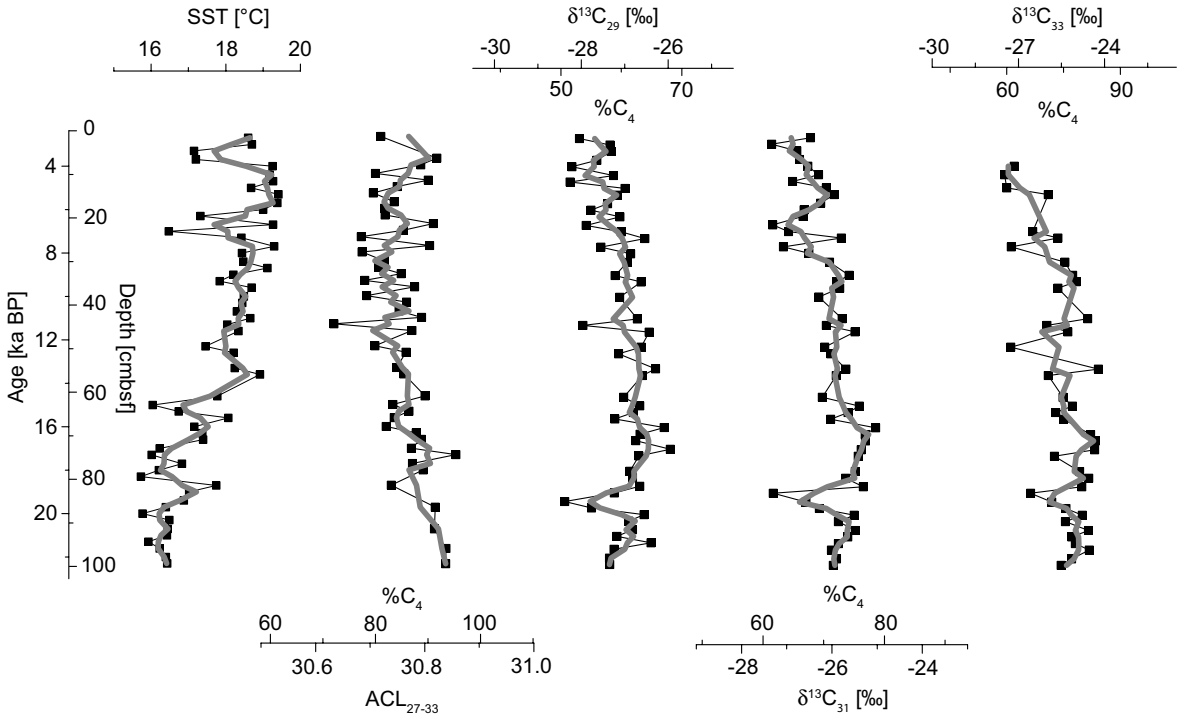


**Fig. 5.3:** Results for GeoB 3711-3 (20°S): Sea surface temperature (SST), age model and *n*-alkane parameters with corresponding calculated $C_4$ contribution; grey: three-point moving average.

5 cm $ka^{-1}$ is similar to that determined by Kirst et al. (1999). With the age assumption in combination with a uniform sedimentation rate and taking into account the core loss, the investigated core section represents material of a time interval from 23 to 2 ka. Due to the extent of scattering in the SST data, however, this age model only serves as an approximation.

### 5.4.2. Age model for GeoB 4917-8 (12°S)

The age model for GeoB 4917-8 is based on radiocarbon dating of seven selected samples and verified by evaluation of alkenone-derived SST data (Fig. 5.4). The conversion of $^{14}C$ ages into calendar ages employs a marine reservoir age of 400 years (Hughen et al., 2004; Fairbanks et al., 2005). For the vicinity of GeoB 4917-8 no other local reservoir effect has been reported (Lewis et al., 2008; Dewar et al., 2012). The assumption of a 400 year reservoir effect was likewise made by Dupont et al. (2008) for Ocean Drilling Project (ODP) site 1078 less than 50 km away from GeoB 4917-8 (Fig. 5.1b). The study area is influenced by the Angola Current, a warm surface current. There open ocean effect is pronounced (van Bennekom and Berger, 1984; Peterson and Stramma, 1991; Wefer et al., 1998), which supports our approximation. Butzin et al. (2005), however, estimated a present-day surface reservoir effect of 400 years and a glacial reservoir effect of maximally 600 years for this region based on radiocarbon simulation. They acknowledged, however, that systematic uncertainties in modelling past climatic conditions may occur. On the

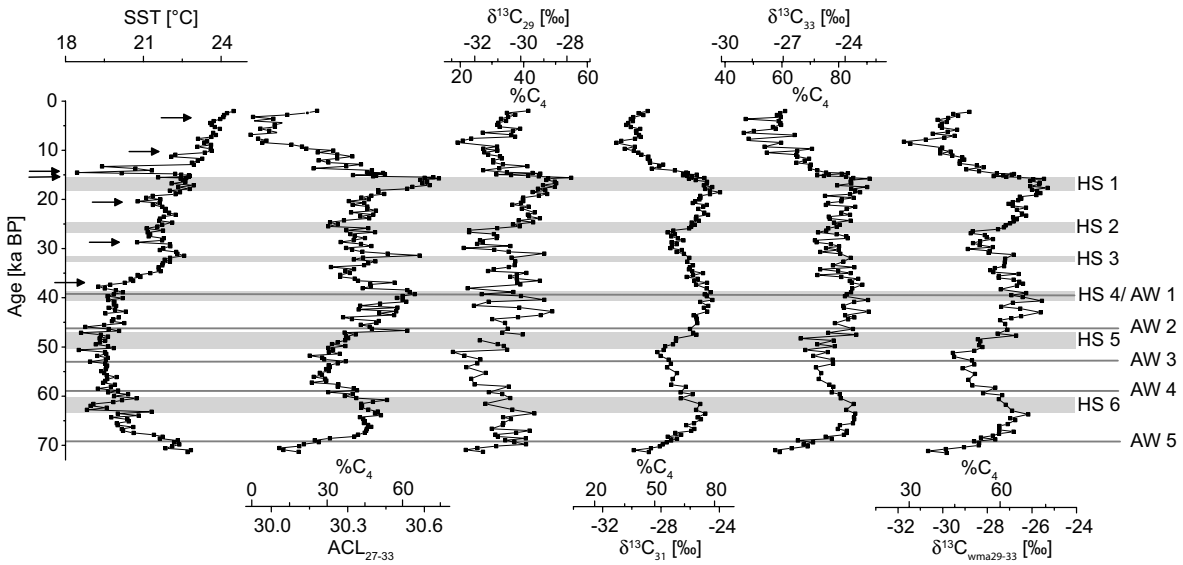


**Fig. 5.4:** Results for GeoB 4917-8 (12°S): SST, age model and *n*-alkane parameters with corresponding calculated $C_4$ contribution; arrows indicate radiocarbon-dated samples; HS - Heinrich Stadial (Sanchez Goñi and Harrison, 2010), AW - Antarctic warming periods (Blunier et al., 2001).

other hand, a shift of an additional 200 years during the glacial does not change our age approximation significantly. Thus, a potential change in reservoir effect was not taken into account.

With the assumptions made, the radiocarbon-dated samples have calibrated ages ranging from 37.4 to 3.4 ka (Table 5.1, Fig. 5.4). Assuming a uniform sedimentation between two radiocarbon dated samples and in the deeper core section, the age range of the analysed core section extends from 73 to 2 ka.

To verify the age model estimated by radiocarbon dating, we analysed alkenone-derived SST values. The data vary between 18°C and 25°C with highest temperatures calculated for the upper part of the core (Fig. 5.4). SSTs decrease between 73 and 65 ka from 23°C to ca. 20°C and remain uniform around 19°C until 38 ka. Further upcore, values increase to ca. 24°C. At ca. 14 ka SST drops to a minimum value of 18°C. A similar albeit less pronounced temperature decline was found by Dupont et al. (2008) in a similar time interval.

Based on radiocarbon dating the investigated core contains material from a glacial (Late Pleistocene) and an interglacial (Holocene) time period. High SST values (>22°C) were found for the Holocene, whereas Late Pleistocene SSTs are below 20°C. In the Late Pleistocene the coolest SSTs occur between 65 and 35 ka. Hessler et al. (2011) estimated SSTs of Southern Hemisphere summer and winter by Mg/Ca analyses of two planktonic foraminifera at ODP site 1078. They found coldest SST

**Table 5.1:** Radiocarbon dates (estimated with Calib- software 5.1.0 beta for samples from 0.2 to 2.75 m bsf and software of Fairbanks et al., 2005 for samples from 3.80 to 4.85 m bsf) and sedimentation rates; all ages = BP, calendar age = mean value.

| Depth [m bsf] | $^{14}$C ages | Calendar age | Sedimentation rate [cm ka$^{-1}$] |
|---|---|---|---|
| 0.2 | 3 510 ± 40 | 3 393 | |
| | | | 12.40 |
| 1.05 | 9 400 ± 60 | 10 245 | |
| | | | 12.42 |
| 1.58 | 12 880 ± 90 | 14 513 | |
| | | | 35.76 |
| 2.05 | 13 750 ± 100 | 15 828 | |
| | | | 13.92 |
| 2.75 | 18 090 ± 160 | 20 857 | |
| | | | 12.49 |
| 3.80 | 24 440 ± 390 | 29 262 | |
| | | | 12.77 |
| 4.85 | 32 100 ± 1 300 | 37 483 | |

values between 50 ka (their oldest sample) and 35 ka and associated them with an intensification of the Benguela Current. Our mean annual SSTs are within the range of their results.

Schneider et al. (1995) analysed alkenone-derived SST data for the last 200 ka from a sediment core (11°35`S) with a minimum in SST at around 50 ka. Their SST development was similar to ours in temperature trend as well as values. For example, in our and their cores the increase of SST from the Last Glacial Maximum (LGM) to the Holocene is ca. 3°C. As a difference, SST values of Schneider et al. (1995) did not show the decline at around 14 ka. But the resolution for their core was about 2 ka. Therefore, the ≈1.4 ka temperature drop observed here could have been missed due to the lower time resolution.

The sedimentation rate for core GeoB 4917-8 estimated from the presented age model is around 13 cm $ka^{-1}$ except for sediments between 15.8 to 14.5 ka (36 cm $ka^{-1}$). A similarly high sedimentation rate, up to three times higher than average, during this time interval was also found for site ODP 1078 (Dupont et al., 2008).

Comparison with SST and literature data appears to verify the presented age model for GeoB 4917-8 as a sufficiently substantiated approximation.

## 5.5. Results

All data are available in the PANGAEA database (http://doi.pangaea.de/10.1594/PANGAEA.831446). All samples from the two core locations contain long chain *n*-alkanes with an odd/even carbon number predominance. Carbon preference indices ($CPI_{27\text{-}33}$) are 5.9 and 5.5 on average for GeoB 3711-3 (20°S) and GeoB 4917-8 (12°S), respectively (Marzi et al., 1993).

### 5.5.1. GeoB 3711-3 (20°S)

The *n*-alkane distribution patterns are dominated by the $C_{31}$ homologue. To determine chain length variations, we calculated the average chain length (ACL) for the $C_{27}$ to $C_{33}$ *n*-alkanes (Poynter, 1989). $ACL_{27\text{-}33}$ values increase slightly downcore (Fig. 5.3).

The carbon isotopic composition of the $C_{29}$ *n*-alkane is fairly uniform throughout the core whereas $\delta^{13}C_{31}$ and $\delta^{13}C_{33}$ just slightly increase downcore. The analytical variation of the isotope ratios of only 1‰ on average additionally masks the trends. Therefore, lines representing the three-point moving average were added to the graphs (Fig. 5.3).

To estimate the proportion of $C_4$ plants from *n*-alkane parameters ($ACL_{27\text{-}33}$, $\delta^{13}C_{29}$, $\delta^{13}C_{31}$, $\delta^{13}C_{33}$), we used a binary mixing equation according to Vogts et al.

**Table 5.2:** End member data with standard deviation representing the variation width within the dataset. Data for $C_3$ plants represent the mean value of two averaged datasets (24 rainforest and 44 ($\delta^{13}C$)/45 ($ACL_{27\text{-}33}$) savannah plants; Vogts et al., 2009); data for $C_4$ plants consist of 33 average values from Rommerskirchen et al. (2006b).

| End member data for | $\delta^{13}C_{29}$ [‰] | $\delta^{13}C_{31}$ [‰] | $\delta^{13}C_{33}$ [‰] | $\delta^{13}C_{WMA29\text{-}33}$ [‰] | $ACL_{27\text{-}33}$ |
|---|---|---|---|---|---|
| $C_3$ plants | -35.4 ± 2.6 | -35.7 ± 2.8 | -35.3 ± 1.9 | -35.6 ± 2.6 | 29.9 ± 0.8 |
| $C_4$ plants | -21.6 ± 2.0 | -22.1 ± 2.1 | -22.2 ± 1.8 | -22.0 ± 1.9 | 30.9 ± 0.6 |

(2012). As end member data for $C_3$ and $C_4$ plants values were used from Vogts et al. (2009) and Rommerskirchen et al. (2006b), respectively (Table 5.2). All calculated proportions show a $C_4$ domination ranging from 50 to 97% (Fig. 5.3). Similar values for *n*-alkane parameters in this region were found by Collins et al. (2011), Rommerskirchen et al. (2003), Rommerskirchen et al. (2006a) and Vogts et al. (2012).

### 5.5.2. GeoB 4917-8 (12°S)

The *n*-alkane distribution patterns were dominated either by the $C_{29}$ or $C_{31}$ homologues. $ACL_{27\text{-}33}$ values for the oldest samples and during the Holocene are lower than during times in between (Fig. 5.4). From 65 to 15 ka $ACL_{27\text{-}33}$ values fluctuate with high values at around 40 and 16 ka and low values at around 55 ka.

The carbon isotopic compositions of the three dominant *n*-alkanes show a consistent pattern throughout the core: $C_{29}$ is the lightest *n*-alkane while $C_{33}$ is heavier than $C_{31}$ (Fig. 5.4). The $\delta^{13}C_{29}$ values stay nearly uniform in the analysed core section. Even though $C_{31}$ varies the most, $C_{33}$ and $C_{31}$ follow the same trends. $\delta^{13}C$ values for the latter two components increase from 73 to 65 ka and stay fairly uniform until 15 ka with minima around 50 and 29 ka. The lowest $\delta^{13}C$ values occur during the Holocene. Similar results for $CPI_{27\text{-}33}$, $ACL_{27\text{-}33}$ and $\delta^{13}C$ in the Southeast Atlantic Ocean and in these time sections were found by Rommerskirchen et al. (2003), Rommerskirchen et al. (2006a), Schefuß et al. (2004) and Vogts et al. (2012), even though they only employed surface sediments or single samples for each time interval.

In order to take different hydrocarbon proportions into account, the weighted mean average (WMA) for the $C_{29}$, $C_{31}$ and $C_{33}$ *n*-alkanes was calculated. $\delta^{13}C_{WMA29\text{-}33}$ follows the trend of the *n*-$C_{31}$ alkane (Fig. 5.4).

All percentages of $C_4$ (calculated from $ACL_{27\text{-}33}$, $\delta^{13}C_{29}$, $\delta^{13}C_{31}$, $\delta^{13}C_{33}$, $\delta^{13}C_{WMA29\text{-}33}$; cf. Section 4.1) range from $C_3$ dominated to $C_4$ dominated vegetation albeit to different extents depending on the parameter used for calculation (Fig. 5.4).

## 5.6. Discussion

### 5.6.1. GeoB 3711-3 (20°S)

High $CPI_{27\text{-}33}$ values (>>1) representing the odd/even carbon number predominance of long chain *n*-alkanes are a typical indicator for an unaltered land plant signal in sediments (Eglinton et al., 1962; Eglinton and Hamilton, 1967; Collister et al., 1994; Rommerskirchen et al., 2006b; Vogts et al., 2009).

The numerical values of the LGM *n*-alkane data at 20°S overlap with those of the Holocene samples (Fig. 5.3). Apparently, during deglaciation (20 to 10 ka) vegetation remained largely unchanged.

All *n*-alkane parameters ($ACL_{27\text{-}33}$, $\delta^{13}C_{29}$, $\delta^{13}C_{31}$, $\delta^{13}C_{33}$) reveal that the terrestrial organic matter in the Southeast Atlantic Ocean sediments is mainly derived from $C_4$ plants (Fig. 5.3). Land plant material in this area is transported from the African continent to the ocean by easterly winds because there is no major river mouth near the coring location (Bremner and Willis, 1993; Dupont and Wyputta, 2003). On the adjacent continent vegetation changes from a small $C_3$ plant-dominated coastal area to mainly or nearly exclusively $C_4$ plant-dominated regions further inland (Fig. 5.1a). The vegetation signal in the sediments is a mixture of both regions with the main contribution coming from the $C_4$ dominated interior of the continent (Vogts et al., 2012).

Except for the $\delta^{13}C_{29}$ data, the *n*-alkane parameters indicate a marginal shift to decreasing $C_4$ plant proportions from the LGM to the Holocene. In some of the LGM samples the percentage of $C_4$ plant material is as low as during the Holocene (Fig. 5.3). Thus, we assume that the vegetation in the source area hardly changed during the last 20 ka even though climate during the LGM was described as having been cooler and more arid than today (Shi et al., 1998). The other way around, no stringent deductions about climate changes can be drawn from our results.

### 5.6.2. GeoB 4917-8 (12°S)

#### *5.6.2.1. Origin of n-alkanes*

All samples show $CPI_{27\text{-}33}$ >>1 which excludes a petroleum origin for the long chain *n*-alkanes (Simoneit, 1984). High CPI values and an odd/even carbon number predominance, like for core GeoB 3711-3, point to an origin primarily from terrestrial higher plants (Eglinton et al., 1962; Eglinton and Hamilton, 1967; Collister et al., 1994; Rommerskirchen et al., 2006b; Vogts et al., 2009).

$ACL_{27\text{-}33}$ values are in the range reported for terrestrial plants of the adjacent

continent (Fig. 5.4; Rommerskirchen et al., 2006b; Vogts et al., 2009). The $ACL_{27\text{-}33}$ value of the youngest sample in this study is close to that determined by Vogts et al. (2012) in a surface sediment sample from the same location to here (Fig. 5.1b). In Holocene and LGM sediments recovered near the investigation area of this study Rommerskirchen et al. (2003) and Rommerskirchen et al. (2006a) found quite similar $ACL_{27\text{-}33}$ values. The $ACL_{27\text{-}33}$ graph correlates noticeably well with the graphs of $\delta^{13}C_{31}$, $\delta^{13}C_{33}$, and $\delta^{13}C_{WMA29\text{-}33}$ ($r^2$= 0.68, $r^2$= 0.66 and $r^2$= 0.74, respectively; Figs. 5.5a, b and c). This relationship was also found by Rommerskirchen et al. (2003) but on a much smaller number of samples.

The trend to isotopically heavier *n*-alkanes from $C_{29}$ over $C_{31}$ to $C_{33}$ results from the different contribution of plants with different metabolic pathways to the members of the homologous series (Rommerskirchen et al., 2006a; Vogts et al., 2012). $C_4$ plants produce longer and isotopically heavier *n*-alkanes than $C_3$ plants

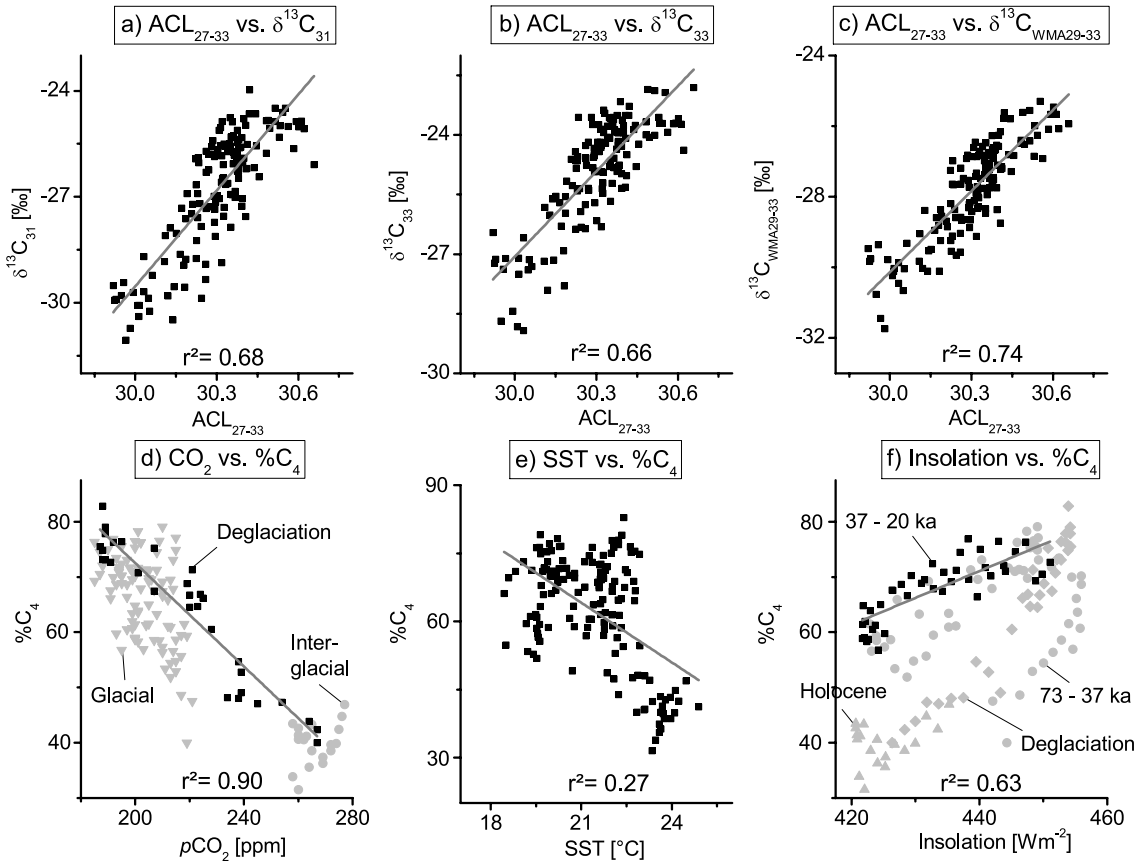


**Fig. 5.5:** Linear correlations (black rectangles) of $ACL_{27\text{-}33}$ with isotopic composition (GeoB 4917-8; 12°S, a, b and c) and of $\%C_4$ with $pCO_2$ (d; Petit et al., 1999; Indermühle et al., 2000; Monnin et al., 2004), SST (e) and local insolation of the postulated source area (f; 14°S, calculated with La2004; Laskar et al., 2004); $\%C_4$ is calculated from $\delta^{13}C_{31}$; grey symbols: data are not included to the correlation.

(Rommerskirchen et al., 2006b; Vogts et al., 2009). Thus, $C_4$ plants contribute more to the $C_{33}$ *n*-alkane in the sediments than to the $C_{29}$ homologue, which is relatively more abundantly produced by $C_3$ plants. Therefore, the $\delta^{13}C_{29}$ values stay largely uniform throughout the core. This is in agreement with a study near the Congo River mouth where $\delta^{13}C_{29}$ changes since the LGM were observed to be even smaller than here (Schefuß et al., 2005).

The $C_{31}$ *n*-alkane is produced in high proportions by both plants types. Hence, in the upper and lower part of the core, where the contribution of $C_4$ plants is low, $\delta^{13}C_{31}$ is similar to $\delta^{13}C_{29}$. In the middle core section, where $C_4$ plants contributed significant amounts of plant material to the sediment, $\delta^{13}C_{31}$ values are similar to $\delta^{13}C_{33}$ values. An analogous isotopic pattern of these *n*-alkanes was found by Vogts et al. (2012) in surface sediments of the Southeast Atlantic Ocean in a north to south transect with vegetation derived from rain forest in the north (mainly $C_3$) to grass savannah plant material further south (mainly $C_4$). Thus, in this study the carbon isotopic composition of the $C_{31}$ *n*-alkane data most sensitively reflect the secular vegetation changes on the nearby African continent throughout the core. Therefore, the following carbon isotope-based discussion is focused on $\delta^{13}C_{31}$.

The $\%C_4$ value of recent sediments analysed by Vogts et al. (2012) matches with our most recent sample. $\%C_4$ calculated by Rommerskirchen et al. (2006a) differs slightly. But for their calculations different end member values were used. End member values used here are based on a significantly extended dataset (Vogts et al., 2009). If they are applied to the $\delta^{13}C$ values of Rommerskirchen et al. (2006a), this leads to the same $C_4$ contribution. On the adjacent continent current vegetation contains less $C_4$ plants than elucidated from the sediments (Figs. 5.1a and 5.4). This is a result of prevailing east-southeast winds which transport material from areas with higher $C_4$ vegetation (Dupont and Wyputta, 2003; Vogts et al., 2012).

$C_4$ abundance calculated with $ACL_{27\text{-}33}$ is similar in its general appearance but systematically lower than calculations using $\delta^{13}C_{31}$ (Fig. 5.4). Vogts et al. (2012) attributed this to the limited database of end member values used for the calculations. In addition, a direct link to photosynthesis pathways was discovered for the carbon isotope composition but not for *n*-alkane chain length (O'Leary, 1981; Schidlowski, 1987). Therefore, the correlation between ACL and $\%C_4$ is most likely indirect and may be related to the different environmental conditions of the habitats.

#### *5.6.2.2. Source area*

Compared to other studies in this area, our results (ACL, $\delta^{13}C_{31}$, $\%C_4$) match the best those of Vogts et al. (2012). Schefuß et al. (2004) found a higher proportion of $C_4$

plants in recent sediments at ca. 10°S (5300 m water depth) than at this site (70% $C_4$ and <50%, respectively). Comparing our data with those of Rommerskirchen et al. (2006a; ODP site 1079 from 740 m water depth and GeoB 1016-3, 3400 m water depth; Fig. 5.1b), $\delta^{13}C_{31}$ values are similar for the mid- to late-Holocene but differ up to 4‰ between 18 and 19 ka.

Collins et al. (2011) investigated a nearby core from 500 m water depth (ODP site 1078; Fig. 5.1b) and calculated $\%C_3$ from $\delta^{13}C_{31}$ using end member values similar to those used in this study. Their estimation of vegetation composition is similar to ours for the LGM and the late Holocene. For deglaciation and mid-Holocene their data show up to 35% lower abundances of $C_4$ plants.

The discrepancies between our and the above mentioned studies may be attributed to different water depths of sampling sites or significantly different distances to the continent. A dependence of *n*-alkane parameters, including isotopic composition, from these geographic parameters was already discussed by Vogts et al. (2012) and Rommerskirchen et al. (2003). The trend in decreasing $ACL_{27-33}$ values with increasing water depths in this and the studies of Rommerskirchen et al. (2003) and Rommerskirchen et al. (2006a; ODP site 1079 and GeoB 1016-3; Fig. 5.1b) supports the idea of the geographic influence.

Especially shallow sediments receive material from neighbouring rivers. Collins et al. (2011) concluded that the main proportion of the material contributing to their core (ODP 1078; Fig. 5.1b) has been delivered from Balombo river drainage and that wind transport was not abundant. The prevailing wind direction in this area is southeast, whereas the Balombo river flows from the highlands to the coast and discharges north of the sampling sites. Material is then transported southward by the Angola Current (Fig. 5.1a; van Bennekom and Berger, 1984). As a result, wind carries terrestrial material from further south than the Balombo river. At our site, however, the sediments received land plant material probably exclusively via wind transport (Vogts et al., 2012).

In order to support the idea of different source areas further, we have compared our results with pollen studies from the same core that Collins et al. (2011) had investigated (ODP 1078; Dupont et al., 2008; Hessler et al., 2012). The pollen data of the last 50 ka concur with the results of Collins et al. (2011) regarding the vegetation change from grassland/savannah (mainly $C_4$) to woodland (mainly $C_3$). At their site (ODP 1078), *n*-alkane parameters show a vegetation change from $C_4$ dominated to mainly $C_3$ between 22 and 19 ka. In our study, however, the transition during deglaciation begins slightly later (ca. 20 ka; Fig. 5.4). Comparing the northern source area of ODP 1078 land plant material with our results indicates that woodlands spread

from north to south during deglaciation. Therefore, results from Collins et al. (2011) should differ from our results only during deglaciation. Thus, we conclude that differences between neighbouring cores in this case are due to different source areas.

### *5.6.2.3. Influence of global climate on vegetation*

The percentage of $C_4$ plants based on $\delta^{13}C_{31}$ varies between 30% and 90% (Fig. 5.4). $C_4$ plants outcompete $C_3$ plants at high temperatures, high light intensity and more arid conditions as well as lower $pCO_2$ (Ehleringer et al., 1997; Maley, 1991; Tipple and Pagani, 2007). The interplay of these climatic parameters is quite complex and not for all parameters data are available for the past. Some information can, however, directly or indirectly be deduced. Analyses of Antarctic ice cores reveal past global $pCO_2$ data, which correlate with global temperature (Barnola et al., 1987; Petit et al., 1999). Another global climate signal are glacial-interglacial cycles reflected by $\delta^{18}O$ values (e.g., Hoefs, 2004; Sharp, 2007). Both parameters display the shift from Pleistocene to Holocene (Fig. 5.6). This shift is also reflected by the contemporaneous vegetation deduced in this study. Furthermore, $pCO_2$ correlates well with $\%C_4$ ($r^2$= 0.90; Fig. 5.5d) during deglaciation (Petit et al., 1999; Indermühle et al., 2000; Monnin et al., 2004). In addition, samples from Late Pleistocene (low $pCO_2$ values and high $\%C_4$) and Holocene (high $pCO_2$ values and low

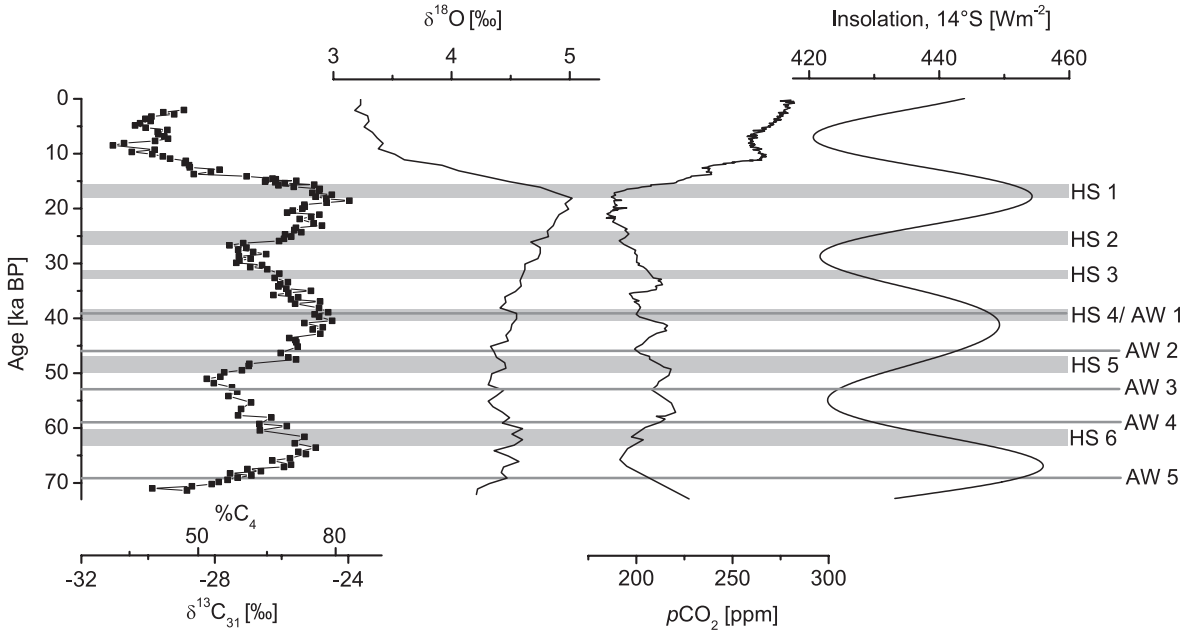


**Fig. 5.6:** Comparison of $\delta^{13}C_{31}$ and calculated $\%C_4$ (GeoB 4917-8, 12°S) with benthic foraminiferal $\delta^{18}O$ data (Lisiecki and Raymo, 2005), $pCO_2$ (Petit et al., 1999; Indermühle et al., 2000; Monnin et al., 2004) and local insolation of the postulated source area (14°S, calculated with La2004; Laskar et al., 2004); HS - Heinrich Stadial (Sanchez Goñi and Harrison, 2010), AW - Antarctic warming periods (Blunier et al., 2001).

$\%C_4$) are clearly separated.

The shift to higher $pCO_2$ and warmer climate during deglaciation is accompanied by a trend to higher $C_3$ plant abundance in southwest Africa. At first sight, the lower temperatures of the Late Pleistocene should be advantageous for $C_3$ plants (e.g., Ehleringer et al., 1997). But the Late Pleistocene was also dryer than the Holocene, which favours $C_4$ plants (e.g., Gasse, 2000; Weldeab et al., 2007). In addition, lower $pCO_2$ shifts the crossover point above which $C_4$ plants benefit from higher temperatures to lower values (Ehleringer et al., 1997).

In contrast to the vegetation change during deglaciation, the smaller maxima in $\%C_4$ (about 60 ka, 40 ka and 20 ka; Fig. 5.6) are not reflected by the $pCO_2$ curve. Thus, we evaluated if the $\%C_4$ maxima correlate with other known climate events, such as Northern Hemisphere Heinrich Stadials and Antarctic warming periods. The Northern Hemisphere is coupled via atmosphere and ocean to the Southern Hemisphere. High latitude temperature fluctuations may be coupled to tropical temperatures (Charles et al., 1996).

Heinrich Stadials are characterised by short-term warmer conditions in the Southern Hemisphere (Crowley, 1992; Broecker, 1998; EPICA, 2006; Barker et al., 2009). This should lead to more humid conditions on the continent and thus to more abundant $C_3$ plants (Hessler et al., 2010, 2012). Our results, however, do not show any change in vegetation composition during Heinrich Stadials (Fig. 5.4). These findings concur with those for the sediments from ODP 1078 (Hessler et al., 2012). There, the absence of vegetation variations was attributed to changes in the intensified hydrological cycle during warmer conditions: Precipitation and evaporation both intensified and resulted in a small net moisture supply for plant communities. Consequently, the effect on vegetation was considered negligible.

Antarctic warming periods were shown to occur by Antarctic ice core studies (Blunier et al., 1998; Blunier and Brook, 2001). A warming of the Southern Hemisphere should lead to wetter conditions, which in turn are advantageous for $C_3$ plants. Our results include the last five warmings but neither show an increase nor a decrease in $C_4$ composition exceeding the variation width of the data. Vegetation composition, thus, may have been insensitive to Antarctic warming events.

High-latitude climate fluctuations during the Late Pleistocene seem to have a negligible influence on southwestern African vegetation. Blunier et al. (1998) discussed that the coupling between the hemispheres is only weak, which would also indicate a weak coupling between high and low latitudes. This may explain why our results do not show significant effects of high-latitude climate fluctuations on low-latitude vegetation. Additionally, SST data show only a weak correlation with

$\%C_4$ ($r^2$= 0.27; Fig. 5.5e), which points to a minor influence of marine conditions on continental vegetation.

### *5.6.2.4. Insolation effects on local vegetation*

Another determining climate factor acting on local scale is the astronomical forcing which results, for example, in varying insolation (e.g., Hays et al., 1976). We calculated climatic conditions and local insolation for a continental region (ca. 350 km from the coast, 14°S) using the WebWIMP modeling program (Table 5.3; Matsuura et al., 2009) and La2004 (Fig. 5.6; Laskar et al., 2004). For this postulated source region, Vogts et al. (2012) found the best correlation between sedimentary *n*-alkane signals and vegetation composition. In this area today's growing season lasts from November to April with highest water availability (here defined as precipitation minus evaporation) for plants during March (Table 5.3). Although growing season length was two month shorter during the LGM than today, LGM wind patterns deviated only insignificantly from today's conditions (Dupont and Wyputta, 2003; Collins et al., 2011). We therefore assume that the growing season was shorter during LGM but its seasonality was unaltered during the last 70 ka. In contrast to $C_3$ plants, $C_4$ plants start growth at the end of the growing season (Winslow et al., 2003). For this reason and because of the highest water availability during March, we used the mean monthly insolation for March in our approach. However, the illustrated insolation is not equal to the insolation that reaches the plant because insolation will be

**Table 5.3:** Mean monthly temperature and water availability (precipitation minus evapotranspiration) in the postulated source area (ca. 350 km from the coast, 14°S) of GeoB 4917-8 (12°S) calculated by the WebWIMP modeling program (Matsuura et al., 2009).

| Month | Temperature [°C] | Water availability [mm month$^{-1}$] |
|---|---|---|
| Jan | 22 | 100 |
| Feb | 22 | 73 |
| Mar | 22 | 104 |
| Apr | 21 | 13 |
| May | 19 | -56 |
| Jun | 17 | -45 |
| Jul | 17 | -46 |
| Aug | 19 | -66 |
| Sep | 22 | -83 |
| Oct | 23 | -51 |
| Nov | 22 | 32 |
| Dec | 22 | 71 |

reduced in the atmosphere (e.g., due to reflection).

The oscillating local insolation in March shows great similarity to the variation of $\%C_4$ between 50 and 10 ka (Fig. 5.6). Between 73 and 50 ka both curves appear to be slightly out of phase. This may be due to dating uncertainties in the deeper part of the core. The oldest radiocarbon-dated sample is at 37 ka (Table 5.1). Sedimentation rates were assumed to be uniform downcore but sedimentation rates and estimated ages may not be totally exact. However, during the radiocarbon-dated period prior to the LGM (37 - 20 ka) $\%C_4$ positively correlates with insolation ($r^2$= 0.63; Fig. 5.5f). During deglaciation the insolation effect on $C_4$ plant abundance are overlain by the above mentioned global climatic factors and therefore not taken into account. A correlation between insolation and $C_4$ plant abundance was also found for East Africa (Schefuß et al., 2003a). In contrast, in northwest Africa vegetation remained unaffected by insolation variations (Niedermeyer et al., 2010). In the African rainforest tree pollen abundance ($C_3$) changes simultaneously with insolation (Dupont, 2011).

Higher insolation potentially favours the growth of $C_4$ plants because of their lack of photorespiration (Long, 1999; Still et al., 2003). As a result, growth of $C_4$ plants is not limited by higher levels of insolation. Global $C_4$ distribution, however, is not well correlated with insolation (Teeri, 1988 and references therein). Thus, higher insolation may only indirectly lead to conditions favourable to $C_4$ plants by affecting temperature and precipitation.

Higher insolation leads to increased temperature (e.g., Kutzbach, 1981). Growing season temperature was described as the dominant factor controlling the distribution of $C_3$ and $C_4$ plants (Teeri and Stowe, 1976; Teeri, 1988; Sage et al., 1999b). The distribution of $C_3$ and $C_4$ plants is further dependent on timing of precipitation (Ehleringer and Monson, 1993; Amundson et al., 1994; Sage et al., 1999b). $C_4$ plants dominate in regions where summers are hot and wet followed by dry winters. In contrast, $C_3$ plants grow during cooler wet seasons. Although $C_3$ plants dominate in wet African regions, $C_4$ plants can also occur in wet regions if some other factors rule out $C_3$ dominance (Sage et al., 1999b).

With higher insolation sea-land temperature contrast and monsoon activity increase. This leads to higher precipitation on the continent (Kutzbach, 1981; Kutzbach and Liu, 1997; Partridge et al., 1997; Niedermeyer et al., 2010). Other studies postulated that an enhancement of rain and temperature may not result in greater water availability for plants because evaporation also increases (Hessler et al., 2012). But also the timing of precipitation is essential: If precipitation and water availability increase during the warmer end of the growing season, this may lead to an increased growth of $C_4$ vegetation.

The effect of increased growth of $C_4$ plants may be further increased because this highly productive plant would provide more fuel for fire during dry seasons. Fire would promote the expansion of $C_4$ plants by destroying and replacing $C_3$ with $C_4$ plants (Bond et al., 2005; Beerling and Osborne, 2006; Osborne and Beerling, 2006; Daniau et al., 2010). Thus, fire effects may explain why $C_4$ plants spread during times of increasing insolation. But they do not explain the decreasing $C_4$ distribution when insolation declines.

Another factor enhancing the observed $C_4$ variations may be the shading of these plants. $C_4$ plants thrive in an open habitat where they recieve full sunlight, but they grow poorly in shaded regions, e.g., under the canopy of trees ($C_3$ plants). As a results, if $C_3$ plants shade $C_4$ plants, those $C_4$ plants would not be able to outcompete these $C_3$ plants (Sage and Kubien, 2003). But if $C_3$ distribution decreases, $C_4$ plants obtain more sunlight and can thrive and spread.

In general, the interplay of climatic factors and their influence on the distribution of $C_3$ and $C_4$ plants is complex (Teeri, 1988). In the source area studied, insolation may have been the key factor during the Late Pleistocene. Whether insolation is directly or indirectly responsible for vegetation changes needs to be verified. In other regions, however, different factors may control the climate-dependent change of vegetation composition.

### 5.6.3. Glacial-interglacial differentiation by single samples

General informations on vegetation during glacials or interglacials, such as predominant plant type, are given by the cores from both locations studied. In this regard, single samples are representative for a given period. However, single samples approaches may become biased if extreme values are taken into account. Here, extreme values are revealed for 20 ka at 20°S and, e.g., 40 ka or 50 ka at 12°S, and they differ by up to 20% $C_4$ plants. During periods of great vegetation changes, such as glacial-interglacial transitions, a single sample cannot be representative in all cases. In addition, a reliable age model is required for a single sample approach.

At 12°S, values for most *n*-alkane parameters are clearly separated between the Late Pleistocene and the Holocene (Fig. 5.4). In these cases, single samples may be assigned to a glaciation state based on their *n*-alkane signal. But where vegetation variation is minimal, e.g. at 20°S, this is not possible.

## 5.7. Conclusions

On the basis of terrestrial *n*-alkanes we investigated the changes of southwest African vegetation during 23 to 2 ka (20°S) and 73 to 2 ka (12°S), respectively. At

20°S, the $C_4$ domination in the continental source area remains fairly unaltered from the LGM to today. In contrast, at 12°S most *n*-alkane parameters clearly separate the Late Pleistocene (66% $C_4$ on average) from the Holocene (40% $C_4$ on average).

For both cores single samples are representative for the glacial or interglacial, but glacial-interglacial transitions need to be avoided for such approaches. Nevertheless, smaller vegetation changes or extreme values during a period will most likely be missed by single sample analyses or bias them.

At 12°S $C_4$ vegetation decreases from the LGM to the Holocene simultaneously with $pCO_2$ increase ($r^2$= 0.90). The smaller maxima in $C_4$ distribution during the Late Pleistocene occur neither during Heinrich Stadials nor during Antarctic warming events. But they are reasonably well correlated with local insolation changes ($r^2$= 0.63).

## 5.8. Acknowledgements

We are grateful to the organisers and participants of RV Meteor cruises M34/2 and M41/1. J. Pätzold (University of Bremen) is appreciated for help during sample retrieval. We thank L. Dupont, S. Mulitza and M. Segel (University of Bremen) for support regarding sample preparation for radiocarbon dating. B. Kopke helped and gave advice during carbon isotope analysis and B. Schnetger and M. Schulz (all ICBM) supported XRF analysis. M. Fischer, H. Haase, J. Jasper, M. Kurtz, L. Meiners, S. Schüler and I. Ulber (all ICBM) are acknowledged for their support during sample workup. We are indebted to G. Eglinton (University of Bristol) for valuable discussions regarding data interpretation. Parts of this study were financially supported by the Deutsche Forschungsgemeinschaft (DFG, grant nos. Ru 458/35 and Ru 458/40).

# 6. Summary and perspectives

The main aim of this thesis was to further elaborate information on continental vegetation and climate derived from sedimentary *n*-alkanes in marine geological archives. The investigated region of southwest Africa was chosen because the vegetation zones are broadly parallel to the latitude and the plant material is zonally transported from the continent to the ocean.

To investigate possible trends of *n*-alkane parameters for $C_3$ and $C_4$ plants in southwest Africa, 41 $C_3$ and 11 $C_4$ plant species from the wood- and shrubland of Angola were analysed. The wood- and shrubland is located between the rain forest and the savannah. A comparison of plant *n*-alkane data from these vegetation zones reveals that the carbon isotopic composition of the $C_3$ plants increase towards the south. This increase is probably due to changing environmental conditions like increasing water stress, light intensity and less incorporation of recycled $CO_2$. The distribution patterns of the *n*-alkanes show an increase in chain length towards the south for both $C_3$ and $C_4$ plants. Numerically, this increase is best reflected by an ACL parameter comprising the most abundant homologues ($C_{29}$-$C_{33}$). No distinct relations were observed between ACL and the mean annual temperature or the aridity indices of the respective vegetation zones. In addition, the plants are grouped according to the plant height in different growth forms and in different habitats. The plant heights are correlated with the mean chain length of each group in order to evaluate the influence of a vertical temperature gradient (temperature decrease with height above the ground) on the chain length. Thereby, it was revealed that the $ACL_{27\text{-}33}$ values for trees in the different vegetation zones are fairly uniform. The averaged $ACL_{27\text{-}33}$ value of all trees and all grasses were further used as end member values to calculate the abundance of tree organic matter in sediments of a transect in the southeast Atlantic analysed previously. The calculated tree abundance reflects the tree proportion on the adjacent continent with respect to the transport pathways.

An isobathic transect of surface sediment samples off southwest Africa (1°N to 28°S) was investigated to find out how the *n*-alkane parameters (chain length distribution and stable carbon isotopic composition) reflect the adjacent continental vegetation. To estimate the $C_4$ contribution to the sediments, a binary mixing equation was employed using *n*-alkane end member parameters (ACL, $\delta^{13}C_{29}$, $\delta^{13}C_{31}$ and $\delta^{13}C_{33}$) for $C_3$ and $C_4$ plants. Across the different parameters used for the calculations, the $C_4$ proportions roughly match each other. In southwest Africa, the

vegetation changes from $C_3$ plant dominated in the equatorial rain forest to $C_4$ plant dominated towards the south. The calculated $C_4$ abundance with $\delta^{13}C_{31}$ reflects the continental vegetation if long range transport of plant material by wind and rivers is taken into account. The four northern samples probably receive large amounts of aeolian material from distant, unknown locations via the Harmattan winds. For this reason, these samples were excluded from further evaluation. The $C_4$ abundances of the other samples correlated significantly with the mean annual precipitation and the aridity indices in the catchment areas.

The hydrogen isotopic composition of the *n*-alkanes was determined for the $C_{29}$, $C_{31}$ and $C_{33}$ *n*-alkanes. The sediment-derived signals reflect the δD composition of the precipitation on the adjacent continent. However, correlations of the *n*-alkane δD values with precipitation δD values at different distances to the coast reveal that the area 350 km inland is a major source region of the sedimentary *n*-alkanes. The hydrogen isotopic composition of the precipitation varies over the year, but taking into account the seasonality does not lead to a significant increase in correlation. The apparent fractionation between the *n*-alkanes and the precipitation at 350 km distance to the coast is quite uniform in the course of the transect despite the gradient in climatic conditions and vegetation composition. This leads to the conclusion that the δD change due to the increasing aridity towards the south is superimposed by the concurrent δD variation due to the change of the plant groups. Thus, palaeoenvironmental studies should evaluate the $C_3$ or $C_4$ contribution in parallel.

To study the influence of different climatic parameters on the past vegetation, two sediment cores from the southeast Atlantic (12°S and 20°S) covering the current interglacial and parts of the last glacial were analysed for their *n*-alkane parameters. Single samples are representative for the glacial or interglacial they derive from for the northern core but not significantly for the southern core. For such an approach, however, glacial-interglacial transitions need to be avoided, and small vegetation changes might be missed. The southern core is located adjacent to a $C_4$ plant dominated region and reveals a fairly uniform contribution of $C_4$ material to the sediments during the last 23 ka. No stringent deductions about climatic changes were drawn from these results. In contrast, the core at 12°S covering the last 73 ka indicates a $C_4$ plant domination during the Last Pleistocene, a $C_3$ plant domination during the Holocene and a gradual change of the vegetation during deglaciation. During deglaciation, the increasing atmospheric $CO_2$ content correlates well with the $\%C_4$ values. During the Late Pleistocene, small $\%C_4$ fluctuations were detected which do not occur simultaneously with Heinrich Stadials or Antarctic warming periods. Instead, the local insolation from the end of the growing season shows great

similarities with the $\%C_4$ fluctuations. Higher insolation leads to higher temperatures and to higher precipitation rates at the end of the growing season which may have favoured the growth of $C_4$ plants.

This thesis expands the knowledge about the *n*-alkane parameters and their deductions on vegetation and climatic parameters. However, there are still knowledge gaps which should be addressed in subsequent studies. The small variation of the end member data when updated with new results from additional plant series indicate that the general vegetation aspects are depicted by this dataset. For special locations like areas, where epiphytes or swamp grasses are abundant, additional data would be valuable or necessary. Furthermore, the hypothesis on the connection between ACL and growth height/vertical temperature gradient should be confirmed. Therefore, ACL values of plants with known growth height and known local temperature during growing season should be studied. Expanding the use of ACL to a tree abundance indicator may lead to a valuable proxy for life form abundance which in turn can be employed to interpret *n*-alkane hydrogen isotopic data. In addition, a study of δD values of plant samples and precipitation δD values could further elaborate the fractionation mechanisms between the hydrogen isotopic composition of precipitation and plant waxes. *n*-Alkane data from the transport pathways (dust or sediment traps) could furthermore reveal possible changes in the *n*-alkane composition during aeolian transport and while sinking through the water column. This approach could be accompanied by modelling of more detailed wind trajectories and the determination of the fractionation of different material sizes during aeolian transport. Regarding the sediments, a thorough transect of samples from different water depths may shed light on the effect of water depth on *n*-alkane parameters. For climatic deductions, the influence of insolation on vegetation composition should be verified at different locations and during different time frames. Thereby, it could be investigated if the *n*-alkane δD values reflect the insolation patterns because it was emphasised that higher insolation leads to wetter conditions which in turn should be mirrored by the δD values. With regard to the current increase in atmospheric $pCO_2$, the effects on the vegetation distribution could be modelled and influences on the agriculture could be evaluated.

Despite these remaining knowledge gaps, this thesis contributes to the currently on-going research by (i) updating the literature *n*-alkane plant database, (ii) confirming that the *n*-alkane parameters reflect the continental vegetation and precipitation and (iii) detecting possible dependencies of the current and past vegetation distribution on climatic parameters like aridity, $pCO_2$ and insolation. Even though the *n*-alkanes are chemically quite simple molecules, they provide important information

whose interpretation may lead to a better understanding of the Earth´s climate.

# 7. References

Aichner, B., Herzschuh, U., Wilkes, H., Vieth, A., Böhner, J., 2010. δD values of *n*-alkanes in Tibetan lake sediments and aquatic macrophytes - A surface sediment study and application to a 16 ka record from Lake Koucha. Organic Geochemistry 41, 779-790.

Alley, R.B., 1998. Icing the North Atlantic. Nature 392, 335-337.

Amundson, R., Franco-Vizcaíno, E., Graham, R.C., DeNiro, M., 1994. The relationship of precipitation seasonality to the flora and stable isotope chemistry of soils in the Vizcaíno desert, Baja California, México. Journal of Arid Environments 28, 265-279.

Arens, N.C., Hope Jahren, A., Amundson, R., 2000. Can $C_3$ plants faithfully record the carbon isotopic composition of atmospheric carbon dioxide? Paleobiology 26, 137-164.

Barbosa, P.M., Stroppiana, D., Grégoire, J.-M., 1999. An assessment of vegetation fire in Africa (1981-1991): Burned areas, burned biomass, and atmospheric emissions. Global Biogeochemical Cycles 13, 933-950.

Barker, S., Diz, P., Vautravers, M.J., Pike, J., Knorr, G., Hall, I.R., Broecker, W.S., 2009. Interhemispheric Atlantic seesaw response during the last deglaciation. Nature 457, 1097-1102.

Barnola, J.M., Raynaud, D., Korotkevich, Y.S., Lorius, C., 1987. Vostok ice core provides 160,000-year record of atmospheric $CO_2$. Nature 329, 408-414.

Bassham, J.A., Benson, A.A., Kay, L.D., Harris, A.Z., Wilson, A.T., Calvin, M., 1954. The path of carbon in photosynthesis. XXI. The cyclic regeneration of carbon dioxide acceptor. Journal of the American Chemical Society 76, 1760-1770.

Beerling, D.J., Osborne, C.P., 2006. The origin of the savanna biome. Global Change Biology 12, 2023-2031.

van Bennekom, A.J., Berger, G.W., 1984. Hydrography and silica budget of the Angola Basin. Netherlands Journal of Sea Research 17, 149-200.

Bi, X., Sheng, G., Liu, X., Li, C., Fu, J., 2005. Molecular and carbon and hydrogen isotopic composition of *n*-alkanes in plant leaf waxes. Organic Geochemistry 36, 1405-1417.

Bird, M.I., Summons, R.E., Gagan, M.K., Roksandic, Z., Dowling, L., Head, J., Keith Fifield, L., Cresswell, R.G., Johnson, D.P., 1995. Terrestrial vegetation change inferred from *n*-alkane $\delta^{13}C$ analysis in the marine environment. Geochimica et Cosmochimica Acta 59, 2853-2857.

Björkman, O., 1976. Adaptive and genetic aspects of $C_4$ photosynthesis. In: R.H. Burris, C.C. Black (Eds.), Metabolism and Plant Productivity. University Park Press, Baltimore, pp. 287-309.

Björkman, O., Berry, J., 1973. High-efficiency photosynthesis. Scientific American 229, 80-93.

Blunier, T., Brook, E.J., 2001. Timing of millennial-scale climate change in Antarctica and Greenland during the last glacial period. Science 291, 109-112.

Blunier, T., Chappellaz, J., Schwander, J., Dällenbach, A., Stauffer, B., Stocker, T.F., Raynaud, D., Jouzel, J., Clausen, H.B., Hammer, C.U., Johnsen, S.J., 1998. Asynchrony of Antarctic and Greenland climate change during the last glacial period. Nature 394, 739-743.

Bond, W.J., Woodward, F.I., Midgley, G.F., 2005. The global distribution of ecosystems in a world without fire. New Phytologist 165, 525-538.

Bowen, G.J., Revenaugh, J., 2003. Interpolating the isotopic composition of modern meteoric precipitation. Water Resources Research 39.

Bowen, G.J., Wilkinson, B., 2002. Spatial distribution of $\delta^{18}O$ in meteoric precipitation. Geology 30, 315-318.

Bowen, G.J., Wassenaar, L.I., Hobson, K.A., 2005. Global application of stable hydrogen and oxygen isotopes to wildlife forensics. Oecologia 143, 337-348.

Bremner, J.M., Willis, J.P., 1993. Mineralogy and geochemistry of the clay fraction of sediments from the Namibian continental margin and the adjacent hinterland. Marine Geology 115, 85-116.

Brodribb, T., 1996. Dynamics of changing intercellular $CO_2$ concentration ($c_i$) during drought and determination of minimum functional $c_i$. Plant Physiology 111, 179-185.

Broecker, W.S., 1998. Paleocean circulation during the last deglaciation: A bipolar seesaw? Paleoceanography 13, 119-121.

Broecker, W., Bond, G., Klas, M., Clark, E., McManus, J., 1992. Origin of the northern Atlantic's Heinrich events. Climate Dynamics 6, 265-273.

Burdige, D.J., 2005. Burial of terrestrial organic matter in marine sediments: A re-assessment. Global Biogeochemical Cycles 19, doi:10.1029/2004GB002368.

Bush, R.T., McInerney, F.A., 2013. Leaf wax *n*-alkane distributions in and across modern plants: Implications for paleoecology and chemotaxonomy. Geochimica et Cosmochimica Acta 117, 161-179.

Butzin, M., Prange, M., Lohmann, G., 2005. Radiocarbon simulations for the glacial ocean: The effects of wind stress, Southern Ocean sea ice and Heinrich events. Earth and Planetary Science Letters 235, 45-61.

Carr, A.S., Boom, A., Grimes, H.L., Chase, B.M., Meadows, M.E., Harris, A., 2014. Leaf wax *n*-alkane distributions in arid zone South African flora: Environmental controls, chemotaxonomy and palaeoecological implications. Organic Geochemistry 67, 72-84.

Castañeda, I.S., Werne, J.P., Johnson, T.C., Filley, T.R., 2009. Late Quaternary vegetation history of southeast Africa: The molecular isotopic record from Lake Malawi. Palaeogeography, Palaeoclimatology, Palaeoecology 275, 100-112.

Charles, C.D., Lynch-Stieglitz, J., Ninnemann, U.S., Fairbanks, R.G., 1996. Climate connections between the hemisphere revealed by deep sea sediment core/ice core correlations. Earth and Planetary Science Letters 142, 19-27.

Chase, B.M., Meadows, M.E., 2007. Late Quaternary dynamics of southern Africa's winter rainfall zone. Earth-Science Reviews 84, 103-138.

Chester, R., 2003. Marine Geochemistry, 2nd ed., Blackwell Science Ltd, Malden.

Chibnall, A.C., Piper, S.H., Pollard, A., Williams, E.F., Sahai, P.N., 1934. The constitution of the primary alcohols, fatty acids and paraffins present in plant and insect waxes. Biochemical Journal 28, 2189-2208.

Chikaraishi, Y., Naraoka, H., 2003. Compound-specific δD-$\delta^{13}$C analyses of *n*-alkanes extracted from terrestrial and aquatic plants. Phytochemistry 63, 361-371.

Chikaraishi, Y., Naraoka, H., 2007. $\delta^{13}$C and δD relationships among three *n*-alkyl compound classes (*n*-alkanoic acid, *n*-alkane and *n*-alkanol) of terrestrial higher plants. Organic Geochemistry 38, 198-215.

Cleugh, H., Miller, J., Böhm, M., 1998. Direct mechanical effects of wind on crops. Agroforestry Systems 41, 85-112.

Cole, M.M., 1986. The Savannas: Biogeography and Geobotany, Academic Press, London.

Collatz, G.J., Berry, J.A., Clark, J.S., 1998. Effects of climate and atmospheric $CO_2$ partial pressure on the global distribution of $C_4$ grasses: Present, past, and future. Oecologia 114, 441-454.

Collins, J.A., Schefuß, E., Heslop, D., Mulitza, S., Prange, M., Zabel, M., Tjallingii, R., Dokken, T.M., Huang, E., Mackensen, A., Schulz, M., Tian, J., Zarriess, M., Wefer, G., 2011. Interhemispheric symmetry of the tropical African rainbelt over the past 23,000 years. Nature Geosciences 4, 42-45.

Collins, J.A., Schefuß, E., Mulitza, S., Prange, M., Werner, M., Tharammal, T., Paul, A., Wefer, G., 2013. Estimating the hydrogen isotopic composition of past precipitation using leaf-waxes from western Africa. Quaternary Science Reviews 65, 88-101.

Collister, J.W., Rieley, G., Stern, B., Eglinton, G., Fry, B., 1994. Compound-specific

$\delta^{13}C$ analyses of leaf lipids from plants with differing carbon dioxide metabolisms. Organic Geochemistry 21, 619-627.

Cranwell, P.A., 1981. Diagenesis of free and bound lipids in terrestrial detritus deposited in a lacustrine sediment. Organic Geochemistry 3, 79-89.

Crowley, T.J., 1992. North Atlantic Deep Water cools the Southern Hemisphere. Paleoceanography 7, 489-497.

Dai, A., Trenberth, K.E., 2002. Estimates of freshwater discharge from continents: Latitudinal and seasonal variations. Journal of Hydrometeorology 3, 660-687.

Dale, J.E., 1988. The control of leaf expansion. Annual Review of Plant Physiology and Plant Molecular Biology 39, 267-295.

Daniau, A.-L., Harrison, S.P., Bartlein, P.J., 2010. Fire regimes during the last glacial. Quaternary Science Reviews 29, 2918-2930.

Dewar, G., Reimer, P.J., Sealy, J., Woodborne, S., 2012. Late-Holocene marine radiocarbon reservoir correction (ΔR) for the west coast of South Africa. The Holocene 22, 1481-1489.

Downes, R.W., 1969. Differences in transpiration rates between tropical and temperate grasses under controlled conditions. Planta 88, 261-273.

Dupont, L., 2011. Orbital scale vegetation change in Africa. Quaternary Science Reviews 30, 3589-3602.

Dupont, L.M., Wyputta, U., 2003. Reconstructing pathways of aeolian pollen transport to the marine sediments along the coastline of SW Africa. Quaternary Science Reviews 22, 157-174.

Dupont, L.M., Behling, H., Kim, J.-H., 2008. Thirty thousand years of vegetation development and climate change in Angola (Ocean Drilling Programm Site 1078). Climate of the Past 4, 107-124.

Eckert, S., Brumsack, H.-J., Severmann, S., Schnetger, B., März, C., Fröllje, H., 2013. Establishment of euxinic conditions in the Holocene Black Sea. Geology 41, 431-434.

Eglinton, T.I., Eglinton, G., 2008. Molecular proxies for paleoclimatology. Earth and Planetary Science Letters 275, 1-16.

Eglinton, G., Hamilton, R.J., 1967. Leaf epicuticular waxes. Science 156, 1322-1335.

Eglinton, G., Gonzalez, A.G., Hamilton, R.J., Raphael, R.A., 1962. Hydrocarbon constituents of the wax coatings of plant leaves: A taxonomic survey. Phytochemistry 1, 89-102.

Ehleringer, J.R., Monson, R.K., 1993. Evolutionary and ecological aspects of photosynthetic pathway variation. Annual Review of Ecology and Systematics 24,

411-439.

Ehleringer, J.R., Cerling, T.E., Helliker, B.R., 1997. $C_4$ photosynthesis, atmospheric $CO_2$ and climate. Oecologia 112, 285.

EPICA, 2006. One-to-one coupling of glacial climate variability in Greenland and Antarctica. Nature 444, 195-198.

Fairbanks, R.G., Mortlock, R.A., Chiu, T.-C., Cao, L., Kaplan, A., Guilderson, T.P., Fairbanks, T.W., Bloom, A.L., Grootes, P.M., Nadeau, M.-J., 2005. Radiocarbon calibration curve spanning 0 to 50,000 years BP based on paired $^{230}Th/^{234}U/^{238}U$ and $^{14}C$ dates on pristine corals. Quaternary Science Reviews 24, 1781-1796.

Farquhar, G.D., 1983. On the nature of carbon isotope discrimination in $C_4$ species. Australian Journal of Plant Physiology 10, 205-226.

Farquhar, G.D., Ehleringer, J.R., Hubick, K.T., 1989. Carbon isotope discrimination and photosynthesis. Annual Review of Plant Physiology and Plant Molecular Biology 40, 503-537.

Feakins, S.J., Sessions, A.L., 2010a. Controls on the D/H ratios of plant leaf waxes in an arid ecosystem. Geochimica et Cosmochimica Acta 74, 2128-2141.

Feakins, S.J., Sessions, A.L., 2010b. Crassulacean acid metabolism influences D/H ratio of leaf wax in succulent plants. Organic Geochemistry 41, 1269-1276.

Feakins, S.J., deMenocal, P.B., Eglinton, T.I., 2005. Biomarker records of late Neogene changes in northeast African vegetation. Geology 33, 977-980.

Ficken, K.J., Li, B., Swain, D.L., Eglinton, G., 2000. An *n*-alkane proxy for the sedimentary input of submerged/floating freshwater aquatic macrophytes. Organic Geochemistry 31, 745-749.

Fischer, G., Wefer, G., 1996. Long-term observation of particle flux in the eastern Atlantic: Seasonality, changes of flux with depth and comparison with the sediment record. In: G. Wefer, W.H. Berger, G. Siedler, D.J. Webb (Eds.), The South Atlantic - Present and Past Circulation. Springer, Berlin.

Frierson, D.M.W., Lu, J., Chen, G., 2007. Width of the Hadley cell in simple and comprehensive general circulation models. Geophysical Research Letters 34, L18804.

Gagosian, R.B., Peltzer, E.T., 1986. The importance of atmospheric input of terrestrial organic material to deep sea sediments. Organic Geochemistry 10, 661-669.

Gao, L., Zheng, M., Fraser, M., Huang, Y., 2014. Comparable hydrogen isotopic fractionation of plant leaf wax *n*-alkanoic acids in arid and humid subtropical ecosystems. Geochemistry, Geophysics, Geosystems 15, 361-373.

Garcin, Y., Schwab, V.F., Gleixner, G., Kahmen, A., Todou, G., Séné, O., Onana, J.-M., Achoundong, G., Sachse, D., 2012. Hydrogen isotope ratios of lacustrine

sedimentary *n*-alkanes as proxies of tropical African hydrology: Insights from a calibration transect across Cameroon. Geochimica et Cosmochimica Acta 79, 106-126.

Gasse, F., 2000. Hydrological changes in the African tropics since the Last Glacial Maximum. Quaternary Science Reviews 19, 189-211.

Gasse, F., Chalié, F., Vincens, A., Williams, M.A.J., Williamson, D., 2008. Climatic patterns in equatorial and southern Africa from 30,000 to 10,000 years ago reconstructed from terrestrial and near-shore proxy data. Quaternary Science Reviews 27, 2316-2340.

Gat, J.R., 1996. Oxygen and hydrogen isotopes in the hydrologic cycle. Annual Review of Earth and Planetary Sciences 24, 225-262.

Gingele, F.X., 1996. Holocene climatic optimum in southwest Africa - Evidence from the marine clay mineral record. Palaeogeography, Palaeoclimatology, Palaeoecology 122, 77-87.

Hatch, M.D., 1987. $C_4$ photosynthesis: A unique elend of modified biochemistry, anatomy and ultrastructure. Biochimica et Biophysica Acta - Reviews on Bioenergetics 895, 81-106.

Hatch, M.D., Slack, C.R., 1966. Photosynthesis by sugar-cane leaves - A new carboxylation reaction and pathway of sugar formation. Biochemical Journal 101, 103-111.

Hayes, J.M., 1993. Factors controlling $^{13}C$ contents of sedimentary organic compounds: Principles and evidence. Marine Geology 113, 111-125.

Hays, J.D., Imbrie, J., Shackleton, N.J., 1976. Variations in the Earth's orbit: Pacemaker of the Ice Ages. Science 194, 1121-1132.

Heinrich, H., 1988. Origin and consequences of cyclic ice rafting in the Northeast Atlantic Ocean during the past 130,000 years. Quaternary Research 29, 142-152.

Hessler, I., Dupont, L., Bonnefille, R., Behling, H., González, C., Helmens, K.F., Hooghiemstra, H., Lebamba, J., Ledru, M.-P., Lézine, A.-M., Maley, J., Marret, F., Vincens, A., 2010. Millennial-scale changes in vegetation records from tropical Africa and South America during the last glacial. Quaternary Science Reviews 29, 2882-2899.

Hessler, I., Steinke, S., Groeneveld, J., Dupont, L., Wefer, G., 2011. Impact of abrupt climate change in the tropical southeast Atlantic during Marine Isotope Stage (MIS) 3. Paleoceanography 26, PA4209.

Hessler, I., Dupont, L., Handiani, D., Paul, A., Merkel, U., Wefer, G., 2012. Masked millennial-scale climate variations in South West Africa during the last glaciation. Climate of the Past 8, 841 - 853.

Heyns, P., 2003. Water-resources management in Southern Africa. In: M. Nakayama (Ed.), International Waters in Southern Africa. United Nations University Press, Hong Kong, pp. 5-37.

Hoefs, J., 2004. Stable Isotope Geochemistry, 5th ed., Springer, Berlin.

Hoffmann, B., Kahmen, A., Cernusak, L.A., Arndt, S.K., Sachse, D., 2013. Abundance and distribution of leaf wax *n*-alkanes in leaves of Acacia and Eucalyptus trees along a strong humidity gradient in northern Australia. Organic Geochemistry 62, 62-67.

Hou, J.Z., D'Andrea, W.J., MacDonald, D., Huang, Y.S., 2007. Hydrogen isotopic variability in leaf waxes among terrestrial and aquatic plants around Blood Pond, Massachusetts (USA). Organic Geochemistry 38, 977-984.

Hou, J., D'Andrea, W.J., Huang, Y., 2008. Can sedimentary leaf waxes record D/H ratios of continental precipitation? Field, model and experimental assessments. Geochimica et Cosmochimica Acta 72, 3503-3517.

Hren, M.T., Pagani, M., Erwin, D.M., Brandon, M., 2010. Biomarker reconstruction of the early Eocene paleotopography and paleoclimate of the northern Sierra Nevada. Geology 38, 7-10.

Huang, Y., Dupont, L., Sarnthein, M., Hayes, J.M., Eglinton, G., 2000. Mapping of $C_4$ plant input from North West Africa into North East Atlantic sediments. Geochimica et Cosmochimica Acta 64, 3505-3513.

Hughen, K.A., Baille, M.G.L., Bard, E., Beck, J.W., Bertrand, C.J.H., Blackwell, P.G., Buck, C.E., Burr, G.S., Cutler, K.B., Damon, P.E., Edwards, R.L., Fairbanks, R.G., Friedrich, M., Guilderson, T.P., Kromer, B., McCormac, G., Manning, S., Bronk Ramsey, C., Reimer, P.J., Reimer, R.W., Remmele, S., Southon, J.R., Stuiver, M., Talamo, S., Taylor, F.W., van der Plicht, J., Weyhenmeyer, C.E., 2004. Marine04 marine radiocarbon age calibration, 0-26 cal kyr BP. Radiocarbon 46, 1059-1086.

Indermühle, A., Monnin, E., Stauffer, B., Stocker, T.F., Wahlen, M., 2000. Atmospheric $CO_2$ concentration from 60 to 20 kyr BP from the Taylor Dome ice core, Antarctica. Geophysical Research Letters 27, 735-738.

IPCC, 2013. Climate change 2013, the physical science basis, working group I contribution. In: T.F. Stocker, Q. Dahe, G.-K. Plattner, M.M.B. Tignor, S.K. Allen, J. Boschung, A. Nauels, Y. Xia, V. Bex, P.M. Midgley (Eds.), Fifth Assessment Report of the Intergovernmental Panel on Climate Change, Cambridge University Press, Cambridge.

Jetter, R., Kunst, L., Samuels, A.L., 2006. Composition of plant cuticular waxes. In: M. Riederer, C. Müller (Eds.), Annual Plant Reviews 23: Biology of the Plant Cuticle. Blackwell, Oxford, pp. 145-181.

Kahmen, A., Hoffmann, B., Schefuß, E., Arndt, S.K., Cernusak, L.A., West, J.B., Sachse, D., 2013a. Leaf water deuterium enrichment shapes leaf wax *n*-alkane δD values of angiosperm plants II: Observational evidence and global implications. Geochimica et Cosmochimica Acta 111, 50-63.

Kahmen, A., Schefuß, E., Sachse, D., 2013b. Leaf water deuterium enrichment shapes leaf wax *n*-alkane δD values of angiosperm plants I: Experimental evidence and mechanistic insights. Geochimica et Cosmochimica Acta 111, 39-49.

Keeley, Jon E., Rundel, Philip W., 2003. Evolution of CAM and $C_4$ carbon-concentrating mechanisms. International Journal of Plant Sciences 164, S55-S77.

Kemp, D.R., 1980. The location and size of the extension zone of emerging wheat leaves. New Phytologist 84, 729-737.

Kirst, G.J., Schneider, R.R., Müller, P.J., von Storch, I., Wefer, G., 1999. Late Quaternary temperature variability in the Benguela current system derived from alkenones. Quaternary Research 52, 92.

Kolattukudy, P.E., 1976. Introduction to natural waxes. In: P.E. Kolattukudy (Ed.), Chemistry and Biochemistry of Natural Waxes. Elsevier Scientific Publishing Company, Amsterdam, pp. 1-17.

Kunst, L., Samuels, A.L., 2003. Biosynthesis and secretion of plant cuticular wax. Progress in Lipid Research 42, 51-80.

Kutzbach, J.E., 1981. Monsoon climate of the early Holocene: Climate experiment with the Earth's orbital parameters for 9000 years ago. Science 214, 59-61.

Kutzbach, J.E., Liu, Z., 1997. Response of the African monsoon to orbital forcing and ocean feedbacks in the middle Holocene. Science 278, 440-443.

Laskar, J., Robutel, P., Joutel, F., Gastineau, M., Correia, A.C.M., Levrard, B., 2004. A long-term numerical solution for the insolation quantities of the Earth. Astronomy and Astrophysics 428, 261-285.

Leegood, R.C., 1999a. Carbon dioxide-concentrating mechanisms: $C_4$ photosynthesis and Crassulacean Acid Metabolism. In: P.J. Lea, R.C. Leegood (Eds.), Plant Biochemistry and Molecular Biology. John Wiley & Sons Ltd., West Sussex, pp. 51-79.

Leegood, R.C., 1999b. Photosynthesis in $C_3$ plants: The Benson-Calvin cycle and photorespiration. In: P.J. Lea, R.C. Leegood (Eds.), Plant Biochemistry and Molecular Biology. John Wiley & Sons Ltd., West Sussex, pp. 29-50.

Lewis, C.A., Reimer, P.J., Reimer, R.W., 2008. Marine reservoir corrections: St. Helena, South Atlantic Ocean. Radiocarbon 50, 275-280.

Lisiecki, L.E., Raymo, M.E., 2005. A Pliocene-Pleistocene stack of 57 globally distributed benthic $\delta^{18}O$ records. Paleoceanography 20, PA1003.

Liu, W., Yang, H., 2008. Multiple controls for the variability of hydrogen isotopic compositions in higher plant *n*-alkanes from modern ecosystems. Global Change Biology 14, 2166-2177.

Liu, W., Yang, H., Li, L., 2006. Hydrogen isotopic compositions of *n*-alkanes from terrestrial plants correlate with their ecological life forms. Oecologia 150, 330-338.

Long, S.P., 1999. Environmental responses. In: R.F. Sage, R.K. Monson (Eds.), $C_4$ Plant Biology. Academic Press, San Diego, pp. 215-249.

Lüttge, U., 2002. $CO_2$-concentrating: Consequences in Crassulacean Acid Metabolism. Journal of Experimental Botany 53, 2131-2142.

Lüttge, U., 2004. Ecophysiology of Crassulacean Acid Metabolism (CAM). Annals of Botany 93, 629-652.

Macková, J., Vašková, M., Macek, P., Hronková, M., Schreiber, L., Šantrůček, J., 2013. Plant response to drought stress simulated by ABA application: Changes in chemical composition of cuticular waxes. Environmental and Experimental Botany 86, 70-75.

Maley, J., 1991. The African rain forest vegetation and palaeoenvironments during late Quaternary. Climatic Change 19, 79-98.

Marzi, R., Torkelson, B.E., Olson, R.K., 1993. A revised carbon preference index. Organic Geochemistry 20, 1303-1306.

Matsuura, K., Willmott, C., Legates, D., 2009. WebWIMP: The web-based water-budget interactive modelling programm, http://climate.geog.udel.edu/~wimp/ (last accessed 04.11.14).

Mayaux, P., Bartholomé, E., Fritz, S., Belward, A., 2004. A new land-cover map of Africa for the year 2000. Journal of Biogeography 31, 861-877.

McDuffee, K.E., Eglinton, T.I., Sessions, A.L., Sylva, S., Wagner, T., Hayes, J.M., 2004. Rapid analysis of $^{13}C$ in plant-wax *n*-alkanes for reconstruction of terrestrial vegetation signals from aquatic sediments. Geochemistry Geophysics Geosystems 5, doi:10.1029/2004GC0772.

McInerney, F.A., Helliker, B.R., Freeman, K.H., 2011. Hydrogen isotope ratios of leaf wax *n*-alkanes in grasses are insensitive to transpiration. Geochimica et Cosmochimica Acta 75, 541-554.

Mead, R., Xu, Y., Chong, J., Jaffé, R., 2005. Sediment and soil organic matter source assessment as revealed by the molecular distribution and carbon isotopic composition of *n*-alkanes. Organic Geochemistry 36, 363-370.

Medina, E., Minchin, P., 1980. Stratification on $\delta^{13}C$ values of leaves in Amazonian rain forests. Oecologia 45, 377-378.

Medina, E., Montes, G., Cuevas, E., Rokzandic, Z., 1986. Profiles of $CO_2$ concentration and $\delta^{13}C$ values in tropical rain forests of the upper Rio Negro Basin, Venezuela. Journal of Tropical Ecology 2, 207-217.

Michalak, J., 2004. DEM data obtained from the shuttle radar topography Mission - SRTM-3. Annals of Geomatics 2, 33-46.

Milton, S.J., Yeaton, R.I., Dean, W.R.J., Vlok, J.H.J., 1997. Succulent karoo. In: R.M. Cowling, D.M. Richardson, S.M. Pierce (Eds.), Vegetation of Southern Africa. Cambridge University Press, Cambridge, pp. 131-166.

Monnin, E., Steig, E.J., Siegenthaler, U., Kawamura, K., Schwander, J., Stauffer, B., Stocker, T.F., Morse, D.L., Barnola, J.-M., Bellier, B., Raynaud, D., Fischer, H., 2004. Evidence for substantial accumulation rate variability in Antarctica during the Holocene, through synchronization of $CO_2$ in the Taylor Dome, Dome C and DML ice cores. Earth and Planetary Science Letters 224, 45-54.

Monson, K.D., Hayes, J.M., 1980. Biosynthetic control of the natural abundance of carbon 13 at specific positions within fatty acids in *Escherichia coli* - Evidence regarding the coupling of fatty acid and phospholipid synthesis. Journal of Biological Chemistry 255, 11435-11441.

Morales, C., 1986. The airborne transport of Saharan dust: A review. Climatic Change 9, 219-241.

Nicholson, S., 2000. The nature of rainfall variability over Africa on time scales of decades to millenia. Global and Planetary Change 26, 137-158.

Nicholson, S., 2009. A revised picture of the structure of the “monsoon” and land ITCZ over West Africa. Climate Dynamics 32, 1155-1171.

Nicholson, S., 2013. The West African Sahel: A review of recent studies on the rainfall regime and its interannual variability. ISRN Meteorology 2013, 32.

Niedermeyer, E.M., Schefuß, E., Sessions, A.L., Mulitza, S., Mollenhauer, G., Schulz, M., Wefer, G., 2010. Orbital- and millennial-scale changes in the hydrologic cycle and vegetation in the western African Sahel: Insights from individual plant wax $\delta D$ and $\delta^{13}C$. Quaternary Science Reviews 29, 2996-3005.

Nilsson, C., Reidy, C.A., Dynesius, M., Revenga, C., 2005. Fragmentation and flow regulation of the world’s large river systems. Science 308, 405-408.

O’Leary, M.H., 1981. Carbon isotope fractionation in plants. Phytochemistry 20, 553-567.

Osborne, C.P., Beerling, D.J., 2006. Nature´s green revolution: The remarkable evolutionary rise of $C_4$ plants. Philosophical Transactions of the Royal Society Series B 361, 173-194.

Pancost, R.D., Boot, C.S., 2004. The palaeoclimatic utility of terrestrial biomarkers

in marine sediments. Marine Chemistry 92, 239-261.

Partridge, T.C., Demenocal, P.B., Lorentz, S.A., Paiker, M.J., Vogel, J.C., 1997. Orbital forcing of climate over South Africa: A 200,000-year rainfall record from the Pretoria Saltpan. Quaternary Science Reviews 16, 1125-1133.

Peterson, R.G., Stramma, L., 1991. Upper-level circulation in the South Atlantic Ocean. Progress in Oceanography 26, 1-73.

Petit, J.R., Jouzel, J., Raynaud, D., Barkov, N.I., Barnola, J.-M., Basile, I., Bender, M., Chappellaz, J., Davis, M., Delaygue, G., Delmotte, M., Kotlyakov, V.M., Legrand, M., Lipenkov, V.Y., Lorius, C., Pépin, L., Ritz, C., Saltzman, E., Stievenard, M., 1999. Climate and atmospheric history of the past 420,000 years from the Vostok ice core, Antarctica. Nature 399, 429-436.

Philander, S.G.H., Gu, D., Lambert, G., Li, T., Halpern, D., Lau, N.C., Pacanowski, R.C., 1996. Why the ITCZ is mostly north of the equator. Journal of Climate 9, 2958-2972.

Pierrehumbert, R.T., 2010. Principles of Planetary Climate, Cambridge University Press, Cambridge.

Polissar, P.J., Freeman, K.H., 2010. Effects of aridity and vegetation on plant-wax δD in modern lake sediments. Geochimica et Cosmochimica Acta 74, 5785-5797.

Polissar, P.J., Freeman, K.H., Rowley, D.B., McInerney, F.A., Currie, B.S., 2009. Paleoaltimetry of the Tibetan Plateau from D/H ratios of lipid biomarkers. Earth and Planetary Science Letters 287, 64-76.

Poynter, J.G., 1989. Molecular stratigraphy: The recognition of palaeoclimatic signals in organic geochemical data. PhD thesis, University of Bristol.

Prahl, F.G., Wakeham, S.G., 1987. Calibration of unsaturation patterns in long chain ketone compositions for palaeotemperature assessment. Nature 330, 367-369.

Prospero, J.M., Charlson, R.J., Mohnen, V., Jaenicke, R., Delany, A.C., Moyers, J., Zoller, W., Rahn, K., 1983. The atmospheric aerosol system: An overview. Reviews of Geophysics 21, 1607-1629.

Radke, M., Willsch, H., Welte, D.H., 1980. Preparative hydrocarbon group type determination by automated medium pressure liquid chromatography. Analytical Chemistry 52, 406-411.

Rao, Z., Zhu, Z., Jia, G., Henderson, A.C.G., Xue, Q., Wang, S., 2009. Compound specific δD values of long chain *n*-alkanes derived from terrestrial higher plants are indicative of the δD of meteoric waters: Evidence from surface soils in eastern China. Organic Geochemistry 40, 922-930.

Ratkowski, D.A., 1990. Handbook of Nonlinear Regression Models, Marcel Dekker, Inc., New York, Basel.

Richards, P.W., 1996. The Tropical Rain Forest, 2nd ed., Cambridge University Press, Cambridge.

Richardson, A., Franke, R., Kerstiens, G., Jarvis, M., Schreiber, L., Fricke, W., 2005. Cuticular wax deposition in growing barley (*Hordeum vulgare*) leaves commences in relation to the point of emergence of epidermal cells from the sheaths of older leaves. Planta 222, 472-483.

Rommerskirchen, F., 2006. Fossil $C_4$ plant signals in southeast Atlantic Ocean continental margin sediments indicate climate-dependent vegetation changes on the adjacent continent. PhD thesis, University of Oldenburg.

Rommerskirchen, F., Eglinton, G., Dupont, L., Güntner, U., Wenzel, C., Rullkötter, J., 2003. A north to south transect of Holocene southeast Atlantic continental margin sediments: Relationship between aerosol transport and compound-specific $\delta^{13}C$ land plant biomarker and pollen records. Geochemistry Geophysics Geosystems 4, doi:10.1029/2003GC000541.

Rommerskirchen, F., Eglinton, G., Dupont, L., Rullkötter, J., 2006a. Glacial/interglacial changes in southern Africa: Compound-specific $\delta^{13}C$ land plant biomarker and pollen records from southeast Atlantic continental margin sediments. Geochemistry Geophysics Geosystems 7, doi:10.1029/2005GC001223.

Rommerskirchen, F., Plader, A., Eglinton, G., Chikaraishi, Y., Rullkötter, J., 2006b. Chemotaxonomic significance of distribution and stable carbon isotopic composition of long chain alkanes and alkan-1-ols in $C_4$ grass waxes. Organic Geochemistry 37, 1303-1332.

Rullkötter, J., 2003. Geochemistry, Organic. In: R.A. Meyers (Ed.), Encyclopedia of Physical Science and Technology. Academic Press, New York, pp. 549-574.

Rullkötter, J., Mukhopadhyay, P.K., Schaefer, R.G., Welte, D.H., 1984. Geochemistry and petrography of organic matter in sediments from Deep Sea Drilling Project Sites 545 and 547, Mazagan Escarpment. In: K. Hinz, E.L. Winterer, et al. (Eds.), Initial Reports of the Deep Sea Drilling Project, Vol. 79, Washington DC, pp. 775-806.

Sachse, D., Radke, J., Gleixner, G., 2004. Hydrogen isotope ratios of recent lacustrine sedimentary *n*-alkanes record modern climate variability. Geochimica et Cosmochimica Acta 68, 4877-4889.

Sachse, D., Kahmen, A., Gleixner, G., 2009. Significant seasonal variation in the hydrogen isotopic composition of leaf-wax lipids for two deciduous tree ecosystems (*Fagus sylvativa* and *Acer pseudoplatanus*). Organic Geochemistry 40, 732-742.

Sachse, D., Gleixner, G., Wilkes, H., Kahmen, A., 2010. Leaf wax *n*-alkane δD

values of field-grown barley reflect leaf water δD values at the time of leaf formation. Geochimica et Cosmochimica Acta 74, 6741-6750.

Sachse, D., Billault, I., Bowen, G.J., Chikaraishi, Y., Dawson, T.E., Feakins, S.J., Freeman, K.H., Magill, C.R., McInerney, F.A., van der Meer, M.T.J., Polissar, P., Robins, R.J., Sachs, J.P., Schmidt, H.-L., Sessions, A.L., White, J.W.C., West, J.B., Kahmen, A., 2012. Molecular paleohydrology: Interpreting the hydrogen-isotopic composition of lipid biomarkers from photosynthesising organisms. Annual Review of Earth and Planetary Sciences 40, 221-249.

Sage, R.F., 1999. Why $C_4$ photosynthesis? In: R.F. Sage, R.K. Monson (Eds.), $C_4$ Plant Biology. Academic Press, San Diego, pp. 3-16.

Sage, R.F., 2001. $C_4$ plants. In: S.A. Levin (Ed.), Encyclopedia of Biodiversity. Academic Press, San Diego, pp. 575-598.

Sage, R.F., 2004. The evolution of $C_4$ photosynthesis. New Phytologist 161, 341-370.

Sage, R.F., Kubien, D.S., 2003. Quo vadis $C_4$? An ecophysiological perspective on global change and the future of $C_4$ plants. Photosynthesis Research 77, 209-225.

Sage, R.F., Li, M., Monson, R.K., 1999a. The taxonomic distribution of $C_4$ photosynthesis. In: R.F. Sage, R.K. Monson (Eds.), $C_4$ Plant Biology. Academic Press, San Diego, pp. 551-584.

Sage, R.F., Wedin, D.A., Li, M., 1999b. The biogeography of $C_4$ photosynthesis: Patterns and controlling factors. In: R.F. Sage, R.K. Monson (Eds.), $C_4$ Plant Biology. Academic Press, San Diego, pp. 313-373.

Sanchez Goñi, M.F., Harrison, S.P., 2010. Millennial-scale climate variability and vegetation changes during the Last Glacial: Concepts and terminology. Quaternary Science Reviews 29, 2823-2827.

Sayed, O.H., 2001. Crassulacean Acid Metabolism 1975–2000, a check list. Photosynthetica 39, 339-352.

Schefuß, E., Ratmeyer, V., Stuut, J.-B.W., Jansen, J.H.F., Sinninghe Damsté, J.S., 2003a. Carbon isotope analyses of *n*-alkanes in dust from the lower atmosphere over the central eastern Atlantic. Geochimica et Cosmochimica Acta 67, 1757-1767.

Schefuß, E., Schouten, S., Jansen, J.H.F., Sinninghe Damste, J.S., 2003b. African vegetation controlled by tropical sea surface temperatures in the mid-Pleistocene period. Nature 422, 418-421.

Schefuß, E., Versteegh, G.J.M., Jansen, J.H.F., Sinninghe Damsté, J.S., 2004. Lipid biomarkers as major source and preservation indicators in SE Atlantic surface sediments. Deep-Sea Research Part I - Oceanographic Research Papers 51,

1199-1228.

Schefuß, E., Schouten, S., Schneider, R.R., 2005. Climatic controls on central African hydrology during the past 20,000 years. Nature 437, 1003-1006.

Schefuß, E., Kuhlmann, H., Mollenhauer, G., Prange, M., Pätzold, J., 2011. Forcing of wet phases in southeast Africa over the past 17,000 years. Nature 480, 509-512.

Schidlowski, M., 1987. Application of stable carbon isotopes to early biochemical evolution on Earth. Annual Review of Earth and Planetary Sciences 15, 47-72.

Schimmelmann, A., Sessions, A.L., Mastalerz, M., 2006. Hydrogen isotopic (D/H) composition of organic matter during diagenesis and thermal maturation. Annual Review of Earth and Planetary Sciences 34, 501-533.

Schneider, R.R., Müller, P.J., Ruhland, G., 1995. Late Quaternary surface circulation in the east equatorial South Atlantic: Evidence from alkenone sea surface temperatures. Paleoceanography 10, 197-219.

Schubert, C.J., Nielsen, B., 2000. Effects of decarbonation treatments on $\delta^{13}C$ values in marine sediments. Marine Chemistry 72, 55-59.

Schulz, H.D., Devey, C.W., Pätzold, J., Fischer, G., 1999. Meteor-Berichte 99-3, University of Bremen.

Sessions, A.L., Burgoyne, T.W., Schimmelmann, A., Hayes, J.M., 1999. Fractionation of hydrogen isotopes in lipid biosynthesis. Organic Geochemistry 30, 1193-1200.

Sharp, Z., 2007. Principles of Stable Isotope Geochemistry, Pearson Education, New Jersey.

Shepherd, T., Wynne Griffiths, D., 2006. The effects of stress on plant cuticular waxes. New Phytologist 171, 469-499.

Shi, N., Dupont, L.M., Beug, H.-J., Schneider, R., 1998. Vegetation and climate changes during the last 21 000 years in S.W. Africa based on a marine pollen record. Vegetation History and Archaeobotany 7, 127-140.

Simoneit, B.R.T., 1984. Organic matter of the troposphere - III. Characterization and sources of petroleum and pyrogenic residues in aerosols over the western United States. Atmospheric Environment (1967) 18, 51-67.

Simoneit, B.R.T., 1997. Compound-specific carbon isotope analyses of individual long chain alkanes and alkanoic acids in Harmattan aerosols. Atmospheric Environment 31, 2225-2233.

Simoneit, B.R.T., 2002. Biomass burning - A review of organic tracers for smoke from incomplete combustion. Applied Geochemistry 17, 129-162.

Simoneit, B.R.T., 2006. Atmospheric transport of terrestrial organic matter to the

sea. In: J.K. Volkman (Ed.), Marine Organic Matter: Biomakers, Isotopes and DNA. Springer, Berlin, Heidelberg, New York, pp. 165-208.

Simoneit, B.R.T., Chester, R., Eglinton, G., 1977. Biogenic lipids in particulates from the lower atmosphere over the eastern Atlantic. Nature 267, 682-685.

Simoneit, B.R.T., Cox, R.E., Standley, L.J., 1988. Organic matter of the troposphere - IV. Lipids in harmattan aerosols of Nigeria. Atmospheric Environment (1967) 22, 983-1004.

Sinninghe Damsté, J.S., Verschuren, D., Ossebaar, J., Blokker, J., van Houten, R., van der Meer, M.T.J., Plessen, B., Schouten, S., 2011. A 25,000-year record of climate-induced changes in lowland vegetation of eastern equatorial Africa revealed by the stable carbon-isotopic composition of fossil plant leaf waxes. Earth and Planetary Science Letters 302, 236-246.

Smith, F.A., Freeman, K.H., 2006. Influence of physiology and climate on δD of leaf wax *n*-alkanes from $C_3$ and $C_4$ grasses. Geochimica and Cosmochimica Acta 70, 1172-1187.

Sternberg, L.D.L., 1988. D/H ratios of environmental water recorded by D/H ratios of plant lipids from submerged plants. Nature 333, 59-61.

Stevens, P.F., 2001. Angiosperm Phylogeny Website, Version 13, http://www.mobot.org/MOBOT/research/APweb/ (last accessed 03.02.15).

Still, C.J., Powell, R.L., 2010. Continental scale distribution of vegetation stable carbon isotope ratios. In: J.B. West, G.J. Bowen, T.E. Dawson, K.P. Tu (Eds.), Isoscapes - Understanding Movement, Pattern, and Progress on Earth Through Isotope Mapping. Springer, New York, pp. 179-194.

Still, C.J., Berry, J.A., Collatz, G.J., DeFries, R.S., 2003. Global distribution of $C_3$ and $C_4$ vegetation: Carbon cycle implications. Global Biogeochemical Cycles 17, 1006.

Stuiver, M., Reimer, P.J., 1993. Extended $^{14}C$ data base and revised Calib 3.0 $^{14}C$ age calibration program. Radiocarbon 35, 215-230.

Sulzman, E.W., 2007. Stable isotope chemistry and measurement: A primer. In: R. Michener, K. Lajtha (Eds.), Stable Isotopes in Ecology and Environmental Science. Blackwell Publishing Ltd, Malden, Oxford, Victoria.

Summerhayes, C.P., Kroon, D., Rosell-Melé, A., Jordan, R.W., Schrader, H.-J., Hearn, R., Villanueva, J., Grimalt, J.O., Eglinton, G., 1995. Variability in the Benguela current upwelling system over the past 70,000 years. Progress In Oceanography 35, 207-251.

Swap, R., Garstang, M., Macko, S.A., Tyson, P.D., Maenhaut, W., Artaxo, P., Kållberg, P., Talbot, R., 1996. The long-range transport of southern African aerosols to

the tropical South Atlantic. Journal of Geophysical Research: Atmospheres 101, 23777-23791.

Teeri, J.A., 1988. Interaction of temperature and other environmental variables influencing plant distribution. In: S.P. Long, F.I. Woodward (Eds.), Plants and Temperature. Society for Environmental Biology, Cambridge, pp. 77-89.

Teeri, J.A., Stowe, L.G., 1976. Climatic patterns and the distribution of $C_4$ grasses in North America. Oecologia 23, 1-12.

Tierney, J.E., Oppo, D.W., Rosenthal, Y., Russell, J.M., Linsley, B.K., 2010a. Coordinated hydrological regimes in the Indo-Pacific region during the past two millennia. Paleoceanography 25, doi:10.1029/2009PA001871.

Tierney, J.E., Russell, J.M., Huang, Y., 2010b. A molecular perspective on Late Quaternary climate and vegetation change in the Lake Tanganyika basin, East Africa. Quaternary Science Reviews 29, 787-800.

Tipple, B.J., Pagani, M., 2007. The early origins of terrestrial $C_4$ photosynthesis. Annual Review of Earth and Planetary Sciences 35, 435-461.

Tulloch, A.P., 1976. Chemistry of waxes of higher plants. In: P.E. Kolattukudy (Ed.), Chemistry and Biochemistry of Natural Waxes. Elsevier Scientific Publishing Company, Amsterdam, pp. 236-250.

UNEP, 1992. World Atlas of Desertification, 1st ed., John Wiley & Sons, Inc., New York.

UNEP, 1997. World Atlas of Desertification, 2nd ed., John Wiley & Sons, Inc., New York.

Vellinga, M., Wood, R.A., 2002. Global climatic impacts of a collapse of the Atlantic Thermohaline Circulation. Climatic Change 54, 251-267.

Vogts, A., 2011. Plant wax alkanes and alkan-1-ols in ocean sediments as indicators of continental climate change - Validation of a molecular proxy. PhD thesis, University of Oldenburg.

Vogts, A., Moossen, H., Rommerskirchen, F., Rullkötter, J., 2009. Distribution patterns and stable carbon isotopic composition of alkanes and alkan-1-ols from plant waxes of African rain forest and savanna $C_3$ species. Organic Geochemistry 40, 1037-1054.

Vogts, A., Schefuß, E., Badewien, T., Rullkötter, J., 2012. *n*-Alkane parameters from a deep sea sediment transect off southwest Africa reflect continental vegetation and climate conditions. Organic Geochemistry 47, 109-119.

Wang, Y., Sessions, A.L., Nielsen, R.J., Goddart III, W.A., 2009. Equilibrium $^2H/^1H$ fractionation in organic molecules. II: Linear alkanes, alkenes, ketones, carboxylic acids, esters, alcohols and ethers. Geochimica et Cosmochimica Acta 73,

7076-7086.

Wefer, G., Bleil, U., Schulz, H., Fischer, G., 1997. Meteor-Berichte 97-1, University of Bremen.

Wefer, G., Berger, W.H., Richter, C., 1998. Initial Reports, Site 1078. In: Proceedings of the Ocean Drilling Programm, Initial Reports, Vol. 175, pp. 143-176.

Weijers, J.W.H., Schefuß, E., Schouten, S., Sinninghe Damsté, J.S.S., 2007. Coupled thermal and hydrological evolution of tropical Africa over the last deglaciation. Science 315, 1701-1704.

Weijers, J.W.H., Schouten, S., Schefuß, E., Schneider, R.R., Sinninghe Damsté, J.S., 2009. Disentangling marine, soil and plant organic carbon contributions to continental margin sediments: A multi-proxy approach in a 20,000 year sediment record from the Congo deep-sea fan. Geochimica et Cosmochimica Acta 73, 119-132.

Weldeab, S., Lea, D.W., Schneider, R.R., Andersen, N., 2007. 155,000 years of West African monsoon and ocean thermal evolution. Science 316, 1303-1307.

Werner, R.A., Bruch, B.A., Brand, W.A., 1999. ConFlo III – An interface for high precision $\delta^{13}C$ and $\delta^{15}N$ analysis with an extended dynamic range. Rapid Communications in Mass Spectrometry 13, 1237-1241.

White, F., 1983. The vegetation of Africa: A descriptive memoir to accompany the UNESCO/AEFTAT/UNSO vegetation map of Africa, UNESCO, Paris.

Whittaker, R.H., 1975. Communities and Ecosystems, Macmillan, New York.

Willmott, C.J., Rowe, C.M., Mintz, Y., 1985. Climatology of the terrestrial seasonal water cycle. International Journal of Climatology 5, 589-606.

Winslow, J.C., Hunt Jr., E.R., Piper, S.C., 2003. The influence of seasonal water availability on global $C_3$ versus $C_4$ grassland biomass and its implications for climate change research. Ecological Modelling 163, 153-173.

Winter, K., Aranda, J., Holtum, J.A.M., 2005. Carbon isotope composition and water-use efficiency in plants with Crassulacean Acid Metabolism. Functional Plant Biology 32, 381-388.

Zhao, M., Dupont, L., Eglinton, G., Teece, M., 2003. *n*-Alkane and pollen reconstruction of terrestrial climate and vegetation for NW Africa over the last 160 kyr. Organic Geochemistry 34, 131-142.

Zimmerman, J., Ehleringer, J., 1990. Carbon isotope ratios are correlated with irradiance levels in the Panamanian orchid *Catasetum viridiflavum*. Oecologia 83, 247-249.

## Acknowledgements (in German)

Während meiner Zeit als Doktorandin haben mich viele Menschen auf unterschiedlichste Weise begleitet und unermüdlich unterstützt. Dafür bin ich sehr dankbar.

Prof. Dr. Jürgen Rullkötter danke ich für das mir entgegengebrachte Vertrauen, die wertvollen Anregungen und die Möglichkeit, in diesem spannenden Forschungsgebiet zu promovieren. Weiter möchte ich mich bei Prof. Dr. Hans-Jürgen Brumsack bedanken für die Bereitschaft, diese Arbeit als Korreferent zu begutachten. Prof. Dr. Hans-Jürgen Brumsack, Prof. Dr. Thorsten Dittmar und Prof. Dr. Jürgen Rullkötter gaben mir im Rahmen des „Thesis Komittees" hilfreiche Rückmeldungen und Ratschläge, wofür ich mich herzlich bedanke.

Mein ganz besonderer Dank gilt Dr. Angela Vogts für die gute, stimmungsvolle und unkomplizierte Zusammenarbeit, die vielen fruchtbaren Diskussionen, Anmerkungen und Informationen. Für die gute Zusammenarbeit bin ich Prof. Dr. Geoffrey Eglinton, Dr. Florian Rommerskirchen und Dr. Enno Schefuß dankbar, die mit Ideen und hilfreichen Vorschlägen die Interpretation der Ergebnisse wesentlich vorangebracht haben. Dr. Bernhard Schnetger danke ich für Probenmaterial und Hilfe bei den RFA-Messungen. Weiteres Probenmaterial wurde von Dr. Lydie Dupont (Universität Bremen), Dr. Wolfram Lobin (Universität Bonn), Dr. Jürgen Pätzold (Universität Bremen), Dr. Jan Wieringa (Universität Wageningen) und Dr. Matthias Zabel (Universität Bremen) bereitgestellt, wofür ich mich herzlich bedanke. Mein weiterer Dank gilt Dr. Rebecca Powell (University of Denver) und Dr. Christopher Still (Oregon State University) für die Bereitstellung einer Abbildung. Ich danke zudem den Organisatoren und Teilnehmern der Fahrten M34/2, M41/1 und M76/2 des Forschungsschiffes Meteor.

Ich möchte mich ganz herzlich bei den Mitarbeitern der AG Organische Geochemie für die freundliche, kollegiale Stimmung und die stete Hilfsbereitschaft bedanken. Insbesondere danke ich Dr. Barbara Scholz-Böttcher und Dr. Jürgen Köster für die vielen Antworten und Diskussionen sowie Regina Grundmann, Bernd Kopke, Anke Müllenmeister-Sawall und Charlotte Versteegen für die unermüdliche Hilfe bei technischen und praktischen Problemen. Mein besonderer Dank gilt Bernd Kopke, der mich freundlich, hilfsbereit und sehr engagiert bei den Isotopenmessungen unterstützt hat. Im Rahmen dieser Arbeit entstanden mehrere studentische Arbeiten, welche die Aufarbeitung der Proben wesentlich beschleunigt haben. Dafür danke ich Marten Fischer und Anna Lau. Bei den praktischen Laborarbeiten

unterstützten mich zusätzlich zahlreiche Auszubildende (Hergen Haase, Jan Jasper, Denis Lorenz, Lene Sophie Meiners, Patrick Neumann, Kristin Petersen, Katrin Reinken, Steffen Schüler und Ina Ulber) und studentische Hilfskräfte (Katharina Bengard, Robert Brünjes und Markus Kurtz), denen mein Dank gilt. Ich bedanke mich bei Dr. Philipp Böning, Dr. Christian März, Dr. Donata Monien, Dr. Martina Nullmeier, Dr. Harald Poigner und René Ungermann für schnelle Literaturzugänge und bei Gordon Schroeder für ein Programm zur schnelleren Auswertung von GC-irm-MS-Daten.

Im und außerhalb vom Arbeitsalltag haben mich die “Familia Geochimica” und meine Bürofamilie (Dr. Melanie Beck, Dr. Philipp Böning, Dr. Christian März, Dr. Donata Monien und Anja Reckhardt) wunderbar unterstützt und aufgefangen. Meiner „echten” und „zweiten” Familie, insbesondere Gordon Schroeder, danke ich für den Rückhalt und die zahlreichen Erholungen in meiner Freizeit.

Abschließend danke ich der Deutschen Forschungsgemeinschaft, die Teile dieser Arbeit finanziell gefördert hat.

## Curriculum Vitae (in German)

| Persönliche Daten | |
|---|---|
| Name | Tanja Badewien |
| Geburtsdatum und -ort | 01.12.1983, Leer |
| Staatsangehörigkeit | Deutsch |
| E-Mail | t.badewien@uni-oldenburg.de |

| Schulbildung und Freiwilliges Soziales Jahr | |
|---|---|
| 1990 - 1994 | Grundschule, Leer |
| 1994 - 1996 | Orientierungsstufe, Leer |
| 1996 - 2003 | Gymnasium, Leer |
| 2003 - 2004 | Freiwilliges Soziales Jahr, Leer |

| Akademischer Werdegang | |
|---|---|
| 10.2004 - 10.2009 | Carl von Ossietzky Universität Oldenburg,<br>Marine Umweltwissenschaften (Diplom),<br>Diplomarbeit in der AG Organische Geochemie am Institut für Chemie und Biologie des Meeres (ICBM) mit dem Titel: „Geochemische Analyse von rezenten Sedimenten des südwestafrikanischen Kontinentalhanges”,<br>Diplom: 13.10.2009 |
| seit 01.2010 | Promotionsstudentin in der AG Organische Geochemie am ICBM |

## Eidesstattliche Erklärung

Ich versichere hiermit, dass ich die vorliegende Arbeit selbstständig verfasst, die Leitlinien der guten wissenschaftlichen Praxis der Carl von Ossietzky Universität berücksichtigt und keine anderen als die angegebenen Hilfsmittel und Quellen verwendet habe. Ich habe keine kommerziellen Vermittlungs- und Beratungsdienste in Anspruch genommen. Ferner erkläre ich, dass diese Dissertation keiner anderen wissenschaftlichen Hochschule zur Begutachtung in einem Promotionsverfahren vorliegt oder vorgelegen hat. Teile dieser Dissertation sind, wie angegeben, bereits veröffentlicht.

Oldenburg, im Februar 2015

Tanja Badewien